

A STUDY OF PIPE-SOIL-CLIMATE INTERACTION OF BURIED WATER AND GAS PIPES

By

Derek Chun Chuen Chan

A thesis submitted in fulfilment of the requirements for
the degree of Doctor of Philosophy

Department of Civil Engineering



MONASH University

February 2014

Notice 1

Under the Copyright Act 1968, this thesis must be used only under the normal conditions of scholarly fair dealing. In particular no results or conclusions should be extracted from it, nor should it be copied or closely paraphrased in whole or in part without the written consent of the author. Proper written acknowledgement should be made for any assistance obtained from this thesis.

To my family

DECLARATION

I hereby declare that this thesis contains no material which has been accepted for the award of any other degree or diploma in any university or institution. To the best of my knowledge and belief, this thesis contains no material previously published or written by another person, except when due reference is made in the text of the thesis.



DEREK CHUN CHUEN CHAN

Department of Civil Engineering

Monash University

Clayton, Australia

February 2014

SUMMARY

In Australia, buried water and gas pipes are reported to have more frequent failures in hot and dry summers, which suggests that soil shrinkage and thermal effects are the main factors associated with pipe failure. Shrinkage and swelling are common behaviours of soils especially for reactive clays due to seasonal variation of soil moisture content. As a result, the differential soil movement beneath buried pipe can lead to flexural bending and circumferential fracture of the pipe. In addition, seasonal variation of soil moisture content can cause cyclic upward and downward pipe bending and ultimately lead to fatigue failure. However, the relationships between pipe failure, soil behaviour and seasonal climatic change have not been studied in detail. Consequently, the effect of soil moisture content variation on the performance of buried pipes is not clear.

This research study is aimed at extending the current knowledge on the interaction between pipes, soils and climate. Field instrumentation was undertaken to study the behaviour of buried cast iron pipes in the natural environment. The collected data confirmed that significant flexural stress was induced by the soil movement on the buried pipe due to the seasonal variation of soil moisture content. Upward and downward bending of the pipe was found to occur at wet and dry seasons, respectively.

Regional field measurements of soil moisture content were undertaken in conjunction with field instrumentation to study the seasonal variation of soil moisture content at sites with different soil profiles and geological formations. The 23 sites considered in the study were classified into three categories based on the geological profiles. The study showed that change in soil moisture content was associated with rainfalls and the geological profiles of the site. Variations of soil moisture content can lead to swelling and shrinking of soils and corresponding bending of buried pipes. These data provided the necessary information to understand the likely behaviour of pipes buried in different types of soils.

The ground-atmosphere models were used for prediction of soil moisture content variation of the field sites. The Winkler spring models were used to simulate the pipe-soil interaction, and in conjunction with the long term moisture content variation, pipe flexural stress was calculated.

Taking into account the deterioration of cast iron pipe strength with time, the relationship between pipe failure probability and pipe age was obtained.

This research provides a prediction tool for pipe failure associated with soil behaviour and seasonal climate change. The prediction model can be used to plan for asset management and rehabilitation of the buried pipe networks, thus providing savings on repair of unexpected pipe failures and consequence loss of water and gas services to the communities.

ACKNOWLEDGEMENTS

I wish to express sincere appreciation to my main supervisor Professor Jayantha Kodikara for his endless assistance, guidance and support which enable me to complete my research. I could not have imagined having a better supervisor for my study. My sincere thanks also go to my co-supervisors Professor Malek Bouazza and Professor James Cull for their assistance and encouragement during my pursuit of the research.

I would also like to thank the members of the MAPPS group; Nathan Rajeev, Scott Gould and Chaminda Gallage for their contribution to my personal and professional time. The group has been a source of friendships as well as assistance and collaboration for the research project.

I wish to express my deep and sincere gratitude to my colleagues at Monash University; Ben Shannon, Asli Acikel, Kok Yun Lee and Siavash Hasemi for their friendship and the wonderful memories in the laboratory.

My warm thanks are due to the administrative and technical staff at the Department of Civil Engineering of Monash University; Jenny Manson, Chris Powell, Mike Leach, Long Goh and Alan Taylor for their help during my research, in the workshop and during experimental setup.

I would like to acknowledge Australia Research Council (ARC) for being the main contributor of this research project from the ARC Linkage Grant (LP 100200441). I would also like to acknowledge Danielle Roache from City West Water Limited; Professor Stewart Burn, Dr David Marlow and Dr Paul Davis from CSIRO; Mark Beech from Jemena; Nithi Nithianandan from SP AusNet; Ian Stewart from Envestra Limited; Paul Vanderwal from Water Corporation; Chris Egbers from Ipswich Water; Kevin Dyt from South East Water Limited; and Professor Ian Moore from Queen's University (Canada) for their financial and in-kind support through this project.

Finally I owe my loving thanks to my parents, sister and my lovely dog Happy. This thesis would not have been possible without their love, encouragement and understanding.

LIST OF PUBLICATIONS

Journal papers

Rajeev, P., Kodikara, J., **Chan, D.** and Gallage, C. (2013) Soil moisture monitoring at the field scale using neutron probe, Canadian Geotechnical Journal, ahead of print

Chan, D., Gallage, C., Rajeev, P. and Kodikara, J. (Submitted 2013) Field performance of in-service cast iron water reticulation pipe buried in reactive clay, International journal of Geomechanics – ASCE

Chan, D., Rajeev, P. and Kodikara, J. (Submitted 2013) Field performance of in-service cast iron gas reticulation pipe buried in reactive clay, Journal of Geotechnical and Geoenvironmental Engineering – ASCE

Rajeev, P., Kodikara, J. and **Chan, D.** (In Prep 2013) Estimating apparent thermal diffusivity of soil using field temperature time series

Rajeev, P., **Chan, D.** and Kodikara, J. (2012) Atmosphere-ground interaction modelling for long-term prediction of soil moisture and temperature, Canadian Geotechnical Journal, 49(9): 1059-1073

Conference papers

Chan, D., Rajeev P., Gallage, C. and Kodikara, J. (2010) Regional field measurement of soil moisture content with neutron probe, 17th Southeast Asia Geotechnical conference, 10th – 13th May, Taipei, Taiwan

Gallage, C., **Chan, D.**, Gould, S. and Kodikara, J. K. (2009) Stress-strain development of an in-service cast iron water reticulation pipe buried in expansive soil. Proceedings of OzWater 09. AWA, 16th-18th March, Melbourne, Australia.

Chan, D., Gallage, C., Gould, S., Kodikara, J., Bouazza, A. and Cull, J. (2009) Field instrumentation of water reticulation pipe buried in reactive soil. Proceedings of OzWater 09. AWA, 16th-18th March, Melbourne, Australia.

Gallage, C., Kodikara, J., **Chan, D.** and Davis, P. (2009) A comparison of the results of the numerical analysis and the physical behaviour of a pipe buried in reactive clay. 11th International conference of the International Association for Computer Methods and Advances in Geomechanics, 1st – 6th Oct, Goa, India, (CD Rom publication).

Kodikara, J., Davis, P., Gallage, C. **Chan, D.**, Gould, S. and Zaho, X-L. (2008). Behaviour of a polyethylene pipe buried in reactive soil, the 7th National ASTT Conference, Sydney, Australia (CD Rom publication).

Chan, D., Kodikara, J., Gould, S., Ranjith, P., Choi, X. S. K. and Davis, P. (2007) Data analysis and laboratory investigation of the behaviour of pipes buried in reactive clay. Proceedings of 10th Australia New Zealand Conference on Geomechanics - Common Ground 2007, 21st-24th October, Brisbane, Australia, Volume 2, pp. 206-211.

Technical reports

Rajeev P., **Chan, D.**, and Kodikara, J. (2010) Field measurement of soil moisture content with neutron probe (Melbourne, Australia), Research report No. RR 16, Monash University, Australia

Chan, D., Rajeev P., and Kodikara, J. (2010) Field measurement of the behaviour of an in-service gas reticulation pipe buried in reactive soil (Fawkner, VIC) – Part 2, Research report No. RR 15, Monash University, Australia

Chan, D., Rajeev P., and Kodikara, J. (2010) Field measurement of the behaviour of an in-service water reticulation pipe buried in reactive soil (Altona North, VIC) – Part 2, Research report No. RR 14, Monash University, Australia

Gallage, C., **Chan, D.**, Gould, S. and Kodikara, J. (2008) Field measurement of the behaviour of an in-service water reticulation pipe buried in reactive soil (Altona North, VIC), Research report No. RR 10, Monash University, Australia.

NOTATIONS

α typical thermal coefficient of strain gauge	$\sqrt{\varepsilon}$ square root of dielectric constant
α soil expansion coefficient	ε soil strain
α' apparent thermal coefficient of strain gauge	ε_θ hoop pipe strain
α_σ 1D soil expansion coefficient	ε_x longitudinal pipe strain
$\alpha_{\sigma,i}$ 1D soil expansion coefficient at time step i	ψ_t total soil suction
α_{er} fitting parameters	γ_b bulk unit weight
$\Delta\varepsilon_v$ change of volumetric soil strain	γ_w unit weight of water
$\Delta\omega$ change in gravimetric soil moisture content	ν Poisson's ratio
Δe change in void ratio	π osmotic soil suction
Δh change in soil height of the soil layer	θ volumetric soil moisture content
Δh_ω change in soil height due to change in gravimetric soil moisture content, ω	θ_c bulk density correction of volumetric soil moisture content
ΔT change of temperature	θ_r residual volumetric soil moisture content
ΔV potential voltage difference between the Wenner electrodes	θ_s saturated volumetric soil moisture content
	θ_w volumetric soil moisture content
	ρ_a ground resistivity

ρ_b	bulk density of soil	b	slope of the linear regression of θ_c on n_c
ρ_{bi}	bulk density of soil at a given depth	b	fitting parameters
σ	total normal soil stress	b	corrosion rate constant
σ_h	hoop pipe stress	C	number of neutron counts
σ_0	nominal net soil stress	C	volumetric heat capacity of soil
σ_x	longitudinal pipe stress	C_ψ	correction function of SWCC
ω	gravimetric soil moisture content	C_s	number of neutron counts in a standard material
ψ_m	matric soil suction	c	corrosion rate constant
ψ_i	suction corresponding to the moisture content at the inflection point of SWCC	D	pipe diameter
ψ_r	matric soil suction corresponding to θ_r	$d\varepsilon$	change in soil strain
A	cross sectional area	dh	change in height of a soil element
a	spacing of the Wenner electrodes	dz	height of a soil element
a	y intercept of the linear regression of θ_c on n_c	d_p	depth of pipe centre
a	curve fitting parameter of SWCC	E_c	1D soil constrained modulus
a	constant corresponding to minimum corrosion rate	E_p	Young's modulus of pipe material
α_a	fitting parameters	E_s	elastic modulus of soil
α_0	fitting parameters	e	natural number, 2.71828
		e	soil void ratio

e_0	initial void ratio	L	length of the modelled pipe section
$e_{r,0}$	fitting parameters	L_f	depth of wetting front
G	height of manometer above ground level	m	curve fitting parameter of SWCC
G_s	specific gravity of soil	m	fitting parameters
H	height of water level in AEP cylinder above ground level	N	neutron count rate
H	total height of soil beneath pipe	N_s	neutron count rate in a standard material
I	electric current generated by the Wenner electrodes	n	curve fitting parameter of SWCC
I	infiltration of water	n_c	bulk density correction of neutron count rate
I_f	depth factor	P_{\max}	maximum suction measured by manometer
I_s	shape factor	p_{cr}	pipe corrosion growth rate
i	hydraulic gradient	p_i	internal pipe pressure
K	thermal conductivity of soil	p_e	external pipe pressure
k	soil hydraulic conductivity	P_u	pressure difference in hydraulic conductivity test
k_s	soil spring modulus	Q	volume of one dimensional flow
k_{sat}	saturated soil hydraulic conductivity	r_i	inner pipe radius
L	length of specimen in hydraulic conductivity test	r_e	inner pipe radius

S_r	degree of saturation	t	time interval in AEP test
s	slope of the tangent line that passes through the inflection point of SWCC	t	pipe exposure time in year
T	time of neutron counts	u_a	pore air pressure
T_s	time of neutron counts in a standard material	u_w	pore water pressure
t	pipe wall thickness		

ABBREVIATIONS

AC	Asbestos Cement	IAEA	International Atomic Energy Agency
AE	Actual Evaporation	LAI	Leaf Area Index
AEP	Air Entry Permeameter	PE	Potential Evaporation Energy
AEV	Air Entry Value	PI	Plasticity Index
AS	Australian Standards	PML	Plant Moisture Limiting function
ASTM	American Society for Testing and Materials	PVC	Polyvinyl Chloride
AT	Actual Transpiration	RD	Root Depth
BOM	Bureau of Meteorology	ROCOF	Rate of Occurrence of Failure
CCTV	Closed-circuit Television	SEW	South East Water
CI	Cast Iron	SWCC	Soil Water Characteristics Curve
CSIRO	Commonwealth Scientific and Industrial Research Organisation	TCS	Thermal Conductivity Sensor
CWW	City West Water	wPI	Weighted Plasticity Index
EPC	Earth Pressure Cell	WSAA	Water Services Association of Australia
GPR	Ground Penetrating Radar	YVW	Yarra Valley Water

TABLE OF CONTENTS

DECLARATION.....	v
SUMMARY	vii
ACKNOWLEDGEMENTS.....	ix
LIST OF PUBLICATIONS	xi
NOTATIONS.....	xv
ABBREVIATIONS	xix
TABLE OF CONTENTS	xxi
LIST OF FIGURES.....	xxxix
LIST OF TABLE	xli
1 INTRODUCTION	1
1.1 Background.....	1
1.2 Research Objectives	4
1.3 Research Approach	5
1.4 Thesis Structure	7
2 LITERATURE REVIEW	9
2.1 Introduction.....	9
2.2 Performance of Buried Pipes.....	9
2.3 Interaction of Soil, Climate and Buried Pipe.....	10

2.4	Behaviour of Unsaturated Soils	17
2.4.1	The vadose zone	17
2.4.2	Soil moisture content and suction.....	19
2.4.3	Soil reactivity	21
2.5	Field Studies of Buried Pipe Behaviour.....	31
2.6	Monitoring of Soil Moisture Content.....	34
2.6.1	Variation of soil moisture content and pipe deformation	34
2.6.2	Time or frequency domain reflectometry method	35
2.6.3	Radiometric logging method.....	36
2.7	Pipe Failure Prediction Models.....	38
2.7.1	Statistically based models.....	38
2.7.2	Physically based models.....	40
2.7.3	Comparison of pipe failure prediction models.....	40
2.8	Conclusions	47
3	STUDY OF IN-SERVICE BURIED PIPES BY FIELD INSTRUMENTATIONS.....	49
3.1	Introduction.....	49
3.2	Forensic Analysis	50
3.3	Site Selection Criteria	54
3.4	Soil Characteristics of the Selected Sites	57
3.4.1	Particle size distribution.....	57

3.4.2	Atterberg limits	58
3.4.3	Swelling properties	61
3.4.4	Soil profiles	64
3.5	Field Monitoring Systems.....	65
3.5.1	Measurements of soil and pipe temperature.....	66
3.5.2	Measurement of soil suction	66
3.5.3	Measurement of soil moisture content.....	69
3.5.4	Measurement of soil pressure	72
3.5.5	Measurement of soil displacement.....	72
3.5.6	Measurement of pipe strain.....	73
3.5.7	Measurements of pipe water pressure and temperature	74
3.5.8	Measurement of site weather	74
3.5.9	Summary of the monitoring systems	75
3.5.10	Data acquisition systems.....	75
3.6	Field Instrumentation for Monitoring of the Water Pipe.....	78
3.6.1	Preliminary works	78
3.6.2	Field instrumentations and site layout.....	79
3.6.3	Site excavations	80
3.6.4	Measurement of pipe wall thickness	84
3.6.5	Strain gauging	85

3.6.6	Installation of earth pressure cells.....	87
3.6.7	Installations of soil monitoring sensors	88
3.6.8	Installations of pipe water temperature and pressure gauges.....	91
3.6.9	Wiring and cable connection.....	92
3.6.10	Backfilling and soil compaction.....	92
3.6.11	Installation of weather station	94
3.6.12	Installation of rod extensometer	94
3.7	Field Instrumentation for Monitoring of the Gas Pipe	95
3.7.1	Preliminary works	95
3.7.2	Installation of weather station	95
3.7.3	Field instrumentation and site layout.....	96
	99
3.7.4	Site excavation.....	100
3.7.5	Measurement of pipe wall thickness	101
3.7.6	Pipe instrumentations	101
3.7.7	Installation of dummy pipe	104
3.7.8	Installation of earth pressure cells.....	105
3.7.9	Installations of soil monitoring sensors	106
3.7.10	Wiring and cable connection.....	107
3.7.11	Backfilling and soil compactions	107

3.7.12	Installation of rod extensometer	108
3.8	Conclusions	109
4	INTERACTION OF BURIED PIPES WITH SOILS AND CLIMATE.....	111
4.1	Introduction.....	111
4.2	Effect of Variations of Pipe Water Pressure	112
4.3	Relationship between Air, Soil, and Pipe Temperature	114
4.3.1	Altona North results	114
4.3.2	Fawkner results	117
4.3.3	Summary	120
4.4	Relationship between Rainfall, Soil Moisture Content, and Soil Suction.....	120
4.4.1	Altona North results	121
4.4.2	Fawkner results	124
4.4.3	Summary	128
4.5	Relationship between Soil Moisture Content and Soil Pressure.....	129
4.5.1	Altona North results	129
4.5.2	Fawkner results	130
4.5.3	Summary	133
4.6	Relationship between Soil Moisture Content and Soil Displacement	133
4.6.1	Altona North results	134
4.6.2	Fawkner results	135

4.6.3	Summary	135
4.7	Relationship between Pipe, Soil, and Climate	137
4.7.1	Pipe strain measurements	137
4.7.1.1	Altona North results	137
4.7.1.2	Fawkner results	138
4.7.1.3	Summary	138
4.7.2	Calculation of pipe stress	142
4.7.3	Analysis of pipe flexural stress	146
4.7.3.1	Altona North results	146
4.7.3.2	Fawkner results	151
4.7.3.3	Summary	153
4.7.4	Behaviour of buried in-service pipes	153
4.8	Conclusions	156
5	REGIONAL FIELD MEASUREMENT OF SOIL MOISTURE CONTENT	157
5.1	Introduction	157
5.2	Overview of the Neutron Scattering Method	158
5.2.1	Principal of the neutron method	158
5.2.2	Interaction of neutron and soils	160
5.2.3	Measurement procedure	161
5.2.4	Calibration of neutron probe	162

5.3	Field Measurement of Soil Moisture Content	165
5.3.1	Site selection criteria.....	165
5.3.2	Site classification	166
5.3.2.1	Soil samples collection.....	166
5.3.2.2	Soil particle size distribution.....	166
5.3.2.3	Atterberg limits.....	168
5.3.2.4	Geological profiles	168
5.3.2.5	Summary of site classification	168
5.3.3	Field instrumentations	172
5.3.3.1	Requirements of access tube	172
5.3.3.2	Tube installation procedure	172
5.3.4	Field calibrations.....	175
5.4	Seasonal Variations of Soil Moisture Content.....	182
5.5	Conclusions	196
6	GROUND-ATMOSPHERE INTERACTION MODELLING FOR PREDICTION OF SOIL MOISTURE CONTENT AND TEMPERATURE.....	197
6.1	Introduction.....	197
6.2	Ground-atmosphere Modelling of Soil Column in Vadose/W	198
6.2.1	Governing equations.....	198
6.2.2	Soil water characteristic curves (SWCCs).....	200

6.2.3	Hydraulic conductivity-suction functions	205
6.2.4	Soil thermal conductivities and volumetric heat capacities	215
6.2.5	Vegetation functions	218
6.2.6	Initial and boundary conditions.....	223
6.2.7	Summary of the Vadose/W models	225
6.2.8	Numerical analysis of soil column	226
6.3	Ground-atmosphere Model Prediction	229
6.3.1	Prediction of soil moisture content.....	229
6.3.2	Prediction of soil temperature	233
6.3.3	Comparison of field measurements and model predictions.....	237
6.4	Conclusions	240
7	PROBABILITY OF PIPE FAILURES DUE TO CHANGES OF SOIL MOSITURE CONTENT OVER TIME	241
7.1	Introduction.....	241
7.2	Long Term Ground-atmosphere Model	242
7.2.1	Overview of long term ground-atmosphere model.....	242
7.2.2	Prediction of soil moisture content.....	242
7.3	Probability of Soil Moisture Content Variations.....	244
7.4	Numerical Modelling of Pipe-Soil Interaction	246
7.4.1	Overview of numerical pipe-soil models	246

7.4.2	Theoretical framework of pipe-soil interaction.....	247
7.4.3	Setup of pipe-soil interaction model.....	254
7.4.3.1	Description of model.....	254
7.4.3.2	Determination of linear soil expansion coefficient, α_σ	256
7.4.3.3	Determination of soil spring modulus, k_s	258
7.4.3.4	Soil and pipe properties.....	259
7.4.4	Pipe-soil interaction modelling results.....	260
7.5	Estimation of Buried Pipe Life.....	263
7.5.1	Change in pipe stresses	263
7.5.2	Relationship between pipe strength and pipe failure	264
7.5.3	Relationship between pipe strength and pipe age.....	265
7.5.4	Relationship between pipe failure and pipe age	268
7.6	Conclusions	269
8	CONCLUSIONS AND RECOMMENDATIONS.....	271
8.1	Conclusions	271
8.2	Recommendations for Future Research.....	274
	REFERENCES.....	277
	APPENDIX A.....	295
	APPENDIX B	297
	APPENDIX C	299

APPENDIX D.....	303
APPENDIX E.....	305
APPENDIX F.....	317
APPENDIX G.....	325
APPENDIX H.....	333

LIST OF FIGURES

Figure 1-1 Flow chart of research approach.....	6
Figure 2-1 Monthly variation of water pipe failures in Winnipeg, Manitoba (Rajani <i>et al.</i> 1996).....	11
Figure 2-2 Correlation of pipe breakage, rainfall, evaporation and temperature in Horsham, Victoria (Kassiff and Holland, 1965)	13
Figure 2-3 Annual break rates of AC water pipes in City of Regina, Canada (Hu <i>et al.</i> 2008)	15
Figure 2-4 Water pipe failures and corresponding net evaporation trend (Ibrahimi 2005).....	15
Figure 2-5 Schematic diagram of saturated and unsaturated soil mechanics (Fredlund 1996).....	18
Figure 2-6 Schematic diagram of soil moisture profile (Fredlund 1996).....	19
Figure 2-7 Schematic diagram of generalised soil mechanics (Fredlund 1996)	20
Figure 2-8 Typical SWCC for different soil types (Fredlund and Xing 1994)	21
Figure 2-9 Postulated mechanism of soil volume change: (a) Bending of flat particles; (b) Interlayer expansion; (c) External layer expansion (after Ring 1965)	23
Figure 2-10 Modified correlation between EI_{AZ} and wPI (Dye 2008).....	26
Figure 2-11 Climatic zones of Victoria (Standards Australia 2011).....	30
Figure 2-12 Schematic diagram of neutron probe	37
Figure 2-13 The bathtub curve of life cycle of a typical buried pipe (Kleiner and Rajani 2001)	39
Figure 3-1 Detection of water pipe leaks by acoustic method: (a) Steel “T” bars placed along suspected pipe leak location; (b) “Listening” to the acoustic noise of water pipe leaks	51
Figure 3-2 Failure of water pipe: (a) Exposed circumferential fractured pipe; (b) Pipe replacement with PVC section	51
Figure 3-3 Detection of gas pipe leaks with gas emission sensor: (a) A gas emission sensor inserted into the ground close to the suspected leak location; (b) Detergent sprayed on the failed pipe joint 52	
Figure 3-4 Pipe tensile strength and maximum corrosion pit depth (Gould <i>et al.</i> 2009)	53

Figure 3-5 Geological map of selected sites locations.....	56
Figure 3-6 Particle size distribution of the selected sites	58
Figure 3-7 Plasticity chart for classification of fine grained soils (after Das 1998)	60
Figure 3-8 Oedometers used in swelling test: (a) Typical oedometer; (b) New oedometer.....	61
Figure 3-9 Swelling pressure of samples from Altona North	62
Figure 3-10 Swelling pressure of samples from Fawkner	63
Figure 3-11 Bore hole logs of the selected sites	65
Figure 3-12 Thermocouples	66
Figure 3-13 Thermal conductivity sensors: (a) in saturation; (b) in a pressure plate for calibration ...	68
Figure 3-14 Calibration curves of thermal conductivity sensors for Altona North.....	68
Figure 3-15 Calibration curves of thermal conductivity sensors for Fawkner.....	69
Figure 3-16 Theta probe	70
Figure 3-17 Calibration plot of Theta probes for Altona North	71
Figure 3-18 Calibration plot of Theta probes for Fawkner.....	71
Figure 3-19 Earth pressure cells: (a) vibrating wire type; (b) micro-strain type.....	72
Figure 3-20 Rod extensometer (Geotechnical Systems Australia 2011)	73
Figure 3-21 Strain gauges: (a) 3-wire waterproof biaxial strain gauges; (b) 3-wire uniaxial strain gauges.....	73
Figure 3-22 Water pressure and temperature transmitters (Siemens AG 2011).....	74
Figure 3-23 Components of the weather station	75
Figure 3-24 Data acquisition system installed at Fawkner.....	77
Figure 3-25 Metal cabinet at Altona North: (a) layout of the cabinet; (b) conduit bends at the base of the cabinet.....	78
Figure 3-26 Detailed plan of Altona North	81

Figure 3-27 Detailed plan of a typical instrumentation pit in Altona North	82
Figure 3-28 Vertical long-section of instrumentation pits in Altona North	83
Figure 3-29 Excavations at Altona North: (a) location marking; (b) excavator in operation; (c) a view of the site during excavations.....	84
Figure 3-30 Measurement of water pipe wall thickness with ultrasonic gauge.....	85
Figure 3-31 Vertical cross-section of a typical instrumentation Pit A in Altona North.....	86
Figure 3-32 Strain gauging on water pipe: (a) strain gauge glued on pipe; (b) curing with heated vacuum pads; (c) coated with SEMKIT®.....	87
Figure 3-33 Earth pressure cell installation: (a) placed beneath water pipe; (b) with steel plate placed on top.....	88
Figure 3-34 Vertical Cross-section of Pit 3 in Altona North	89
Figure 3-35 Preparation of horizontal holes: (a) drilling with hand auger; (b) a view of the drilled holes	90
Figure 3-36 Installation of thermocouples: (a) prepare a cavity with screw driver; (b) sensor inserted	90
Figure 3-37 Installation of thermal conductivity sensors: (a) prepare a cavity with wooden rod; (b) sensor to be inserted.....	90
Figure 3-38 Installation of Theta probes: (a) sensor with pins; (b) sensor inserted.....	91
Figure 3-39 Pipe water temperature and pressure gauges in Altona North.....	91
Figure 3-40 Wiring at Altona North: (a) sensors cables pinned to the wall; (b) sending of sensors cables through conduits	92
Figure 3-41 Backfilling and reinstatement of Altona North: (a) Backfill with original soils; (b) water sprayed on dry soils; (c) soil compacted with vibrating plate; (d) a view of the site in one year after instrumentation	93
Figure 3-42 Weather station on Altona North	94
Figure 3-43 Rod extensometer in Altona North.....	95
Figure 3-44 Detailed plan of Fawkner	97

Figure 3-45 Detailed plan of instrumentation pits in Fawkner.....	98
Figure 3-46 Vertical long-section and cross-section of instrumentation pits in Fawkner	99
Figure 3-47 Excavation of Fawkner: (a) location marked; (b) excavator in operation; (c) a view of the site	100
Figure 3-48 Vertical long-section of pipe instrumentation in Fawkner.....	102
Figure 3-49 Cross-section of the gas pipe and strain gauge	103
Figure 3-50 Instrumentation on gas pipe: (a) strain gauges and thermocouple installed on the pipe; (b) after application of SEMKIT®	104
Figure 3-51 Instrumented dummy pipe: (a) Schematic diagram; (b) strain gauges and thermocouples installed.....	105
Figure 3-52 Earth pressure cell: (a) a micro-strain type installed above the pipe; (b) a vibrating wire type installed beneath the pipe.....	106
Figure 3-53 Horizontal drilling in preparation of sensor installation.....	107
Figure 3-54 Reinstatement of Fawkner: (a) temporary driveway; (b) a view of the site after reinstatement	108
Figure 3-55 Schematic diagram of rod extensometer installed in Fawkner	109
Figure 4-1 Typical pipe water pressure at Altona North for a three week period	113
Figure 4-2 Daily average pipe water pressure at Altona North.....	113
Figure 4-3 Soil and pipe temperature in Pit 1 at Altona North	115
Figure 4-4 Soil and pipe temperature in Pit 2 at Altona North	116
Figure 4-5 Soil and pipe temperature in Pit 3 at Altona North	116
Figure 4-6 Soil and pipe temperature in Pit 3 on roadside at Altona North.....	117
Figure 4-7 Soil and pipe temperature in Pit 1 at Fawkner	118
Figure 4-8 Soil and pipe temperature in Pit 2 at Fawkner	118
Figure 4-9 Soil and pipe temperature in Pit 3 at Fawkner	119

Figure 4-10 Soil and pipe temperature in Pit 2 on roadside at Fawkner	119
Figure 4-11 Soil volumetric moisture content, suction and daily rainfall in Pit 1 at Altona North..	122
Figure 4-12 Soil volumetric moisture content, suction and daily rainfall in Pit 2 at Altona North..	123
Figure 4-13 Soil volumetric moisture content, suction and daily rainfall in Pit 3 roadside at Altona North	124
Figure 4-14 Soil volumetric moisture content, suction and daily rainfall in Pit 1 at Fawkner.....	126
Figure 4-15 Soil volumetric moisture content, suction and daily rainfall in Pit 2 at Fawkner.....	126
Figure 4-16 Soil volumetric moisture content, suction and daily rainfall in Pit 3 at Fawkner.....	127
Figure 4-17 Soil volumetric moisture content, suction and daily rainfall in Pit 3 roadside at Fawkner	127
Figure 4-18 Soil volumetric moisture content, suction and daily rainfall in nature strip and under footpath at Fawkner	128
Figure 4-19 Soil pressure and volumetric moisture content versus time in Altona North	130
Figure 4-20 Locations of earth pressure cells in Fawkner	131
Figure 4-21 Soil pressure and volumetric moisture content versus time in Pit 2 of Fawkner	132
Figure 4-22 Soil pressure and volumetric moisture content versus time in Pit 2 of Fawkner	132
Figure 4-23 Soil displacement in Altona North	134
Figure 4-24 Schematic diagram of soil displacement gauge	136
Figure 4-25 Supplementary soil displacement in Fawkner	136
Figure 4-26 Location and labelling of strain gauges on water pipe	139
Figure 4-27 Location and labelling of strain gauges on gas pipe	140
Figure 4-28 Daily average longitudinal and hoop strains of water pipe in Altona North at each pit	141
Figure 4-29 Daily average longitudinal and hoop strains of gas pipe in Fawkner at each pit	142
Figure 4-30 Comparison of water pipe hoop stress.....	145
Figure 4-31 Flexural stress in vertical direction in Altona North	148

Figure 4-32 Flexural stress in horizontal direction in Altona North.....	150
Figure 4-33 Flexural stress in vertical direction in Fawkner.....	152
Figure 4-34 Behaviour of buried pipes in vertical direction due to changes in soil moisture content	154
Figure 4-35 Behaviour of buried pipes in horizontal direction due to changes in soil moisture content.....	155
Figure 5-1 503DR hydroprobe	159
Figure 5-2 Locations of monitoring sites on geological map of Victoria (after Douglas and Spencer- Jones 1993).....	167
Figure 5-3 Plasticity chart for classification of fine grained soils.....	169
Figure 5-4 Preparation of the access hole: (a) preparing an access hole with hand auger; (b) cross- section of soil augering.....	173
Figure 5-5 Installation of the access tube: (a) push the tube by hand; (b) drove the tube with a hammer.....	174
Figure 5-6 Installation of the protection box: (a) protection box installed above the tube; (b) cross- section of the tube and box after installation	175
Figure 5-7 Field calibration of neutron probe: (a) moisture measurement with neutron probe; (b) core samples collected on site	177
Figure 5-8 Corrected volumetric soil moisture content against neutron count ratio of the calibration sites: (a) Site 4 Oakleigh South; (b) Site 5 Doveton; (c) Site 7 Heidelberg West; (d) Site 9 Forest Hill; (e) Site 10 Bulleen; (f) Site 11 Avondale Heights; (g) Site 12 Deer Park	179
Figure 5-9 Combined data with linear regression line.....	181
Figure 5-10 Cleaned data with linear regression line	182
Figure 5-11 Volumetric soil moisture content in Site 1 Altona North: (a) 150 to 550 mm; (b) 550 to 1400 mm.....	184
Figure 5-12 Volumetric soil moisture content in Site 2 Fawkner: (a) 150 to 550 mm; (b) 550 to 1400 mm	184

Figure 5-13 Volumetric soil moisture content in Site 11 Avondale Heights: (a) 150 to 550 mm; (b) 550 to 1400 mm	185
Figure 5-14 Volumetric soil moisture content in Site 7 Heidelberg West: (a) 150 to 550 mm; (b) 550 to 1200 mm.....	186
Figure 5-15 Volumetric soil moisture content in Site 9 Forest Hill: (a) 150 to 550 mm; (b) 550 to 1400 mm.....	186
Figure 5-16 Volumetric soil moisture content in Site 10 Bulleen: (a) 150 to 550 mm; (b) 550 to 1400 mm	187
Figure 5-17 Volumetric soil moisture content in Site 3 Carrum: (a) 150 to 550 mm; (b) 550 to 1400 mm	188
Figure 5-18 Volumetric soil moisture content in Site 4 Oakleigh south: (a) 150 to 550 mm; (b) 550 to 1400 mm.....	188
Figure 5-19 Volumetric soil moisture content in Site 15 Keysborough: (a) 150 to 550 mm; (b) 550 to 1400 mm.....	189
Figure 5-20 Soil moisture variations of basaltic clay sites	194
Figure 5-21 Soil moisture variations of non-basaltic clay sites.....	195
Figure 5-22 Soil moisture variations of Quaternary alluvials and Tertiary sediments sites.....	195
Figure 6-1 SWCC test using filter papers: (a) soil specimen placed in the container with filter papers; (b) specimen container sealed with plastic wrap and lid	202
Figure 6-2 SWCCs of Altona North	204
Figure 6-3 SWCCs of Fawkner.....	204
Figure 6-4 Schematic diagram of AEP (Daniel 1989)	206
Figure 6-5 Field hydraulic conductivity test using AEP: (a) the stainless steel ring embedded in soil; (b) the ring sealed with top plate; (c) filling of permeameter; (d) measurement of hydraulic conductivity with a plastic cylinder	208
Figure 6-6 Constant head method with flow pumps (Lee 2004).....	210
Figure 6-7 Saturated hydraulic conductivity plot of Altona North	212

Figure 6-8 Saturated hydraulic conductivity plot of Fawkner	212
Figure 6-9 Hydraulic conductivity-suction functions of Altona North	214
Figure 6-10 Hydraulic conductivity-suction functions of Fawkner.....	214
Figure 6-11 KD2 Pro thermal properties analyser.....	216
Figure 6-12 Thermal conductivity functions of Altona North	216
Figure 6-13 Thermal conductivity functions of Fawkner	217
Figure 6-14 Volumetric heat capacity functions of Altona North.....	217
Figure 6-15 Volumetric heat capacity functions of Fawkner	218
Figure 6-16 Estimated LAI function for both sites	220
Figure 6-17 Estimated root depth function	221
Figure 6-18 Typical PML function for most types of vegetation	221
Figure 6-19 Initial soil profiles : (a) moisture content; (b) suction	224
Figure 6-20 Initial soil temperature profiles.....	224
Figure 6-21 Summary of the Vadose/W model of Altona North (SWCC in Figure 6-2 and k function in Figure 6-9)	227
Figure 6-22 Summary of the Vadose/W model of Fawkner North (SWCC in Figure 6-3 and k function in Figure 6-10)	228
Figure 6-23 Volumetric moisture content output: (a) Altona North at 300 mm; (b) Fawkner at 250 mm	230
Figure 6-24 Volumetric moisture content output: (a) Altona North at 800 mm; (b) Fawkner at 500 mm	231
Figure 6-25 Volumetric moisture content output: (a) Altona North at 1000 mm; (b) Fawkner at 1000 mm	232
Figure 6-26 Temperature output: (a) Altona North at 300 mm; (b) Fawkner at 250 mm.....	234
Figure 6-27 Temperature output: (a) Altona North at 800 mm; (b) Fawkner at 500 mm.....	235

Figure 6-28 Temperature output: (a) Altona North at 1000 mm; (b) Fawkner at 900 mm.....	236
Figure 6-29 Model prediction against neutron probe measurement: (a) Altona North; (b) Fawkner	238
Figure 6-30 Model prediction against thermocouple measurement: (a) Altona North; (b) Fawkner	239
Figure 7-1 Long term prediction of soil moisture content in Altona North	243
Figure 7-2 Long term prediction of soil moisture content in Altona North with random climate at 800 mm.....	245
Figure 7-3 Change in soil moisture content at soil depth of 800 mm.....	246
Figure 7-4 Idealised surface between void ratio, moisture content, and net stress (Gould 2011)....	249
Figure 7-5 Schematic diagram of attenuation of stress with depth (after Gould 2011)	252
Figure 7-6 Flowchart of pipe-soil interaction modelling procedure (after Gould 2011)	255
Figure 7-7 Schematic diagram of Winkler spring model.....	255
Figure 7-8 Plot of void ratio against moisture content	256
Figure 7-9 Simplified springs at all soil layers to the representative layer	260
Figure 7-10 Model prediction for pinned end support conditions.....	261
Figure 7-11 Model outputs of bending moment for fixed end support conditions	262
Figure 7-12 Pipe flexural stress with average support condition	264
Figure 7-13 Correlation between pipe strength and pipe failure probability	265
Figure 7-14 Correlation between graphitization depth to specimen thickness ratio and tensile strength (Gould <i>et al.</i> 2009)	267
Figure 7-15 Correlation between pipe strength and pipe age.....	267
Figure 7-16 Correlation between pipe age and failure probability.....	269

LIST OF TABLE

Table 2-1 Factors affecting pipe breakage rates (Kleiner and Rajani 2002)	16
Table 2-2 Identification criteria of soil reactivity based on plasticity index	24
Table 2-3 Classification of EI_{AZ} based on wPI (after Dye 2008).....	26
Table 2-4 Identification of soil reactivity based on soil swell.....	27
Table 2-5 Classification of Victorian soil reactivity (after Standard Australia 2011)	29
Table 2-6 Comparison of pipe failure prediction models	41
Table 3-1 Summary of Mechanical testing of cast iron pipes (after Gould <i>et al.</i> 2009).....	53
Table 3-2 Summary of Atterberg limits of the selected sites.....	59
Table 3-3 Properties of oedometer test specimens.....	63
Table 3-4 Summary of soil properties of the selected sites	64
Table 3-5 Summary of sensors and equipment	76
Table 5-1 Summary of soil properties of the monitoring sites	170
Table 5-2 Soil bulk density of the calibration sites	177
Table 5-3 Summary of the least-squares linear regression equations of the calibration sites	180
Table 5-4 Analysis of seasonal soil moisture content variations.....	190
Table 6- 6-1 AEP test results	209
Table 6-2 Laboratory hydraulic conductivity test results	211
Table 6-3 Summary of hydraulic conductivity of the field instrumentation sites.....	213
Table 7-1 Soil and pipe properties used in the pipe-soil interaction model.....	260
Table 7-2 Model outputs of maximum flexural stress.....	262
Table 7-3 Typical constants for exponential corrosion equation (Rajani <i>et al.</i> 2000)	266

CHAPTER 1

INTRODUCTION

1.1 Background

In cities worldwide, buried water and gas pipe networks form part of the critical infrastructure providing essential services to the community. However, in most developed countries this vital infrastructure was installed several decades ago, and dealing with frequent pipe failures has become a major problem. Failure of buried pipes can lead to the loss of water and gas services to communities and produce negative social and economic impacts (Chan 2008). Subsequent repairs may also affect water quality, interrupt traffic and business activities and consume already constrained infrastructure funding (Hu *et al.* 2008). Furthermore, the costs of replacing and rehabilitating existing pipe networks are increasing due to ageing of pipes, causing significant concern to pipe asset owners.

In 2009, Australian water utilities supplied urban water services to 18.3 billion users, with total urban water consumption of 1505 GL in the main cities of Australia. Current water pipe assets in Australia with over 80,000 km of pipe networks are estimated to be worth nearly A\$ 100 billion (WSAA 2010a). Based on current population trends increase in water usage in 2026 is expected to be 600 billion litres annually (WSAA 2010b). With the increase in water usage and the prospect of increasing maintenance costs, the sustainable management of pipe network has become a

challenging task. Over the last five years, annual capital investment by Australian water utilities has increased from A\$ 1.7 billion to A\$ 8.1 billion, where a significant proportion of this investment is related to maintaining and renewing existing pipe assets (CSIRO 2010). Similarly, Australian gas utilities are in a similar situation with the estimated replacement cost in 2011 for approximately 25,000 km of gas transmission pipe networks (APIA 2011a) exceeding A\$ 40 billion (APIA 2011b).

The global maintenance costs and economic lost due to pipe breaks and leakages are very high. In China, annual economical lost due to leaks and breaks of water service pipes in 612 cities are approximately US\$ 36 to 60 million (Zhang and Shao 2000). The Environmental Protection Agency in the United States of America estimated that an investment of US\$ 138 billion is required to rehabilitate and renew current water distribution system in the 20 years from 1997 to 2017 (Hertzler and Davies 1997). The gas industries in the United States, which operates approximately 60,000 miles of cast iron pipe networks, are also spending a considerable portion of their maintenance budgets on rehabilitation of pipes (Jeon *et al.* 2004). Water utilities in Canada are also concerned about the deterioration of ageing water mains and the estimated substantial financial costs for repair and replacement of the pipe networks (Rajani and Tesfamariam 2007).

In general, pipe fails when the applied stress exceeded the material strength. The performance of pipes and time of failure are closely related to the environmental and operational conditions. Australian and international researches on buried pipes (Kassiff and Zeitlen 1962; Rajani *et al.* 1996; Jarrett *et al.* 2001a; Ibrahim 2005) indicate that pipe failures mainly depend on stresses exerted on the pipe due to seasonal shrinkage and swelling of soils and thermal expansion and contraction of pipe materials. In order to address this problem, it is important to consider the pipe-soil-climate interaction in pipe asset management, failure prediction, and rehabilitation and failure mitigation strategies planning. Under current Australian climatic conditions, it has been clearly established that water and gas pipe failure rates rise markedly during hot and dry summers and to a lesser extent in relatively cold and wet winters (Ibrahim 2005; Chan *et al.* 2007). Analysis of Australian buried pipe data (Chan 2008; Gould and Kodikara 2008; Gould and Kodikara 2009) indicates that these effects are much more pronounced after a prolonged hot and dry period, highlighting the susceptibility of the existing pipe networks to local climatic change.

Current understanding on interaction between pipe-soil-climate is that seasonal variations of soil moisture content in the vicinity of the buried pipes is leading to soil shrinkage and swelling and consequential ground movement. The magnitude of the ground movement depends on the soil types. For example, soils that exhibit high shrink and swell behaviour (i.e., reactive clays) can be expected to experience significant movement between dry and wet seasons. Therefore, the knowledge of moisture variation within the soil close to the buried pipes is of substantial value in determining the stress on the pipe through the soil and climate interaction. The overall ground movement due to change in soil moisture content is uneven because of the variation of the soil profile, ground cover, presence of trees and vegetation, and the source of water such as irrigation or small pipe leaks. In residential areas, reticulation pipes buried in nature strips between driveways are subjected to differential ground movement due to variation in permeability between the concrete driveways and the nature strips. The change of soil moisture content beneath the concrete driveways will be less than that in the nature strips. Hence when the soil moisture content fluctuates, pipe sections buried in the nature strips will move up and down with respect to swelling and shrinkage of soils, while the pipe sections beneath the driveways stay at the same level. Differential movement of various sections along the pipe can induce tensile stress in the flexural direction of the pipe, and may ultimately lead to circumferential failure when those stresses exceed the tensile strength of the pipe material.

Study of pipe failure types in Victoria, Australia (Gould and Kodikara 2008) has shown that circumferential failures are the most common mode of failures in reticulation pipes, which accounted for up to 60 % of total reticulation pipe failures per 100 km per annum. Statistics of pipe failure modes vary from city to city, but on average 70 % of water pipe failures are circumferential and the other 30 % are either longitudinal breaks, blow outs, or hydrant and service connection leaks (Rajani *et al.* 1996). In addition, circumferential fractures were found to increase in periods of extreme weather conditions (Gould and Kodikara 2008; Gould and Kodikara 2009) suggesting that longitudinal pipe movement is the principal failure mechanism. Nevertheless, the actual mechanisms and parametric variations governing the pipe failure behaviour need to be established from field evidence. Furthermore, fluctuation of temperature may induce thermal stress in the pipes. Pipe

failures occur when these stress are increased to a magnitude that can break the pipes particularly when the pipe integrity may have already been compromised by other factors such as corrosion.

In spite of the importance of the effect of seasonal soil moisture variations on the performance of buried pipes, particularly in reactive soils, little work has been carried out to quantify this relationship and model the interaction. The determination of the precise relationship is quite difficult as other factors including the physical properties of pipe, the soil and the seasonal climate of the local area also play significant roles. As a result an Australian Research Council Linkage Project (known as the Pipe Linkage Project, LP0667936) was established to address this issue. The research study presented in this thesis is part of this ARC Linkage Project which focused on field measurement and monitoring of the buried pipes and soil behaviour with computer modelling of ground behaviour. Quantitative understanding and precise modelling of this interaction would enable engineers to improve the design, construction, maintenance and management of buried pipes in reactive soils.

1.2 Research Objectives

The board objective of this research is to understand the interaction of the behaviour of buried reticulation pipes and seasonal variation of soil moisture content in Melbourne, Australia. The specific research objectives were:

1. To understand the behaviour of in-service buried reticulation water and gas pipes by field instrumentation.
2. Study the variation in soil moisture content in regional Melbourne due to seasonal fluctuation of soil moisture and associated ground movement.
3. Examine the interaction between seasonal climate change and soil moisture content by analyse of field instrumentation data.

4. Develop a model for prediction of pipe performance due to seasonal change and in soil moisture content.

1.3 Research Approach

A summary of the research approach of this project is shown in Figure 1-1. Detailed procedures on field instrumentation, sample collection, laboratory testing and modelling are presented in the relevant chapters.

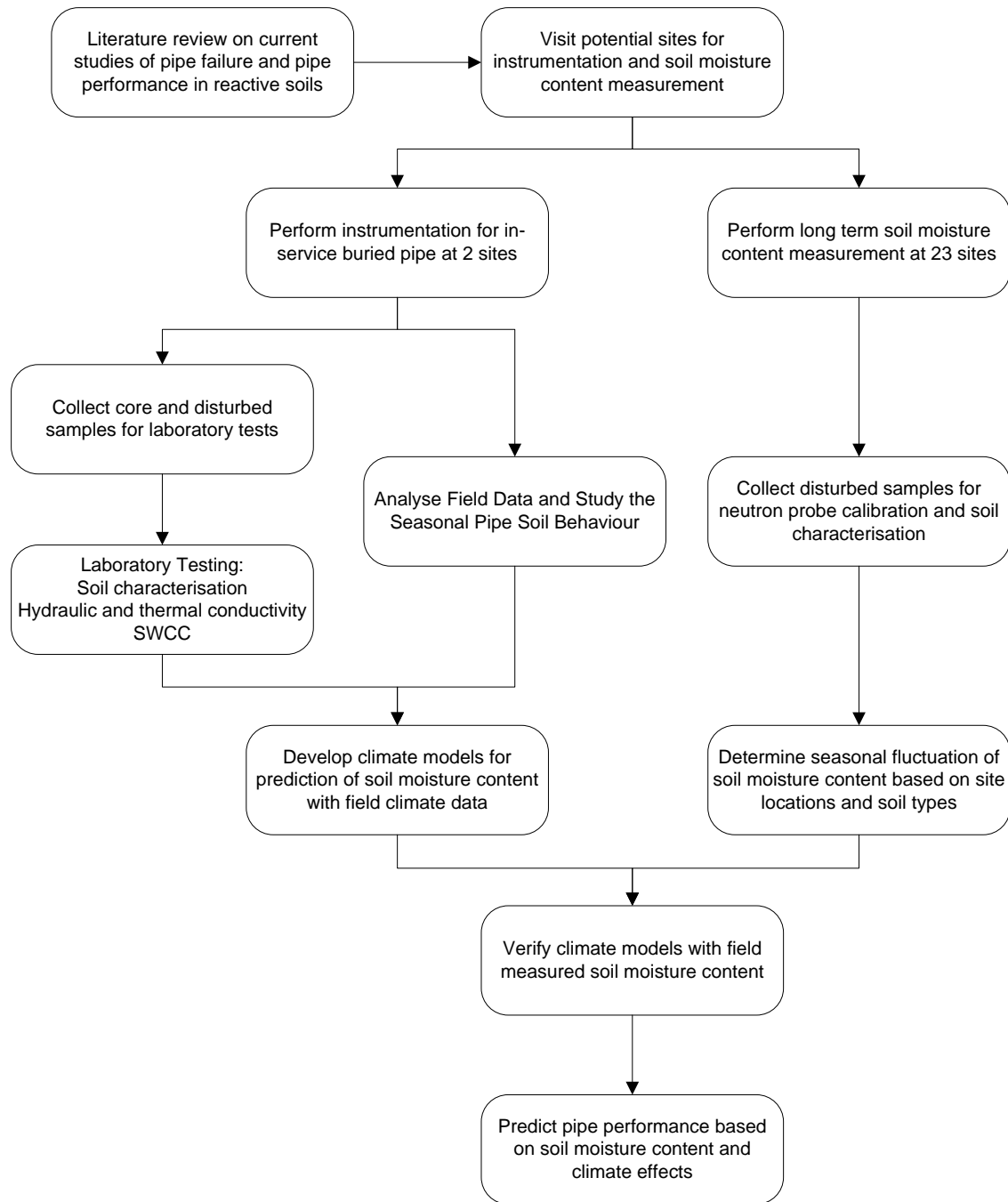


Figure 1-1 Flow chart of research approach

1.4 Thesis Structure

The thesis is organized into eight chapters. A brief description of each chapter is given below.

Chapter 1: Introduction

Chapter 1 provides an introduction on the main objectives of the project with background information and previous studies on buried pipe failure. The research approach is outlined in the chapter.

Chapter 2: Literature review

Chapter 2 reviews previous research into soils, seasonal climate change and behaviour of buried pipes. Studies of unsaturated soil properties and reactivity are described. A brief background history of the geophysical method for ground surveying is also discussed. The chapter ends with a review of pipe failure prediction models with the main features of major models summarised.

Chapter 3: Study of in-service buried pipes by field instrumentations

Chapter 3 provides an overview of the field instrumentation that was implemented to study the behaviour of in-service water and gas pipes buried in reactive clay soils. A preliminary investigation of field sites, forensic analysis of buried pipes and site selection criteria are described. The procedures of site selection, sensor calibration and installation, pipe instrumentation, and data collection are presented.

Chapter 4: Interaction of buried pipes with soils and climate

Chapter 4 discusses the analysis of data collected from the field instrumentations. The behaviour of buried pipes with interaction of soils and seasonal climatic change on site is discussed.

Chapter 5: Regional field measurement of soil moisture content

Chapter 5 discusses the detailed field study of soil moisture content using neutron probe measurements. Site selection criteria, field installation and the probe calibration process are described. Analysis of field data and seasonal fluctuation of soil moisture content amongst the monitoring sites are discussed with classification based on the geological formation and the properties of the soil on site.

Chapter 6: Ground-atmosphere interaction modelling for prediction of soil moisture content and temperature

Chapter 6 presents the soil and climate interaction modelling using the soil properties and climate data obtained from the field sites. The soil and climate parameters used as inputs to the models and the modelling approach are described. Outputs from the models are compared with the field measured data for validation of the developed models.

Chapter 7: Probability of pipe failures due to changes of soil moisture content over time

Chapter 7 describes the numerical model developed to estimate the probability of pipe failure according to the condition of the pipe material. The model was developed based on the interaction of pipes and soils with long-term soil moisture content data generated from the soil and climate interaction model presented in Chapter 6.

Chapter 8: Conclusions and Recommendations

Chapter 8 provides the conclusions of the research project and recommendations for future research.

CHAPTER 2

LITERATURE REVIEW

2.1 Introduction

This chapter reviews previous research and current state of knowledge on the behaviour of buried water and gas pipes in relation to soils and seasonal climate change. It begins with a review of the studies of interaction between soil, climate and buried pipes, and the factors that are reported to affect the performance of pipes. The identified factors which include properties of unsaturated soils, soil reactivity, soil moisture content and the methods of field measurements of such properties are then described. Consequently, field investigations of buried incorporating with the quantification of these factors are discussed. The chapter ends with a summary of the developed pipe failure prediction models based on the identified factors and their main features.

2.2 Performance of Buried Pipes

Performance of buried pipes in the field is affected by both physical and environmental properties, including climate, soil, and pipe variables. Typically, pipe fails when the environmental and operational conditions exert stresses that exceed their diminishing structural resiliency (Kleiner and

Rajani 2002). The operational conditions are related to the physical properties of the pipes, while the environmental conditions are governed by the seasonal climatic change and the geological properties of soils, especially the shrink and swell behaviours due to soil reactivity (Chan, 2008).

The physical and environmental conditions affecting buried pipes have not been fully understood. In previous studies (Kuraoka *et al.* 1996b; Rajani *et al.* 1996) theoretical models were developed to assess the pipe-soil interaction of buried pipes. However, these existing models considered only some of the influencing physical variables, and the influence of soils and climate were not properly taken into account. Fundamental studies (Morris 1967; Clark 1971; Rajani *et al.* 1996) on pipe asset data analysis revealed that pipe failures were related to seasonal climate change and soil properties, where higher pipe failure rates were recorded in months of extremely hot and cold seasons. In Australia, it was reported that a high number of pipe failures occurred in hot and dry summers (Kassiff and Holland, 1965; Ibrahimi, 2005; Chan, 2008; Gould *et al.*, 2009) when soil moisture content decreased. Previous studies on the interaction between soils, seasonal climate change and performance of buried pipes are reviewed in the following sections.

2.3 Interaction of Soil, Climate and Buried Pipe

Studies of buried water and gas pipe failure data can provide information on the pipe failure patterns and reveal factors that are affecting the behaviour of the pipes. In 1953, a study of pipe failure data of cast iron (CI) and asbestos cement (AC) water pipes was undertaken in the City of Winnipeg, Canada (Baracos *et al.* 1955). The analysis results showed a definite cyclic pattern in monthly circumferential failure with two peaks occurred in January and September. A comparison of circumferential failure with monthly temperature, precipitation and depth of snow cover reviews a close correlation with seasonal climatic change. The reactive behaviour of clay soils in Winnipeg was believed to be the cause of this phenomenon.

The studies of Morris (1967) and Clark (1971) on the performance of water pipes indicated that failure was influenced by seasonal climatic variation and volume change of clay soils. Another study of water pipe failures in the City of Winnipeg (Rajani *et al.* 1996) also showed that pipe failure is

influenced by the seasonal climates. Figure 2-1 shows the typical annual pipe failure pattern. The pipe failure rates peak at months when the ground temperature was below normal. Similar studies (Needham and Howe 1981; Lochbaum 1993) were conducted on gas pipes and essentially draw similar conclusions.

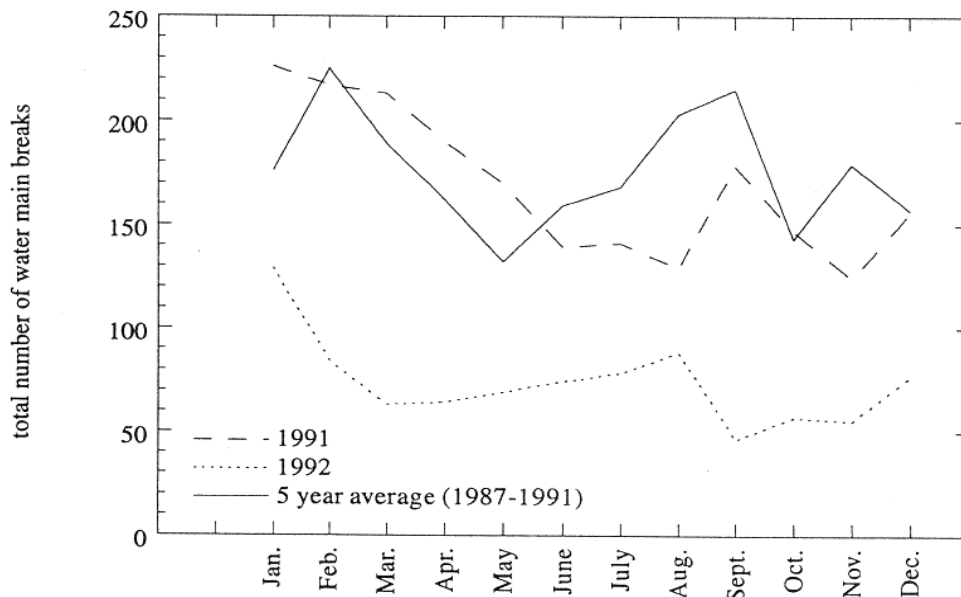


Figure 2-1 Monthly variation of water pipe failures in Winnipeg, Manitoba (Rajani *et al.* 1996)

Analysis of pipe failure data during the period of 1952 to 1982 from four water authorities in UK (Mordak and Wheeler 1988) with large number of AC pipes, indicated that pipe failure rates increased significantly for pipes laid in aggressive environments, such as reactive clay. It was also identified that most of the failures in clay soil areas occurred during the dry summer months and years with long dry periods, while distribution of failures in sandy soils and gravel is fairly random. Furthermore, over 60% of pipe failures occurred at the months when soil moisture deficit was at maximum. The pipe failure patterns were attributed to shrinkage of clays, which causes extra loading

on the buried pipes. High incidences of circumferential failures were also found to be associated with smaller diameter pipes, and the failure rates of these pipes showed a linear relationship with pipe age.

Kassiff and Zeitlen (1962) reported that the correlation between buried pipe failure and ground movement due to expansive nature of clay. It was found that high stresses produced by swelling of reactive clays may damage pipelines by introducing cracks and ruptures at longitudinal and circumferential directions. Kassiff and Holland (1965; 1966) have studied the behaviour of pipes buried in reactive clay in Victoria, Australia. It was found that high intensity of pipe failures resulting from excessive longitudinal tensile stresses occurred within the areas of reactive clay as well as relatively low annual rainfall. Pipe failures were mostly occurred in summer or early autumn months in Victoria, when rainfall was generally at minimum while evaporation and temperature were at maximum as shown in Figure 2-2. In Victoria, the effect of shrinkage phenomena on pipes is more severe than swelling, and the reactive properties of the clay would cause differential longitudinal bending action on the pipes.

Association between plasticity index and failure density was observed by Hudak et al. (1998) on a study of CI and PVC pipes failure in an area having soils with moderate to very high shrink and swell potential in Texas, US. It was found that the highest density of pipe failures occurred in area of highest plasticity indices, suggesting that reactive soils play an important role in rupturing water pipes. Pipe failures were reported to be more common in small diameter pipes of 150 or 200 mm. In the extreme dry periods of months which had below average rainfall, an above average number of pipe failures were observed signifying the effect of soil shrinkage on premature pipe failure. Similar behaviour was observed in UK (Newport 1981) where failure of water pipes peaked soon after very hot and dry summers.

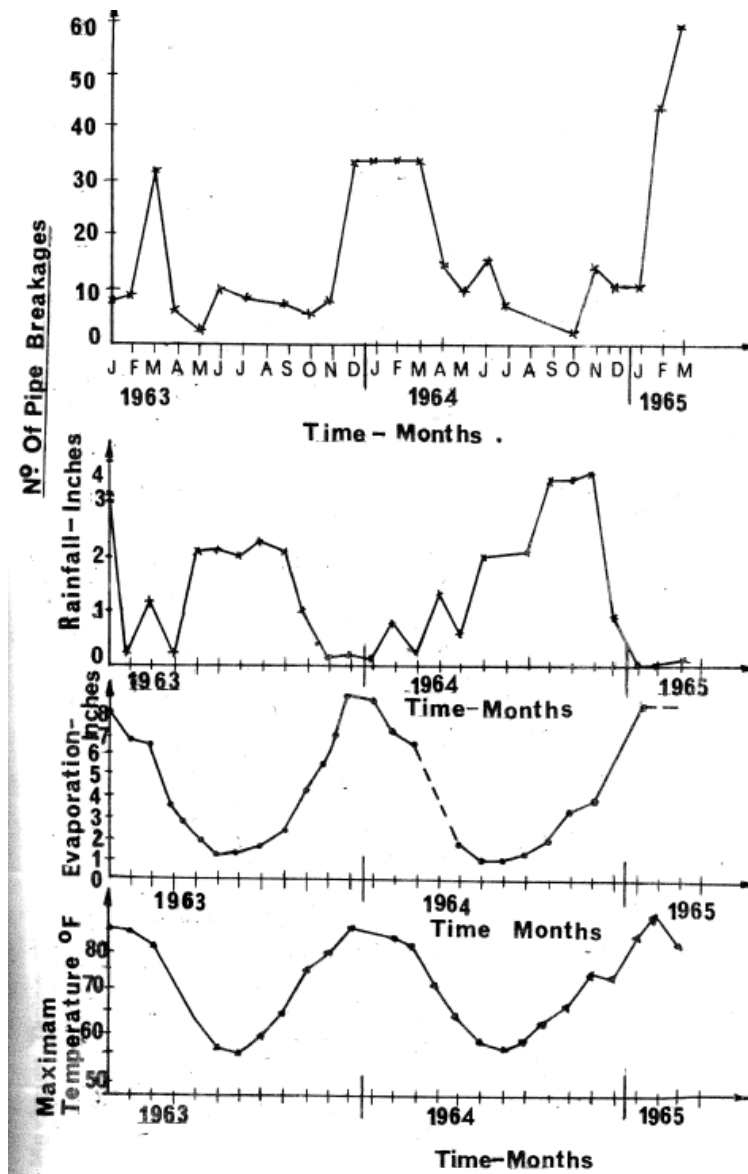


Figure 2-2 Correlation of pipe breakage, rainfall, evaporation and temperature in Horsham, Victoria (Kassiff and Holland, 1965)

The analysis of failure data of AC water pipes in the City of Regina, Canada from 1980 to 2004 (Hu and Hubble 2007) suggested that differential soil movement due to soil shrinkage is the primary cause of high incidence of circumferential failures and large proportion of failures on small diameter

pipes. Soils in the study area were reported as reactive clays with high shrink and swell potential. It was found that most of the annual failure rates corresponded to the highest rainfall deficit and freezing indices, while the highest annual failure rates corresponded to the year with the highest rainfall deficit. A further study (Hu *et al.* 2008) of the annual AC pipe failure rates indicated that from 1995 to 2004 the average failure rate at the City of Regina was 0.27 breaks/year/km, more than double the annual pipe failure rates of 0.13 breaks/year/km for the period of 1985 to 1994. Figure 2-3 illustrates the AC failure rates from 1980 to 2004. The study identified that different factors including pipe age, pipe diameter, climate, soil type, water quality, construction method and pipe maintenance method had contributed to the failure of pipes. Climates and local soil conditions were also identified to be critical factors contributing to the failures. The reactive montmorillonite type clay soils in the area were reported to undergo significant swelling and shrinkage due to seasonal moisture change. Development of stress caused by differential soil movement due to change in soil volume was found to be the main failure mechanism of buried AC pipes.

A study of water pipe failure data in Victoria, Australia from 1993 to 2005 (Ibrahimi 2005) also shows similar behaviour as in the US, UK and Canada. High numbers of pipes and other infrastructure breaks have occurred in dry and hot summers. Figure 2-4 shows the comparison of net evaporation and water pipe failures. Net evaporation is inversely related to soil moisture content, which is an indication similar to the rainfall deficit. The soil moisture content decreases as net evaporation increases and vice versa. The number of water pipe failures fluctuates with the change of net evaporation and peaks at extremely dry weather. Similar results have been obtained by Chan (2008) for the study of water and gas pipe failures in the period of 1996 to 2003. Higher pipe failure rates during summer have been attributed to dry weather, while higher pipe failure rates were recorded in reactive soils than non-reactive soils. Studies on the failure of water and gas pipes in Victoria, Australia (Gould and Kodikara 2008; 2009) for the year of 1996 to 2006 drew the same conclusion that pipe failure rates increase with net evaporation. Higher failure rates were observed for pipes which are older in age, with longer length in-service, buried in reactive soils, and with diameters of 100 to 150 mm. Furthermore, the study revealed that the rate of circumferential fractures increased with the increase in net evaporation suggesting that longitudinal bending of pipes could be the predominant failure mechanism related to drying of soils.

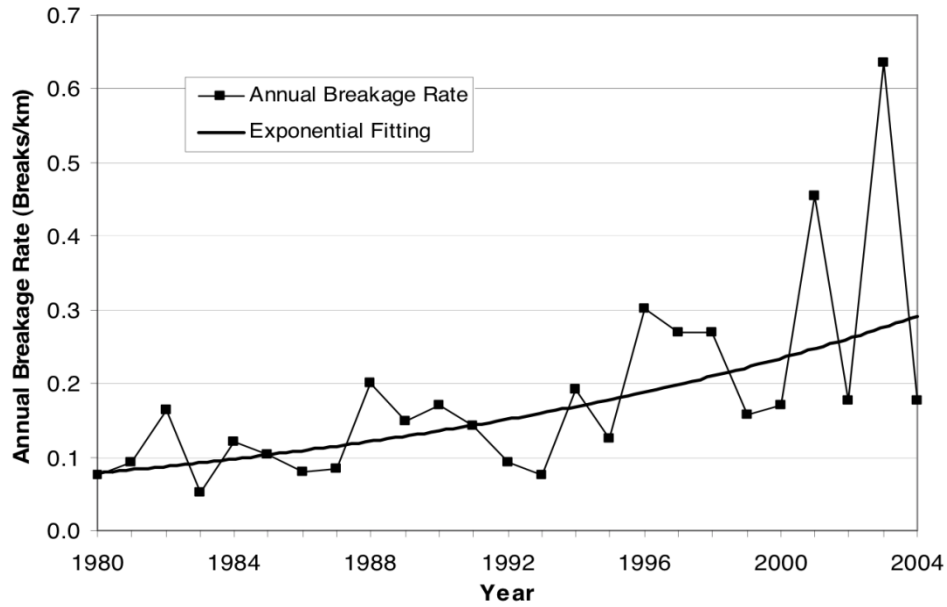


Figure 2-3 Annual break rates of AC water pipes in City of Regina, Canada (Hu *et al.* 2008)

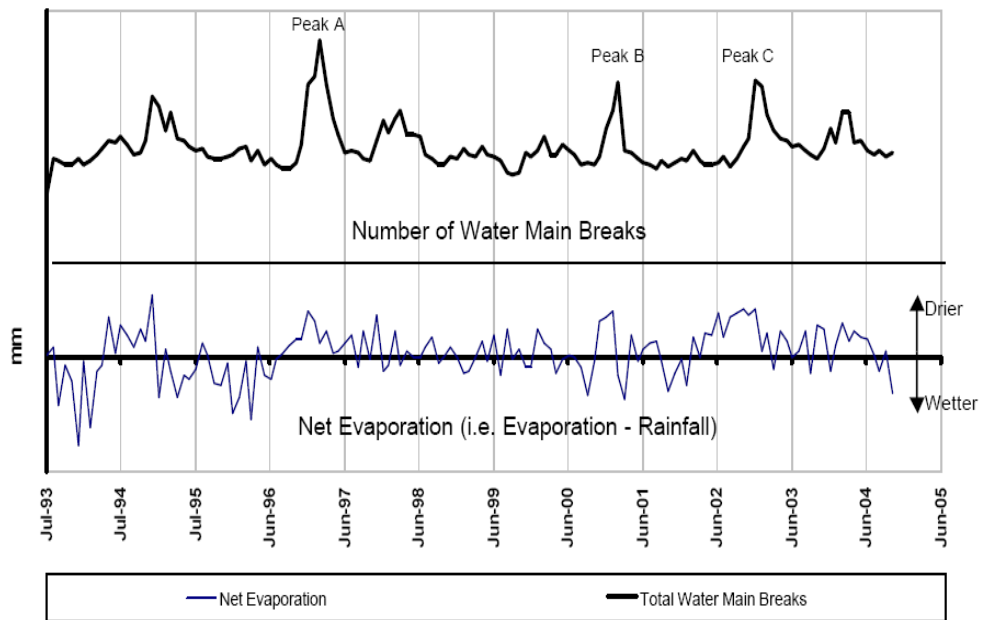


Figure 2-4 Water pipe failures and corresponding net evaporation trend (Ibrahimi 2005)

There are several more studies (O'Day 1982; Walski and Pelliccia 1982; Bahmanyar and Edil 1983; Kettler and Goulter 1985; Goulter and Kazemi 1988; Karaa and Marks 1990; Habibian 1994) on determining the cause of pipe failures by identifying a correlation between pipe failures and influential factors such as age of pipes, soil corrosivity, pipe diameter, temperature, water pressure, and external loads. All of these studies reveal that multiple factors have, in certain extent, contributed to the failure of buried pipes. These factors can generally be identified as environmental and operational conditions, some of which are static while others vary with time. Table 2-1 illustrates the main factors affecting pipe failures, where the factors related to the pipe properties and installation process are static, while factors relating to the environmental and surrounding area of the pipes are dynamic. Soil being a static factor is exception, the properties of soil, e.g., temperature, moisture content, and electrical resistivity, vary over time (Kleiner and Rajani 2002).

Table 2-1 Factors affecting pipe breakage rates (Kleiner and Rajani 2002)

Static	Dynamic	Operational
material	age	replacement rates
diameter	temperatures (soil, water)	cathodic protection
wall thickness	soil moisture	water pressure
soil (backfill) characteristics	soil electrical resistivity	
installation	bedding condition	
	dynamic loadings	

The studies of buried pipe failure data drew similar conclusions that higher rate of pipe failures occur for pipes buried in reactive clay during extreme meteorological conditions. In some cases, longitudinal stress induced by differential soil movement are believed to be of such magnitude that could cause failure of pipes whose integrity may have already been compromised by other factors, such as chemical attack from the inside water and outside soils (Hu and Vu 2011). Consequently, circumferential fractures were found to increase at period of high rainfall deficit in hot summer suggesting that longitudinal pipe movement due to drying of soils is the principle failure mechanism.

2.4 Behaviour of Unsaturated Soils

2.4.1 The vadose zone

As previously discussed, seasonal variation of soil moisture content is identified as one of the major factors related to the failure of buried pipes. Swelling and shrinkage of soils due to seasonal change of moisture content primarily occurred in unsaturated soils located in the region above water table, which is known as the vadose zone. In Melbourne region in Australia, the vadose zone is considered to extended 1.5 to 2 m below the ground surface, where most of the reticulation pipes are buried.

Inside the vadose zone, negative pore water pressure is acting in the soil, which is considered to be in a three phases medium consisting of air, water and solid, while the soil below the water table is fully saturated with positive water pressure. In general, there are three regions in the vadose zone: the 'capillary fringe'; the 'two fluid phases' and the 'dry soil' regions as shown in Figure 2-5. The region of 'capillary fringe' locates immediately above the water table where the degree of saturation approaches 100%, it is assumed to have a continuous water phase and discontinuous air phase (Fredlund 1996). Above the capillary fringe, soils could be unsaturated due to increase in suction, being the 'two fluid phases' of water and air. The degree of saturation in this region may vary from 20 to 90 % with both water and air phases are continuous. The 'dry soil' region is located at the top of vadose zone, as soils becomes dryer close to the surface; the water phase become discontinuous with air filling most of the voids, although the soil can be wetted during rainfall events.

The location of water table in the ground is basically influenced by the seasonal climate conditions. The water table will be located relatively closer to the ground surface in humid regions than in arid regions as well as in wet or dry seasons. Physical climate processes such as precipitation, evaporation and transpiration are driven by the energy of the sun and can also affect the location of the ground water table. A typical moisture profile in the ground is shown in Figure 2-6 where the pore water pressure in vadose zone is negative due to soil suction. In the event of precipitation, water will infiltrate the soil and suction will be reduced while soil moisture content is increased. Otherwise evaporation of water predominantly due to the sun's energy will dry the soil with time and lead to

increase in suction. Since soil moisture content and ground water table is greatly affected by the climate conditions, seasonal fluctuation of soil suction and moisture content will then occur in the vadose zone. Soil moisture content will generally be higher in wet then in dry season with possible rise of water table, however increase of moisture content at greater depth can be delayed depending on the hydraulic conductivity of soils. This delay could vary from few weeks to months for stiff clay (Chan *et al.* 2010a; Chan *et al.* 2010b). Conversely, below the vadose zone pore water pressure can be assumed to be in equilibrium state and will not be affected by the climate conditions.

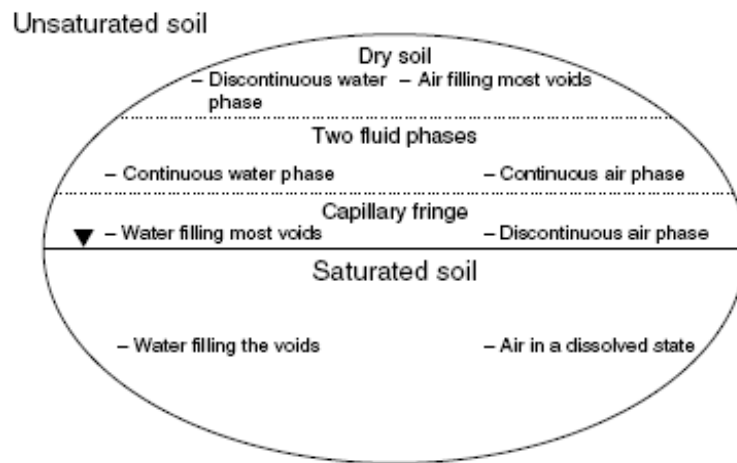


Figure 2-5 Schematic diagram of saturated and unsaturated soil mechanics (Fredlund 1996)

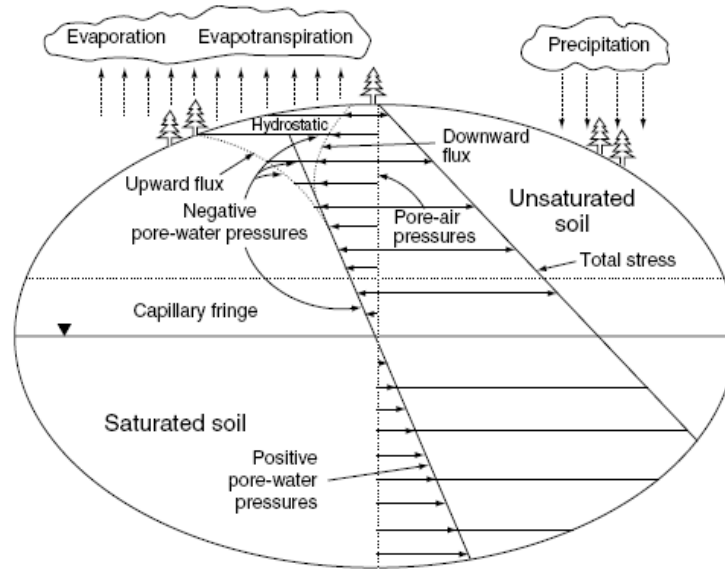


Figure 2-6 Schematic diagram of soil moisture profile (Fredlund 1996)

2.4.2 Soil moisture content and suction

Soil stress is developed in the ground according to the pore water pressure and the depth of the soil. There are generally three possible combination of independent stress as shown in Figure 2-7, the net normal stress ($\sigma - u_a$); the matric suction ($u_a - u_w$); and the effective stress ($\sigma - u_w$), where σ is total normal stress, u_w is pore water pressure and u_a is pore air pressure (Rowe 2001).

Total suction, ψ_t in soils is comprised of matric suction, ($u_a - u_w$) and osmotic suction, π therefore:

$$\psi_t = (u_a - u_w) + \pi \quad \text{Equation 2-1}$$

Total suction is commonly referred to as the free energy state of soil water and can be measured in terms of its partial vapour pressure (Edlefsen and Anderson 1943). It is closely related to the surrounding environment and generally caused by the change of relative humidity in the soil, e.g., presence of curved water surface due to capillary pressure deficit (Fredlund and Rahardjo 1993). Osmotic suction is related to the salt content in pore water of soils, where the relative humidity in a

pore can be reduced due to presence of dissolved salts. Matric suction, as previous noted, is related to the pore water pressure of the soil and can be greatly affected by the surrounding environment and climate conditions. It is known to vary with time due to environmental changes, where stability of the soil can be affected by reduction of matric suction in a heavy rainfall event (Rowe 2001). In general, it is safe to assume that the total suction is mainly governed by matric suction since the change in osmotic suction is relatively less significant. Nevertheless, significant change in osmotic suction can occur in saline soils or marine conditions due to presence of salts, and the total suction of soils needs to be calculated carefully. Since total suction is mainly governed by matric suction, which is affected by surrounding environment and climates, it is important to understand the relationship between moisture content and suction in order to understand the behaviour of unsaturated soils.

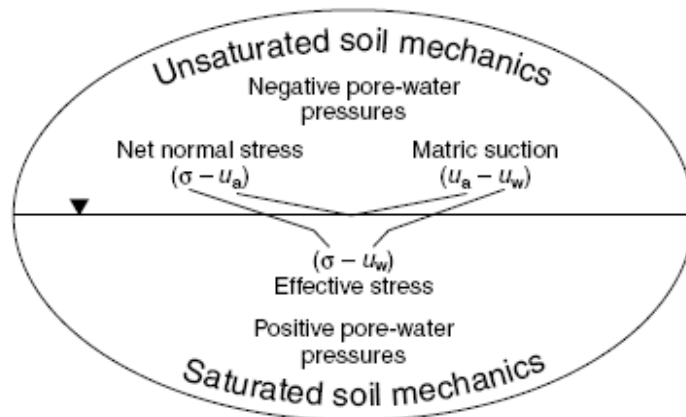


Figure 2-7 Schematic diagram of generalised soil mechanics (Fredlund 1996)

Soil moisture content is commonly quantified in terms of volumetric moisture content but can also be expressed as gravimetric moisture content and degree of saturation. The plot of soil moisture content as a function of suction is known as the soil water characteristics curve (SWCC). The curve describes the capability of the soil to store water under change in suction (GEO-SLOPE International 2010). Both total suction and matric suction can be used in the plot, however as noted

previously total suction can be considered to be equivalent to matric suction at high suction range. The SWCC is usually plotted in log scale due to great range of suction that can be experienced by the soil in the field, especially in the vadose zone.

Figure 2-8 shows the typical SWCC of different types of soils. Shrinkage and swelling behaviour of soils are related to the soil types and SWCC. Clay soils tend to be more reactive than silty and sandy soils due to the fine particles and clay minerals which result in higher saturated moisture content and suction range. As a result, small change in suction due to evaporation or precipitation can result in great change in volumetric moisture content and subsequent change in volume.

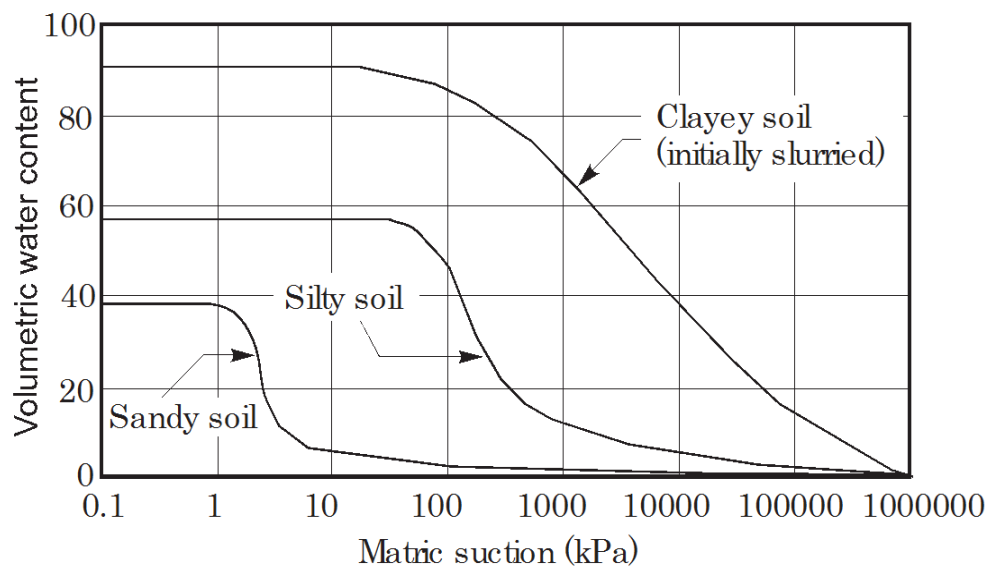


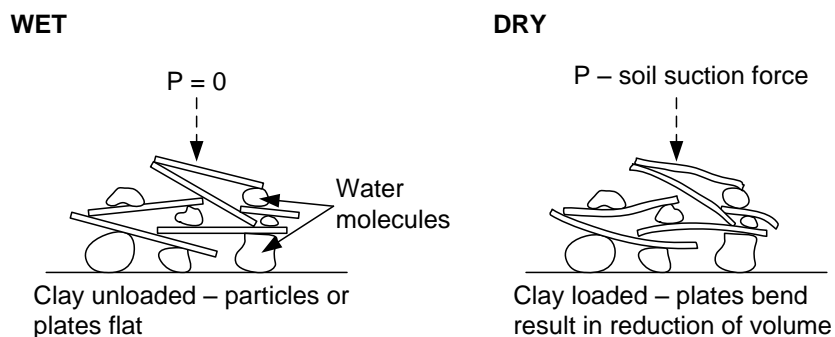
Figure 2-8 Typical SWCC for different soil types (Fredlund and Xing 1994)

2.4.3 Soil reactivity

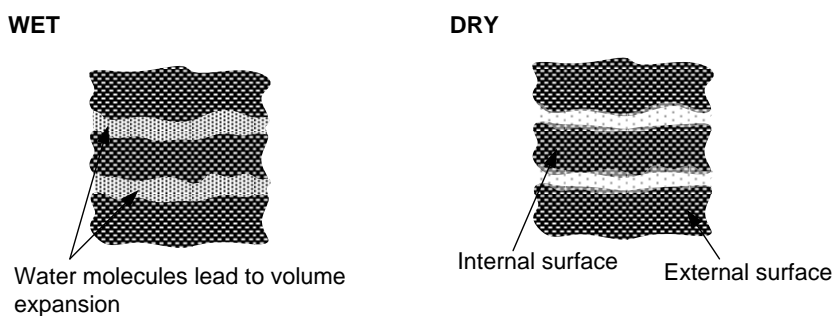
Reactive soils are reported as a main reason for failure of buried infrastructure including pavement, foundations, shallow buried underground structures and pipes (Kassiff and Zeitlen 1962; Seed *et al.* 1962a; Mordak and Wheeler 1988; Cameron 1989; Seddon 1992; Chan 2008; Clayton *et al.* 2010; Hu *et al.* 2010). In geomechanics, soil reactivity is referred to the soil behaviour where the volume of soils changes due to variation of moisture content. Soils that exhibit significant shrink and swell behaviour due to moisture change are referred to as reactive soils. Generally in extensive flat ground condition swelling and shrinking of soils will occur as vertical ground heaving in wet condition and settlement and cracking in dry condition.

The reactivity of soils is a function of the shrink / swell potential and the climate the soil is placed on. There are four components relevant to the determination of soil reactivity, which are mineral composition, particle size, chemical composition and soil profile (Cameron and Walsh 1984). Apart from these factors, the surrounding environment including trees, the level of water table, buildings and foundations constructed on the site, and most importantly the atmospheric climate close to the ground surface can also affect the reactivity of soils (Chan, 2008).

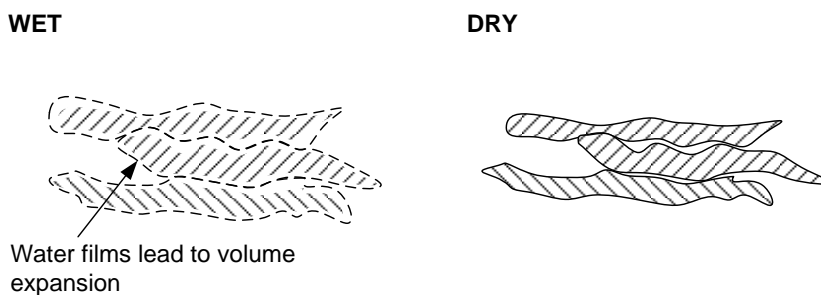
The mechanism of reactive soils was suggested by several researchers (Terzaghi 1931; Ladd 1960; Seed *et al.* 1962a; Ring 1965; Kassiff and Holland 1966) as two components, the mechanical component and the physiochemical component. Terzaghi (1931) described the mechanical component as release of bending forces (from water tension) within the platy clay minerals due to unloading or exposure to free water, which result in volume expansion of soil (Figure 2-9 (a)). When soil is drying, the absorbed water is released and the clay minerals are held in place by the original bending force, consequently decrease of soil volume occurred. The physiochemical component consider swelling of soil volume as a result of negative charged clay minerals attracting water molecules to the internal and external surface (Figure 2-9 (b) and (c)). The interlayer expansion is controlled by the bond forces developed between adjacent minerals, where the smaller the force the greater the quantity of water that can enter between the minerals and so the larger the volume expansion (Kassiff and Holland 1966). External layer expansion is the increase in volume due to absorption of water molecules between individual clay particles (Barshad 1955).



(a) Bending of flat particles (Mechanical)



(b) Interlayer expansion (Physicochemical)



(c) External layer expansion (Physicochemical)

Figure 2-9 Postulated mechanism of soil volume change: (a) Bending of flat particles; (b) Interlayer expansion; (c) External layer expansion (after Ring 1965)

Potentially reactive soils, i.e., clayey soils, are composed of a mineralogical structure of extremely small crystalline particles of the clay minerals. Common types of clay minerals are; allophane,

halloysite, kaolinite, illite and montmorillonite. A common feature among these minerals is the presence of platy surfaces which consist two sheets of closely packed oxygen or hydroxyls with aluminium, iron or magnesium atoms organised into an octahedral network. And a silica tetrahedron arranged to form a hexagonal network with all the apexes pointing in one direction and the bases in a common plane (Barshad 1955; Grim 1962). The montmorillonitic and micaceous minerals consist of the oxygen ions surfaces, while kaolinitic and chloritic minerals consist of both oxygen and hydroxyl ions surfaces. Change in soil volume due to interlayer expansion can be identified and measured only by x-ray analysis, while external layer expansion can be determined from the measurement of total increase in volume of the clay body or clay bearing material with apparatuses designed for these purposes (Keen and Raczkowski 1921; Winterkorn and Bayer 1934). Nevertheless, all methods of clay mineral identification are generally inaccurate, resulting in the estimation to about the nearest 5 % to 10 % only (Kassiff and Holland 1966).

Various laboratory tests can be used as an indication of soil reactivity, e.g., the linear shrinkage test, shrinkage limits test, plasticity index, and free swell test. These tests can be performed in the laboratory without too much difficulty. Several researchers (Holtz and Gibbs 1956; Seed *et al.* 1962b) have described identification criteria for soil reactivity on the basis of plasticity index (PI). Since soil reactivity is generally based on the quantity of water that the soil can imbibe; the higher the PI, the greater the quantity of water that can be imbibed by the soil and hence the greater will be its swelling potential (Rao 2006). Ladd and Lambe (1961) also consider PI as the best indicator of soil reactivity, and have related it to vertical expansion of soils. Table 2-2 shows a summary of identification of soil reactivity based on PI. Large differences can be observed in the PI values presented by various researchers; in particular the results of Seed *et al.* (1962) were based on artificially produced clays and produced higher reactivity at low PI values. Therefore the identification of reactivity with PI must be done with caution as the criteria may imply some uncertainties.

Table 2-2 Identification criteria of soil reactivity based on plasticity index

Reactivity	Holtz and Gibbs (1956)	Ladd and Lambe (1961)	Seed <i>et al.</i> (1962)
Low	PI < 18	PI < 20	PI < 10
Medium	15 ≤ PI ≤ 28	20 ≤ PI ≤ 40	10 ≤ PI ≤ 20
High	25 ≤ PI ≤ 41	40 < PI ≤ 50	20 < PI ≤ 35
Very high	PI > 41	PI > 40	PI > 35

It is important to note that the percentage of reactive minerals or clay particles within a soil plays a significant role for soil reactivity. For example, if the percentage of clay size particles is very low, then the overall soil may not be reactive even if the clay within the soil is highly reactive. This aspect is taken into account by taking weighted plasticity index (wPI), which gives the product of clay-size fraction (percentage of soil particle passing a US Number 200 sieve) and PI (Zapata 1999). A classification system was first presented by Zapata *et al.* (2006) using wPI as the parameter for designating soil reactivity correlated with the expansion index (EI_{AZ}) or Arizona swell potential to quantify soil response to wetting. EI_{AZ} were obtained by performing a swell test according to ASTM D 4829 method (ASTM International 2011) on soil specimens of 25.4 cm height and 61 cm diameter with confined pressure of about 5 kPa. The observed one-dimensional swell is divided by the initial specimen height and expressed as a percentage (Zapata *et al.* 2006). The linear correlation is continued by Dye (2008) with extra data as follow:

$$EI_{AZ} = 0.2655wH + 0.5 \quad \text{Equation 2-2}$$

with R^2 of 0.57 as shown in Figure 2-10. The potential classification shown in Table 2-3 has developed based on this linear correlation.

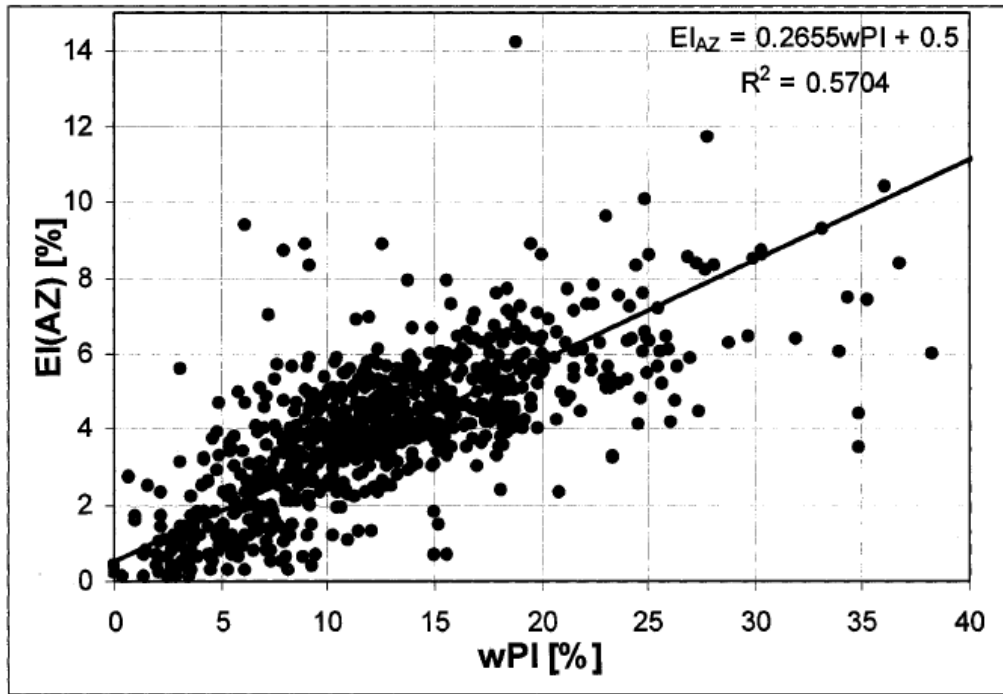


Figure 2-10 Modified correlation between EI_{AZ} and wPI (Dye 2008)

Table 2-3 Classification of EI_{AZ} based on wPI (after Dye 2008)

Reactivity	wPI	EI_{AZ}
Low	< 5.65	< 2.00
Medium	5.70 – 16.95	2.01 – 5.00
Moderate	17 – 35.8	5.01 – 10.00
High	>35.85	> 10.01

The free swell testing method performed using oedometer can also be considered as an indication of soil reactivity, where soils with higher swelling potential will tend to be highly reactive. In spite of this, the oedometer test is not applicable to highly dispersible soils, because of the relatively long period of time required for colloids to settle. Table 2-4 illustrates the results of oedometer tests undertaken by Holtz and Gibbs (1956) and Seed *et al.* (1962). These results were obtained by undertaking a series of oedometer free swelling tests with inundated reactive soil samples. Holtz and Gibbs (1956) obtained the results from undisturbed soil specimens, while Seed *et al.* (1962) conducted the tests on remoulded specimens compacted at maximum dry density and optimum moisture content. These results can be used as a guide to identify the reactivity of soils.

Table 2-4 Identification of soil reactivity based on soil swell

Reactivity	Swell (%)	
	Holtz and Gibbs (1956)	Seed <i>et al.</i> (1962)
Low	0 – 10	0 – 1.5
Medium	10 – 20	1.5 – 5
High	20 – 35	5 – 25
Very high	> 35	> 25

The Australian Standard AS2870 (Standards Australia 2011) provides a relatively simple classification system on soil reactivity. Since the reactivity of soil is a function of the shrink / swell potential and the climates the soil are placed on, the AS classification system for site reactivity in Victoria is based on the known Geological profile, the soil types and the climate zones. This classification system is primarily used for design of residential slab and footing, but can be adopted for general classification of the soil reactivity of a site. Reactivity of a particular site can be classified on the basis of the soil profile as shown in Table 2-5 and the climatic zones (Trewin and Jones 2004) as shown in Figure 2-11. Extremely reactive soils in Victoria are mainly comprised of volcanic residual clays and

limestone clays. The volcanic clays consist of Newer and Older Volcanics, and limestone clays belong to the Shepparton Formation (Birch 2003). The Newer Volcanic and Shepparton Formation are primarily situated in the Western region of Victoria, while Older Volcanics and some of the Newer Volcanics are both situated in the surrounding area of Melbourne. These extremely reactive soils are predominantly located within climatic zones 3 and 4.

The climatic zones in Figure 2-11 showed the climate of Victoria ranged from alpine wet coastal climate to semi-arid climate. A comparison of soil profile with the climatic zone reveals that the reactivity of the same soil type can vary from 'Moderate' to 'Extreme' depending on the climate. The reactivity of soils is directly related to the local climate, where reactivity is lower in wet climates and greater in dry climates. It can be expected that shrinking and cracking will be the dominant mechanism of the extremely reactive soils that are primary located in the zones of dry climates.

The identification and classification of soil reactivity are generally based on simple soil tests that can be conducted in the laboratory and classification system which can be performed with basic information of a site. Soil information can also be obtained on the basis of the visual appearance and the cracks or ground heave on site. Nevertheless, these methods are only indicative and by no means absolute for all expansive soils. It is necessary to conduct a few or all of these methods in order to classify a particular soil sample.

Table 2-5 Classification of Victorian soil reactivity (after Standard Australia 2011)

Soil Profiles	Climatic zone			
	1	2	3	4 and 5
Clays derived from limestone's, marls, and other calcium-rich sediments	Moderate to High	Moderate to High	Moderate to Extreme	Moderate to Extreme
Clays derived from alkaline volcanics or sedimentary rocks with interbedded alkaline volcanics or pryoclastics	Moderate to High	Moderate to High	Moderate to High	Moderate to Extreme
Non-basaltic and non-calcareous residual clays derived from sedimentary, metamorphic, granitic or other acid volcanic rocks	Moderate	Moderate to High	Moderate to High	Moderate to High
Alluvial, glacial and estuarine soils silts, sands or gravels which overlie deep clays.	Non-reactive to moderate	Slightly to High	Slightly to High	Moderate to Extreme
Interbedded silts, sands, and clay mixtures.	Slightly	Slightly to Moderate	Slightly to Moderate	Moderate to Extreme

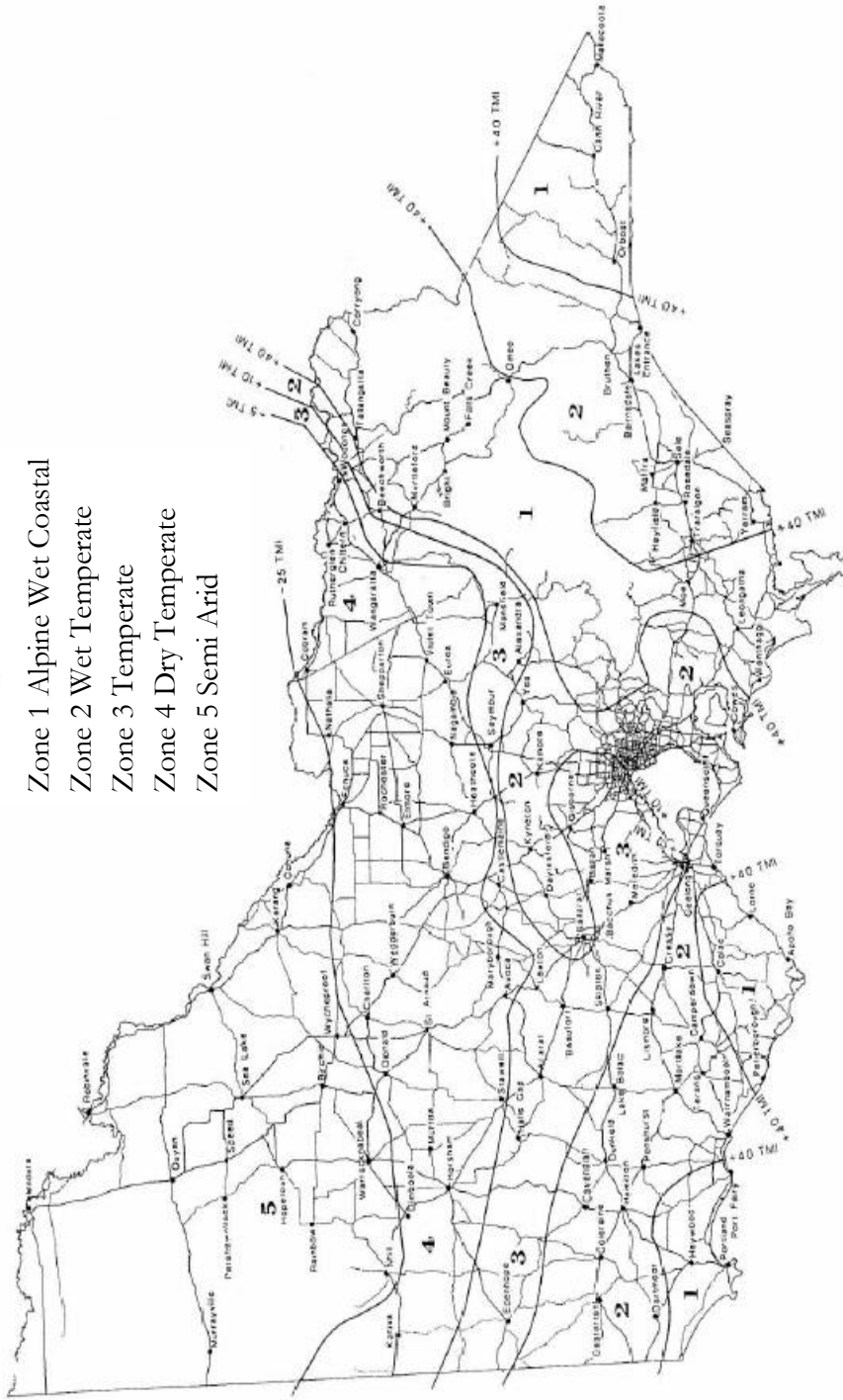


Figure 2-11 Climatic zones of Victoria (Standards Australia 2011)

2.5 Field Studies of Buried Pipe Behaviour

The study of pipe failure mechanisms and influence of different factors on buried pipes can be undertaken by monitoring the working environment, corresponding response of pipes buried in reactive soils condition, and measurement of the soil properties in the vicinity. These studies can be performed by burying instrumented pipe sections in the field, where in some cases these instrumented sections were used to replace in-service pipes. Strain gauges and thermocouples are common types of instrumentation on pipes, while soil displacement, pressure and moisture content surrounding the pipes were usually monitored.

Baracos et al. (1955) reported the field tests in City of Winnipeg, Canada, involving CI and AC pipes laid in 1953. The test pipes installed with waterproofing strain gauges were used as replacement of old water pipes or installed at new residential development areas. Vertical movement of instrumented pipes was measured by rods attached to the pipe top then extended to the ground surface through sleeves. Soils and water temperature of the site was measured by thermocouples placed in a temperature well. Results of the study showed that amount of pipe movement were related to backfilling and, swelling and shrinking of soils. The pipes were subjected to axial and flexural stresses; pipe bending has taken place in both vertical and horizontal directions. It was reported that differential soil movement due to seasonal changes in soil moisture could be the main cause of pipe failures.

Kassiff and Zeitlen (1962) has performed a field test in Israel by burying two AC pipes in the test site contains highly reactive clay soils. The test pipes were approximately 20 m long and buried at a depth of 0.9 m. Pipe stress was determined from vibrating wire strain gauges installed at various locations. The study compares difference in stress due to moisture variation of backfill material, seasonal moisture change and irrigation. A definite relationship was recognised between soil moisture variation, axial loading, and bending stress induced by soil swelling, which was suggested as a cause of pipe failures. The measured maximum combined stresses were higher for the pipes

installed in dry soils than in wet soils, which suggested that the initial moisture content of the soil could also be an important factor for pipe stress development.

Since late 1993, field test of buried PVC water pipes in different trench backfills have been undertaken in Alberta, Canada (Kuraoka *et al.* 1996b). The study was lasted over two years and performed by replacing old water pipes with instrumented PVC pipes backfilled with different materials. Longitudinal and circumferential strain gauges were mounted at various locations of the water pipes. A sinusoidal variation with time of axial and hoop strains was observed due to seasonal variation of pipe temperature, and the effects of change in moisture content, freeze-thaw, and consolidation. However, due to the deep burial depth of 2 m, the effects of pressure change due to moisture content were insignificant.

In South Regina, Canada a field study of water pipes buried in reactive soils (Hu and Vu 2006; 2011) was implemented by replacing a 150 mm diameter AC pipe with a 155 mm diameter instrumented PVC pipe section buried at 2.9 m below ground surface. Soil moisture content, temperature, and earth pressure were monitored by the sensors installed at various depths. The pipe displacement were measured by rod extensometers installed in a borehole below the pipe, so that the top end of the extensometer was attached to the pipe and the bottom end was anchored to the ground. The three years of results showed that soils monitored at all levels experienced periodic temperature change with seasonal changes in air temperature with peak temperature at pipe depth in March (minimum) and August (maximum) (Hu and Vu 2011). The moisture content at shallow clays were following the changes in annual rainfall deficits, and the time required for the moisture content to change in response to atmospheric conditions increased with depth from the surface. In shallow clays of approximately one meter, the frozen ground prevented infiltration of water; hence decrease in soil moisture content was recorded in the winter seasons even though the rainfall surplus increased during this period (Hu and Vu 2011). Significant increase in soil moisture started in spring due to snow-melt and continued until summer even though rainfall deficits increased during this period, while decrease in rainfall deficit started in autumn until the end of the year. The measured moisture content continues to decrease due to accumulated high rainfall deficit experienced during the summer period. The study also found that vertical soil pressure are closely correlated with the

change in rainfall deficit, which increased when rainfall deficit accumulated and peaks when rainfall deficit was at maximum, suggests that increase of soil pressure can be caused by soil shrinkage due to drying. The findings of Hu and Vu (2011) were similar to the studies in UK by Mordak and Wheeler (1988) as described in Section 2.2. Both studies showed that shrinkage of clay causes extra loading on buried pipes. It is also reported that over 60% of pipe failures occurred at the months when rainfall deficit was at maximum. Newport (1981) has also reported similar findings in UK, as the failure records of water pipe peaks following very hot and dry summers. Previously described studies by Kassiff and Holland (1965; 1966) in Victoria, Australia, have also drew the same conclusion that soil shrinkage of reactive clays would cause differential longitudinal bending action on the pipes. These findings showed that the increase of pressure due to soil shrinkage may be related to increase in pipe failure in hot and dry seasons.

A long term field study of deep buried thermoplastic pipes in Ohio, US (Sargand *et al.* 2008) showed that variation of temperature is likely to cause a much larger influence on the soil pressure fluctuations than the changes in soil moisture conditions at greater burial depth. There were totally 18 thermoplastic pipes buried with soils fill at the depth of 6.1 m or 12.2 m for the period of four to five years. Potentiometer, strain gauges and earth pressure cells with thermistors were installed on the pipe. It was found that seasonal fluctuation only occurred in the soil pressure, while the pipe deflections and circumferential shortening stayed relatively constant over time. Apparently the change of moisture content only occurs within 1.5 m from the surface, and hence the pressure exerted on the deep burial pipes was mostly due to the thermally induced soil pressure.

A recent study of long term monitoring of PVC pipes buried in clay soils was undertaken in Cricklewood, North London (Clayton *et al.* 2010). Two 100 mm diameter instrumented PVC pipes were buried 1 m below ground surface in the vicinity of an oak tree. Deflection gauges were installed inside the pipe in vertical and horizontal direction, and a weather station was set up on site. In the monitoring period of over two years, vertical and horizontal bending of pipes results from ground movement was recorded. Maximum pipe bending occurred in summer when soil moisture deficit was high, which can be equalled to increase of tensile stress of 20 to 30 MPa. The study results

suggested that additional stress generated by ground movement can be an important contributor to failure of old pipes buried in clay soils.

The findings of field studies have further supported that the performance of buried pipes are affected by the soil reactivity, soil moisture content, seasonal climatic change and corrosion of the pipe materials. It is also evident that there is a close correlation between development of pipe stress and seasonal variation of soil temperature and moisture content. It is clear that increase of pipe failure is closely related to shrinkage of soils, especially during hot summers when rainfall deficit is high. The seasonal effects of soils on pipes are significantly affected by the burial depth of pipes, as deformation of the pipes at greater burial depth is relatively constant. In the case of buried reticulation pipes in Victoria, Australia the burial depth is generally ranged from 0.5 m to 0.9 m, where significant effect of seasonal fluctuation can be expected.

2.6 Monitoring of Soil Moisture Content

2.6.1 Variation of soil moisture content and pipe deformation

Studies reviewed in the previous sections clearly showed that reactivity of soils and seasonal variation of soil moisture content are two of the major factors influencing shrinkage and swelling of soils and associated pipe deformations. It follows then that the knowledge of soil moisture variation in soils is important to determine the additional stress and deformations that are imposed on the buried pipes.

In general, two different approaches were reported to calculate stresses and deformations on structures buried in soils with reactive behaviour; using soil suction as a governing variable and using soil moisture content as a governing variable. Fredlund and Vu (2003) modelled the stress and deformation under the slab as a function of variation in matric suction, defined as the excess air pressure over the pore water pressure. Masia *et al.* (2004) undertook 3D numerical modelling of the expansive soil movement on the basis of soil suction profiles that developed beneath a structure.

This numerical model is deemed to be capable of generating continuous records over time on the basis of recorded climatic data and representative soil properties.

However, the long term monitoring of suction variation in field is difficult and not reliable (Fityus 1999; Gould *et al.* 2011). In contrast, the measurement of moisture content is relatively easy, hence a ground movement prediction method based on moisture content offers some advantages. A number of researchers have followed this approach including Fityus (1999) and Rajeev and Kodikara (2011).

The accurate measurement of soil moisture content is straightforward by oven drying. However, this requires a soil sample to be retrieved and tested, commonly in the laboratory. Field measurement of soil moisture content can be performed by non-destructive, indirect testing methods such as time or frequency domain reflectometry and radiometric logging method. Each of these indirect methods offers merits and demerits for soil moisture content measurement.

2.6.2 Time or frequency domain reflectometry method

The time domain reflectometry (TDR) method determines moisture content on the basis of the different dielectric constant between each substance. As in soil the dielectric constant is dominated by the amount of water present, which is empirically related to the volumetric soil moisture content.

The measurement of soil moisture content is performed by inserting the rods (i.e., 3 rods or 5 rods) of a TDR probe into the soil. A sinusoidal signal is generated to the internal transmission line in the array of the rods. The impedance of the array varies with the dielectric constant of the soil. Reflections of the signal is affected by the impedance of the rod array and combined with the applied signal to form a voltage standing wave along the transmission line. The output voltage is proportional to the difference in amplitude of the standing wave. A 3rd order polynomial relationship is commonly adopted for the output voltage, V , and the square root of dielectric constant of the soil, $\sqrt{\epsilon}$, where

$$\sqrt{\epsilon} = 1.07 + 6.4V - 6.4V^2 + 4.7V^3$$

Equation 2-3

A linear relationship is then developed between the square root of dielectric constant, $\sqrt{\varepsilon}$ and the volumetric soil moisture content, θ is described by,

$$\sqrt{\varepsilon} = a_0 + a_1\theta \quad \text{Equation 2-4}$$

where a_0 and a_1 are the two soil related coefficients. (Delta-T 1999).

The TDR method is relatively quick to perform and is suited for automatic measurements, however TDR probe needs to be buried in the ground for the measurement and multiple probes are required for multiple measurements of soil moisture content at various depths and locations.

2.6.3 Radiometric logging method

The radiometric logging methods are performed by inputting radioactivity source to the ground to provide information at various depths. The neutron probe, which was developed more than 40 years ago, is now a commonly used radiometric logging method for monitoring of the soil moisture variation in the field.

The working principle of neutron probes is simple and reasonably straightforward. A probe consisting of the neutron source and detector is lowered to a pre-drilled borehole to the required depth. Measurement is operated by emitting high energy neutrons from the encapsulated radioactive source, e.g., Americium-241:Beryllium, which interacts with the soil particles and soil water that surrounds the probe. Since neutrons have no charge, the electric fields associated with the charged soil particles do not affect their movement. The fast neutrons will collide with hydrogen atoms in the soil moisture and get slowed down. The low energy, moderated neutrons are detected by the detector and the volumetric moisture content of the soil is determined by the count of low energy neutrons. A higher count rate means that more moderated neutrons are presented and soil moisture content is higher. The precision of the measurement is depending on the logging time, where a longer count time can provide more precise measurement but it also means that less measurement can be made in a day.

Figure 2-12 shows a typical design of neutron probe for measurements of moisture within the upper 1 to 2 m of the soil, which can provide a description of moisture variations over large study areas but at discrete locations (Schmugge *et al.* 1980). Aluminium tubes are the most commonly used borehole casing for neutron logging method as it is virtually transparent to neutrons and does not affect the sensitivity of measurement. Nevertheless, aluminium tubes are prone to corrosion in soils containing sodium chloride and in very acid or alkaline soils and may require replacement during long-term experiment (Greacen 1981). The neutron probe has proved to provide satisfactory measurements in soil moisture investigations (Evetts and Steiner, 1995), but because of the potential risk of the radioactive source a license is required to operate the probe.

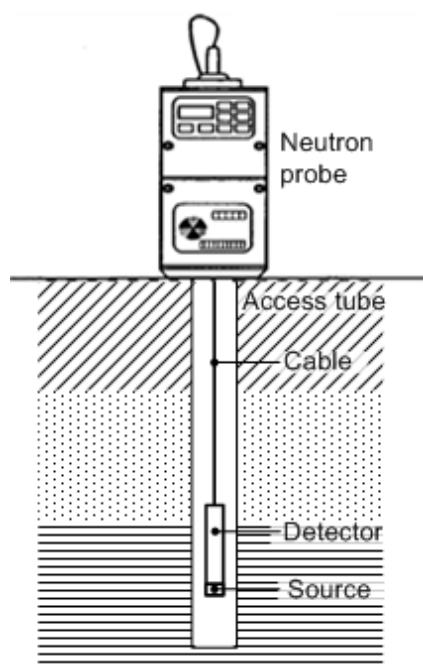


Figure 2-12 Schematic diagram of neutron probe

2.7 Pipe Failure Prediction Models

Studies of the pipe-soil interaction by investigation of soil properties and field instrumentations should eventually lead to development of a pipe failure model. In general, it requires the understanding of the mechanical behaviour and the structural deterioration of the buried pipes by analysing historical data. Pipe failure prediction models are developed from two modelling approaches, statistically based and physically / mechanically based. The statistical models are based on the pipe failure data, where failure rates are described by fitting forms of functions (e.g., time-exponential) to the recorded failure data (Davis *et al.* 2007). Although future failure rates can be predicted by extrapolation (Jarrett *et al.*, 2001b), forecasts are generally restricted to homogeneous groups of pipes with similar attributes (Herz 1998). Furthermore, good quality large failure database are required as a basis for these models. The physical models are based on the soil-structural interaction behaviour. These models may be scientifically more robust but are often limited by availability of the required data, hence are normally applied on major transmission pipes as the cost of failure is significant. A review of both prediction models is presented in the following section with brief description and comparison.

2.7.1 Statistically based models

Prediction of buried pipe failures in statistical models are based on pipe failure patterns identified from historical failure data, then assumed that the failure pattern will be continued in the future. The life cycle of a typical buried pipe was described by Kleiner and Rajani (2001) as the bathtub curve shown in Figure 2-13. The bathtub curve of buried pipes describe the rate of occurrence of failure (ROCOF) of a repairable unit (Ascher and Feingold 1984) which distinguishes between three phases, burn-in, in-usage and wear-out. The burn-in phase is the initial phase that refers to the period after installation, pipe failures occurred within this period are mainly due to installation or manufacturing problems. The second phase of in-usage described the operational periods of the pipes, failure rates are normally low in this period with occasional incidents of random heavy loads or third party damage. The third phase is referred as the wear-out phase when the pipe starts to

deteriorate with increasing failure rates. Some statistical models considered all phases of the bathtub curve, while others may only consider one or two phases. Some models have also assumed a different shape of the bathtub, which can be represented by the line B at the wear-out phase in Figure 2-13.

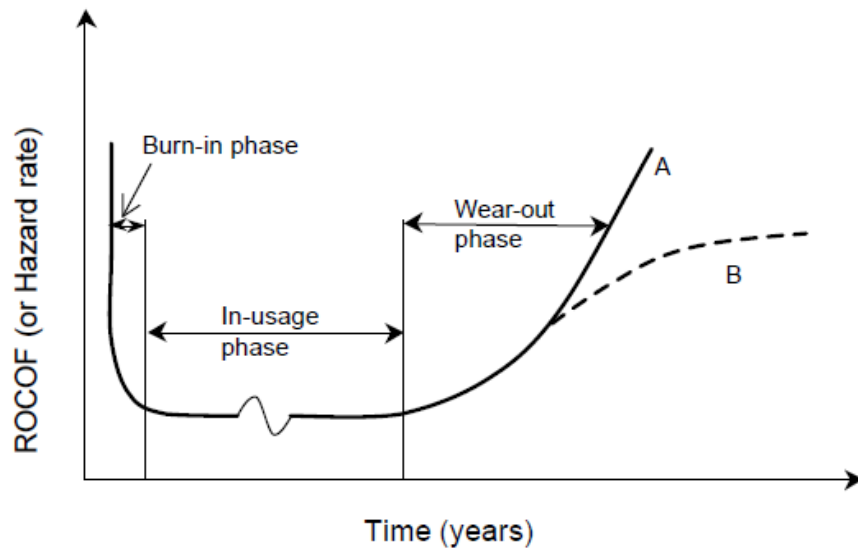


Figure 2-13 The bathtub curve of life cycle of a typical buried pipe (Kleiner and Rajani 2001)

The statistical models can be classified as deterministic and probabilistic models. Subclasses of the probabilistic models are multi-variate and single-variate group processing models. Deterministic models are based on the pipe age and failure data according to the factors considered, which includes pipe properties, operational and environmental factors. According to these factors the pipe data were partitioned into homogenous groups with similar attributes so that future failure patterns can be extrapolated (Davis *et al.* 2007). The probabilistic multi-variate models are able to consider most of the factor related to pipe failure in the analysis, which makes it more powerful on failure prediction but with more complex mathematical framework, while the data have to be carefully examined to identify covariates with best predicting ability. Conversely, the probabilistic single-variate models can be used to derive probabilities of pipe life expectancy, failure and analysis of

failure clustering phenomenon (Kleiner and Rajani 2001). These models are suitable for identification of prioritising pipe replace or rehabilitation, since assessment can be done on individual pipes.

2.7.2 Physically based models

The physical behaviour of buried pipes are based on the environmental and operational conditions as previously described in Table 2-1, as well as quality of manufacturing and installation. The physical mechanisms related to these conditions can be classified into three principal aspects: the pipe structural properties; internal loads during operation; and material deterioration due to chemical (Rajani and Kleiner 2001). The structural behaviour related to these aspects is generally well studied (Young and Trott 1997; Moser 2001) except for other issues, such as pipe-soil interaction and material deterioration. The initial development of physical models was aimed mainly at deterministic models which can be used to estimate the remaining service life of pipes on the basis of corrosion pit depths. Recently some models were developed using probabilistic approaches to consider uncertainties in defining material deterioration and pipe failure processes. It is agreed that a complete physically based model would explicitly encompass all the inter-relations between the factors affecting pipe failures and eliminate the need to use statistics to estimate failure patterns (Rajani and Kleiner 2001). But such robust physical model requires comprehensive pipe asset and data which most of the asset owners have yet to provide, or too costly to acquire.

2.7.3 Comparison of pipe failure prediction models

A comparison of the physically and statistically models in chronological order are shown in Table 2-6 with the references and descriptions of the models. Each of the model offer merits and demerits on pipe failure, some models are only applicable for a specific pipe type, some models considered only certain variate, and some models make assumptions that are questionable. In general, physically based models, due to the cost and data required, are only used for major transmission pipes which have significant maintenance cost. Statistically based models are relatively more economical and hence mostly used for small diameter distribution pipes.

Table 2-6 Comparison of pipe failure prediction models

References	Model types			Pipe types	Description	Data requirements	Remarks
	Physical	Statistical	Classes				
Watkins and Spangler (1958)	X		Deterministic	Flexible	Interaction between pipe in-plane behaviour with soils due to internal pressure and external loads.	Material properties, installation and operational conditions, soil properties	Assumption is inadequate for small diameter pipes.
Doleac (1979); Doleac <i>et al.</i> (1980)	X		Deterministic	Pit cast	Calculation of hoop stress from predicted remaining wall thickness.	Pipe age, soil properties	Predictability of the power function has not been well validated.
Shamir and Howard (1979)		X	Deterministic		Prediction of failure rates based on regression analysis on increase of failure rates with pipe age.	Pipe length, installation date, failure history, homogenous pipe groups with same attributes	Assumption of uniform distribution of failure along all pipes in a group is questionable.
Walski and Pelliccia (1982)		X	Deterministic	Pit cast iron	Enhanced Shamir and Howard (1979) models with two factors, accounted for previous pipe failure and failure rates in large diameter pit cast iron pipes.	Same as for Shamir and Howard (1979) with addition data on the pipe casting methods and diameter	Same as Shamir and Howard (1979).

Clark <i>et al.</i> (1982)		X	Deterministic		A two-phase model with a linear equation to predict the time elapsed to the first pipe failure and an exponential equation to predict pipe failure rates.	Similar to Shamir and Howard (1979) with information of operating pressure, soil corrosivity, additional failure data, e.g., failure types	Further study may be required for suitability of the model to pipe failure prediction.
Kettler and Goulter (1985)		X	Deterministic	Cast iron, ductile iron	A time-linear model based on a linear relationship between pipe failure and pipe age.	Same as Shamir and Howard (1979)	Same as Shamir and Howard (1979).
Mark <i>et al.</i> (1987)		X	Probabilistic multi-variate		Prediction of pipe failure using proportional hazards model to compute the probability of the time duration between consecutive failures.	Pipe length, operating pressure, installation date, pipe age, failure history, soil corrosivity	
Andreou <i>et al.</i> (1987)		X	Probabilistic multi-variate		A two stage pipe failure process consists of the proportional hazards model and the Poisson type model.	Same as for Mark <i>et al.</i> (1985)	Covariates have to be carefully identified.

Kiefner and Vieth (1989)	X		Deterministic	Ductile steel	Prediction of pipe failure pressure based on the assessment of corrosion pits and bulging of the pipes before failure.	Pipe material properties, corrosion characteristic	The model has not been validated with other pipe materials
Randall-Smith <i>et al.</i> (1992)	X		Deterministic	Grey cast iron, ductile iron	A linear model based on constant corrosion rate.	Pipe age, pipe wall thickness, internal and external pit depths	Assumptions are questionable. Stresses have not been considered.
Goutier <i>et al.</i> (1993)		X	Probabilistic single-variate group processing		Prediction of subsequent pipe failures from the first failure using a non-homogeneous Poisson probability distribution.	Failure history, location of failures with precision to the a metre	The model does not provide failure prediction capabilities by itself.
Ahmed and Melchers (1994)	X		Probabilistic	Steel	Estimate the deterioration of pipe wall thickness with time based on Watkins and Spangler (1958) model with a second-moment description method to approximate the dependent variables.	Similar to Watkins and Spangler (1958) model, plus parameters for pipe wall deterioration function	Limitation on pipe materials, stress direction and difficulty in deriving the required parameters

Constantine and Darroch (1993); Constantine et al. (1996)		X	Probabilistic multi-variate		Prediction of pipe failure from a time dependent Poisson model which is also known as a Weibull process.	Pipe age, pipe properties, pressure, soil properties, traffic conditions	
Herz (1996, 1998)		X	Probabilistic single-variate group processing		A lifetime probability distribution density function based on the functions of probability density, hazard and survival.	Pipe age, installation date, failure history, homogenous groups with same attributes	Not suitable for prioritising individual pipes for rehabilitation.
Rajani et al. (1996); Rajani and Tesfamariam (2007)	X		Deterministic	Grey cast iron	Predict time to failure of pipes based on simplified Winkler model in combination with failure theories and fuzzy numbers.	Pipe age, pipe properties, soil properties, seasonal ground and water temperature	
Pandey (1997)	X		Probabilistic	Steel	Based on Kiefner and Vieth (1989) model to estimate the pipeline reliability incorporating the impact of inspection and repair activities planned over the service life.	Pipe age, wall thickness, internal and external corrosion pit depths, corrosion pit length, corrosion characteristic	The model may only be valid for steel pipes.

Hong (1998, 1999)	X		Probabilistic	Steel, ductile material	Probabilistic expression comprised the probability distribution of the pipe strength uncertainty and the corrosion defect size by the ratio of actual pipe operating pressure and the predicted remaining strength of the corroded pipe.	Pipe age, wall thickness, internal and external corrosion pit depths, corrosion pit length, corrosion characteristic	Limited application to ductile pipes with large diameter.
Gustafson and Clancy (1999a, b)		X	Probabilistic single-variate group processing		Prediction of pipe failure interval with a semi-Markov model where the time interval of each failure is depending to the failure order.	Failure history, homogenous groups with same attributes	
Ranjani and Makar (2000)	X		Deterministic	Cast iron	Estimation of remaining service life by structural resistance of a pipe as result of corrosion pits.	Pipe material properties, pipe age, pipe wall thickness, internal and external pit depths, tensile strength, fracture toughness, elastic modulus, flexural strength	Prediction of remaining life is affected by uncertainties in estimating corrosion rates.

Jarrett, <i>et al.</i> (2001b)		X	Probabilistic multi-variate		Extended Constantine and Darroch (1993) and Constantine et al. (1996) models with best linear unbiased predictions to consider extra variation where the Poisson model cannot predict.	Same as for Constantine and Darroch (1993) and Constantine et al. (1996)	
Davis and Burn (2002)	X		Probabilistic	Cast iron	Physical pipe failure model based on the empirical relationship between pipe failures and climate data is combined with statistical model for prediction of failure distributed along the pipe.	Pipe age, pipe properties, corrosion characteristic, soil properties, climate data	

2.8 Conclusions

Current state of the knowledge on performance of buried reticulation pipes shows that the pipes are affected by the physical properties of the pipe and environmental factors of the buried location. The relationship between pipe failures, soils and seasonal climate change were described in this chapter. Existing research in field studies of buried pipes identified that differential soil displacement due to shrinkage of soils has significant effect on pipe loading. However, study of in service buried pipes has not been carried out. Essentially, it is important to understand the behaviour of existing pipes and developed a pipe failure prediction model which incorporates with seasonal soil displacement and the performance of buried pipes.

CHAPTER 3

STUDY OF IN-SERVICE BURIED PIPES BY FIELD INSTRUMENTATIONS

3.1 Introduction

Field instrumentations were aimed to study the behaviour of in-service pipes buried in reactive soils due to seasonal climate changes. A water pipe at Altona North owned by City West Water (CWW) and a gas pipe at Fawkner owned by SP AusNet were selected for this study. The in-service pipes were instrumented with strain gauges and thermocouples, while moisture content, suction and temperature of the surround soils were also monitored. A weather station was installed on each site to record the local rainfall, wind speed, solar radiation, and relative humidity. The details of site selection criteria, instrument calibrations, initial testing of the sensors and field instrumentation are discussed in this chapter. The procedure of the field instrumentation and the calibration process presented in this chapter were published in the research reports, RR10 and RR13 (Gallage *et al.* 2008; 2009) for the Pipe Linkage Project (<http://www.eng.monash.edu.au/civil/research/centres/mapps/>).

3.2 Forensic Analysis

Prior to field instrumentation, forensic investigations were undertaken with the aim to examine the field process related to pipe failure detection, repair, installation, and rehabilitation. Pipe and soil samples were collected for the laboratory testing of material properties and soil characterisation.

Field investigation on twelve sites with the CWW field crew was commenced over a period of two weeks in May and June 2007. Primary operations of the field crew were to locate pipe leaks and repair or replace failed pipes. Water pipe leaks are normally identified either through report from the public or by asset leak detection inspection teams. The major leaks were easier to identify as water flowed out from the ground at the location of leaks, but minor leaks can sometimes be difficult to identify from the ground surface as small water flow could be absorbed by the soil or runoff internally to the nearby storm water drains. In these instances, an acoustic method of 'listening' to the leaks was used. The acoustic detection method required the use of multiple steel 'T' bars be placed on the pipe around the suspected leak location as shown in Figure 3-1 (a) and 'listening' to the acoustic noise generated by the water escaping from the pipe (Fantozzi 2000) as shown in Figure 3-1 (b). Once a leak was located, the ground was excavated to expose the pipe in order to determine the failure type and the appropriate repair method. In general, small leaks or circumferential failures (Figure 3-2 (a)) were repaired by steel clamps, while longitudinal fractures or major leaks were repaired by replacing the failed pipe section with PVC pipe (Figure 3-2 (b)). However, due to pipe samples required for the material testing, failed pipe sections were removed from the sites during the investigation regardless of the failure type. The cast iron (CI) sections removed from the failed pipes were tested for tensile and fracture toughness in the laboratory.



Figure 3-1 Detection of water pipe leaks by acoustic method: (a) Steel “T” bars placed along suspected pipe leak location; (b) “Listening” to the acoustic noise of water pipe leaks



Figure 3-2 Failure of water pipe: (a) Exposed circumferential fractured pipe; (b) Pipe replacement with PVC section

The field investigation of gas pipes was undertaken on May 2008 with SP AusNet sub-contractor, Tenix field crews. Similar to CWW, the works undertaken by Tenix were to locate and repair pipe failures. Three sites within the SP AusNet distribution region were visited in the investigation. Gas pipe leaks were harder to locate than water leaks, as gas leaks were invisible and may only be detected through smell of the gas after continued period of leaking. Furthermore, methods based on the gas detection were usually poor in locating the leakage source of buried pipes since the leakage

gas may flow a long distance before escaping above ground (Liu *et al.* 2000). The location of gas leak could be further made by inserting a gas emission sensor into the ground as shown in Figure 3-3 (a). After the pipe was exposed, the leak may be identified through visual analysis, and detergent could be sprayed on the area in question to identify the leak, especially for a leak at the pipe joints as shown in Figure 3-3 (b). Repairing methods for gas pipes were same as for water pipes, either by using clamps or by replacing the failed pipe with a PVC pipe section. The investigation on variation of the measured pipe tensile strengths with the ratio of maximum corrosion pit depths and specimen thickness was undertaken by Mr Scott Gould, another postgraduate student of the Pipe Linkage Project. The results obtained from the investigation with CI pipe samples collected from CWW, South East Water Limited (SEW), and Yarra Valley Water (YVW) are plotted in Figure 3-4. A clear trend of reduction in tensile strength with increase of maximum corrosion pits can be observed, it is evidenced that the strength of buried pipes are greatly affected by corrosion. A summary of the mechanical test results with pipe samples of water and gas pipes are shown in Table 3-1. Further details of the mechanical tests can be found in Gould *et al.* (2009).



Figure 3-3 Detection of gas pipe leaks with gas emission sensor: (a) A gas emission sensor inserted into the ground close to the suspected leak location; (b) Detergent sprayed on the failed pipe joint

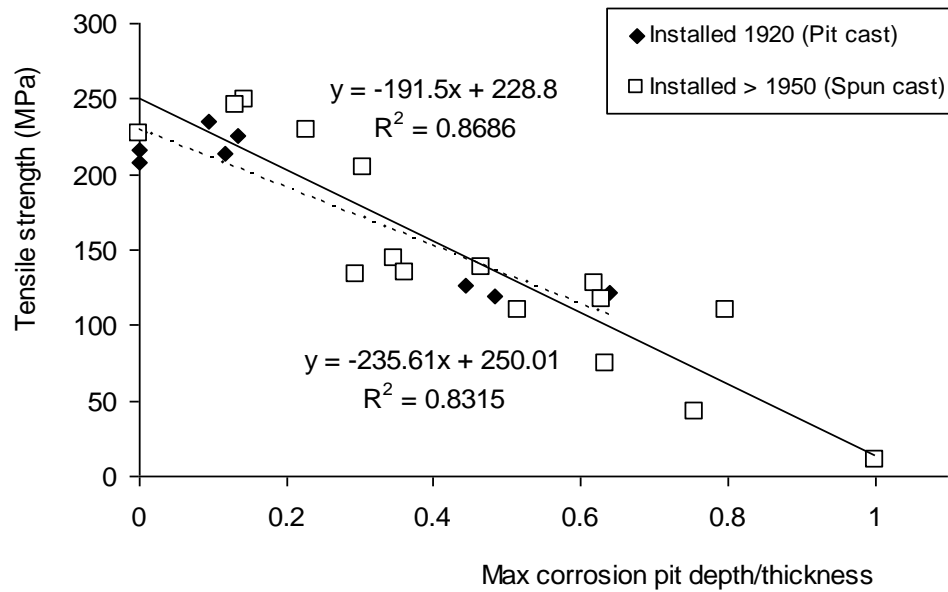


Figure 3-4 Pipe tensile strength and maximum corrosion pit depth (Gould *et al.* 2009)

Table 3-1 Summary of Mechanical testing of cast iron pipes (after Gould *et al.* 2009)

Sample ID*	Service type	Construction Date	Tensile Strength (MPa)	Tangent Modulus (MPa)	Secant Modulus (MPa)	Fracture Toughness (MPa√m)
CWW1	Water	24/07/1920	236	-	64,000	10.6
CWW2	Water	23/12/1953	209	166,582	94181	-
CWW3	Water	28/05/1951	128	-	-	12.6
CWW4	Water	10/12/1951	181	153,749	104948	12.9
CWW5	Water	21/07/1961	168	171,086	119980	10.2
SEW1	Water	13/04/1903	134	121,133	54700	-
SEW2	Water	26/02/1884	145	98,168	51630	9.3
SEW3	Water	10/06/1921	230	-	74216	-
SEW4	Water	11/06/1889	151	175,925	93543	-
YVW2	Water	10/08/1971	203	275,306	118769	-

YVW3	Water	05/07/1972	240	-	125243	-
YVW4	Water	30/01/1973	249	-	159055	-
Alinta 1	Gas	04/01/1970	252	5,504	-	10.48
Alinta 3	Gas	04/01/1970	234	19,971	-	11.31
Envestra 2	Gas	06/01/1960	128	30,284	-	12.01
Envestra 3	Gas	05/01/1960	225	22,304	-	10.09

*Note: CWW– City West Water, SEW – South East Water, YVW – Yarra Valley Water

3.3 Site Selection Criteria

The statistical analysis on buried pipe failures (Gould and Kodikara 2008; Gould and Kodikara 2009) reported that pipes with the nominal diameters of 100 mm are the most numerous in the CWW network, and pipes of 150 to 200 mm have the second longest length in the SP AusNet network. Out of these pipe types those located in reactive soils have the highest failure rate. Similar results were reported by Chan (2008), which indicated over 50% of water pipe failures in Victoria were associated with CI pipes, while about 60% of the failed pipes were 100 mm diameter. In the case of gas pipes, over 73% of pipe failures in reticulation pipes (diameter of 80 to 300 mm) associated with CI pipes. Due to these reasons, it was decided to undertake the instrumentation on a 100 mm CI water pipe in the CWW region, and a 150 mm CI gas pipe in the SP AusNet region. The site was chosen following the criteria described below in order to be effective, safe, convenient, and least complicated for excavation, instrumentation, data-logging and analysis. The selection criteria were:

- An area of high failure rates history;
- A reactive soil region;

- Contains an in-service CI water pipe with diameter of 100 mm, or a CI gas pipe with diameter of 150 mm;
- No previous failure have occurred within the instrumented pipe length;
- A pipe laid across nature strip and driveway to study the effect of previous and impervious surface on buried pipe behaviour;
- A wide nature strip to allow for instrumentation;
- Clear of other utilities such as power cables, telecommunication cables, storm water pipes and sewer pipes;
- A relatively flat ground surface to avoid the effect of sloping ground and risk of potential flooding;
- No trees or other large vegetation on the nature strips within and close to the instrumentation locations; and
- A quiet area with relatively low traffic flow.

Numerous of potential sites were screened using drive-by and walking surveys considering the above criteria. Ten sites were selected from each of the CWW and SP AusNet regions for further investigation on soil depth and site specific properties.

According to the AS 2870 residential slab and footing design (Standards Australia 2011), the change of suction depth (or reactive zone depth) in the Western Melbourne area is approximately 1.5 to 2.3 m. Soil investigations were carried out by hand auguring and undisturbed push tube sampling by a drill rig in order to determine the depth of soils. Two sites were chosen for the field instrumentations, considering the selection criteria and the depth of soils.

3.4 Soil Characteristics of the Selected Sites

3.4.1 Particle size distribution

The soil particle size analysis was performed by sieving in combination with hydrometer in accordance with Australian Standard AS1289.3.6.3 (Standards Australia 2003). The wet sieving method was used to analyse the soil with particle size down to 75 μm , and the hydrometer testing method was used for the proportion of soil particles smaller than 75 μm .

Disturbed soil samples collected from Altona North and Fawkner were soaked in a dispersing solution (diluted hydrated sodium carbonate) for at least one hour before agitating and washing on a 75 μm reinforced sieve. The dispersing solution was used for the washing until the effluent water was clear and all of the fine materials were washed through the sieve. The washed materials was collected in a tray placed under the sieve and oven dried at 105 $^{\circ}\text{C}$ to constant mass.

Accounting to 50 to 100 g of washed samples (i.e., particle size less than 75 μm) were used in the hydrometer analysis. The samples were suspended with the reagents (e.g., diluted hydrated sodium carbonate) and stirred in a dispersion device (e.g., a milk shake maker) for 10 to 15 minutes or until a well-mixed solution was obtained. The mixed solution was poured into a cylinder and further mixed with the reagents to a volume of one litre. The cylinder was shaken for one minute or until the reagents were thoroughly mixed with the soil solution, then it was placed in a stable place with relatively constant temperature. The test was started by submerge the hydrometer in the cylinder and record the incremental readings with time. The test could be stopped when the hydrometer readings became constant, suggested that the fine particles have settled. Percentage passing for soil particle size can be calculated using the hydrometer readings.

Figure 3-6 illustrates the particle distribution curves of the selected sites. The soil at Altona North are generally well graded with 60 % of clay, 30 % of silt, and approximately 10% of sand with very small amount (less than 1 %) of gravel. Soil particles at Fawkner are relatively coarser with 50 % of

clay, 41% of silt, and approximately 6 % and 4 % of sand and gravel, respectively. According to AS 1726 Geotechnical site investigations (Standards Australia 1993), soil samples with 'more than half of material less than 63 mm is smaller than 0.075 mm are classified as fine grained soils. The Atterberg limit tests are used to classify the fine grained soils as described in the following section.

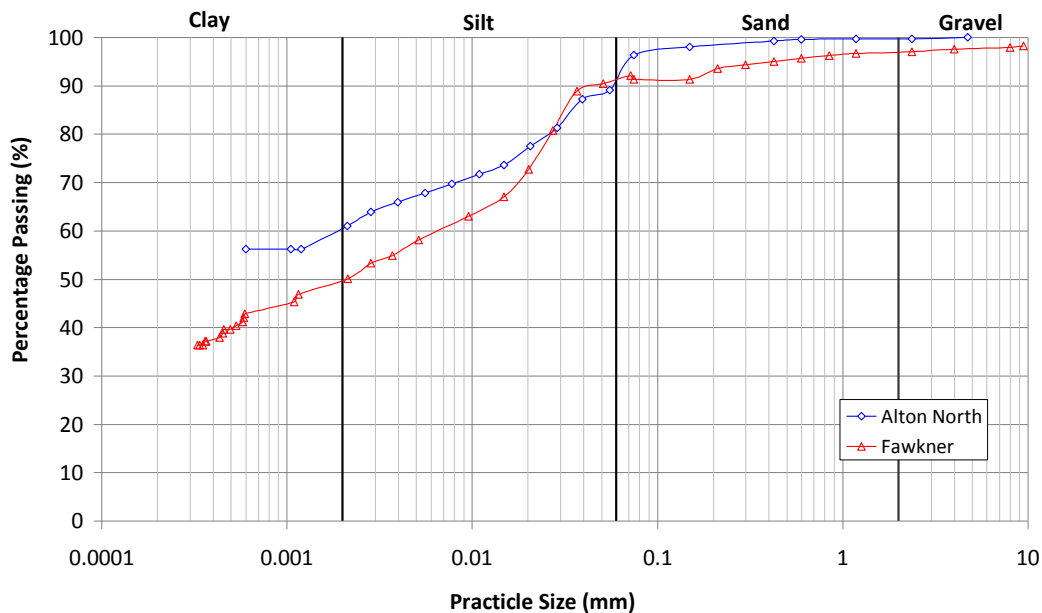


Figure 3-6 Particle size distribution of the selected sites

3.4.2 Atterberg limits

The Atterberg limits tests of the plastic limit, the liquid limit, and the linear shrinkage tests were conducted in accordance with the procedure in AS1289.3.4.1, AS1289.3.2.1 and AS1289.3.1.1 (Standards Australia 2008; 2009a; b). The AS1289.2.1.1 oven drying method (Standards Australia 2005) was used to determine the moisture content for all tests. Linear shrinkage test was undertaken at the same time with liquid limit test, using the soil sample at the moisture content close to the liquid limit. The tests were performed using core samples collected from Altona North and Fawkner

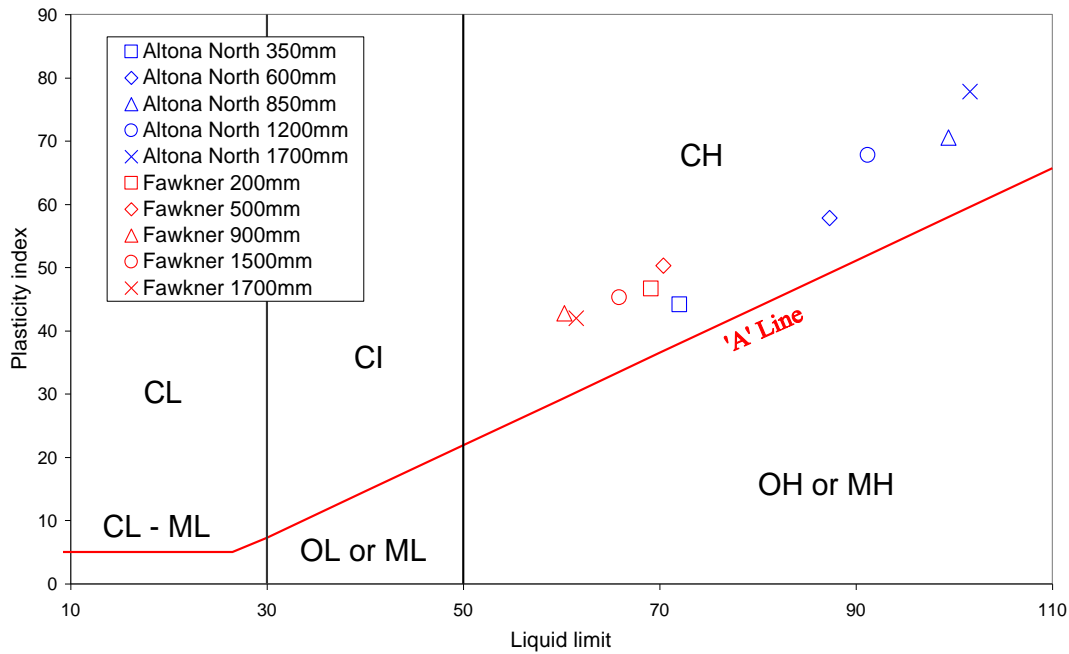
at different depths. A summary of the results is shown in Table 3-2. The soil at Altona North showed higher plasticity index and linear shrinkage than for Fawkner, which suggested that the Altona North site has higher potential for ground movement.

Table 3-2 Summary of Atterberg limits of the selected sites

Altona North					
Depth (mm)	Plastic Limit	Liquid Limit	Plasticity Index	Linear Shrinkage	wPI
350	27.8	72.0	44.2	21.7%	42.6
600	29.5	87.3	57.8	24.0%	55.7
850	28.9	99.4	70.5	21.2%	67.9
1200	23.4	91.2	67.8	26.0%	65.3
1700	23.8	101.6	77.8	24.4%	74.9
Fawkner					
Depth (mm)	Plastic Limit	Liquid Limit	Plasticity Index	Linear Shrinkage	wPI
200	22.4	69.1	46.7	19.7%	42.6
500	20.1	70.4	50.3	20.0%	45.9
900	17.5	60.3	42.8	18.1%	39.1
1500	20.7	65.9	45.2	18.8%	41.3
1700	19.5	61.5	42.0	17.7%	38.3

Figure 3-7 shows the plasticity chart for fine grained soils plotted with the results of the two selected sites. All the samples were plotted above the 'A' line in the region of CH, inorganic clays of high plasticity, fat clays. According to the studies of soil reactivity based on plasticity index as discussed in Section 2.4.3, the reactivity of soil is proportional to wPI. The wPI of the samples are calculated using the clay content obtained from particle size distributions. The percentage of soil particle passing a 75 μm sieve is 96.3 % and 91.3 % for Altona North and Fawkner, respectively. As shown in Table 3-2 soils with wPI greater than 35.85 are considered to be highly reactive. Hence significant ground movement can be expected on both sites. These findings can be further confirmed by the geological map in Figure 3-5 that shows that the selected sites located in the Newer Volcanics

formation, where the basaltic clay belongs to this formation are considered as soil of high to extreme reactivity according to the Australian Standard AS 2870 (Standards Australia 1996).



Legend:

Group symbols	Typical names
ML	Inorganic silts and very fine sands, rock flour, silty or clayey fine sands or clayey silts with slight plasticity
CL, CI	Inorganic clays of low to medium plasticity, gravelly clays, sandy clays, silty clays, lean clays
OL	Organic silts and organic silty clays of low plasticity
MH	Inorganic silts, micaceous or diatomaceous fine sandy or silty soils, elastic silts
CH	Inorganic clays of high plasticity, fat clays
OH	Organic clays of medium to high plasticity, organic silts

Figure 3-7 Plasticity chart for classification of fine grained soils (after Das 1998)

3.4.3 Swelling properties

Swelling properties of the selected sites were measured from core samples at various depths using the oedometer test. The ASTM Standard D4546 (ASTM International 2008) outlined the procedure for measurement of swelling pressure; however two types of oedometer as shown in Figure 3-8 were used for the measurements. The typical oedometer showed in Figure 3-8 (a) loaded the specimen by applying weights on the lever arm. The new apparatus shown in Figure 3-8 (b) was manufactured by the workshop of Monash University. It is relatively smaller in size and installed with digital dial gauges for continuous computer logging. Both oedometer are capable of measuring swelling pressure, the variation is that higher pressure can be applied to the specimen from the lever arm of the typical oedometer while the new oedometer is more compact and can be set up on a small bench.

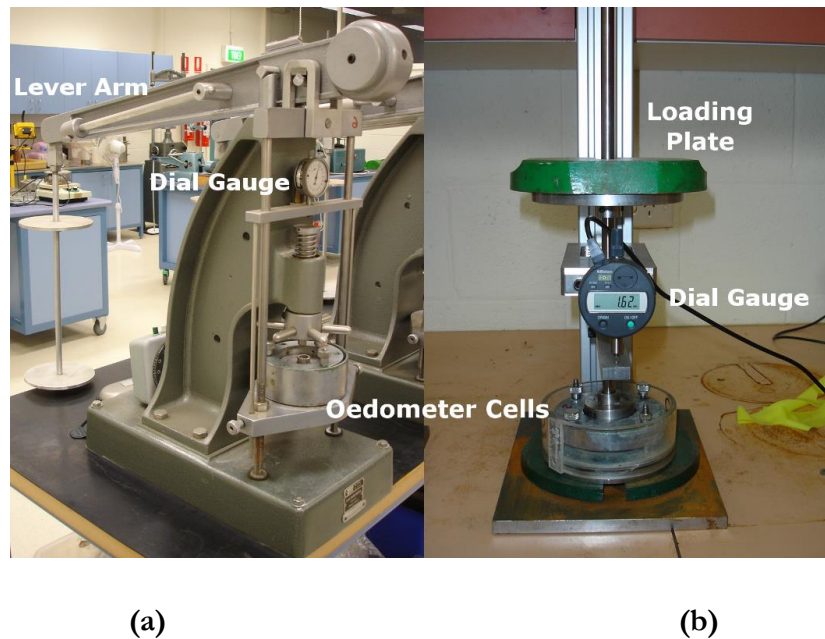


Figure 3-8 Oedometers used in swelling test: (a) Typical oedometer; (b) New oedometer

Core samples from selected sites were cut into the consolidation rings and set up in the oedometer. A seating pressure of 3 kPa was applied, before the specimens were inundated with water and swelling of soils was started. The step loadings were applied when swelling of soils had ceased, then the specimens started to consolidate under the applied load. Next load increment was applied when consolidation ceased, e.g., when the dial gauge readings became constant. The pressure required for bringing the sample height to its initial height was recorded as the swelling pressure (Nelson *et al.* 2006). The swell pressure plots of the selected sites are shown in Figures 3-9 and 3-10. Swelling pressure of the specimens from Altona north and Fawkner vary from 110 to 600 kPa and 80 to 560 kPa, respectively. These variations are predominantly due to different initial moisture content and dry density of the specimens. As showed in Table 3-3 specimens with higher initial dry density tend to have higher swelling pressure. Based on these results, when soil swelling occurred beneath a buried pipe with limited vertical movement (e.g., fully or partially restrained conditions with small vertical strain), on maximum, the swelling pressure applied on the pipe can be as high as 600 kPa and 560 kPa in Altona North and Fawkner, respectively.

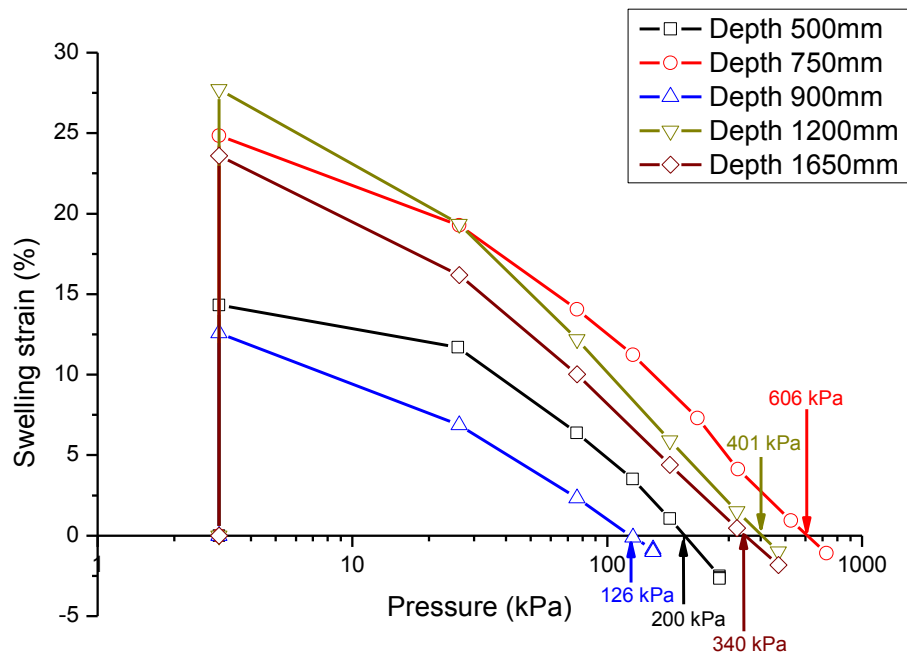


Figure 3-9 Swelling pressure of samples from Altona North

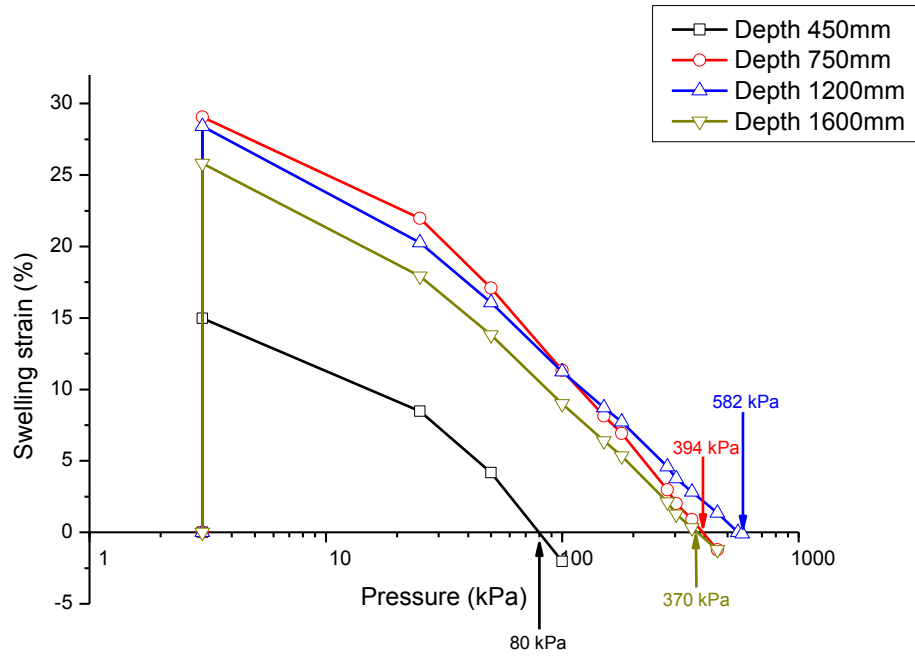


Figure 3-10 Swelling pressure of samples from Fawkner

Table 3-3 Properties of oedometer test specimens

Depth (mm)	Altona North			Depth (mm)	Fawkner		
	Initial Dry Density (kg/m ³)	Initial Moisture Content (%)	Swelling Pressure (kPa)		Initial Dry Density (kg/m ³)	Initial Moisture Content (%)	Swelling Pressure (kPa)
500	1514	22.9	200	450	1447	33.8	80
750	1501	25.3	600	750	1590	27.5	380
900	1359	25.0	110	1200	1698	23.3	560
1200	1573	24.7	400	1600	1636	26.6	370
1650	1562	26.2	350				

3.4.4 Soil profiles

Soil properties obtained from the tests described above are summarised in Table 3-4. These test results confirmed the selected sites contained highly reactive clays that were suitable for field instrumentations. Figure 3-11 shows the observed vertical soil profile at Altona North and Fawkner. Similar soil profiles were observed on both sites with topsoil layer of 0.3 to 0.4 m containing organic material and grass roots. A layer of basalt rock was found at the depth of approximately 2 m which was overlain by consistent layer of residual inorganic clays. The topsoil appeared to be dry at the time of sampling, and soil moisture content increased proportional to the depth below ground surface. Ground water table was not observed for both sites.

Table 3-4 Summary of soil properties of the selected sites

	Altona North	Fawkner
Colour	Light brown / beige	Brown
Clay content	60%	50%
Plastic Limit	26.7	20.1
Liquid Limit	90.3	65.44
Plasticity Index	63.6	45.4
Linear Shrinkage	23.5%	18.9%
Soil Group	CH, Inorganic clays of high plasticity, fat clays	CH, Inorganic clays of high plasticity, fat clays
Swelling pressure	110 to 600 kPa	80 to 560 kPa

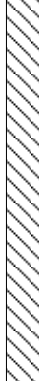
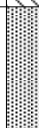
		Altona North		Fawkner	
Boring Method	Inferred Stratigraphy	Graphic Log	Depth (m)	Inferred Stratigraphy	Graphic Log Depth (m)
			0.0		0.0
Push tube	Top soil: MH silty clay, dark grey with root fibers, dry to moist		0.4	Top soil: MH silty clay, brown ashes with root fibers, dry to moist	
	CH inorganic clay of high plasticity, dark to light grey, moist, stiff to very stiff		2.0	CH inorganic clay of high plasticity, brown ashes, moist, stiff	
Rock core	Basalt rock			Basalt rock	

Figure 3-11 Bore hole logs of the selected sites

3.5 Field Monitoring Systems

Soil and pipe sensors were installed in the selected sites for long term pipe-climate-soil interaction study. Measurements of soil temperature, moisture content, suction, pressure, and displacement; and measurements of pipe strain, temperature, and pipe water pressure were undertaken. Weather station was also installed at each site to monitor the local weather. Detail information and calibrations of the sensors are discussed in the following sections.

3.5.1 Measurements of soil and pipe temperature

The Campbell Scientific type T thermocouple burial sensors (105T-L) were used for the measurements of soil and pipe temperature. The thermocouples are coated with rubber shield as shown in Figure 3-12 that can be directly buried in soils and attached to the pipe surface. All thermocouples were tested in the laboratory prior to installation by immersing in water of known temperature and compared with the output values. The thermocouples provided instant measurement of temperature.



Figure 3-12 Thermocouples

3.5.2 Measurement of soil suction

The Campbell Scientific 229 thermal conductivity sensor (Figure 3-13 (a)) was used for measurement of soils suction. These sensors consisted of a heating device embedded within the porous ceramic matrix tips, which will increase the temperature within the sensor momentarily. The temperature difference before and after heating is dependent on the surrounding moisture content of the ceramic (ICT International 2007). Therefore soil suction can be measured indirectly from the soil moisture after the sensors were in equilibrium with the surrounding soils. However, moisture

content and heating time varies with the type of soils, and therefore it is necessary to calibrate the sensors with the soil of the site.

The calibration was undertaken using a pressure plate with soils collected from the selected sites. Soil samples from each site were prepared to the moisture content close to liquid limits and compacted by hand into a metal ring on top of a 15 Bar ceramic disc. The soil specimens and ceramic disc were placed inside the pressure plate, and the thermal conductivity sensors were inserted into the soil so that the ceramic components containing the heating devices were fully enclosed by the soil as shown in Figure 3-13 (b). Cables of the sensors were installed with rubber stoppers which could seal off the holes on the steel cover of the pressure plate where the cables were exited through.

The calibration process was started at atmospheric pressure and the sensors were allowed to equilibrate with the soil (i.e., when the sensor outputs became stable). Internal pressure of the pressure plate was then increased incrementally with stages of 30, 50, 150 and 300 kPa. When the internal pressure was increased, water was forced out of the soil and as a result soil suction was increased corresponding to the applied pressure. This is known as the axis translation technique based on the definition of matric suction ($u_a - u_w$). The output values of the sensors at each equilibrium pressure stage would then correspond to that particular suction.

Figures 3-14 and 3-15 illustrate the calibration curves and exponential equations used to convert the sensors temperature outputs into soil suction. Owing to the size of the pressure plate, only 10 sensors could be calibrated at a time. All sensors were calibrated for Altona North site but due to time constraints only 10 out of 15 sensors used in Fawkner were calibrated, the un-calibrated sensors were assigned with the average calibration characteristics.



Figure 3-13 Thermal conductivity sensors: (a) in saturation; (b) in a pressure plate for calibration

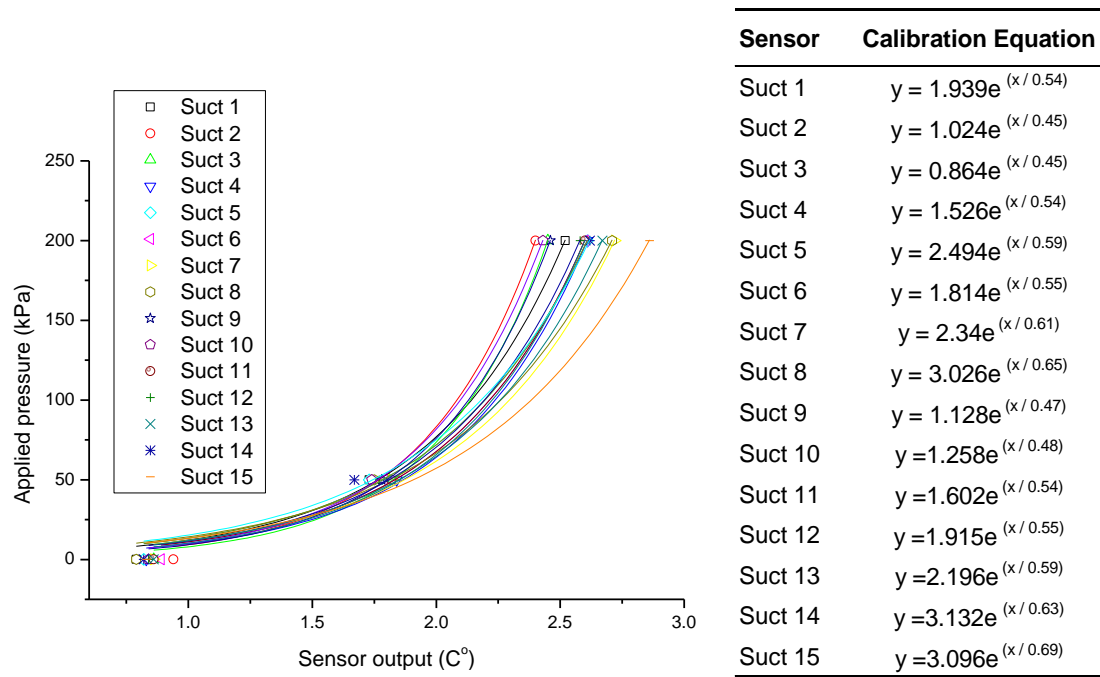


Figure 3-14 Calibration curves of thermal conductivity sensors for Altona North

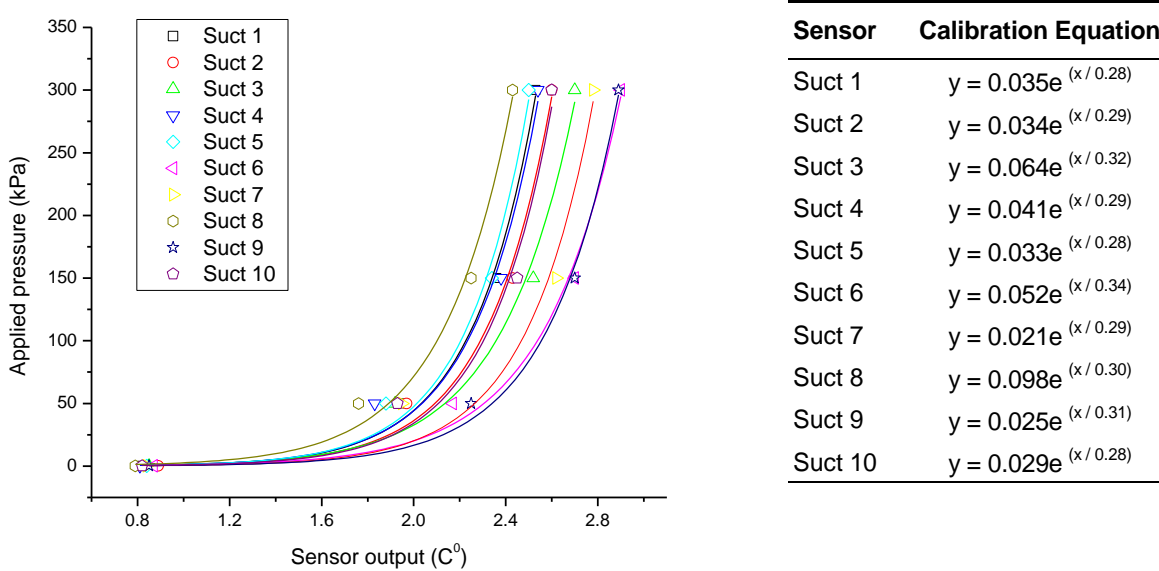


Figure 3-15 Calibration curves of thermal conductivity sensors for Fawkner

3.5.3 Measurement of soil moisture content

The ML2x probes (Theta probes) manufactured by Delta-T Devices (Figure 3-16) were used for measurement of soil moisture content. The Theta probes are capable of measuring volumetric soil moisture content based on the changes of dielectric constant at different soil moisture. Similar to the thermal conductivity sensor, the output of Theta probe varies for soil types. A soil specific calibration was then required for each soil.

Calibration of the Theta probes was undertaken by preparing the soil samples from each site to different moisture content, and then compacted into plastic containers of known volume and mass. The rods of the probes were inserted into the prepared soil samples and the outputs were recorded. The actual gravimetric moisture content of each specimen was determined with the oven drying method (Standards Australia 2005), which was then converted into volumetric moisture content using the dry density of the prepared samples.

Figure 3-17 shows the calibration results of all 15 probes used for Altona North. The relationship between measured volumetric moisture content and the probe output, with factory calibration constant, can be approximated by two straight lines. Hence, two linear equations were used to obtain the volumetric soil moisture content in the field above and below 45% of the probe output. Since the approximately unique two linear relationships can be obtained irrespective of the number of probes, the calibration curve from only one probe was used for Fawkner. Figure 3-18 shows the calibration plot for Fawkner, where a curve and a straight line can approximate the measured volumetric moisture content and probe output. In this case, a logarithm and a linear equation were used to obtain the volumetric moisture content above and below 45% of the probe output.



Figure 3-16 Theta probe

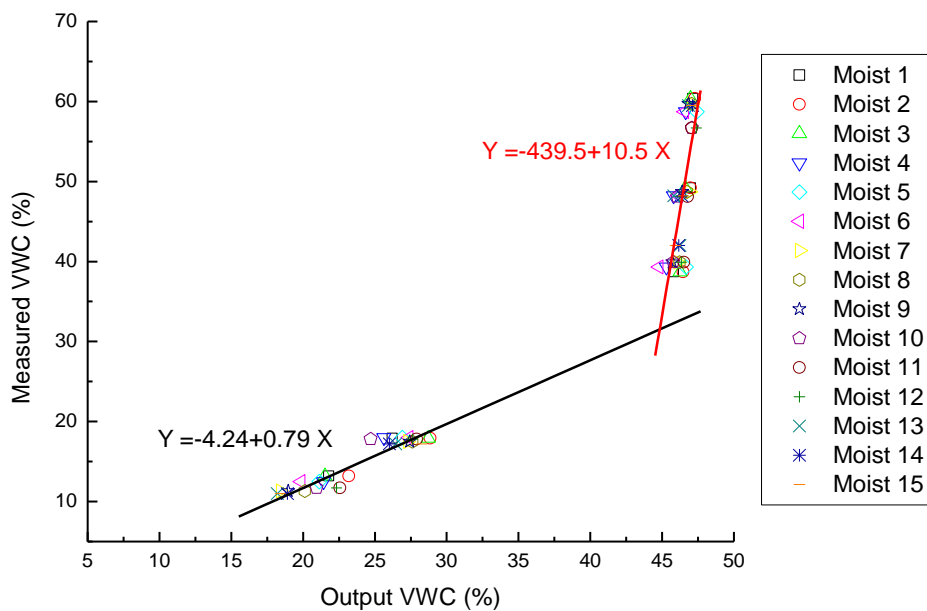


Figure 3-17 Calibration plot of Theta probes for Altona North

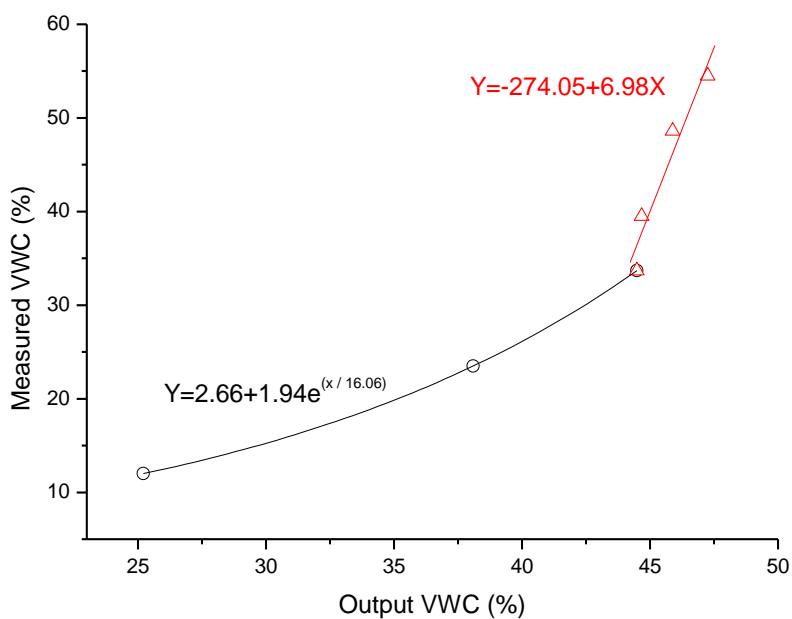


Figure 3-18 Calibration plot of Theta probes for Fawkner

3.5.4 Measurement of soil pressure

Soil pressure exerted on the pipe due to swelling and shrinking was measured by two types of pressure cells; the Geokon model 4800 vibrating wire earth pressure cell (Figure 3-19 (a)) with 1 MPa capacity and the TML model KDE-PA micro-strain earth pressure cell (Figure 3-19 (b)) with 500 kPa capacity. Calibration of the cells was undertaken in the laboratory by applying a known pressure (i.e., dead weight) to the cells and recorded the output values.

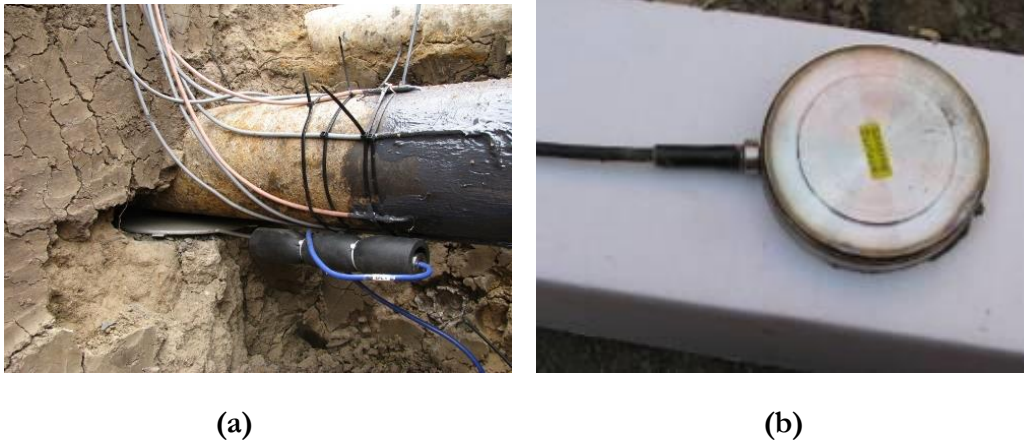


Figure 3-19 Earth pressure cells: (a) vibrating wire type; (b) micro-strain type

3.5.5 Measurement of soil displacement

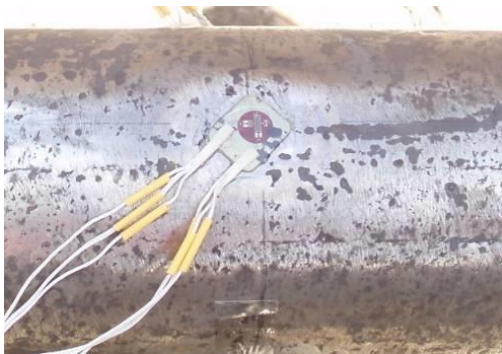
The custom built model 4000 rod extensometer (MPBX) (Figure 3-20) manufactured by Geotechnical Systems Australia was used to monitor the field soil displacement. The rod extensometer consisted of four hydraulic inflatable anchors and a reference head. Depending on the soil profile and depth of the rock on site, the length of the extensometer and location of the anchors may vary. At Altona North, the anchors were located at 0.5, 1.0, 2.0 and 3.0 m from the reference head. At Fawkner, the anchors were located at 0.6, 0.8, 1.0 and 2.0 m from the reference head. The relative soil displacement was measured by the transducers inside the extensometer with respect to the reference head.



Figure 3-20 Rod extensometer (Geotechnical Systems Australia 2011)

3.5.6 Measurement of pipe strain

The 3-wire waterproof biaxial strain gauges (KFW-5-120-D16-11 from Kyowa) as shown in Figure 3-21 (a) and the 3-wire uniaxial strain gauges (N11-FA-5-120-11 from Showa) as shown in Figure 3-21 (b) were used for measurement of pipe strain in Altona North and Fawkner, respectively. The selected strain gauges are thermally compensated for cast iron material with thermal expansion coefficient of $11 \mu\epsilon/^\circ\text{C}$ so that the effect of temperature change could be minimised.



(a)



(b)

Figure 3-21 Strain gauges: (a) 3-wire waterproof biaxial strain gauges; (b) 3-wire uniaxial strain gauges

3.5.7 Measurements of pipe water pressure and temperature

The SITRANS P ZD pressure and temperature transmitters manufactured by Siemens AG (Figure 3-22) were used in Altona North. The pressure and temperature measurement range are 0 to 10 Bar and -50 °C to +200 °C, respectively. Calibrations of the transmitters were performed by applying a known pressure (e.g., controlled air pressure) and by immersing in water of known temperature. The pipe water pressure and temperature were only monitored on the water pipe in Altona North, since the internal pressure of the gas pipe would be almost constant and lower; the pipe temperature was measured by thermocouples installed on the pipe surface.



Figure 3-22 Water pressure and temperature transmitters (Siemens AG 2011)

3.5.8 Measurement of site weather

The local weather of the selected sites was monitored by the Campbell Scientific weather station. The component of the weather station consisted of a tipping bucket rain gauge (CSI model CS700) with measuring range of 0 to 500 mm/hr and resolution of 0.254 mm, an anemometer (wind speed) with measuring range of 0 to 50 m/s and the resolution of 0.5 m/s, a pyranometer (model LI200X) for measurement of solar components, and a temperature and relative humidity sensor (model HMP50) as shown in Figure 3-23. Each component was tested in the laboratory for their responses and the accuracy of measurements in engineering units.

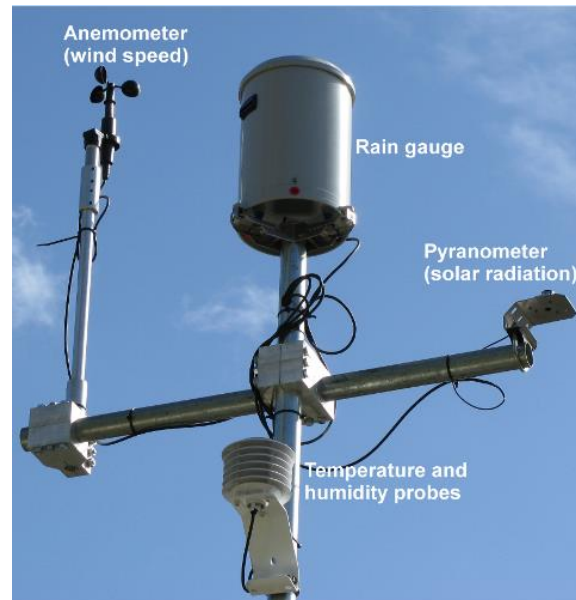


Figure 3-23 Components of the weather station

3.5.9 Summary of the monitoring systems

A summary of sensors and equipment installed at each site is shown in Table 3-5. In addition to these sensors, three sacrificial anodes were attached to the instrumented pipe section close to the strain gauges in order to reduce the corrosion and protect the gauges.

3.5.10 Data acquisition systems

The monitoring system and sensors shown in Figure 3-24 were connected to the Campbell Scientific CR1000 data-logger, CR800 data-logger and the peripherals including, four AM16/32 multiplexers, an AM25T multiplexer to suit thermocouples, an AVWI vibrating wire interface for earth pressure cells, and a CE4 current excitation module for matric suction sensors.

Table 3-5 Summary of sensors and equipment

Measurement	Sensor Type	Altona North	Fawkner
Pipe strain	Biaxial strain gauge (KFW-5-120-D16-11 from Kyowa)	24	-
	Uniaxial strain gauge (N11-FA-5-120-11 from Showa)	-	33
Pipe water pressure & temperature	Pressure and temperature gauges (Sitrans from Seimens)	1	-
Soil temperature	Thermocouple (Type T 105T-L from Campbell Scientific)	15	23
Soil suction	Thermal conductivity sensor (CS229 from Campbell scientific)	15	15
Soil moisture content	Time domain reflectometry (ML2x from Delta-T Devices)	15	18
Soil pressure	Vibrating wire earth pressure cell (Model 4800 from Geokon)	2	2
	Micro-strain type earth pressure cell (TML model KDE-PA from Geokon)	-	4
Soil displacement	Rod extensometer (custom-built 4000 from Geotechnical Systems Australia)	1	1
Air temperature, rainfall, windspeed, relative humidity, solar radiation	Weather station (from Campbell Scientific)	1	1

The data-logging systems were mounted on a wooden board prior to field work to allow for testing of all the sensors in the laboratory. A customized logging program provided by Campbell Scientific was uploaded to the CR1000 data-logger using the Loggernet software. Manufacturer and laboratory calibration factors were embedded in the logging program so that the sensors outputs were converted in the preferred units. The communication of each sensor with the logging systems was

checked by performing benchmark testing. The acquired data were saved on a 2GB compact flash card inserted in the CR1000 data-logger at ten minute intervals. The weather station was connected to the CR800 data-logger for communication and logging. The operation of CR800 was similar to CR1000, and the Loggernet software could be used for both loggers. Data measured by the weather station were stored in the internal memory of CR800 at ten minutes intervals.

Data collection was scheduled for both sites on a monthly basis. The data records in the CR1000 data-logger were collected by swapping the existing flash card with an empty card. The climate data from the weather stations were downloaded from the CR800 data-logger by connecting to a laptop computer using a serial port cable. A view of the data acquisition system in Fawkner is shown in Figure 3-24; the logging systems on both sites were almost identical.

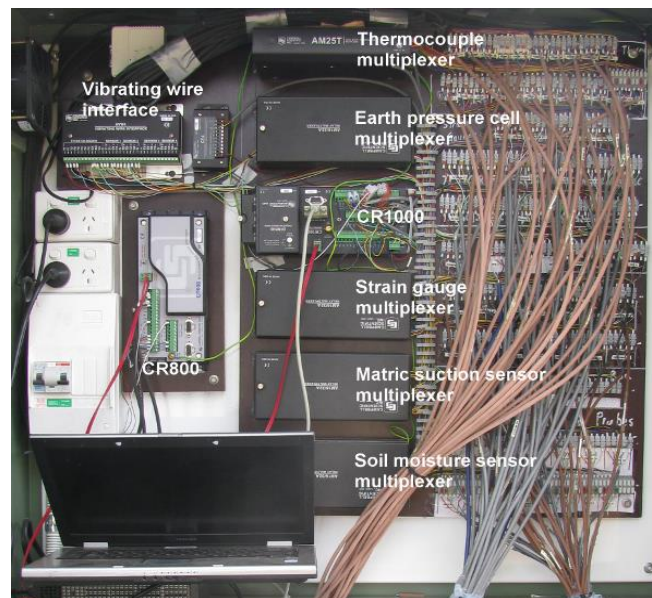


Figure 3-24 Data acquisition system installed at Fawkner

3.6 Field Instrumentation for Monitoring of the Water Pipe

3.6.1 Preliminary works

Preliminary works of the field instrumentation on Altona North, Victoria were carried out on December, 2007. The works were begun with installation of a metal cabinet housing for the data acquisition system. The cabinet with dimensions of 1200 mm x 1000 mm x 300 mm (H x W x B) was mounted on a concrete base of 500 mm x 1300 mm x 400 mm (D x W x B) as shown in Figure 3-25 (a). The concrete base which contained six 63 mm diameter heavy duty electrical 90° conduit bends (Figure 3-25 (b)) was bedded in the soil to a depth of 400 mm. The sensor cables could be sent through the conduits and connected with data acquisition system located inside the cabinet. The cabinet consisted of two compartments; the data acquisition system, and the power outlets and circuit breakers were installed in the top compartment, the 12 V backup battery was stored at the bottom compartment. The two compartments were separated using a partition plate which contained holes the sensor cables could be passed through. Main power was supplied from a nearby power pole to the cabinet through underground cables, and the backup battery would be recharged when the main power was connected.



Figure 3-25 Metal cabinet at Altona North: (a) layout of the cabinet; (b) conduit bends at the base of the cabinet

3.6.2 Field instrumentations and site layout

Majority of the field works, including excavations, sensors installations and connections were carried out on January, 2008. Supplementary field works were undertaken on February and March, 2008 for installations of weather station and rod extensometer, respectively.

The detailed plan of the site with locations of access pits and borehole for rod extensometer is shown in Figure 3-26. The nature strip considered for instrumentation is 23.8 m long and 4.8 m wide, which can provide sufficient access for sensors installation in soils and pipe. The water pipe to be instrumented is buried at 850 mm (to pipe crown) below the ground surface and located 3.16 m away from the boundary of the property. A 100 mm diameter gas pipe was located 2.4 m from the property. A storm water pipe was found at 0.6 m from the road, while overhead power and telecommunication lines were located 6 m above ground surface. Other objects existing on the nature strip were power pole and a small tree as shown in the plan, neither of which interfered with the instrumentation and subsequent measurements.

Instrumentation of the pipe and surrounding soils were undertaken in three primary locations, designated as Pit 1, 2, and 3 as shown in Figure 3-26. Pit 1 was located beneath the driveway, directly under the concrete slab, while Pit 2 and Pit 3 were located 5 m and 15.6 m away from Pit 1, respectively. An additional pit was located 3.4 m away from Pit 3 for installation of the pipe water and temperature transducers. The pit locations were selected to monitor the driveway behaviour of the pipe. In this case, the two driveways were considered as the end supports so that Pit 1 was located at one end, Pit 3 was located at the mid-span and Pit 2 was approximately located at one third of the distance between Pit 1 and 3. Locations of the water pipe joints were not identified, as joints locating by excavations would disturb the current soil condition, while internal pipe scanning with CCTV could have resulted in contamination of potable water supply. Owing to these reasons, the selected locations of the pits and sensors were judged on the basis of intuitive assessment of the likely pipe behaviours.

Each of the Pits 1, 2 and 3 consisted of two pits, the smaller Pit A for instrumentations of the water pipe sections and the larger Pit B for installations of soil sensors. Pit A was excavated to 1.3 m

below the ground surface around the pipe to allow access to the water pipe for instrumentations. Pit B was excavated to 2.5 m or until reaching the basalt rock to allow for installations of the soil sensors. Figure 3-27 illustrates the typical view of an instrumentation pit.

The vertical long-section of the instrumentation pits is shown in Figure 3-28, the locations and types of soil sensors installed at each pit can be identified. Thermocouples, thermal conductivity sensors and Theta probes were installed above and below the pipe by drilling horizontally through the soil at the smaller Pit A of each pit. The installations of these sensors are described in the following sections.

3.6.3 Site excavations

Excavations on the site were preceded with care in order to avoid damaging the buried water pipes and any service connection and buried utility. Designated locations of the pits were marked with spray paint as shown in Figure 3-29 (a). An excavator was used during the operation.

The water pipe was exposed as shown in Figure 3-29 (b). Excavations of soils close to the pipe were undertaken with shovels and crowbars in order to minimise the chance of damaging the pipe. Shoring was set up inside the larger Pit B of each pit to provide protection against soil collapse during installations.

A section of the concrete driveway was removed before excavation of at Pit 1 could be undertaken. The spoils from each pit were transported and stored in another location as separately marked piles. It was deemed to be necessary to avoid the spoils interfering with the site activities. Soils excavated from each pit were backfilled to the same pit after instrumentations. A view of the site during excavation is shown in Figure 3-29 (c).

Address (site-1): 21-23, Mcintosh Rd, Altona North, VIC 3025

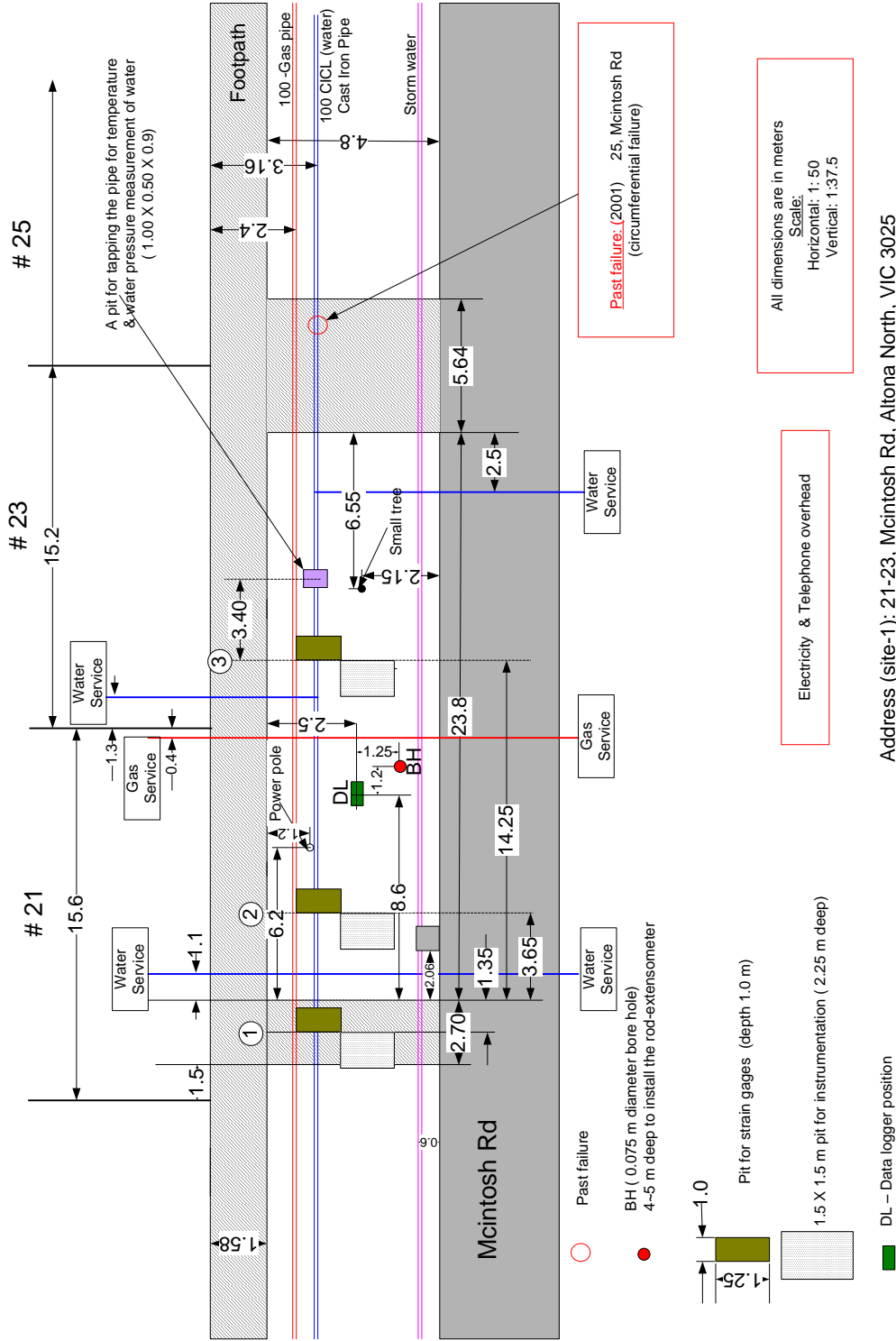


Figure 3-26 Detailed plan of Altona North

Address (site-1): 21-23, Mcintosh Rd, Altona North, VIC 3025

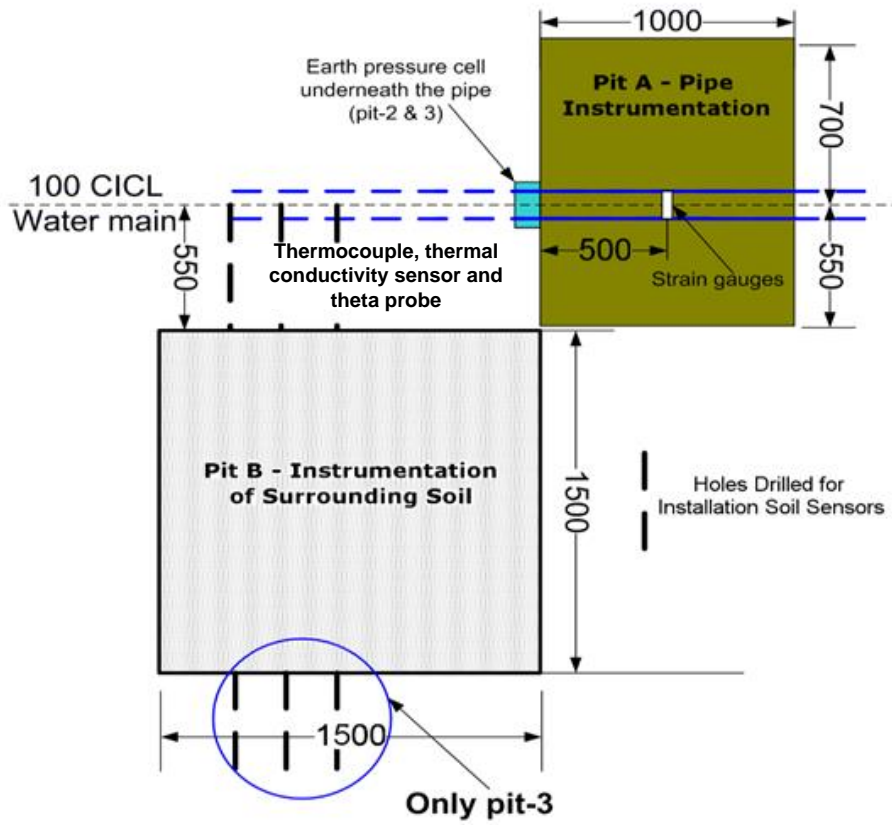


Figure 3-27 Detailed plan of a typical instrumentation pit in Altona North

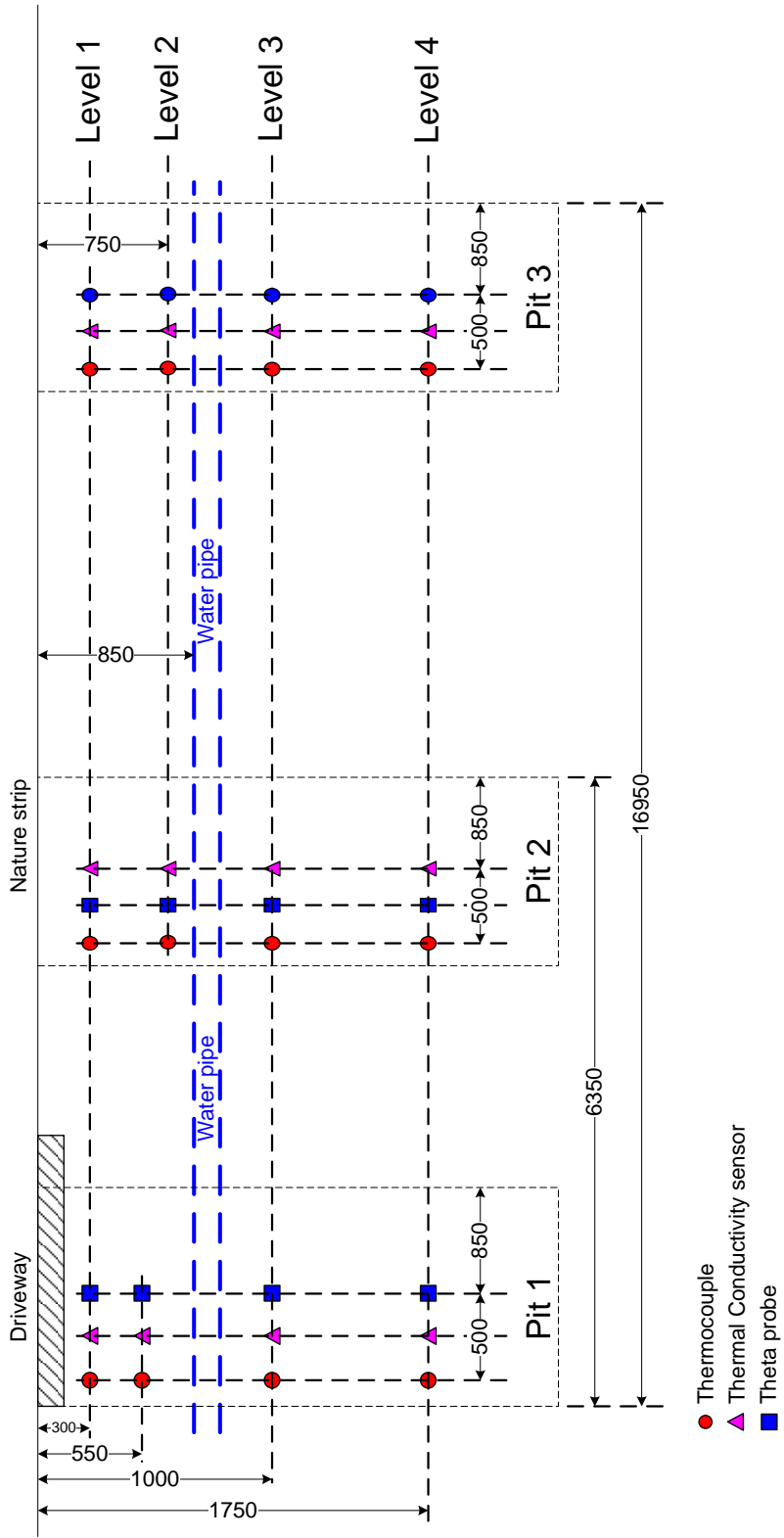


Figure 3-28 Vertical long-section of instrumentation pits in Altona North

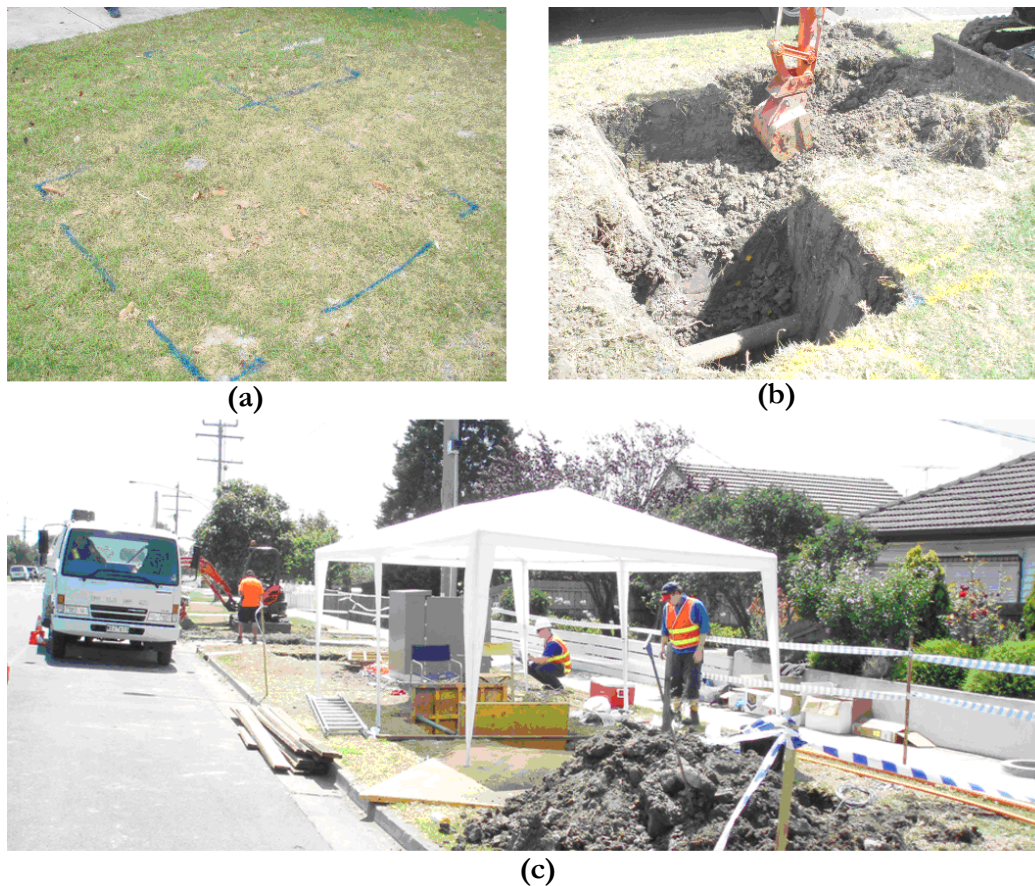


Figure 3-29 Excavations at Altona North: (a) location marking; (b) excavator in operation; (c) a view of the site during excavations

3.6.4 Measurement of pipe wall thickness

The asset data of CWW showed that the cast iron water pipe selected for instrumentation was installed in 1961 with internal diameter of 100 mm. Based on the installation date, it is likely that the pipe has an internal cement lining applied at the time of manufacture. The non-destructive method with the use of ultrasonic gauge was chosen for the pipe wall thickness measurement. Wall thickness of the pipe was determined from the travelling time of ultrasonic waves emitted by the transducer placed on the pipe surface and reflected from the internal pipe surface to the transducer.

The pipe surface was firstly sanded to remove the rust and exposed the bare metal for measurement. A thin layer of glycerine was applied on the bare metal surface to enhance contact between the transducer and the pipe surface. Figure 3-30 shows the pipe wall thickness measurement taken place. Measurements have been undertaken at the top, bottom and two springlines of the pipe in each pit. The average pipe wall thickness was measured to be 8.5 mm.



Figure 3-30 Measurement of water pipe wall thickness with ultrasonic gauge

3.6.5 Strain gauging

Totally twelve strain gauges were installed on the pipe. At each pit, a biaxial strain gauge (consisted of two strain gauges) was installed at the top, bottom, and two springlines of the pipe. The biaxial strain gauges were oriented on the pipe so that one strain gauge would measure the longitudinal pipe strains and the other strain gauge would measure the circumferential pipe strains. The vertical cross-section of the smaller Pit A in Figure 3-31 shows the locations of strain gauges and earth pressure cells. It is important to note that earth pressure cells were only installed in Pits 2 and 3. The details of the installation are discussed in the next section.

Installation of strain gauges was performed with extreme care as the accuracy of the measurements was based on the contact between the strain gauges and the pipe surface. It was necessary to properly protect the strain gauges, especially when the pipe was corroded and would be buried in reactive soils. Fort Burn Pty Ltd., a company which specialises in strain gauging, was

commissioned for the site installation. According to the standard strain gauging procedure, the sections of the pipe to be strain gauged was sanded to expose the bare metal surface and was cleaned with alcohol. Strain gauge adhesive was applied on the strain gauges and carefully attached to the pipe surface using tweezers as shown in Figure 3-32(a). Curing process of the adhesive was accelerated by placing heated vacuum pads on top of the strain gauges as shown in Figure 3-32 (b). The original strain gauges wires were cut off to ensure a good seal when the vacuum pads were placed. Each of the strain gauge was reconnected to a 25 m long shielded data cables. Three layers of waterproofing coating, SEMKIT®, were applied on the strain gauges and the surrounding areas to serve as a protection coating (Figure 3-32 (c)). First coating of SEMKIT® was applied when the adhesive had cured, while the next two coatings were applied 24 and 48 hours after the first coating was applied.

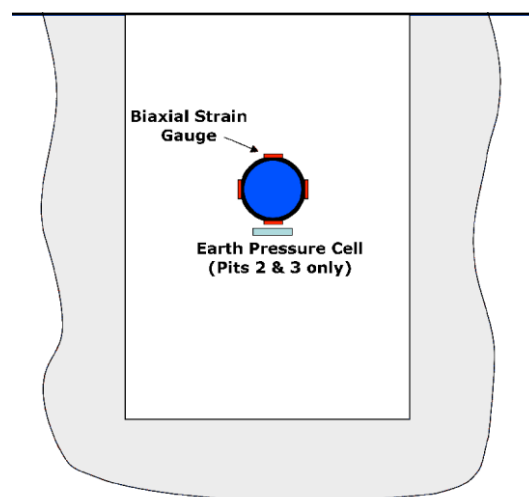


Figure 3-31 Vertical cross-section of a typical instrumentation Pit A in Altona North

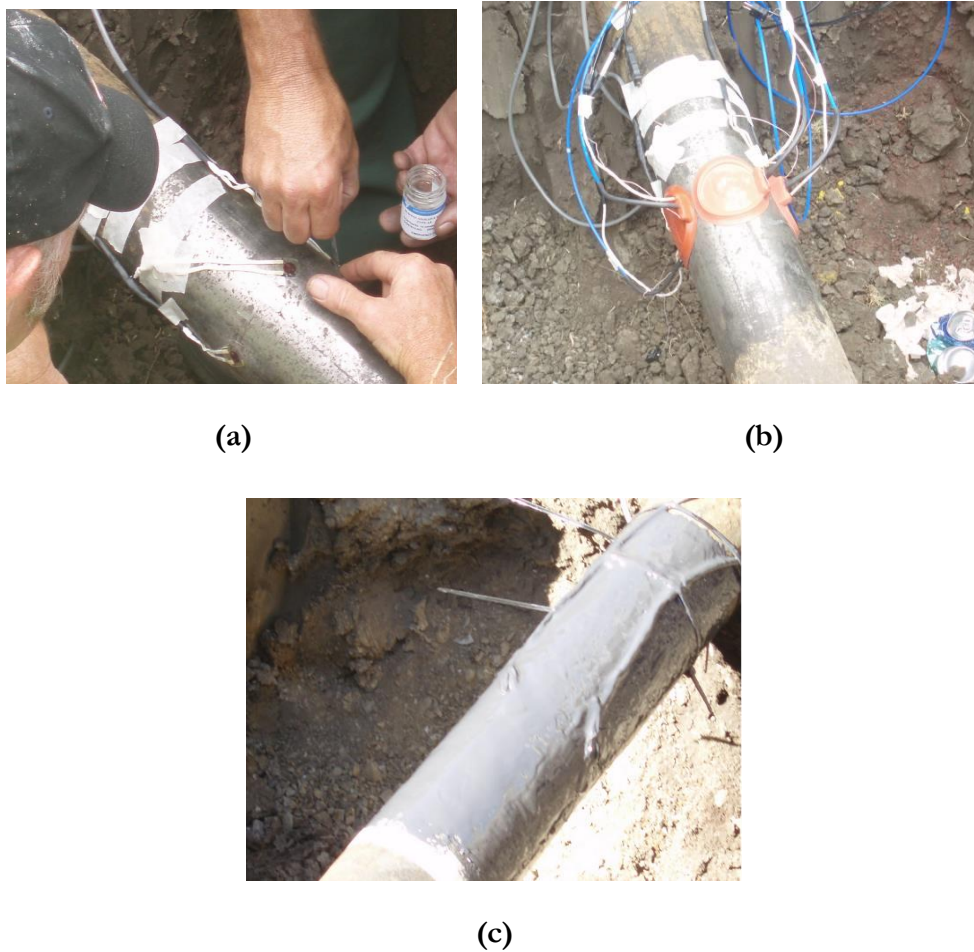


Figure 3-32 Strain gauging on water pipe: (a) strain gauge glued on pipe; (b) curing with heated vacuum pads; (c) coated with SEMKIT®

3.6.6 Installation of earth pressure cells

Earth pressure cells were installed approximately 50 mm beneath the water pipe at Pits 2 and 3, since the change of soil pressure at Pit 1, under the driveway, was expected to be insignificant as the ground surface was sealed off by the impermeable concrete slab. Installation of pressure cells were performed by digging a small hole in the soil wall of the pits beneath the pipe, and prepared a flat base with thin layer of sand to provide a uniform base for the pressure cells to sit on, as shown in Figure 3-33(a). A 200 mm diameter steel plate was placed on each pressure cell to ensure the soil pressure was uniformly disturbed on the cells (Figure 3-33(b)). The same soils

from the hole were filled into the gap between the steel plate and the pipe, and the hole was backfilled close to the initial conditions.



Figure 3-33 Earth pressure cell installation: (a) placed beneath water pipe; (b) with steel plate placed on top

3.6.7 Installations of soil monitoring sensors

Thermocouples, thermal conductivity sensors and Theta probes were installed at four different levels in the smaller Pit B of each pit as shown in the vertical long-section of the instrumentation pits in Figure 3-22. In general, soil sensors were installed in four levels at the depths of 300, 700, 1000 and 1750 mm, except at Pit 1 where a small boulder was found in 700 mm and consequently the sensors were installed at 550 mm. An additional set of soil monitoring sensors was installed in three levels in Pit 3. These sensors were installed at the soil wall closer to the road to monitor the soil conditions on the roadside as shown in Figure 3-34.

The water pipe was located 550 mm inside the pit wall, therefore horizontal holes were drilled to the same length at each level so that the sensors would be located above and below the water pipe. The hole drilling was performed with hand augers (Figure 3-35 (a)) and in total 12 holes was drilled in each pit (Figure 3-35 (b)).

It is essential to maintain good contact between the sensors and soils in order for good measurements to be recorded. As the design of each sensor was different, slightly different installation methods were used. The thermocouple was relatively smaller in size with a flattened sensor head, and therefore a cavity slightly smaller than the sensor head were prepared at the end of the hole with screw drivers prior to installation (Figure 3-36 (a)). The thermocouple was installed by inserting the sensor head into the cavity (Figure 3-36(b)). The thermal conductivity sensor consisted of a circular ceramic head, which were installed by inserting into a cavity slightly smaller than the sensor head created by pushing a wooden dowel into the soil (Figure 3-37(a)). The cavity was enlarged when the sensor head was pushed in (Figure 3-37 (b)) and provided good contact with the soil. The design of Theta probe allowed an easier installation method as it consisted of sensor rods that could be directly inserted into the soil. As shown in Figure 3-38(a), a Theta probe was pushed into the pre-drilled hole with a shortened length electrical conduit and inserted into the soil (Figure 3-38 (b)). All of the soil monitoring sensors were installed horizontal to the ground surface in order to minimise possible measurement error due to non-uniform vertical flow of moisture in soils.

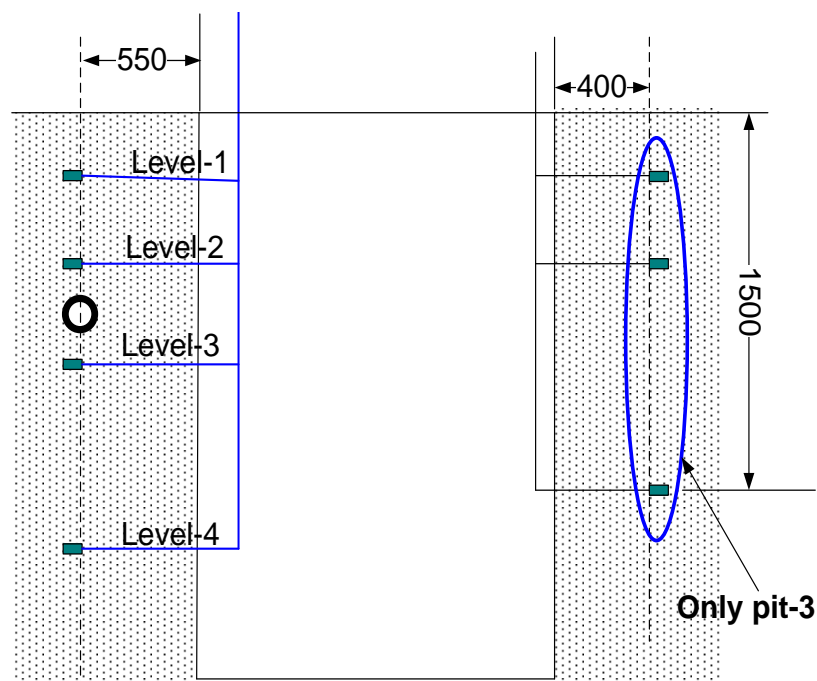


Figure 3-34 Vertical Cross-section of Pit 3 in Altona North



(a)

(b)

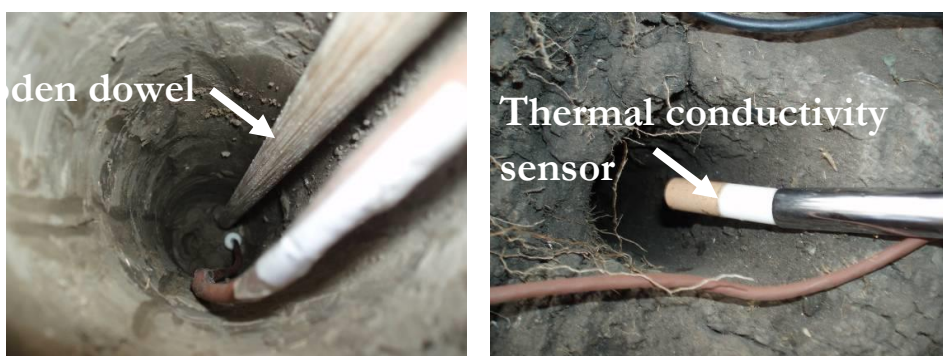
Figure 3-35 Preparation of horizontal holes: (a) drilling with hand auger; (b) a view of the drilled holes



(a)

(b)

Figure 3-36 Installation of thermocouples: (a) prepare a cavity with screw driver; (b) sensor inserted



(a)

(b)

Figure 3-37 Installation of thermal conductivity sensors: (a) prepare a cavity with wooden rod; (b) sensor to be inserted

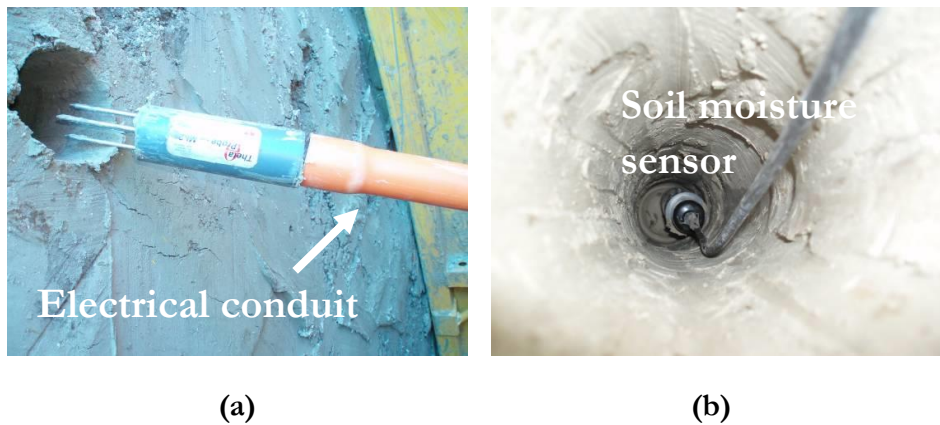


Figure 3-38 Installation of Theta probes: (a) sensor with pins; (b) sensor inserted

3.6.8 Installations of pipe water temperature and pressure gauges

Measurement of pipe water temperature and pressure required the internal sensors of the gauges to be in contact with the water, however due to the regulations of CWW and possible contamination of potable water supply the sensors cannot be placed directly inside the pipe. Instead, a custom built t-piece and a pipe tapping connection were used to divert the pipe water with the gauges installed at the end of the t-piece as shown in Figure 3-39. A plastic manhole with removable cover was installed to enclose the gauges. The manhole was flush with the existing ground surface and provided access to the gauges when required.

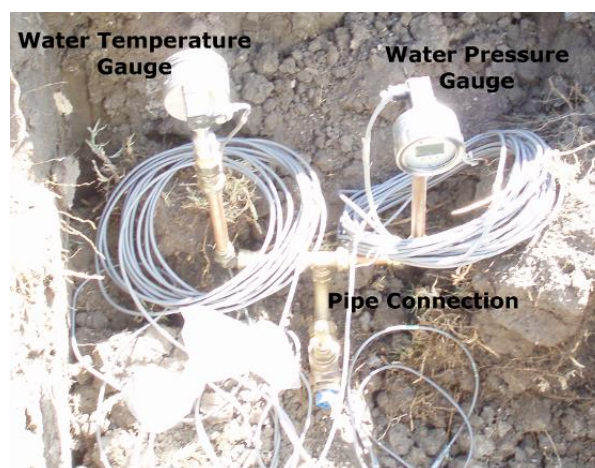


Figure 3-39 Pipe water temperature and pressure gauges in Altona North

3.6.9 Wiring and cable connection

Wiring and connection of sensors cables with the data acquisition systems were undertaken when all sensors were installed. The sensors cables were pinned to the soil wall at each pit as shown in Figure 3-40 (a) to prevent damage during backfill and compaction. The cables were laid out to the full length and tied together, then sent through the conduits to the instrumentation cabinet as shown in Figure 3-40 (b). The sensors cables were trimmed to the required length and connected to the data acquisition system. The measurement data were recorded after connection to ensure the sensors were properly functioning prior to backfilling.



Figure 3-40 Wiring at Altona North: (a) sensors cables pinned to the wall; (b) sending of sensors cables through conduits

3.6.10 Backfilling and soil compaction

Backfilling of the pits were performed with the original soils excavated from each pit (Figure 3-41 (a)) and compacted to the density close to the initial density (same amount of soils excavated from each pit was backfilled), however no *in-situ* density measurements were conducted. The compaction was conducted in four to five layers up to the existing ground level. Water was sprayed on the soil (Figure 3-41 (b)) before compacting with a vibrating plate compactor (Figure 3-41 (c)). Compaction of soils close to the pipe and sensors cables was

conducted manually with hand held compactor and ramming rod to avoid any damage to the pipe and cables.

After backfilling, a temporarily driveway consisted of crushed rock and bitumen surface was built to provide temporarily access for the residents. A new driveway of 300 mm concrete slab was installed few weeks after the field instrumentation was completed. The nature strips were reinstated by grass seeding with topsoil. The turf was watered by CWW from time to time, however the amount of water used for watering has not been recorded. Figure 3-41 (d) shows a view of the site in one year after instrumentation.



(a)



(b)



(c)



(d)

Figure 3-41 Backfilling and reinstatement of Altona North: (a) Backfill with original soils; (b) water sprayed on dry soils; (c) soil compacted with vibrating plate; (d) a view of the site in one year after instrumentation

3.6.11 Installation of weather station

Installation of the weather station was carried out on February 2008. The weather station was pre-assembled on a cross-shaped steel pipe and attached to a 4m long galvanised steel pipe. This setup was installed as an attachment to the instrumentation cabinet so that the weather station was standing 4.5 m above the ground surface (Figure 3-42). The rain bucket was levelled horizontal to the ground surface after installation to ensure the measurement accuracy. The cables of the weather station was sent through the galvanized steel pipe into the instrumentation cabinet, and was connected with the CR 800 data-logger and the data acquisition systems.



Figure 3-42 Weather station on Altona North

3.6.12 Installation of rod extensometer

The installation of rod extensometer was undertaken on March 2008. A bore hole of 75 mm diameter and 3.4 m deep was drilled on site for this installation. The rod extensometer consisted of a reference head and four anchors as illustrated in Figure 3-43. When installed, the rod extensometer was positioned in the hole so that the top 2 m (anchors 1 and 2 which were 0.5 and 1 m from the reference head, respectively) was in the soil, and the bottom 1.4 m (anchors 3 and 4 which were 2 and 3 m from the reference head, respectively) was in the basalt rock.

The rod extensometer was installed by inflating the anchors so that the blades would cut into the soil and the anchors would be moving with the soil when displacement occurred. The bottom section of the rod extensometer was grouted with cement, so that anchors 3 and 4 were fixed to

the rock when the cement was hardened. Remainder of the hole was filled with weak bentonite-cement mixed slurry to provide support for anchors 1 and 2. The extensometer cable was sent through a conduit and connected with the data acquisition systems situated inside the instrumentation cabinet.

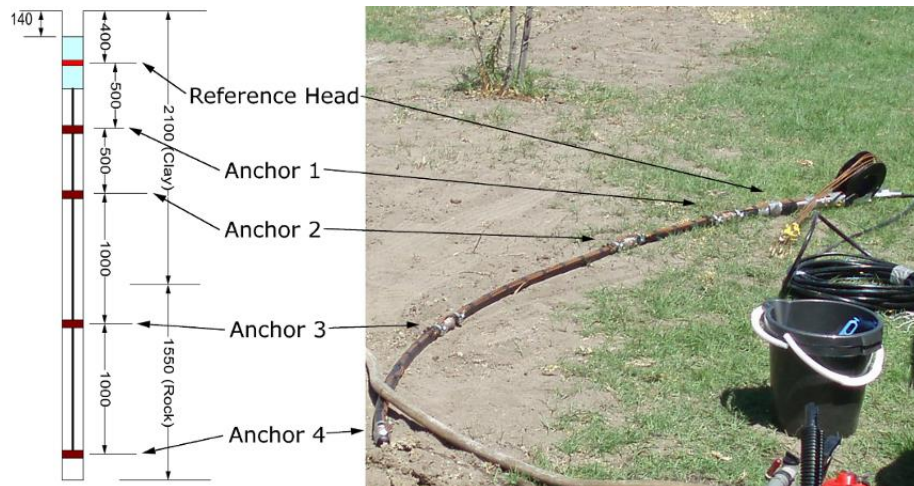


Figure 3-43 Rod extensometer in Altona North

3.7 Field Instrumentation for Monitoring of the Gas Pipe

3.7.1 Preliminary works

The site selected for gas pipe instrumentation was located in Fawkner, Victoria. Preliminary works on installation of the metal instrumentation cabinet was carried out in September 2008. The cabinet in Fawkner was identical to the one installed in Altona North, and the same installation procedure was carried out. Similar to Altona North, power supply was sourced from a nearby power pole with a rechargeable backup battery situated in the cabinet.

3.7.2 Installation of weather station

The installation of the weather station was carried out together with the installation of the cabinet. Same as in Altona North, the weather station was attached to a cross-shaped galvanised

steel pipe and was situated 4.5 m above the ground level. Levelling and wiring were performed and data logging was started when the data acquisition systems were installed in the cabinet.

3.7.3 Field instrumentation and site layout

The main field instrumentation was undertaken approximately a week after the preliminary works on September 2008, while the rod-extensometer was installed in October 2008. The detailed site plan in Figure 3-44 illustrates the location of access pits and other buried utilities on the site. The nature strip considered for instrumentation was 27.5 m long and 3.74 m wide, which provided sufficient spacing for excavations and instrumentations. The gas pipe to be instrumented had an internal diameter of 150 mm and buried at a depth of 650 mm (to pipe centre). It was located 1.8 m away from the property boundary.

The soil and pipe instrumentation was undertaken in three pits similar to instrumentation in Altona North. The locations of the instrumentation pits were designed to avoid interference with other utilities on site. Figure 3-45 illustrates the detailed plan of the instrumentation pits. Pit 1 was located beneath the driveway, while Pit 2 and 3 were located in the nature strip 6.9 and 14.85 m away from the centre of the driveway, respectively. The three pits were selected to monitor the pipe strain between the two driveways similar to the measurement in Altona North, so that Pit 1 was at the end support, Pit 3 was at the mid span, and Pit 2 was located at approximately one third of the distance between Pit 1 and 3. According to the records of SP AusNet, the gas pipe was made up of 2.7 m long pipe segments connected by bolted joints. A joint was found beneath the driveway during excavation and other joints are assumed to be located 2.7 m away from the previous joint as shown in Figure 3-45.

Each of the Pits 1, 2 and 3 consisted of two pits; the smaller pit for pipe instrumentation were excavated to a depth of 1.2 m below the ground level, and the larger pit for soil monitoring sensors installation were excavated to 1.1 to 1.8 m below the ground surface depending on the depth of the found basalt rock. Figure 3-46 shows the vertical long-section (section X-X) and the cross-section (section Y-Y) of the instrumentation pits. Locations of the soil monitoring sensors were also included in the figure.

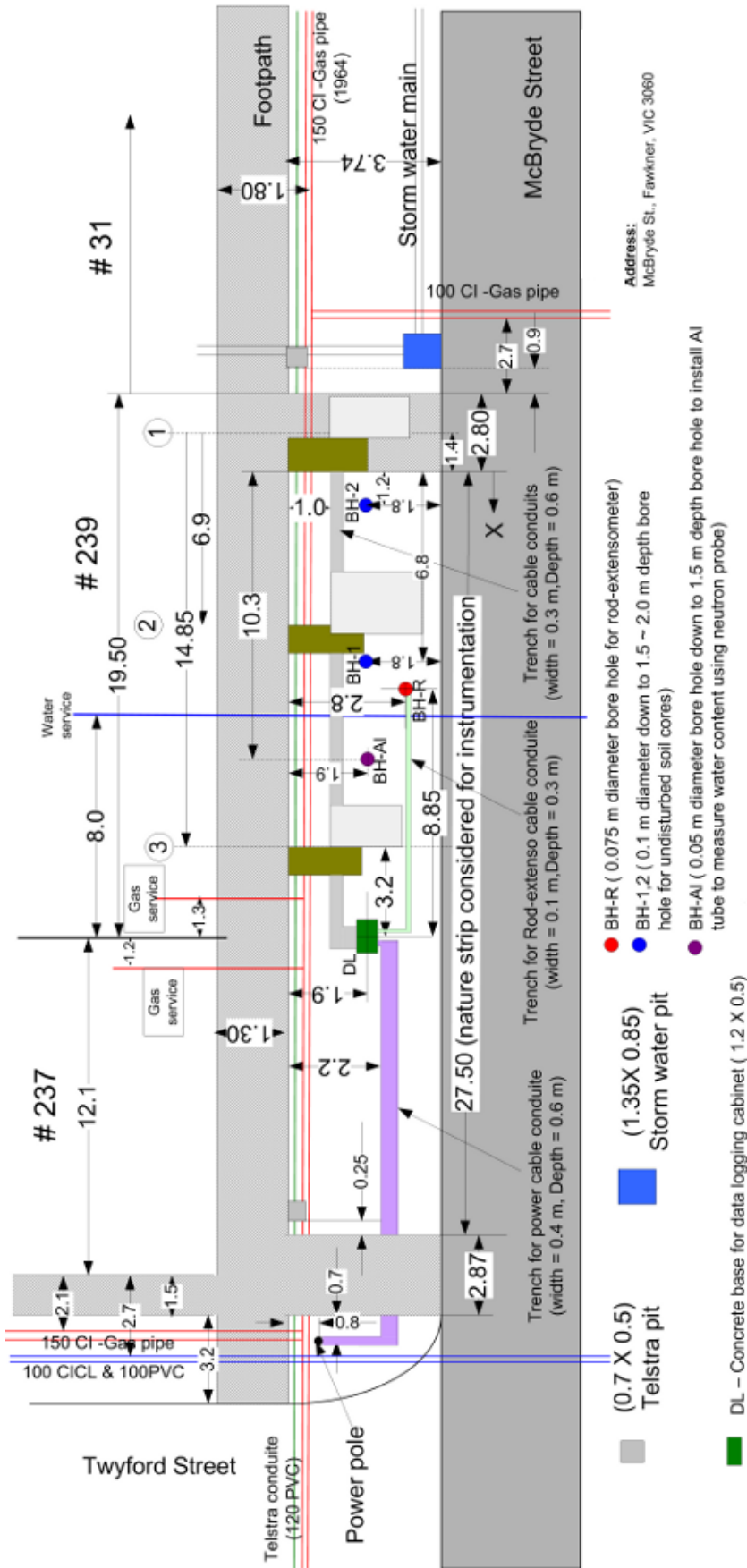


Figure 3-44 Detailed plan of Fawkner

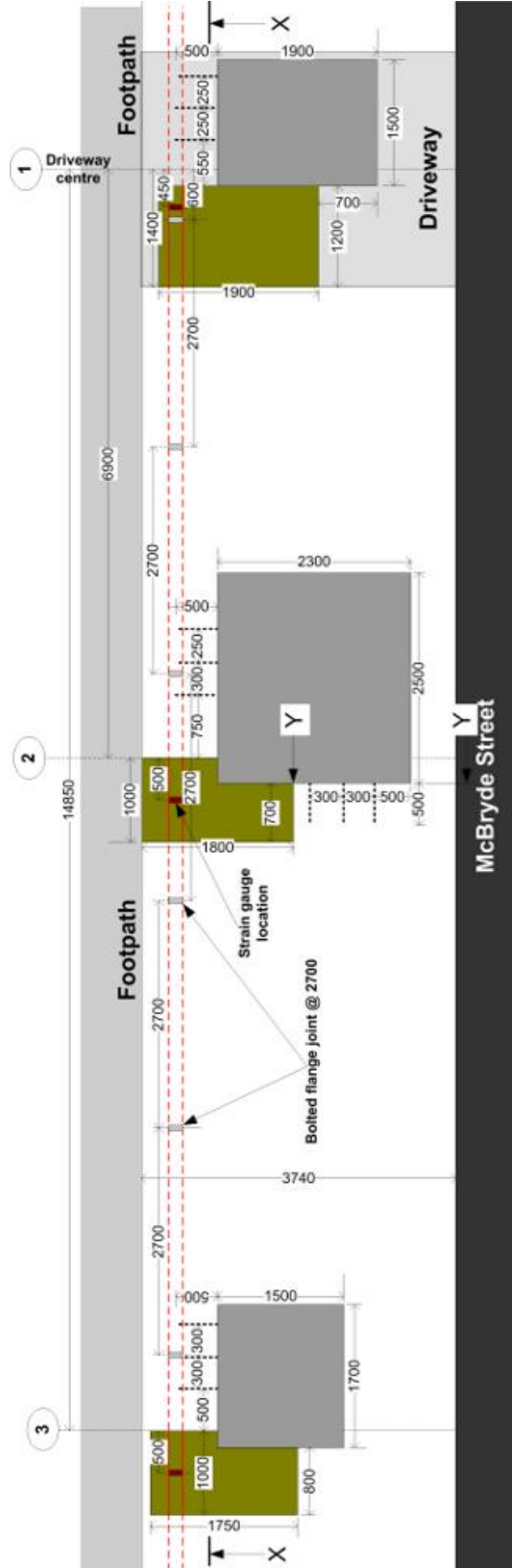


Figure 3-45 Detailed plan of instrumentation pits in Fawkner

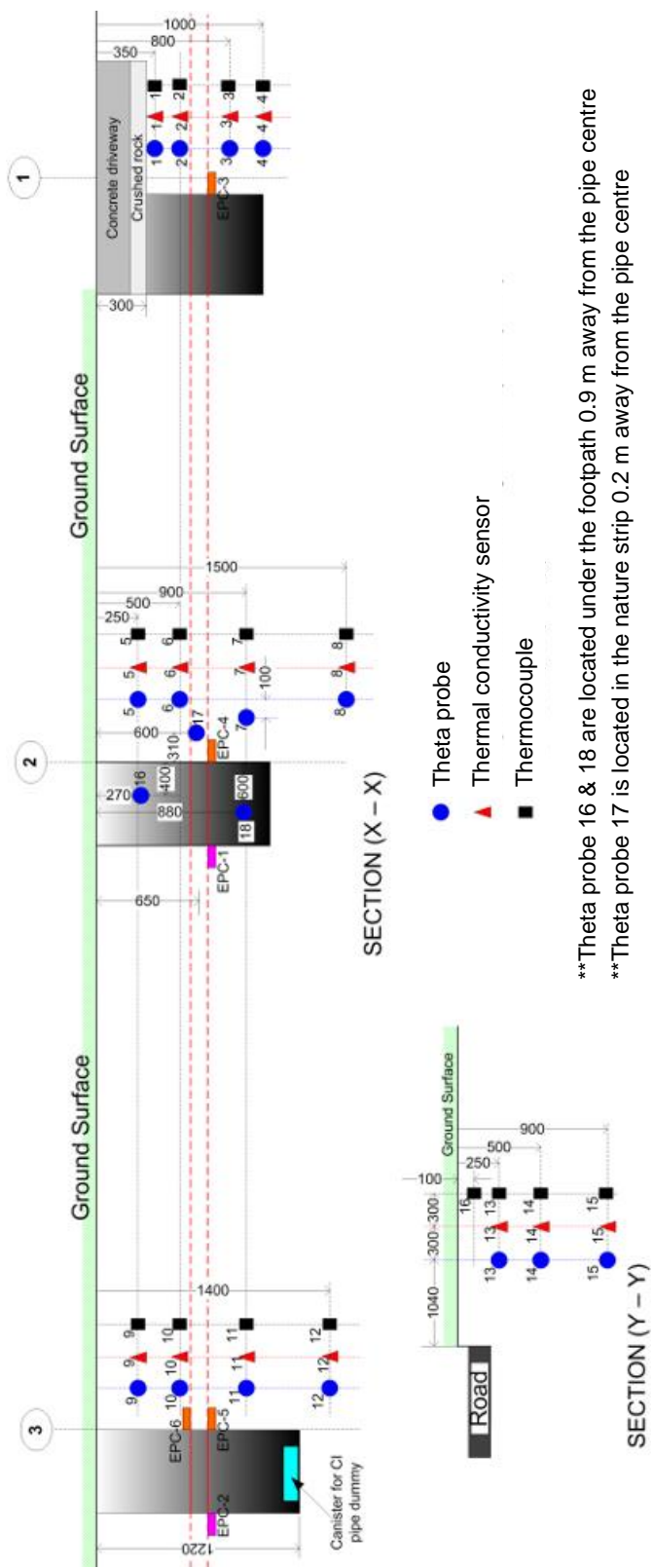


Figure 3-46 Vertical long-section and cross-section of instrumentation pits in Fawkner

3.7.4 Site excavation

The same procedure as in Altona North was implemented during excavation in Fawkner. The locations of buried pipes and other utilities were identified, and the pits locations were marked by spray paint (Figure 3-47 (a)). Site excavations were carried out using an excavator (Figure 3-47 (b)), and the spoils from each pit was transported away and stored in separately marked piles. Figure 3-47 (c) shows that Pit 3 was excavated and safety barriers were set up around Pit 2 at the end of a workday. Shoring was set up in the larger pits prior to sensors installations. Part of the concrete driveway was removed prior to excavation of Pit 1.

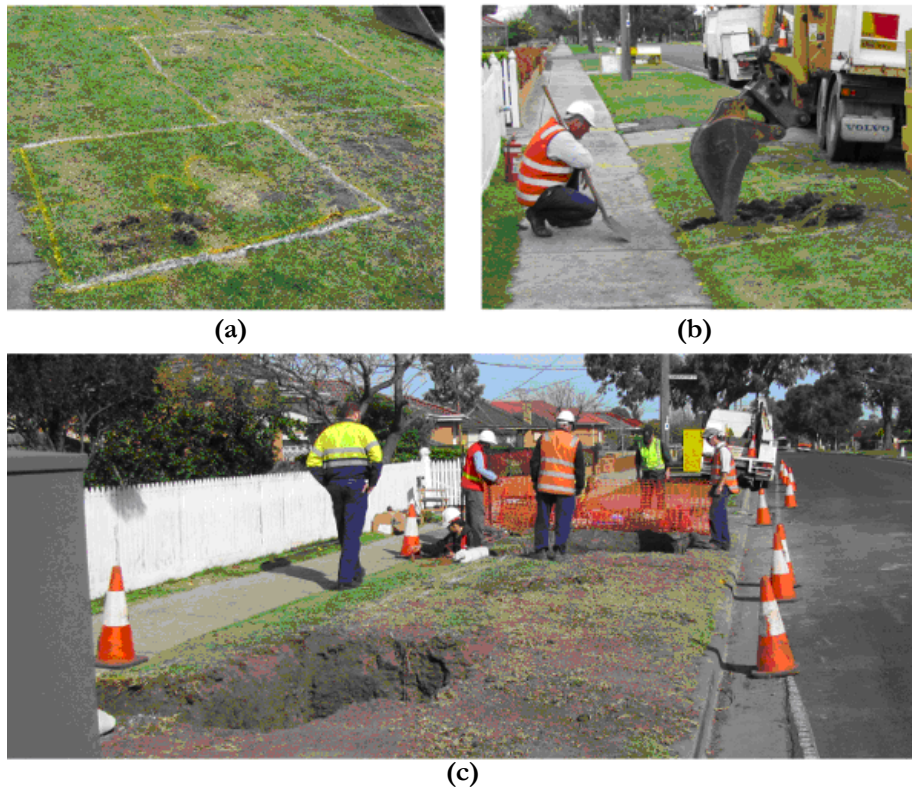


Figure 3-47 Excavation of Fawkner: (a) location marked; (b) excavator in operation; (c) a view of the site

3.7.5 Measurement of pipe wall thickness

According to the SP AusNet records, the cast iron gas pipe installed in 1964 on site has an internal diameter of 150 mm. The pipe surface was cleaned to allow for measurement of pipe wall thickness using the ultrasonic gauge. Same procedure as in Altona North was adopted. Measurements were taken at twelve locations at the pipe top, bottom and two springlines in each pit. The average pipe wall thickness was measured to be 9.9 mm.

3.7.6 Pipe instrumentations

There were totally 30 uniaxial strain gauges installed on the gas pipe. At each pit, two strain gauges (on longitudinal and circumferential directions) were installed at four locations at the pipe top, bottom, and two springlines. In addition, in each pit two uniaxial strain gauges were installed at the top and bottom of the pipe along the longitudinal direction as a backup.

Apart from strain gauges, a thermocouple was also installed on the top and bottom of the pipe in each pit in order to monitor the pipe temperature at locations close to the strain gauges. Figure 3-48 shows the locations of strain gauges, thermocouples and earth pressure cells in a vertical long-section. A cross-sectional view of the gas pipe at each pit is shown in Figure 3-49. Please note that installation of earth pressure cells are described in subsequent section.

The instrumentations of strain gauges and thermocouples were also undertaken by Fort Burn Pty Ltd. The cleaning and preparation process of the gas pipe was same as for the water pipe, and the strain gauges were attached following the same procedures. Figure 3-50 (a) shows the strain gauges and thermocouples installed on the pipe. Layers of waterproofing material, SEMKIT®, were applied as shown in Figure 3-50 (b).

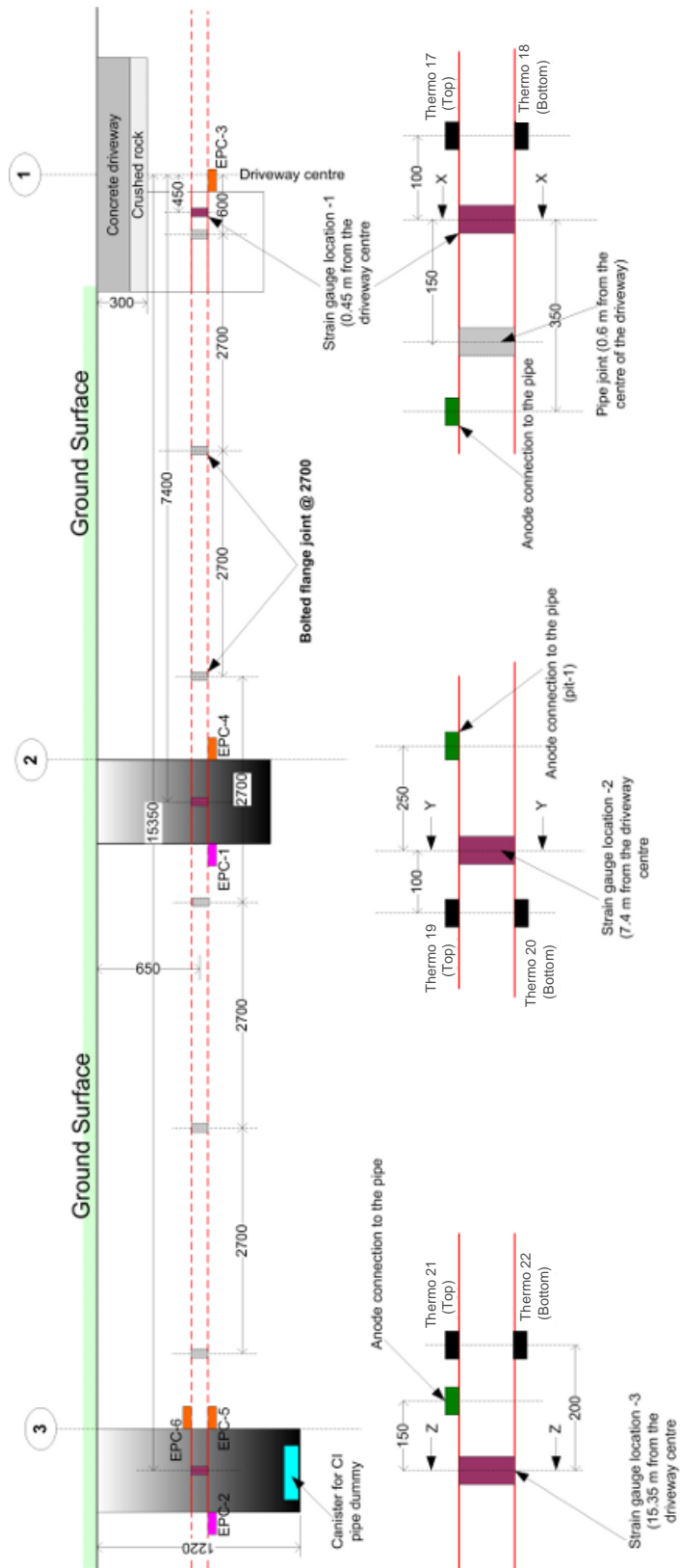


Figure 3-48 Vertical long-section of pipe instrumentation in Fawkner

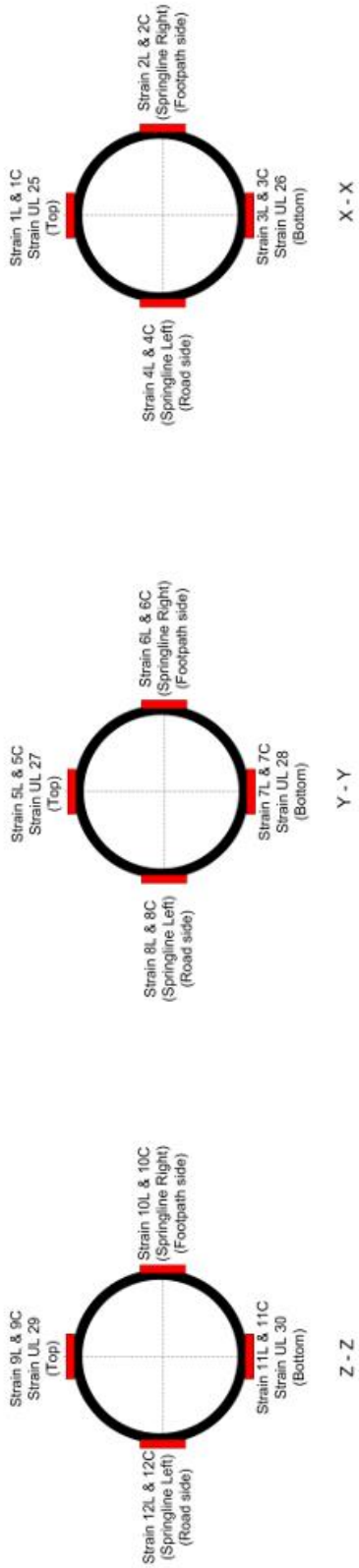


Figure 3-49 Cross-section of the gas pipe and strain gauge



Figure 3-50 Instrumentation on gas pipe: (a) strain gauges and thermocouple installed on the pipe; (b) after application of SEMKIT®

3.7.7 Installation of dummy pipe

Strain gauges could be subjected to expansion and contraction of the cast iron pipe due to temperature change. Correction of this thermal expansion effect can be minimised by using thermally compensated strain gauges. However further correction can be performed by measuring the strains of a cast iron pipe section similar to the instrumented gas pipe, buried in the same conditions, but not subjected to any load.

In order to enhance the pipe strain measurements, a dummy pipe was installed on site to correct the thermal expansion. The dummy pipe was a 280 mm long cast iron pipe section instrumented with two uniaxial strain gauges (on longitudinal and circumferential directions) and a thermocouple as shown in Figure 3-51. The dummy pipe was placed in a plastic canister and buried in the smaller pit of Pit 3 next to the instrumented pipe.

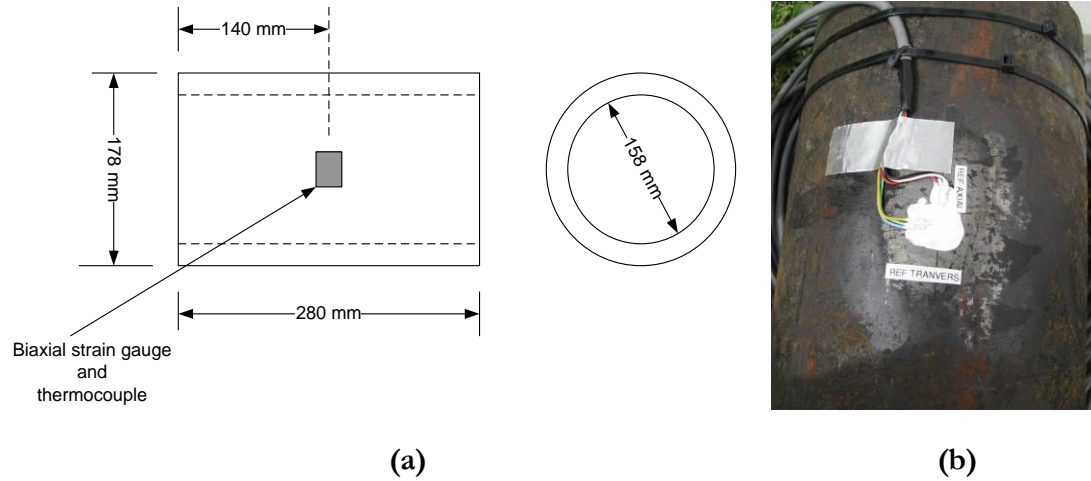


Figure 3-51 Instrumented dummy pipe: (a) Schematic diagram; (b) strain gauges and thermocouples installed

3.7.8 Installation of earth pressure cells

Same type of vibrating wire earth pressure cells as in Altona North was used in Fawkner. In addition, four micro-strain type earth pressure cells were installed directly above and beneath the gas pipe to measure the soil pressure acting on the pipe (Figure 3-48). Installation methods of both pressure cells were similar to Altona North, except that the no steel plates were placed on the pressure cells so that a more direct measure of soil pressure could be obtained. The surrounding areas were then backfilled with the original soil. Figure 3-52 (a) shows a micro-strain type earth pressure cell installed on top of the gas pipe and a vibrating wire type earth pressure cell installed beneath the pipe is shown in Figure 3-52 (b). Only a micro-strain type was installed in Pit 1 as the change of soil pressure under the driveway is expected to be significantly small.



Figure 3-52 Earth pressure cell: (a) a micro-strain type installed above the pipe; (b) a vibrating wire type installed beneath the pipe

3.7.9 Installations of soil monitoring sensors

Soil monitoring sensors were installed at four levels in the larger pits of Pit 1, 2 and 3. The locations of the sensors were shown in Figure 3-46 the vertical long-section and cross-section of the pits. During installations, boulders were found at different depths on the soil walls, and therefore the sensors locations in several pits were shifted as shown in the long-section. An additional set of soil sensors were installed at three levels in Pit 2 away from the pipe. Additional Theta probes were also installed at Pit 2; one in the nature strip at the same depth as the instrumented pipe, and two under the footpath at 270 and 900 mm beneath the ground surface. These probes were installed to monitor the moisture content at the nature strip and beneath the footpath for comparison with the measurements made along the pipe profile. Installation methods of the monitoring sensors were same as in Altona North, except a motor auger was used for hole drilling on the soil wall as shown in Figure 3-53, which speeded up the installation progress.



Figure 3-53 Horizontal drilling in preparation of sensor installation

3.7.10 Wiring and cable connection

The sensors cables were pinned on the soil wall and sent through the conduit as in Altona North. The sensors were connected to the data acquisition systems and the preliminary data were recorded to ensure the functionality of all sensors before backfilling.

3.7.11 Backfilling and soil compactions

All of the pits were backfilled with the original soils and compacted to the density close to the initial following the same procedures as described for Altona North. The compactions at each pit were done in layers of four to five, where loose soils were spread out and sprayed with water before compacted with a vibrating plate compacter. A temporarily driveway was constructed with crushed rock and bitumen as shown in Figure 3-54 (a). Reinstatement of the site was undertaken by SP AusNet after the instrumentation. A view of the site in two years after instrumentation is shown in Figure 3-54 (b).



Figure 3-54 Reinstatement of Fawkner: (a) temporary driveway; (b) a view of the site after reinstatement

3.7.12 Installation of rod extensometer

The rod extensometer was installed in October 2008 following the same procedure as in Altona North. A schematic diagram of the rod extensometer is shown in Figure 3-55. The extensometer was positioned in the pre-drilled hole that anchor 3 was fixed to the rock by the cement grout, while anchors 4, 5 and 6 were situated in the soil by a weak bentonite-cement mix at 1.0, 0.8 and 0.6 m from the reference head, respectively.

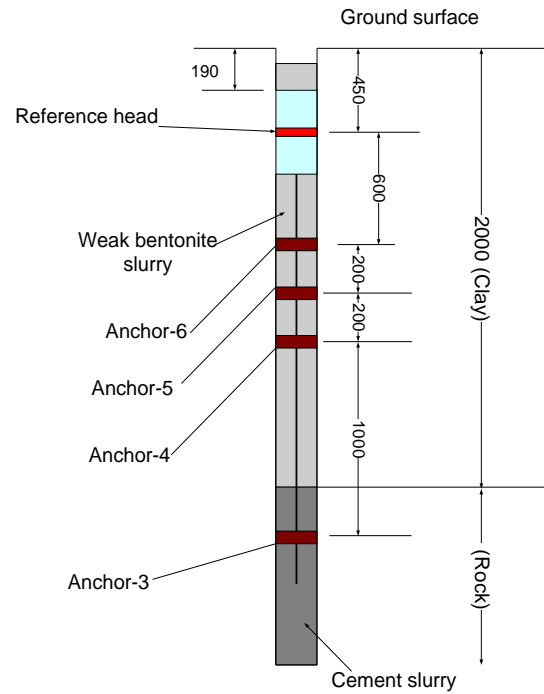


Figure 3-55 Schematic diagram of rod extensometer installed in Fawkner

3.8 Conclusions

The preliminary work and field instrumentation of buried in-service water and gas pipes were presented in this chapter with detailed information on the forensic analysis, site selection criteria, instrumentation procedures, and sensors calibrations and installations. The analysis of field data and the behaviour of soil-pipe interaction based on the data collected from the field are presented in the subsequent chapters.

CHAPTER 4

INTERACTION OF BURIED PIPES WITH SOILS AND CLIMATE

4.1 Introduction

The field instrumentations undertaken on in-service water and gas pipes at Altona North and Fawkner were described in Chapter 3. Analysis of the data collected from Altona North between January 2008 and February 2011, and from Fawkner between September 2008 and May 2011 is presented in this chapter. In particular, the effect of changes in soils and prevailing climate on the behaviour of buried pipes is discussed.

The collected field data were in binary format and converted by the Loggernet software to CSV format files. The converted raw data were processed with corresponding calibration factors and used in the analysis. Part of the field data presented in this chapter was published in research reports, RR 10, 13, 16 and 17 (Gallage *et al.*, 2008; 2009; Chan *et al.*, 2010a; 2010b).

4.2 Effect of Variations of Pipe Water Pressure

The water pressure of the instrumented pipe at the Altona North site was recorded during the monitoring period in order to investigate the effect of variations in the pipe water pressure on the behaviour of buried water pipes.

Since the daily water pressure recorded during the monitoring period was only slightly varied, a typical record of a three week period from the 7th to the 27th of April 2008 is presented. Figure 4-1 shows the cyclic fluctuations of pipe water pressure measured during the selected period. The maximum and minimum water pressures were measured as 754 kPa and 650 kPa, respectively. A plot of the daily water pressure calculated as the average pressure recorded in weekdays and weekends during the three week period is shown in Figure 4-2. The maximum daily pressure was recorded at around 5:00 am on weekdays, and minimum pressure at 9:00 am, showing that pressure changes were due to the morning activities of the residents.

The recorded fluctuations of water pressure were purely related to water usage of the local residents with a water pressure difference of approximately 100 kPa, while major pressure transient events that resulted in a significant increase or decrease of pressure were not observed. As shown in the mechanical testing results in Table 3-1, the tensile strength of failed cast iron pipes ranged from 128 to 252 MPa, and therefore the pressure difference of 100 kPa would not affect the strength of the buried water pipe.

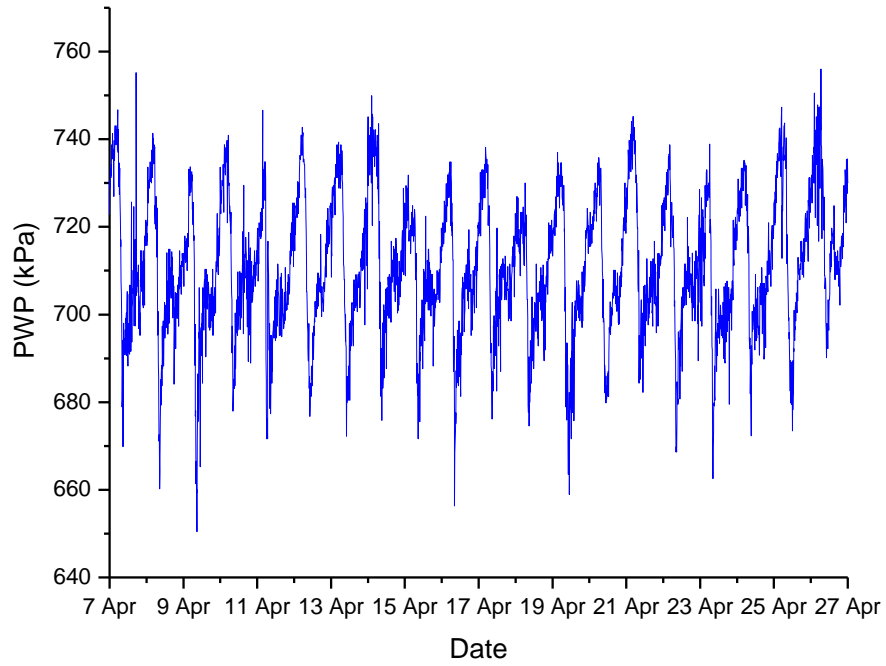


Figure 4-1 Typical pipe water pressure at Altona North for a three week period

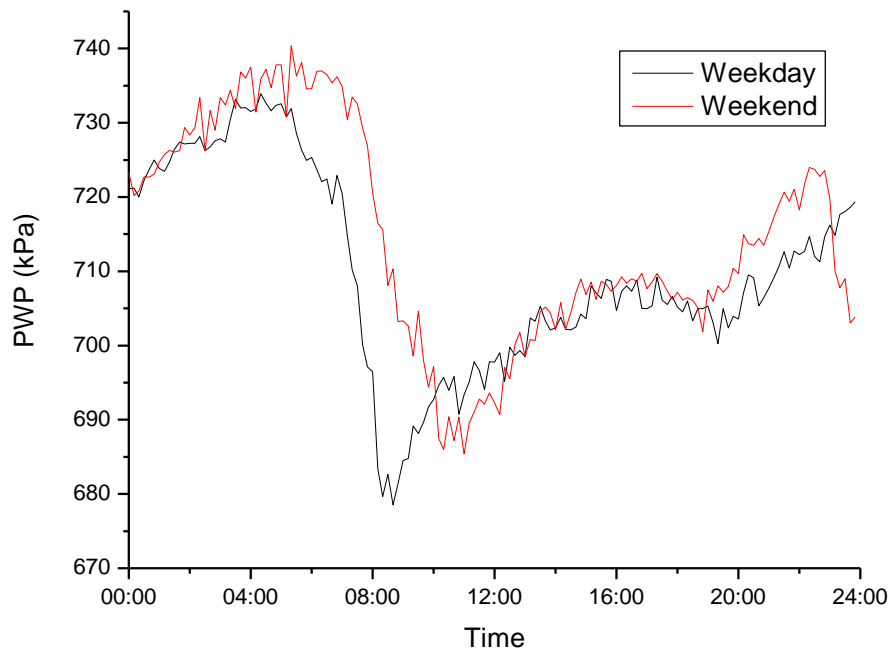


Figure 4-2 Daily average pipe water pressure at Altona North

4.3 Relationship between Air, Soil, and Pipe Temperature

In order to understand the effect of seasonal changes in air temperature on soil and pipe temperatures, the measured air, soil, and pipe temperatures from the instrumentation sites were analysed.

4.3.1 Altona North results

The measured soil temperature is plotted in Figure 4-3 to Figure 4-6 according to the pit locations. The measured air temperature and pipe water temperature are also shown for comparison purposes. The cyclic seasonal variation in soil temperature was observed in all of the pits, where a maximum soil temperature of 28°C was recorded in February and March, and a minimum of 10 °C was recorded in July and August. The soil temperature measured at a depth of 300 mm closely followed the trend of measured air temperature, while the soil temperature at greater depths of 550 to 1750 mm also varied between hot and cold seasons but not as much.

In Pit 1 beneath the driveway, the air temperature has a significant effect on the soil temperature at shallow depths. Figure 4-3 shows that the variation of soil temperature at 300 mm was approximately 2 to 3 °C greater than other pits beneath the nature strips. This is due to the fact that the concrete driveway has higher thermal conductivity than the vegetation and soils on the nature strips. Variations of soil temperature at greater depths (i.e., beyond 1000 mm) in Pit 1, however were very similar to the temperature variations in other pit locations (Figure 4-4, Figure 4-5, and Figure 4-6).

In all pits, the soil temperature at a depth of 1000 mm generally varied between 12 and 23 °C; and at 1750 mm, soil temperature varied between 14 and 22 °C. The variation of soil temperature beneath the nature strips between the depths of 300 to 1750 mm was approximately -2.5 °C per metre in summer and +2.5 °C per metre in winter.

The pipe water temperature measured on the water pipe located at a depth of 850 mm showed a better agreement with the soil temperature measured beneath the nature strip (i.e., Pits 2 and 3) at a depth of 300 mm than the depths of 700 and 1000 mm. A reasonable explanation of this behaviour is that the pipe water temperature transducer was installed on the t-piece located above the pipe in a covered pit and was not buried by soils, so that the temperature of the water inside the t-piece became closer to the temperature inside the pit rather than that in the pipe. Hence, the measured pipe water temperature was not the actual water temperature inside the pipe.

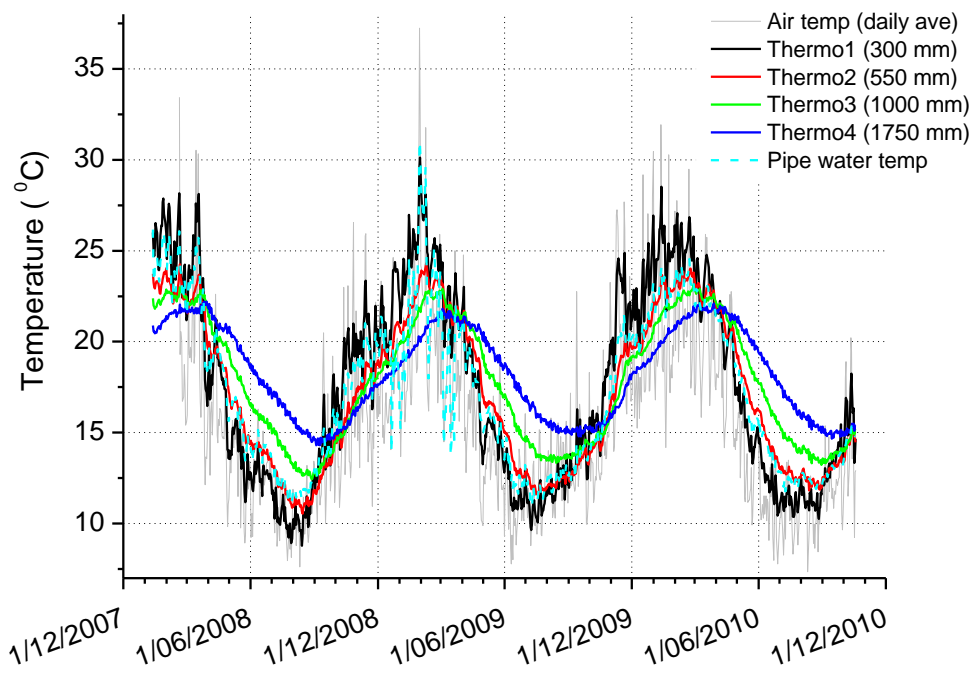


Figure 4-3 Soil and pipe temperature in Pit 1 at Altona North

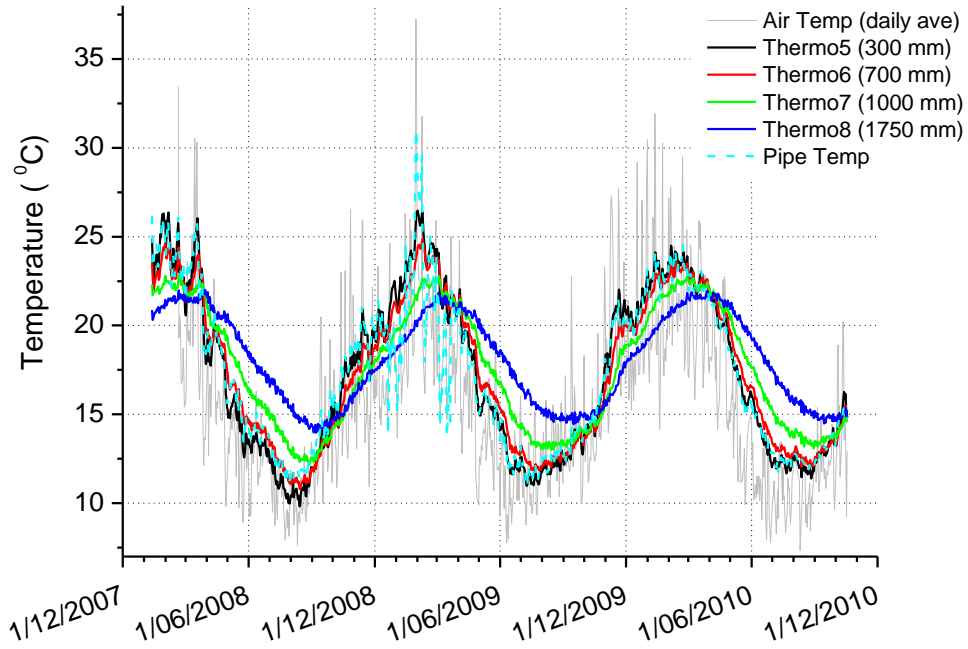


Figure 4-4 Soil and pipe temperature in Pit 2 at Altona North

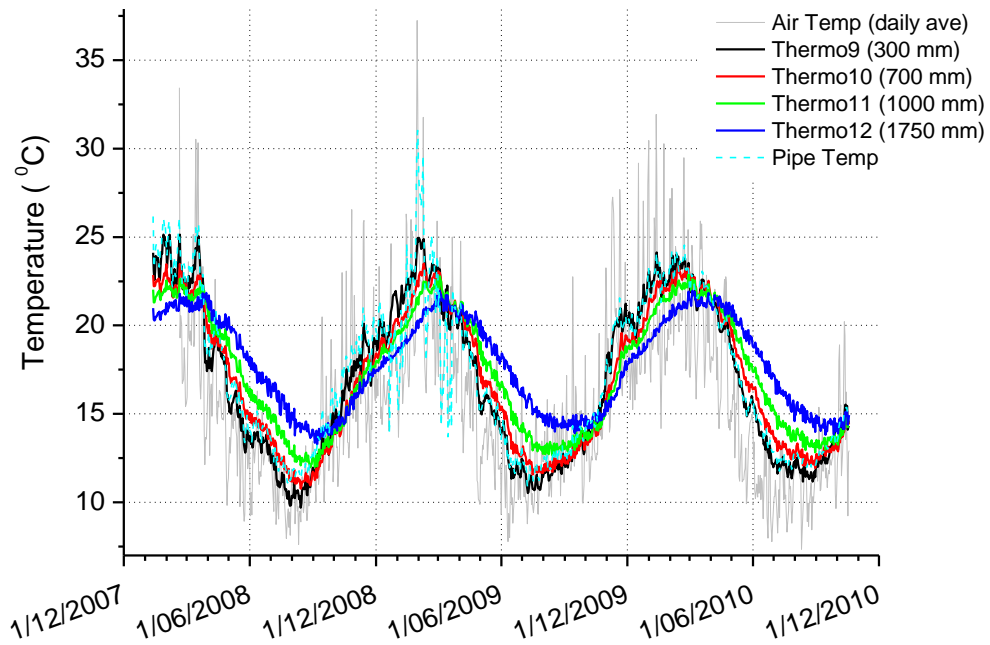


Figure 4-5 Soil and pipe temperature in Pit 3 at Altona North

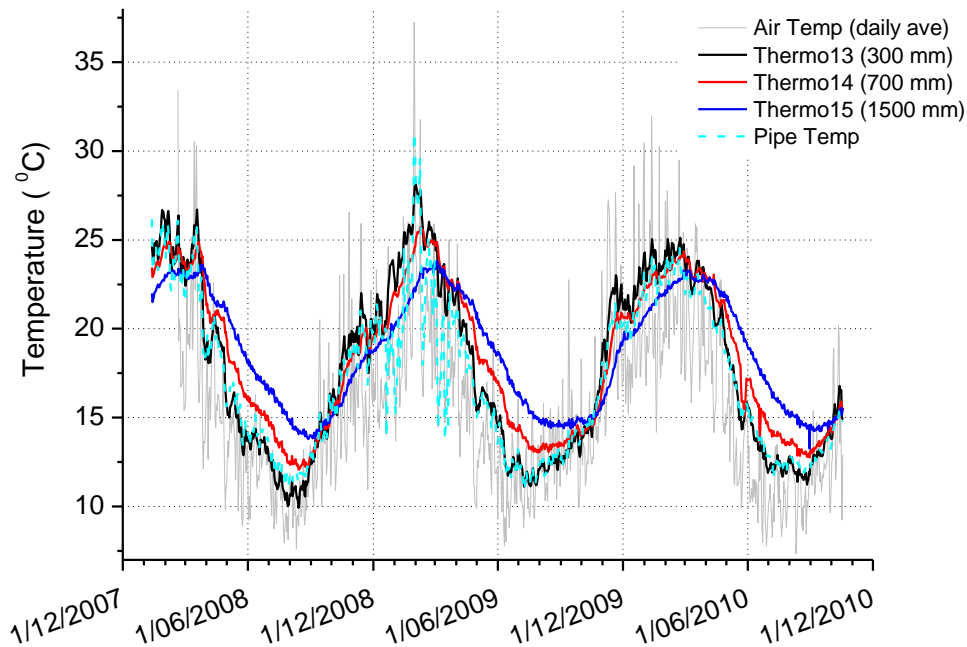


Figure 4-6 Soil and pipe temperature in Pit 3 on roadside at Altona North

4.3.2 Fawkner results

The soil temperature measurements are shown in Figure 4-7 to Figure 4-10. Similar to Altona North, the soil temperature was closely related to seasonal variation of air temperature.

In Pit 1 (Figure 4-7), the thermal effect of soils at shallow depth beneath the concrete driveway, similar to Altona North, was observed. The measured soil temperature at 350 mm in Pit 1 showed greater variation than the temperature measured at the same depth in other pits under the nature strips (Figure 4-8, Figure 4-9, and Figure 4-10), while soil temperature measured at greater depths (i.e., greater than 500 mm) was similar regardless of the pit locations.

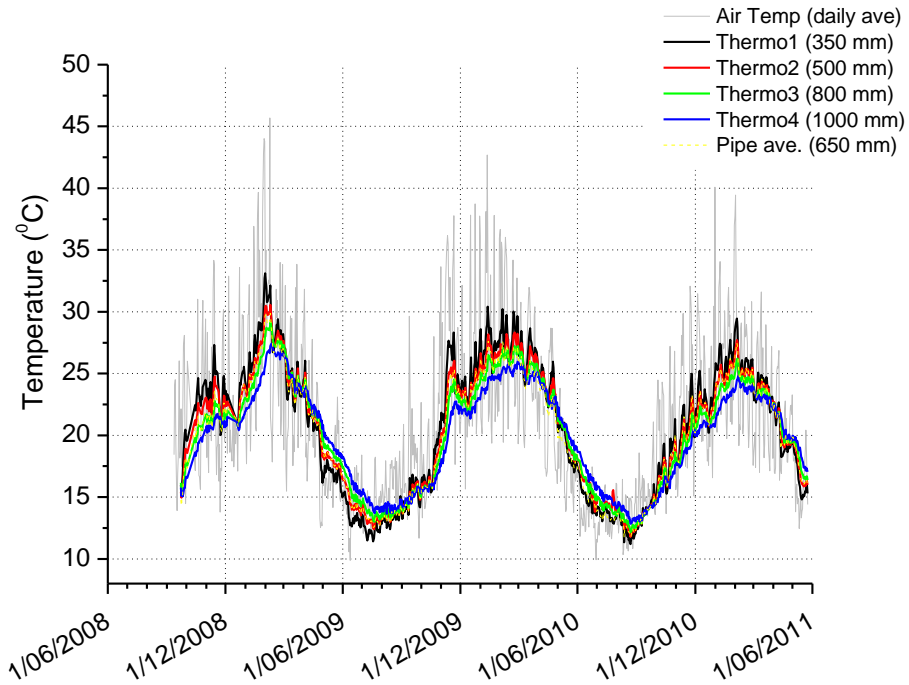


Figure 4-7 Soil and pipe temperature in Pit 1 at Fawkner

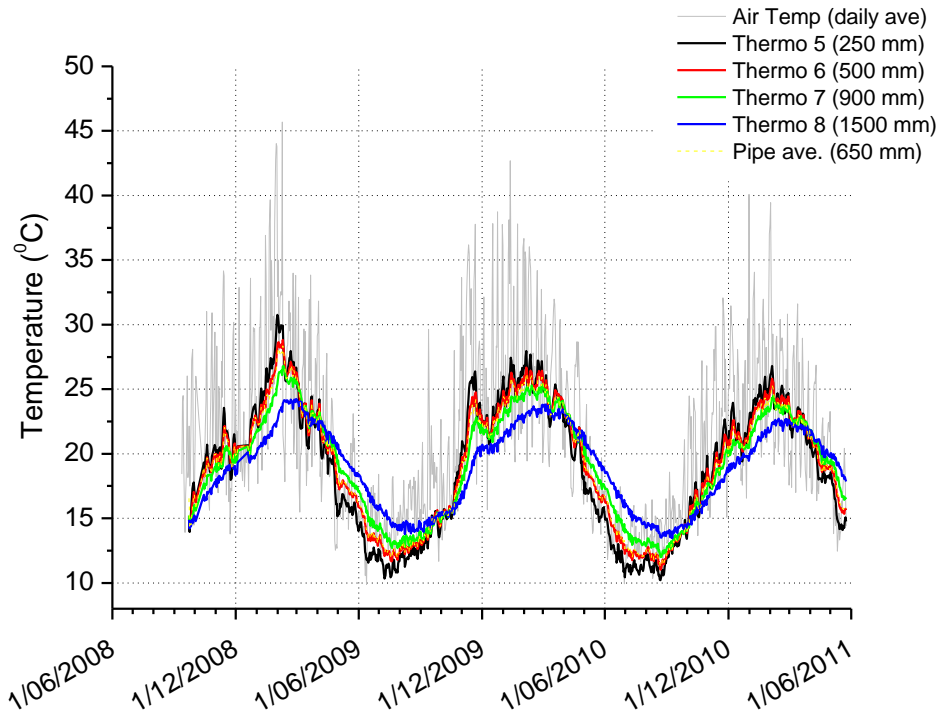


Figure 4-8 Soil and pipe temperature in Pit 2 at Fawkner

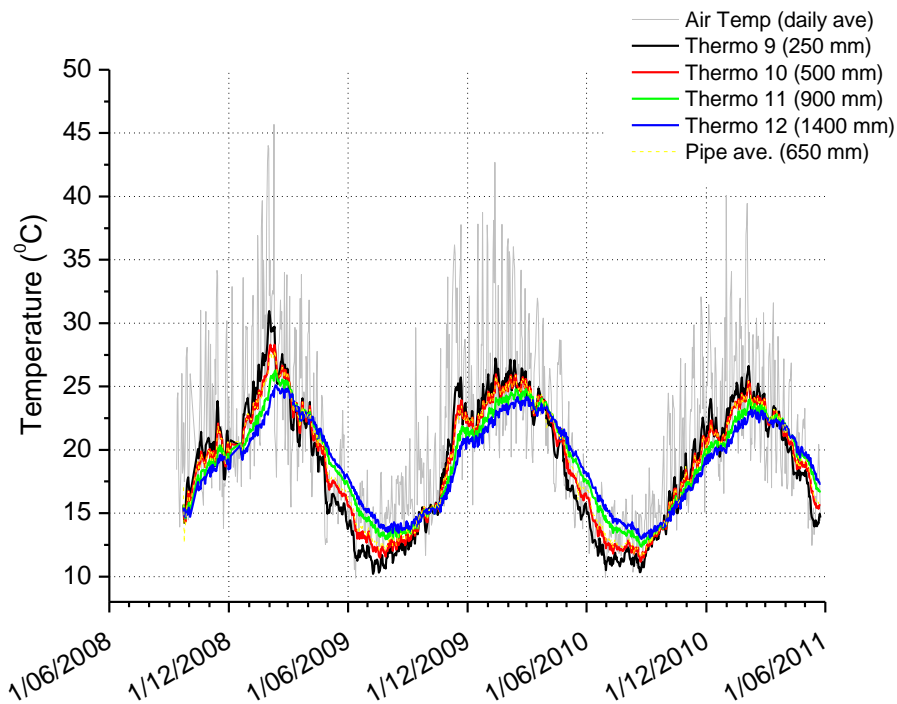


Figure 4-9 Soil and pipe temperature in Pit 3 at Fawkner

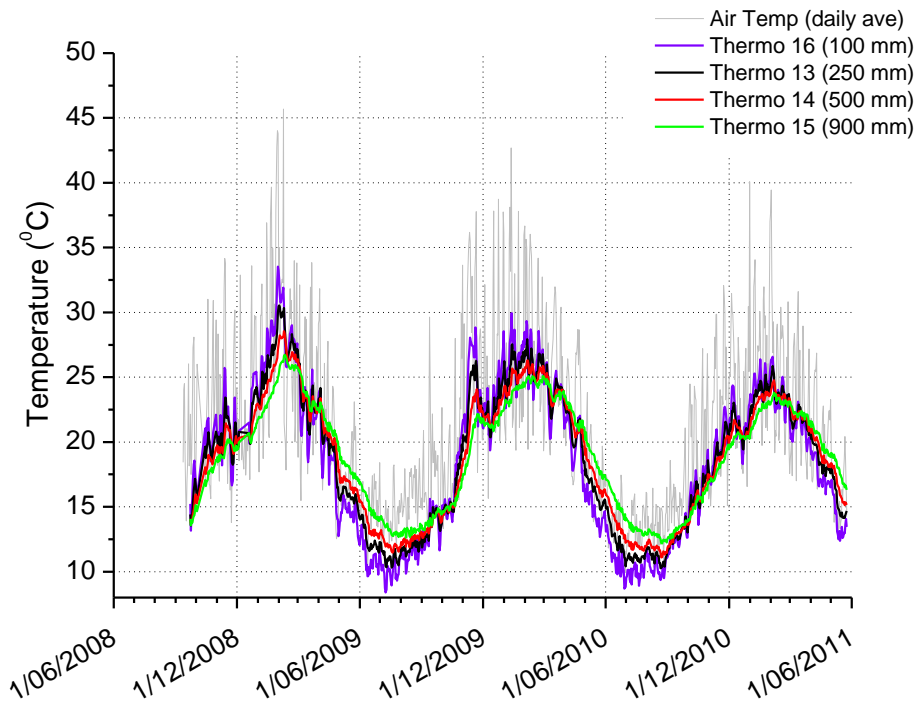


Figure 4-10 Soil and pipe temperature in Pit 2 on roadside at Fawkner

In all pits, the range of soil temperature, measured at the depths of 900 and 1000 mm, was 14 to 27 °C; and at the depths of 1400 and 1500 mm, was 14 to 24 °C. The variation of soil temperature beneath the nature strips from 250 to 1500 mm was approximately -3 °C per metre in summer and +3°C per metre in winter.

The pipe temperature measured on the gas pipe buried at a depth of 650 mm showed good agreement with the soil temperature measured at 500 and 900 mm. Thus, the gas pipe was considered in a state of thermal equilibrium with the surrounding soils. Seasonal variation of pipe temperature was approximately ± 7 °C from an average of 20 °C throughout the monitoring period.

4.3.3 Summary

The temperature measurements from both sites indicate that variations of soil and pipe temperature are directly affected by the seasonal variations of air temperature, and the types of the ground cover. In addition, temperature of the pipe is directly related to the soil temperature at the burial depth.

4.4 Relationship between Rainfall, Soil Moisture Content, and Soil Suction

The matric suction and volumetric moisture content of soils at the instrumentation sites were measured in order to study the relationship between rainfall and variations of soil moisture content at various depths. The data logging interval of the theta probes (TP) and thermal conductivity sensors (TCS) was ten minutes, but the daily average values, which provide smoother curves for analysis, were used for the plots. For comparison purposes, the volumetric soil moisture content, soil matric suction, and daily rainfall are plotted together in the figures.

4.4.1 Altona North results

Figure 4-11 to Figure 4-13 show the measured moisture content and suction values at each depth were generally correlated to each other, as the recorded soil moisture content increased when the soil suction decreased. However, it can be observed that the TPs provided more robust measurements than the TCSs, as the suction values tended to approach zero quickly when soil moisture content increased. Anomalous behaviours were observed in the TPs and TCSs installed along the buried pipe side at Pit 3 that the soil moisture content measurements only varied by 3 to 4 % and matric suction measurements decreased to zero for an extended period of time. These behaviours were possibly due to malfunction of the sensors, and therefore the data of this location were not considered in the analysis. The data measured on the road side at Pit 3 did not show any anomalous behaviour and were considered in the analysis.

In Pit 1 (Figure 4-11), the response of soil sensors to rainfall was not immediate, as the impermeable concrete driveway sealed the ground surface. Changes in soil moisture content and suction were slow and required a few weeks to a month for the sensors at greater depths (i.e., greater than 500 mm) to show a corresponding wetting or drying peak.

In Pit 2 (Figure 4-12), the response of soil sensors beneath the nature strips to rainfall was slightly different to the response in Pit 1. A major difference was a more instantaneous response to rainfall, especially at a depth of 300 mm, where sudden increase of soil moisture content and decrease of soil suction due to intense rainfall were recorded by TP5 and TCS5. These sudden changes can be observed in May, July and December 2008, April and November 2009, and March and October 2010. Similar but slightly delayed responses were recorded by the sensors installed at a depth of 700 mm. At greater depths of 1000 and 1750 mm, Pit 2 showed similar responses to those in Pit 1. A seasonal cyclic variation in moisture content was observed, with maximum value at March and minimum value at September. At the end of 2010, a series of intense rainfall events occurred, and significant increase in soil moisture content was observed at all depths except at the depth of 1750 mm.

At Pit 3 on the roadside away from the pipe (Figure 4-13), good correlation of measured data with rainfall was observed for the sensors at a depth of 300 mm. As for Pit 2, a significant increase in soil moisture content due to a series of intensive rainfall events at the end of 2010 was recorded by the sensors in all depths at Pit 3 roadside. Similarly, the seasonal cyclic variations in soil moisture content recorded at the depths of 1000 and 1750 mm in Pits 1 and 2 were also observed.

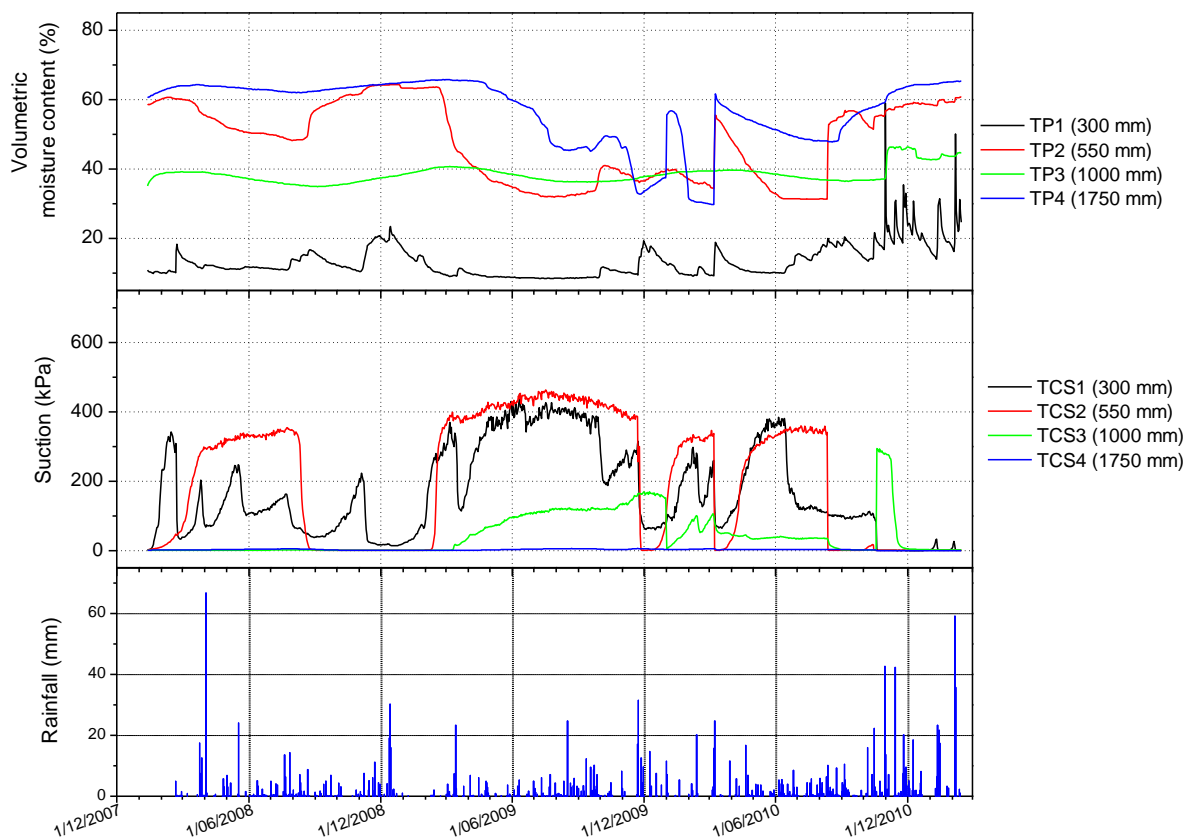


Figure 4-11 Soil volumetric moisture content, suction and daily rainfall in Pit 1 at Altona North

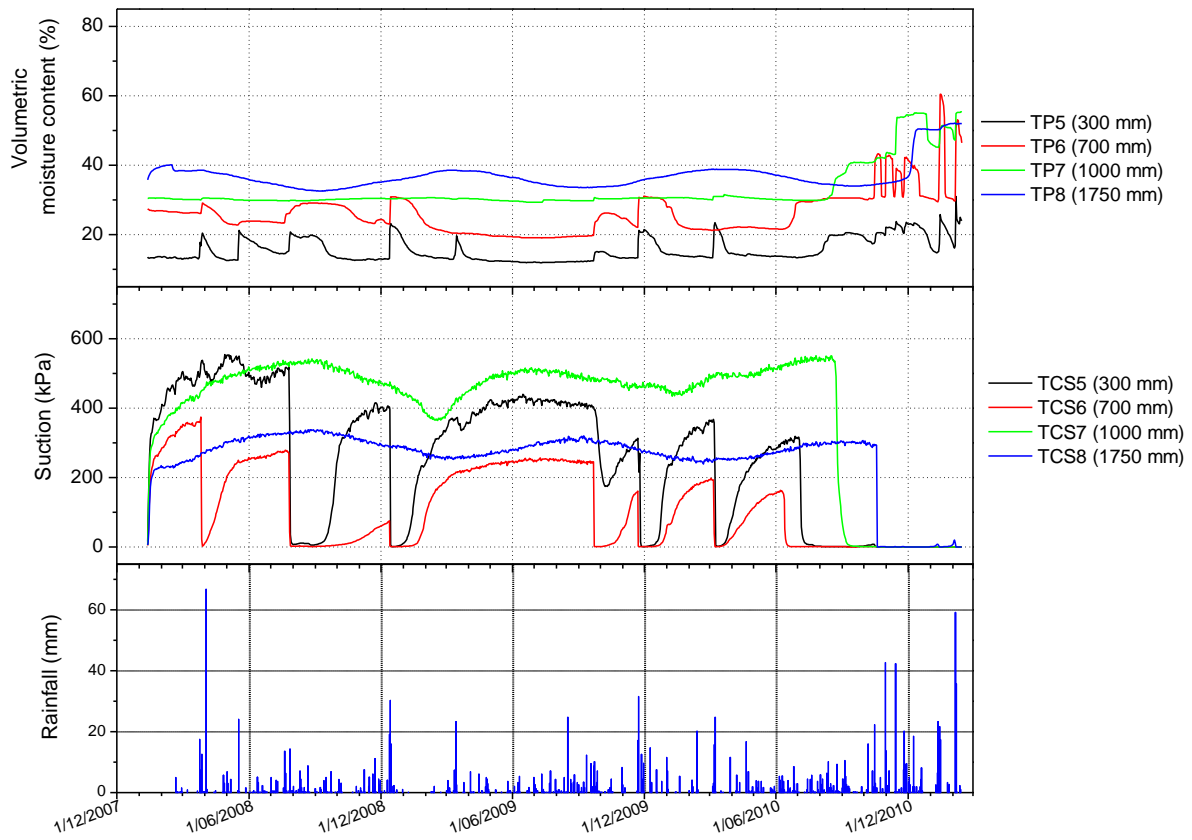


Figure 4-12 Soil volumetric moisture content, suction and daily rainfall in Pit 2 at Altona North

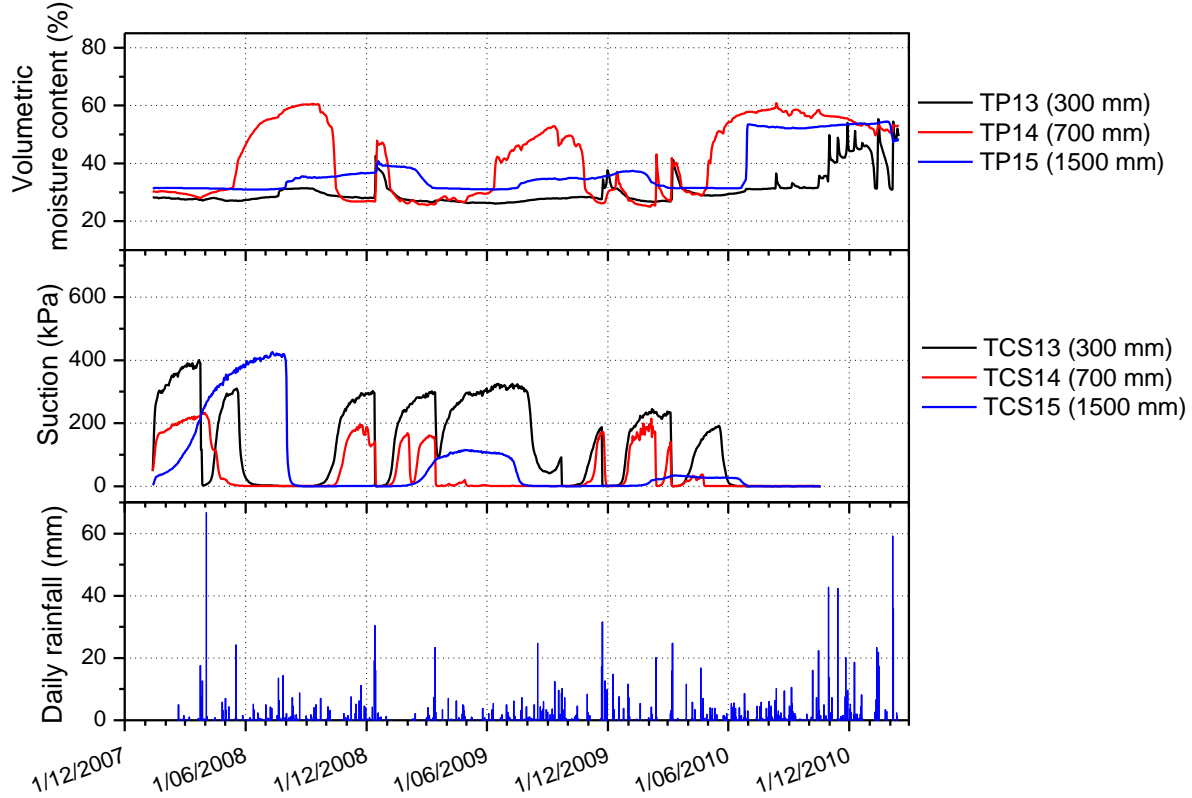


Figure 4-13 Soil volumetric moisture content, suction and daily rainfall in Pit 3 roadside at Altona North

4.4.2 Fawkner results

The measured soil moisture content and suction are plotted in Figure 4-14 to Figure 4-18 for each pit. Similar to Altona North, the recorded measurements in shallow depths of the nature strips showed more immediate response to the rainfall, while seasonal cyclic variation in soil moisture content was observed at the depths of 1000 mm and beyond.

In Pit 1 (Figure 4-14), the data showed that the impermeable concrete driveway has sealed the ground surface, and therefore changes in the soil moisture due to rainfall were delayed. The series of intense rainfall events that occurred during late 2010 resulted in an increase in soil moisture content

along the soil profile. A seasonal cyclic variation in soil moisture content were observed at a depth of 1000 mm with a minimum in September and a maximum in March, except in 2010 with the series of intense rainfall events.

In Pit 2 (Figure 4-15), the changes in soil moisture content at shallow depths beneath the nature strips were closely related to the rainfall. The seasonal cyclic variation of soil moisture was also observed at the depths of 900 mm and beyond similar to the findings at 1000 mm in Pit 1.

In Pit 3 (Figure 4-16) similar results to those in Pit 2 were observed as the measured soil moisture content and suction at depths of 250 and 500 mm were closely related to the rainfall. At depths of 900 and 1400 mm, sudden increase in soil moisture content in late 2010 suggest that a substantial amount of rain water reached these depths.

In Pit 2 roadside (Figure 4-17), the measured moisture content and suction at shallow depths of 250 and 500 mm were similar to that in other pits beneath the nature strips (i.e., Pits 2 and 3). The seasonal cyclic variation of soil moisture content was also observed at 900 mm similar to the findings at 1000 mm in other pits.

The measurements of supplementary sensors installed beneath the footpath and close to the pipe as described in Chapter 3 are shown in Figure 4-18. The changes in soil moisture content under the footpath were very similar to the soil moisture content measured at 350 mm in Pit 1, under the driveway due to similar type of ground surface in these locations. The sensor installed close to the pipe at 600 mm showed responses close to the responses of sensors at similar depths in other pits. All of the sensors recorded the increase in soil moisture content at the end of 2010.

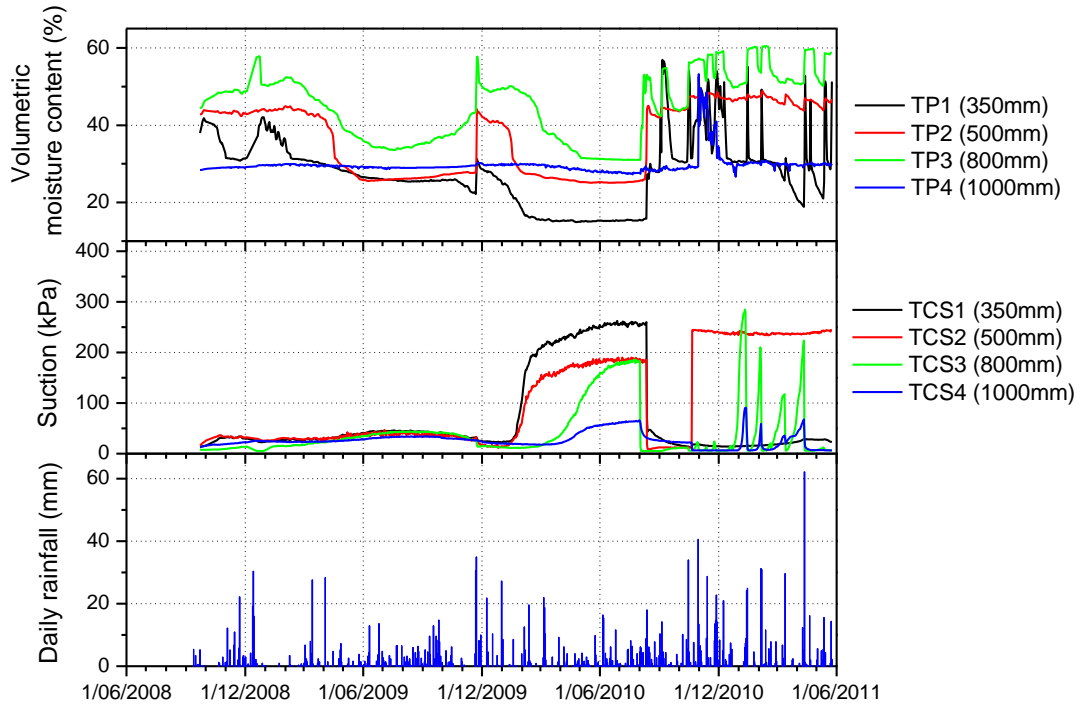


Figure 4-14 Soil volumetric moisture content, suction and daily rainfall in Pit 1 at Fawkner

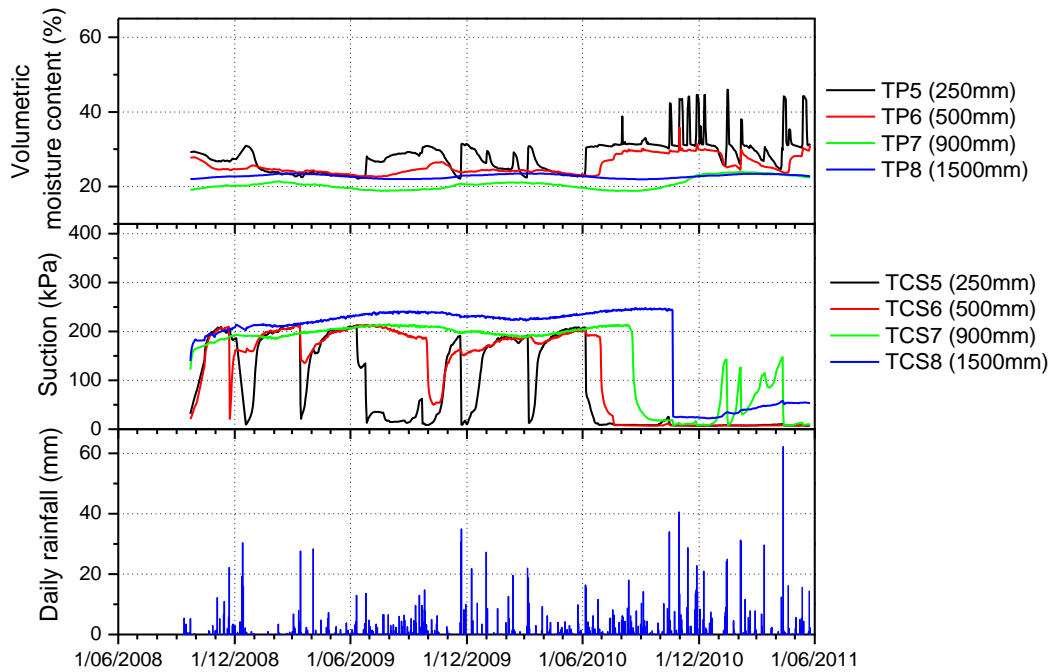


Figure 4-15 Soil volumetric moisture content, suction and daily rainfall in Pit 2 at Fawkner

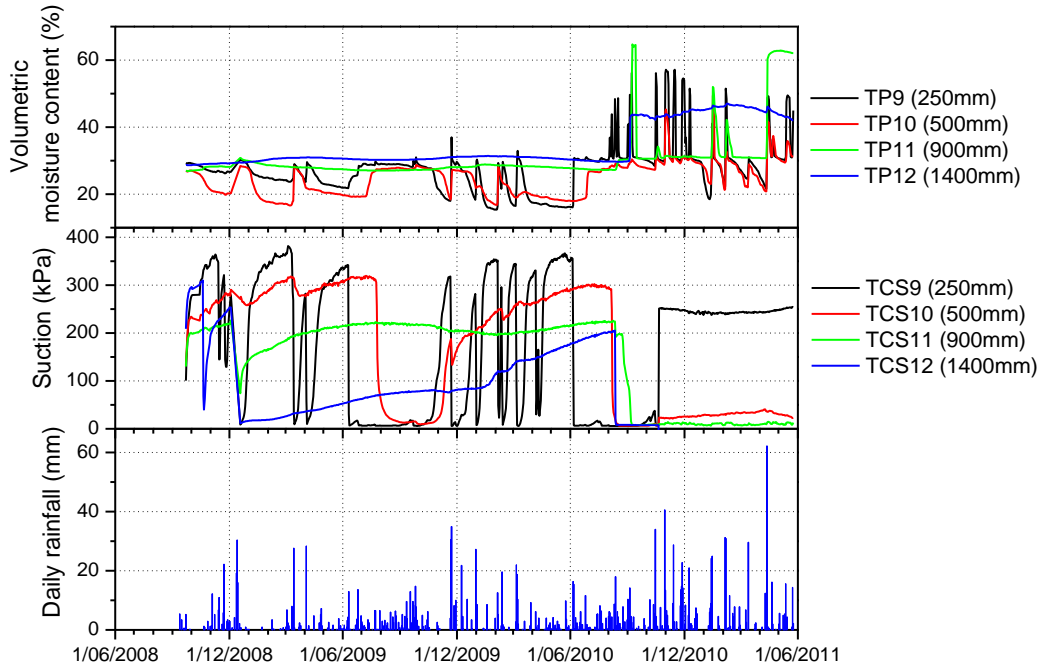


Figure 4-16 Soil volumetric moisture content, suction and daily rainfall in Pit 3 at Fawkner

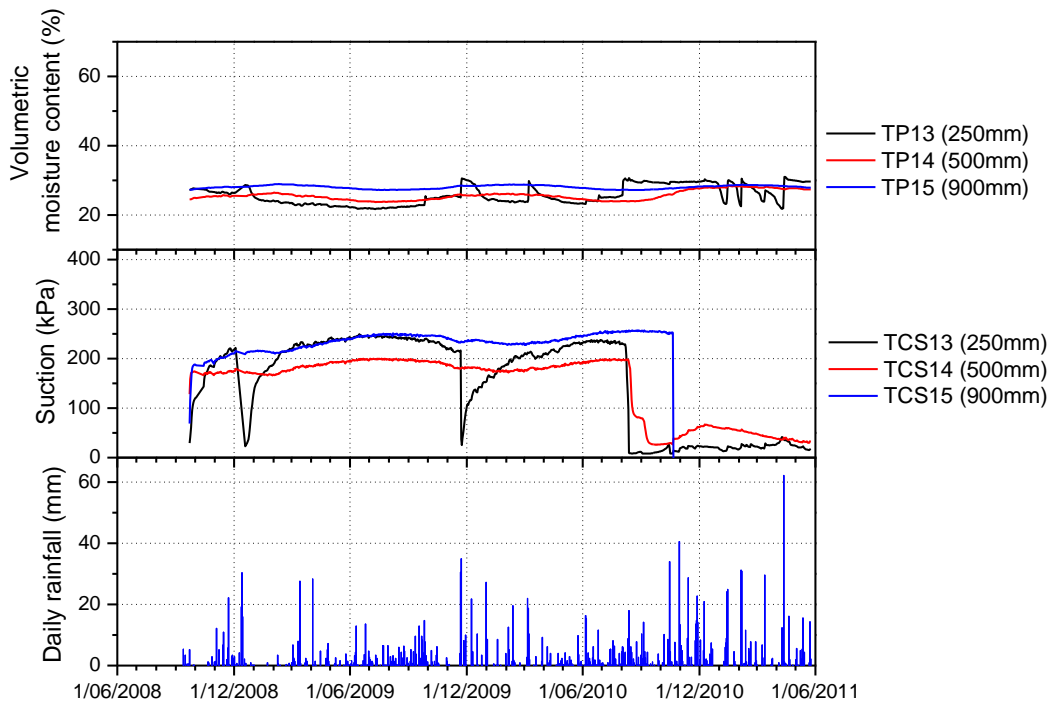


Figure 4-17 Soil volumetric moisture content, suction and daily rainfall in Pit 3 roadside at Fawkner

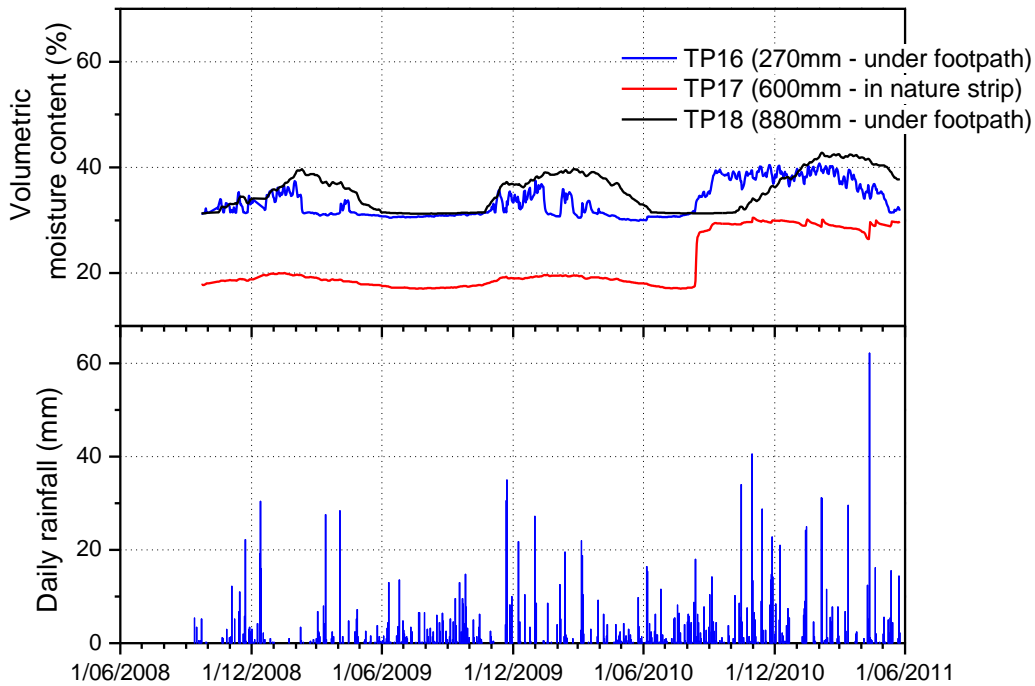


Figure 4-18 Soil volumetric moisture content, suction and daily rainfall in nature strip and under footpath at Fawkner

4.4.3 Summary

The findings from both instrumentation sites show that rainfall, types of ground surface, and burial depths have direct effect on soil moisture content and suction. At shallow depths (i.e., less than 900 mm) changes in soil moisture in response to rainfall were more immediate, while at greater depth (i.e., greater than 1000 mm) a seasonal cyclic variation of soil moisture content was observed. The series of intense rainfall events at the end of 2010 had a significant effect on the soil moisture content at soil depths greater than 1000 mm in both sites. The effect of changes in soil moisture content on the behaviour of the buried pipes will be discussed in the following sections.

4.5 Relationship between Soil Moisture Content and Soil Pressure

In order to understand the effect of changes in soil moisture content on soil pressure, the measured soil pressure beneath and above (only at Fawkner) the pipes during the monitoring period were analysed in this section.

4.5.1 Altona North results

The soil pressure measurements of two earth pressure cells (EPC) installed beneath the buried water pipe in Pits 2 and 3 are shown in Figure 4-19. The theoretical overburden pressure, which calculated on the basis of soil density and depth of pressure cells (i.e., 0.85 m); and the average soil moisture content, which calculated on the basis of the measurements of TPs at a depth of 700 mm, are also plotted in the figure. As can be seen in the figure, the soil pressure recorded in Pit 3 by EPC 1 was always lower than the theoretical overburden pressure and soil pressure measured by EPC 2 in Pit 2, in certain period it also measured negative pressure. This behaviour cannot be explained according to the physical behaviour of the soil and possibly be due to a malfunction of EPC 1, therefore the analysis of soil pressure with moisture content is focused on Pit 2.

The soil pressure measured by EPC 2 showed an “out of phase” pattern with the average soil moisture content measured at 700 mm. Increase in soil pressure occurred when soil moisture content decreased and vice versa. Soil pressure increased between February and March in 2008, 2009, and 2010 when soil moisture content decreased. Conversely, soil pressure decreased in September 2008, 2009, and 2010 when soil moisture approached its maximum. Maximum soil pressure recorded on site is 50 kPa.

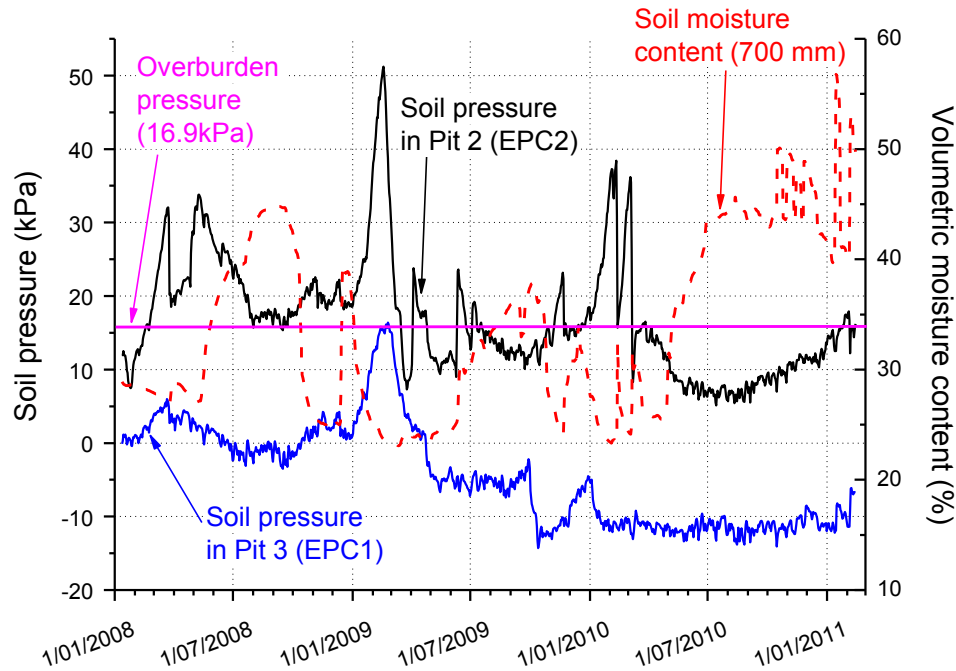


Figure 4-19 Soil pressure and volumetric moisture content versus time in Altona North

4.5.2 Fawkner results

Six EPCs were installed and located in the site as shown in Figure 4-20. EPCs 1 and 2 (in pink colour) were vibrating wire type pressure cells and EPCs 3, 4, 5 and 6 (in black colour) were micro-strain type pressure cells. Unfortunately, EPC 3 in Pit 1 and EPC 6 in Pit 3 gave erratic data where the measured pressure was relative low and negative at certain periods, hence these data were not considered in the analysis. The measured soil pressure is plotted in Figure 4-21 and Figure 4-22 for each pit location. The soil moisture content measurements at soil depth close to the EPCs in each pit are also plotted for comparison purposes.

In Pit 2 (Figure 4-21), the soil pressure recorded by EPCs 1 and 4 were quite different. In general, EPC 1 showed greater variation than EPC 4. The soil pressure measured by EPC 1 peaked when the soil moisture content measured approached minimum indicated soils were drying. The

measurements of EPC 4 were more random, that changes in soil pressure were not related to soil moisture content.

In Pit 3 (Figure 4-22), soil pressure measurements of EPCs 2 and 5 were different. Variation of soil pressure of EPC 2 was relatively low, which varied less than 10 kPa around the theoretical overburden pressure. It may be due to poor compaction of soils around the EPC during backfill. In contrast, the measurements of EPC5 showed greater variations similar to EPC 1 and corresponding to changes of soil moisture content. In general, increase in soil pressure was associated with decrease in soil moisture content and vice versa. Peak soil pressure was recorded by EPC 5 when soil moisture content at 500 mm decreased.

The soil pressure measurements in Fawkner showed a certain degree of randomness; thus a clear conclusion cannot be easily drawn. The data from EPCs 1 and 5 suggested that an increase in soil pressure was associated with a decrease in soil moisture content and vice versa, it was similar to the findings in Altona North. Maximum soil pressure of 75 kPa was measured by EPC5.

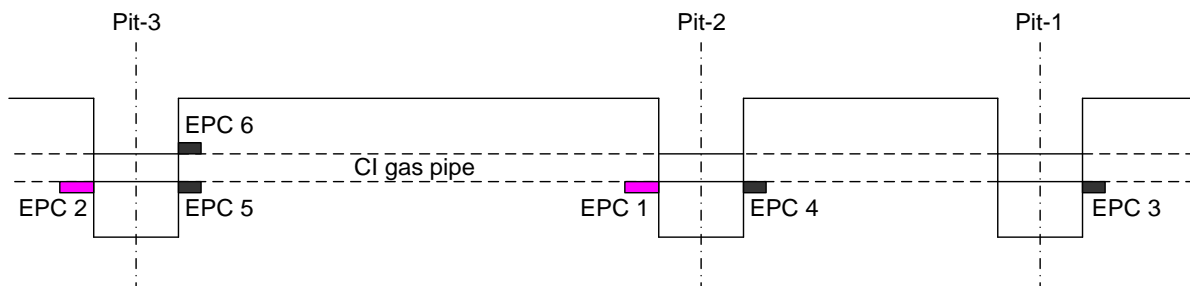


Figure 4-20 Locations of earth pressure cells in Fawkner

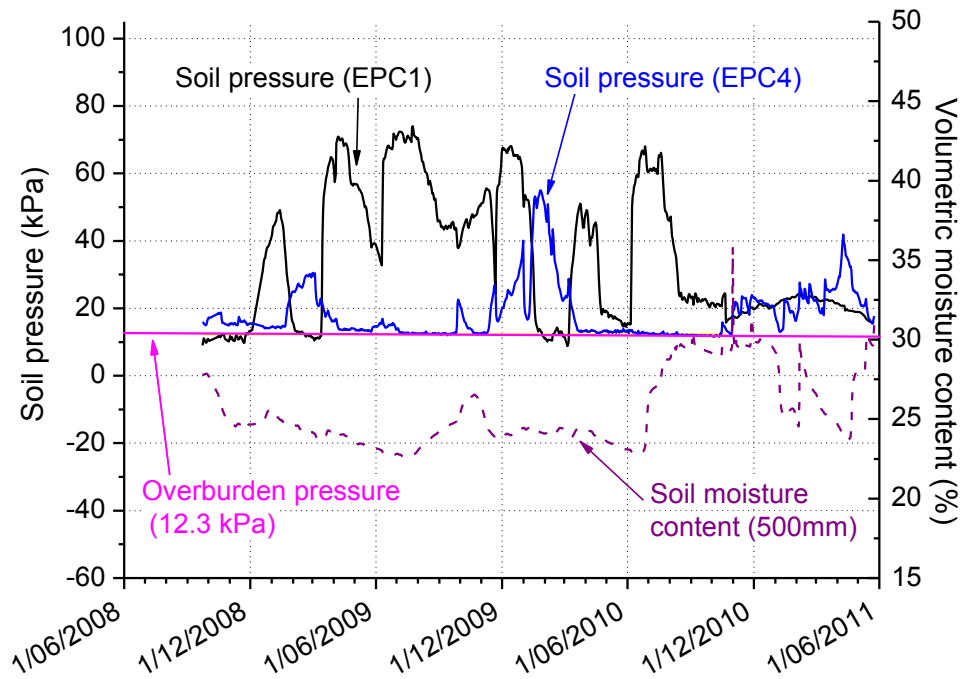


Figure 4-21 Soil pressure and volumetric moisture content versus time in Pit 2 of Fawkner

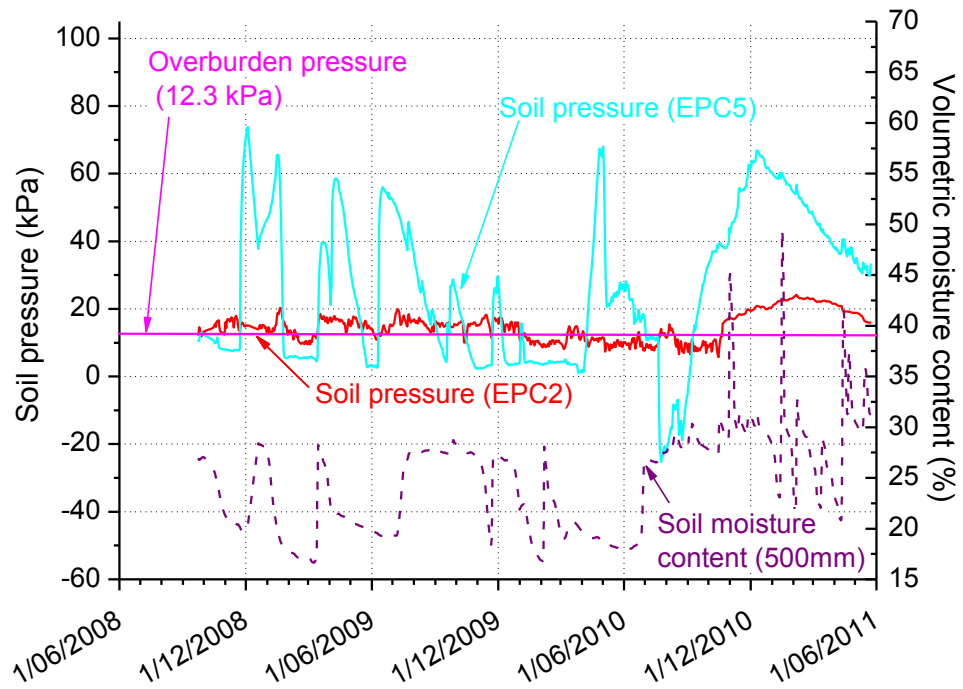


Figure 4-22 Soil pressure and volumetric moisture content versus time in Pit 2 of Fawkner

4.5.3 Summary

The measurements of soil pressure are not very successful due to anomalous behaviour of some EPCs. The generally effect of changes in soil moisture content on soil pressure obtained from the available data are, soil pressure increases when soil moisture content reduces and soil pressure reduces when soil moisture content increases. According to general physical behaviour of soils, shrinkage or swelling occur when moisture content decrease or increase, respectively. Increase in soil pressure due to decrease in moisture content is known as shrinkage induced pressure (Puppala *et al.* 2012). When soil is contracted due to surrounding boundary conditions shrinkage pressure is induced. Decrease in pressure when soil moisture content increase is then associated with the shrunken soils being softened and swelling is initialised, which releases the soil pressure around the pipe and EPCs. In consideration of buried pipes behaviour, in dry and hot summers, shrinkage induced soil pressure will be developed in the nature strips which are exposed to moisture variation and temperature changes. As shown in the field data in Fawkner, an additional load of up to 75 kPa was measured on the pipe. Differential shrinkage induced pressure under the nature strips and concrete driveway can generate flexural movement along buried pipes. Variations of soil pressure can also be considered as a cyclic loading to some extent related to seasonal variations of soil moisture content. Seasonal behaviour of buried pipes due to these variations is discussed in the subsequent sections.

4.6 Relationship between Soil Moisture Content and Soil Displacement

The soil displacement of the instrumentation sites was measured in order to study the swelling and shrinkage behaviour of soils due to seasonal changes in soil moisture content and the effect on buried pipes. The soil displacement was measured by rod extensometers installed in both sites.

4.6.1 Altona North results

The soil displacement measurements at various depths of soils are plotted in Figure 4-23. The displacement of soils was calculated as the distance that the anchors of the extensometer moved from the initial location. As can be seen in the figure, seasonal variations of soil displacement were observed and more pronounced in shallow depth (i.e., 400 mm). Swelling of soil occurred when soil moisture content increased during the wet seasons (i.e., September to November), while shrinkage of soils occurred when soil moisture content decreased during the dry seasons (i.e., February to March). In general, soil swelling occurred gradually over a period of seven month from March to October. Conversely, soil shrinkage occurred more quickly in a short period of time from January to March. The series of intense rainfall events in late 2010 led to increase of soil moisture content and continuous soil swelling. Maximum soil shrinkage at 900 mm (pipe depth is 850 mm in Alton North) was measured as 17 mm and 16 mm in 2009 and 2010, respectively.

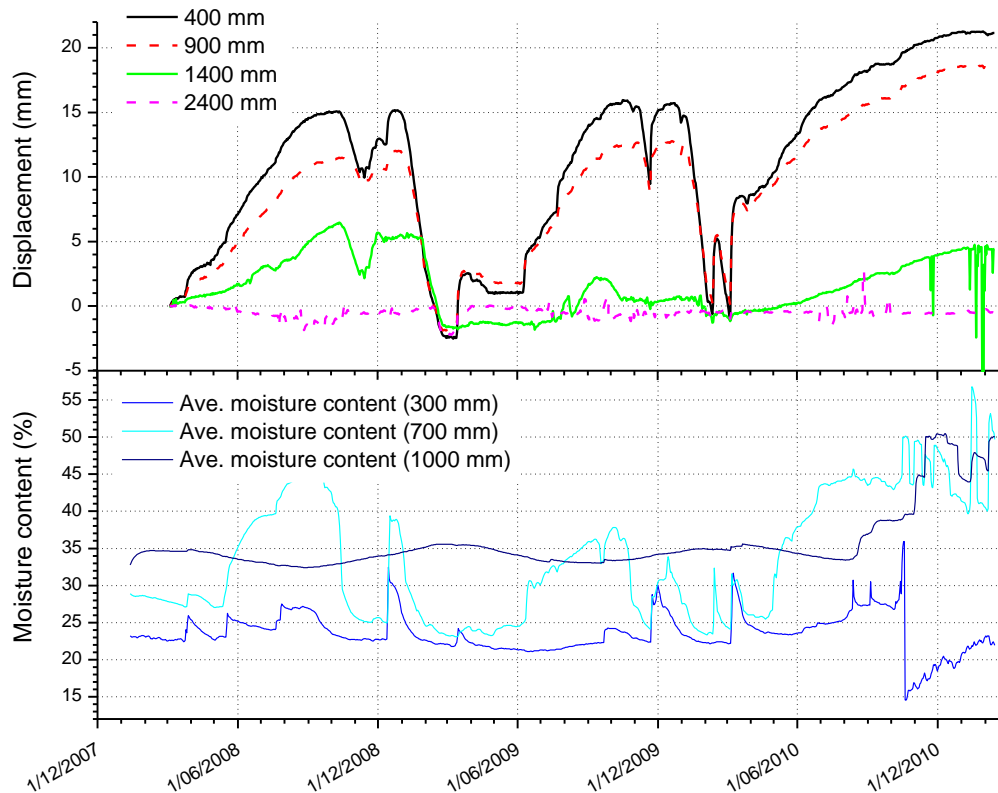


Figure 4-23 Soil displacement in Altona North

4.6.2 Fawkner results

The rod extensometer on site failed to measure the actual soil displacement and showed very small displacement of values less than 1 mm. This is possibly due to malfunctions of the internal transducer of the extensometer. Supplementary displacement measurements were undertaken between June and October 2010 in order to provide some information on the soil displacement. A schematic diagram of the soil displacement gauge used for supplementary measurements is shown in Figure 4-24, which was designed as a stainless steel rod attached to a squared base. The displacement gauges of particular lengths were buried at the depths of 270, 450, and 650 mm, where the small blades on the base were cut into the soil to fix the gauges in position. Displacement of these gauges was measured by a surveying level and a surveying staff placed on top of the rod on the gauge. The concrete slab of the instrumentation cabinet and a point on the power pole were taken as the stationary reference points, so that displacement of each gauge was measured with respect to these points.

Figure 4-25 shows the gauge displacement measurements with average soil moisture content at 250 and 500 mm for comparison purposes. The series of intense rainfall events in late 2010 resulted in significant increase of soil moisture content at both depths, which led to soil swell. Soil displacement of 24 mm due to swelling was recorded at the depth of 270 mm, while smaller displacement of 18 mm and 16 mm were recorded at 450 and 650 mm, respectively. The maximum displacement measured at the depths of 650 mm (i.e., pipe depth in Fawkner) was 19 mm in August and October 2010 corresponding to decrease of soil moisture content and shrinkage of soils.

4.6.3 Summary

The soil displacement measurements on both sites were directly related to the variations of soil moisture content. Swelling of soils occurred gradually when soil moisture content increase, while shrinkage of soils was found to occur more quickly within a shorter period of time. The effect of soil swelling and shrinkage on buried pipes are analysed with the measured pipe stress in the following sections.

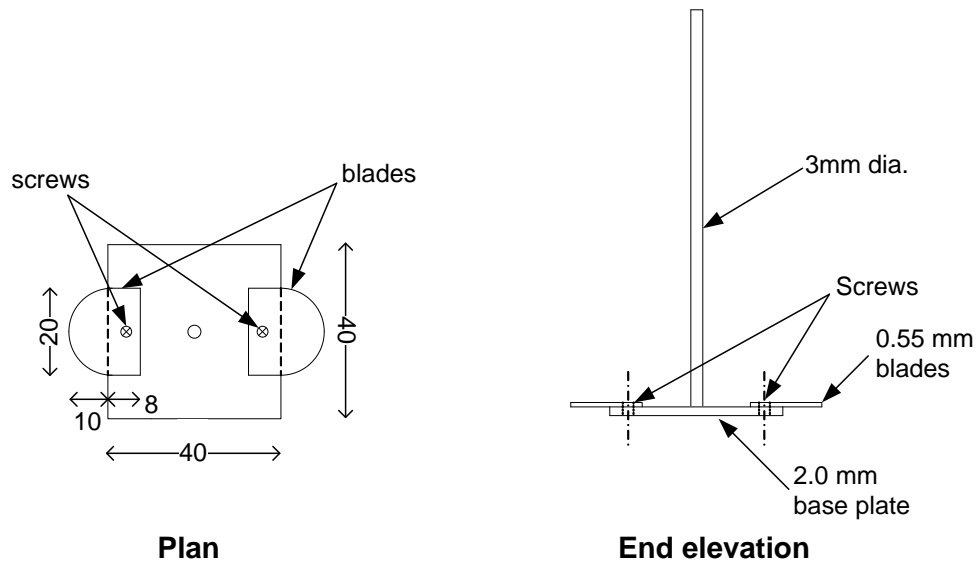


Figure 4-24 Schematic diagram of soil displacement gauge

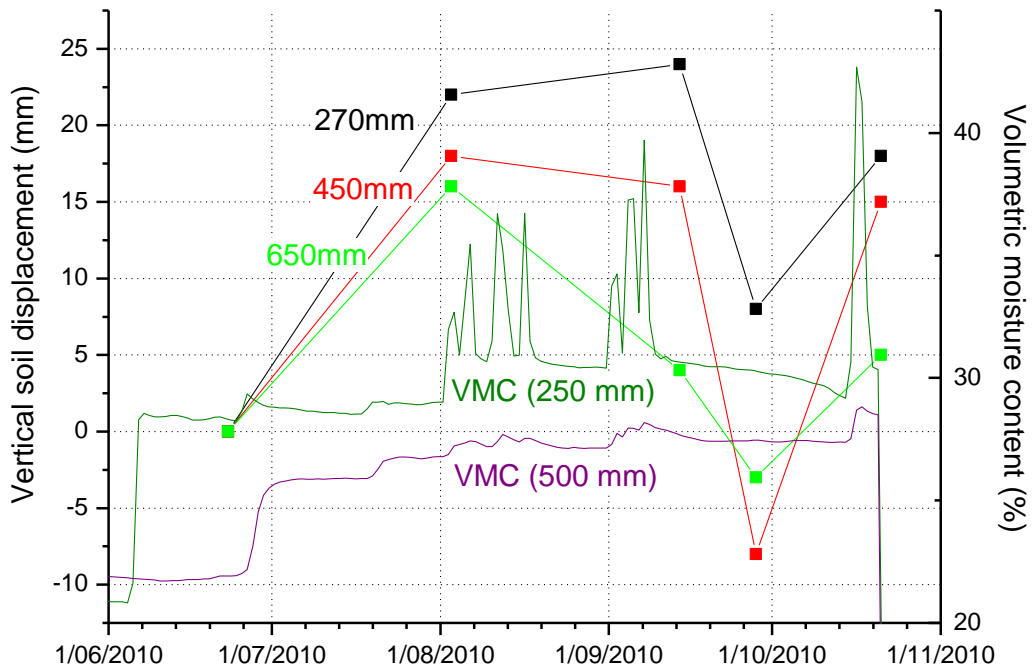


Figure 4-25 Supplementary soil displacement in Fawkner

4.7 Relationship between Pipe, Soil, and Climate

In order to study the effect of flexural pipe stress caused by seasonal changes in soils on pipe deformation, strain gauges were installed on the buried water and gas pipes, as described in Chapter 3, to measure the longitudinal and hoop (circumferential) strains. The measurements of pipe strain were converted to stress and the pipe flexural stress was calculated. Analysis was undertaken for flexural stress with soil moisture content, soil displacement or soil pressure. The following subsections describe the details of analysis.

4.7.1 Pipe strain measurements

The pipe strain measurements from both sites are presented in this section. The orientations of the strain gauges on the water and gas pipes are shown in Figure 4-26 and Figure 4-27. As previously stated in Chapter 3, an internal investigation was not conducted for the instrumented pipes, and the locations of pipe joints were determined on the basis of the information provided by the asset owners. The pipe joints were 6 and 2.7 m apart for the water and gas pipe, respectively, based on a known location of a joint found in the instrumentation pits in both sites. The data acquisition time was at ten minutes intervals and the daily average values were used for analysis and plots. The plots of all strain data from both sites are shown in Appendix A.

4.7.1.1 Altona North results

The measurements of pipe strain were recorded for approximately one and a half year from January 2007 to August 2009. Some of the strain measurements became erratic in April 2009 and more than half of the strain gauges were failed possibly due to delamination from the pipe surface on August 2009. The pipe strain measurements until August 2008 were considered in the analysis.

Figure 4-28 shows the daily average measurement of longitudinal and hoop in each pit in Altona North, the average soil temperature measured at 700 mm is also plotted for comparison purposes. The sign convention for the strain plots is positive for tension and negative for compression.

Seasonal variations of pipe strain were observed from the figure that the pipe strain maximised (in tension) between February and March when soil temperature was high, and minimised (in compression) in August and September when soil temperature was low.

4.7.1.2 Fawkner results

In Fawkner, pipe strain measurements were analysed from September 2008 to May 2011. Two longitudinal strain gauges on the spring line (Strain 2L and 10L) gave erratic data from April 2008, and were believed to be faulty. Unfortunately, these strain gauges were located on the springline and no backup gauge was installed. Therefore, the measurements of these gauges were excluded from the plots and the analysis.

Figure 4-29 shows the daily average longitudinal and hoop strains at each pit. The average pipe temperature is also plotted for comparison purposes. Similar to the findings in Altona North, the seasonal variations of pipe strain were related to the changes of pipe temperature. In general, the pipe was in tension between February and March when soil temperature was high, and in compression between August and September when soil temperature was low.

4.7.1.3 Summary

The measured strain showed that the buried pipes experienced tensile and compressive strain in hot and dry seasons, respectively, due to seasonal variations of temperature. Further analysis of the pipe behaviour is described in the following section by calculation of the flexural pipe stress from the strain measurements.

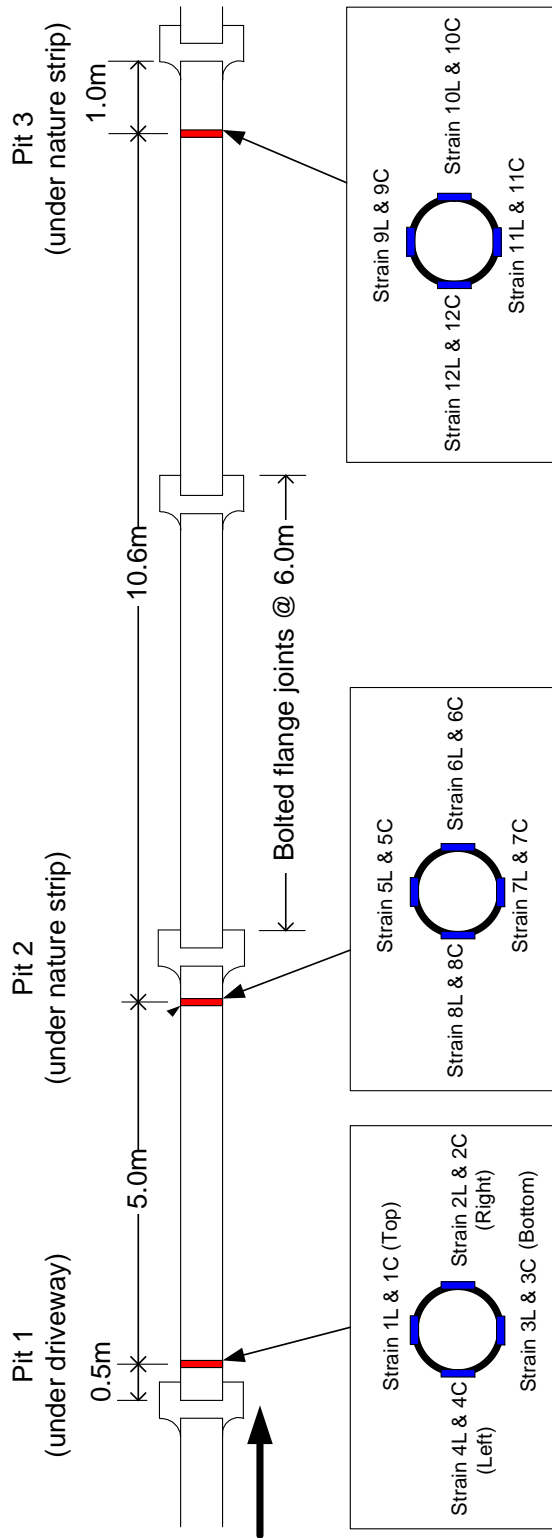


Figure 4-26 Location and labelling of strain gauges on water pipe

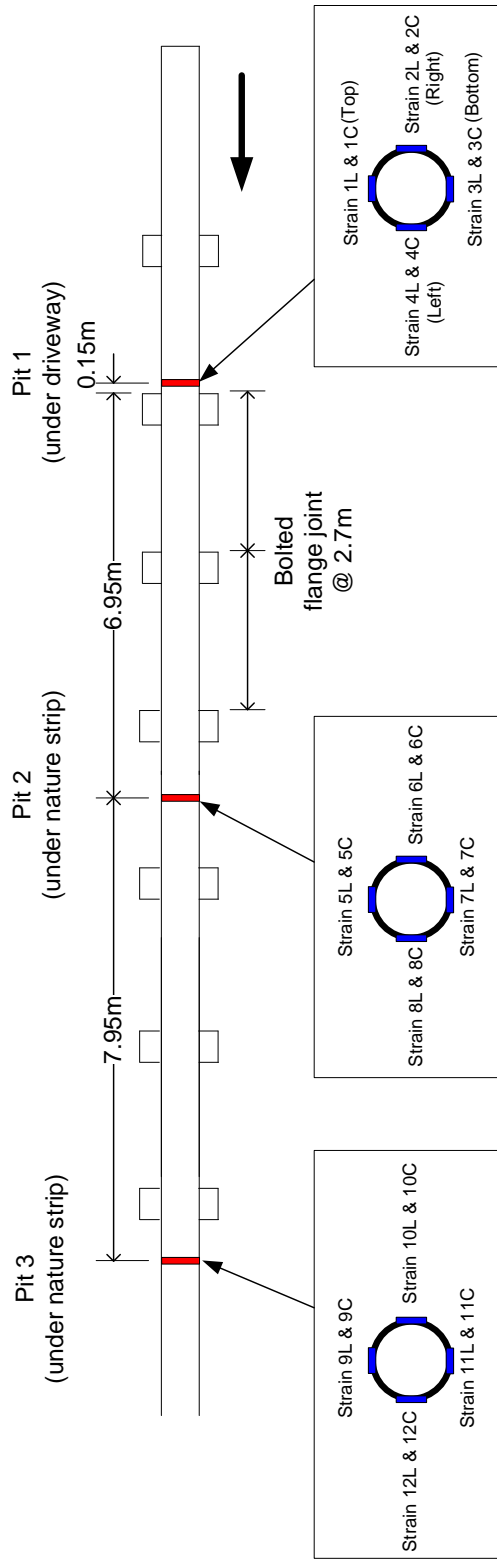


Figure 4-27 Location and labelling of strain gauges on gas pipe

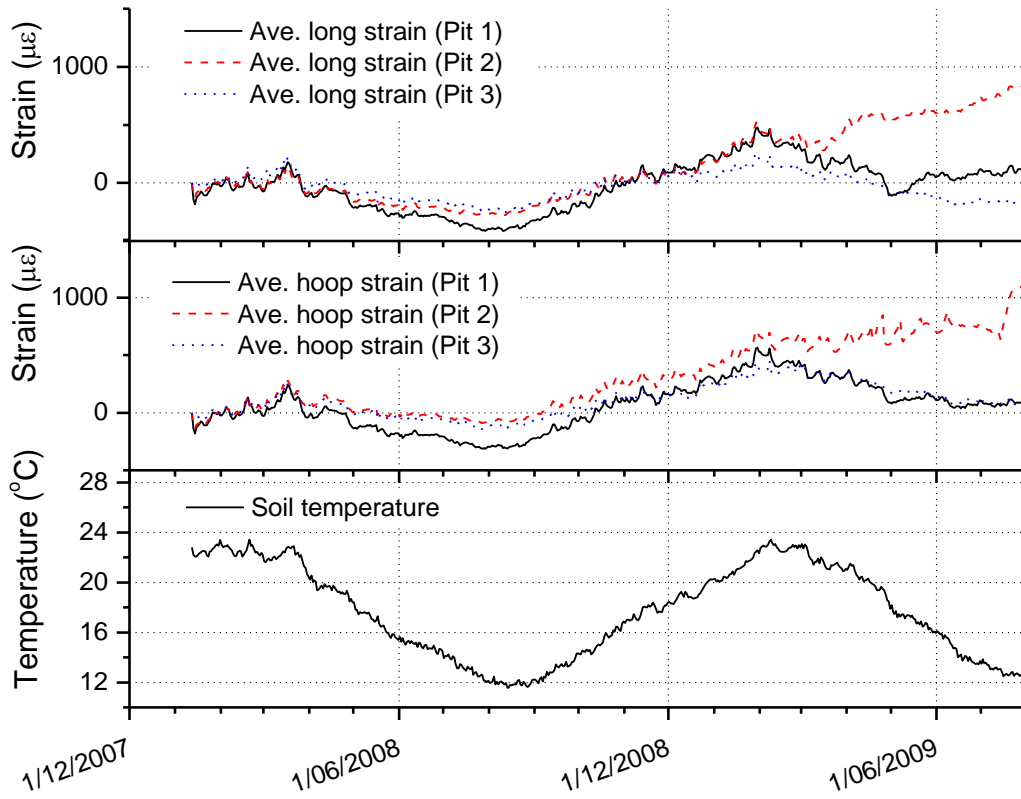


Figure 4-28 Daily average longitudinal and hoop strains of water pipe in Altona North at each pit

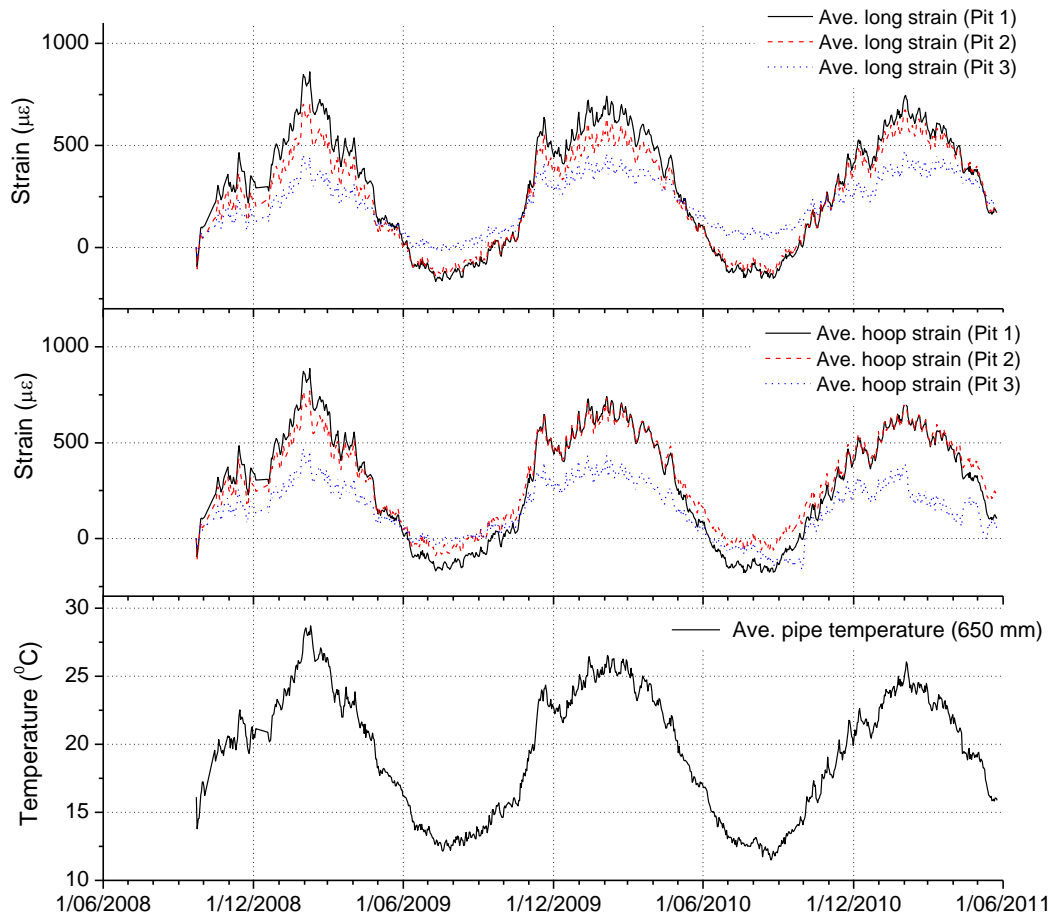


Figure 4-29 Daily average longitudinal and hoop strains of gas pipe in Fawkner at each pit

4.7.2 Calculation of pipe stress

In order to calculate the flexural pipe stress for analysis, the pipe strain measurements were converted to stresses using properties of the buried pipes. Longitudinal and hoop stresses of the buried pipe can be calculated by the following equations:

$$\varepsilon_{\theta} = -\nu \cdot \frac{\sigma_x}{E_p} + \frac{\sigma_h}{E_p} + \nu \cdot \frac{(p_i + p_e)}{2E_p} + \alpha \cdot \Delta T \quad \text{Equation 4-1}$$

$$\varepsilon_x = \frac{\sigma_x}{E_p} - \nu \cdot \frac{\sigma_h}{E_p} + \nu \cdot \frac{(p_i + p_e)}{2E_p} + \alpha \cdot \Delta T \quad \text{Equation 4-2}$$

$$\varepsilon_x - \varepsilon_{\theta} = (1 + \nu) \cdot \frac{\sigma_x}{E_p} - (1 + \nu) \cdot \frac{\sigma_h}{E_p} \quad \text{Equation 4-3}$$

where ε_{θ} is the hoop strain; ν is the Poisson's ratio of the pipe material; σ_x is the longitudinal stress; E_p is the Young's modulus of pipe material; σ_h is the hoop stress; p_i and p_e are the internal and external pressure of the pipe, respectively; α is the thermal coefficient of the strain gauge; ΔT is the change of temperature; and ε_x is the longitudinal strain.

The hoop stress of a thin wall pipe (thickness / diameter < 0.1) is represented by Equation 4-4 (Kuraoka *et al.* 1996a):

$$\sigma_h = \frac{D \cdot (p_i - p_e)}{2 \cdot t} \quad \text{Equation 4-4}$$

where D is the pipe diameter and t is the pipe wall thickness. The hoop stress of a thick wall pipe can be calculated using Equation 4-5 (Hu and Vu 2006):

$$\sigma_h = \frac{2p_i \cdot r_i^2}{r_e^2 - r_i^2} - \frac{p_e \cdot (r_e^2 + r_i^2)}{r_e^2 - r_i^2} \quad \text{Equation 4-5}$$

where, r_i and r_e are the inner radius and outer radius of the pipe, respectively.

The external pipe pressure, p_e is calculated as the overburden soil pressure on the pipe in the field using Equation 4-6,

$$p_e = \gamma_b \cdot d_p$$

Equation 4-6

where, γ_b is bulk unit weight of the soil measured in the field and d_p is the depth of the pipe centre. The water and gas pipes are located at the depth of 0.85 and 0.65 m below the ground surface, hence p_e calculated as 16.9 kPa and 12.3 kPa for Altona North and Fawkner, respectively. Other pipe properties considered in stress calculations are:

- Young's modulus, E_p is 150 GPa (Tangent modulus of pipes sections (Gould *et al.* 2009))
- Pipe external diameter, D is 120 mm and 160 mm for water and gas pipes, respectively;
- Pipe wall thickness, t is 8.5 mm and 9.9 mm for water and gas pipes, respectively, measured by ultrasonic method in the field (refer to Chapter 3);
- Poisson's ration of cast iron pipe, ν is 0.21 (refer to Appendix B);
- Typical thermal coefficient of cast iron, α is $10.5 \times 10^{-6}/\mu^{\circ}\text{C}$ (Rajani and Tesfamariam 2004);
- Measured apparent thermal coefficient, α' is $40 \times 10^{-6}/\mu^{\circ}\text{C}$ in the laboratory (refer to Appendix B); a fixed apparent thermal coefficient cannot be obtained in the field (refer to Appendix C).

According to the above theoretical justification, the instrumented pipes may be considered as thin wall pipes, as the thickness / diameter ratio equals to 0.071 and 0.062 for water and gas pipes, respectively, are less than 0.1. The hoop stress can be calculated using Equation 4-4.

Figure 4-30 shows the hoop stress calculated for a selected period of time using both Equations 4-4 and 4-5. The hoop stress calculated from the thin wall equation was approximately 1000 kPa greater than the values from the thick wall theory, therefore it was considered as more conservative for the

pipe design and prediction of failures. Equation 4-4 was then used for calculation of the hoop stress for both water and gas pipes in the analysis.

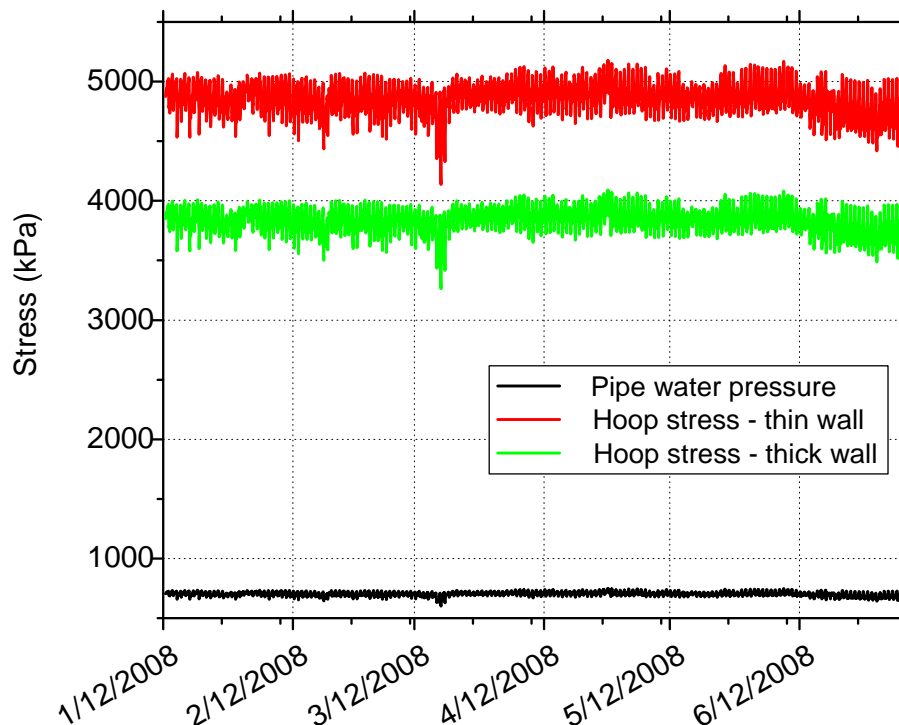


Figure 4-30 Comparison of water pipe hoop stress

The longitudinal stress at each of the pit location was calculated with Equation 4-3 if both longitudinal and hoop strain data were available, and the apparent thermal coefficient, α' was not required in this equation. In locations where either longitudinal or hoop strain data were not available, the relevant equation of either Equation 4-1 or Equation 4-2 was employed with the measured apparent thermal expansion coefficient, α' from the laboratory since a fixed field value cannot be obtained. The calculated pipe stress was the change in stress that the pipe experienced at the time of instrumentation and the stress at each logging time. Sign convention used in the analysis was same as in the strain measurements that tensile stress is positive and compressive stress is

negative. In general, the longitudinal pipe stress was influenced by the flexural stress due to pipe bending, thermal stress, Poisson's effect of radial, and hoop stress of the pipe.

4.7.3 Analysis of pipe flexural stress

In order to study the effect of seasonal changes in soils on pipe deformation, the measured pipe flexural stresses were analysed. Flexural stress of the buried pipe is expected to develop as a result of pipe bending, based on the assumption that the buried pipe obeys the simple bending theory and uniform restrained conditions exist around the pipe circumference. Cast iron pipes are considered as rigid, so that no local buckling will occur on the cross-section of the pipe.

When considering the driveway effect of buried pipes, the instrumented pipe section spanned from the driveway to the centre of the nature strip is assumed to behave like a cantilever beam with rotations at the pipe joints and partially fixed end support at the driveway (Chan 2008). In this analysis, the flexural stress in the vertical direction of the buried pipe was calculated as the difference between the top and bottom longitudinal stress. The flexural stress in the horizontal direction was calculated as the difference between the left springline and right springline longitudinal stress.

When the flexural stress in the vertical direction (i.e., the difference between the top and bottom) is positive, the pipe top experiences greater tensile stress than the bottom and therefore the pipe is bending downward. And when the flexural stress in the vertical direction is negative, the pipe top experienced greater compressive stress than the bottom and therefore the pipe is bending upward. Similarly, in the horizontal direction (i.e., the difference between the left springline and right springline), positive flexural stress shows that the pipe is bending toward the left springline and negative flexural stress shows that the pipe is bending toward the right springline.

4.7.3.1 Altona North results

Figure 4-31 shows the flexural stress in the vertical direction at each pit in Altona North with measured soil displacement, soil moisture content and rainfall. The background of the figure is coloured corresponding to the seasons.

In Pit 1, the calculated flexural stress showed that the pipe section gradually bent upward (in compression) from autumn to spring of 2008 due to an increase in soil moisture content at 700 mm and corresponding soil swelling at the depths of 400 and 900 mm. The pipe section then bent downward (in tension) over the summer of 2009, due to soil shrinkage corresponding to a decrease in soil moisture content. In the winter of 2009, soil swelling occurred and the downward bent pipe reverted to a similar position as in the winter of 2008 (i.e., similar magnitude of flexural stress was recorded in both winters).

In Pits 2 and 3, similar correlations between flexural stress, soil displacement and soil moisture content were observed. The pipe bent upward corresponding to soil swelling during winter, and bent downward corresponding to soil shrinkage in summer.

The calculated flexural stress in the vertical direction showed that the water pipe experienced maximum stress when bending downward in summer. Downward pipe bending was reversed in winter when soil swelling occurred. Maximum flexural stress of the pipe due to soil shrinkage and downward bending was over 35 MPa; and due to soil swelling and upward bending was approximately 20 MPa.

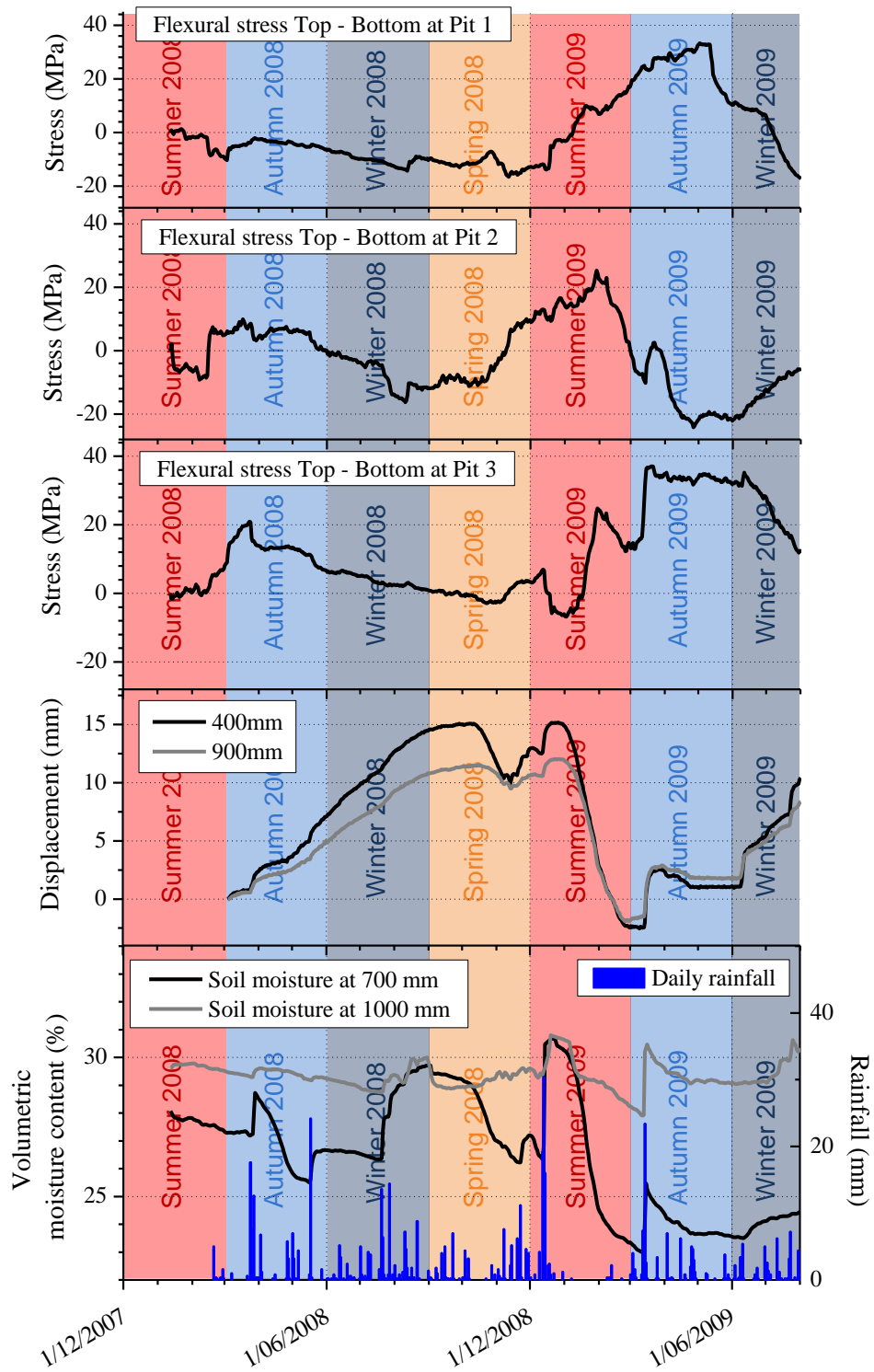


Figure 4-31 Flexural stress in vertical direction in Altona North

Figure 4-32 shows the flexural stress in the horizontal direction in Altona North. The left springline refers to the side of the pipe on the footpath, and the right springline refers to the side of the pipe on the road as shown in Figure 4-26. As stated before, negative flexural stress (in compression) indicates that the pipe section was bending left (i.e., toward the footpath), and positive flexural stress (in tension) indicates that the pipe section was bending right (i.e., towards the road). The measured soil pressure, moisture content and rainfall are also plotted for comparison.

In Pit 1, the pipe section gradually bent toward the road (in tension) during the winter of 2008 corresponding to increases in soil moisture recorded at 700 mm and decreases of soil pressure indicating soil swelling as described in Section 4.5. In the summer of 2009, the bending direction changed to the footpath when soil moisture content decreased and the measured soil pressure increased to its maximum indicating soil shrinkage.

In Pit 2, a similar behaviour as in Pit 1 was observed, but with reduced range as changes in flexural stress was lower. The bending of the pipe section during the autumn of 2008 to the spring of 2009 was insignificant as variations in flexural stress were relatively small. In the summer of 2009, a significant decrease in flexural stress was observed with a decrease in soil moisture content and an increase in the soil pressure implying that soil shrinkage was occurring and the pipe section was bending toward the footpath.

In Pit 3, changes in flexural stress were smaller compared to the changes in other pits. The effect of seasonal soil changes on the pipe stress was not very significant at this location. This is possibly due to the lower magnitude of pipe bending in the horizontal direction.

These findings showed that the pipe was generally bending toward the road during the winter period due to soil swelling and bending toward the footpath in summers due to soil shrinkage. Flexural stress measured in the horizontal direction was lower than the vertical direction with maximum stress of 25 MPa at Pit 1 due to soil swelling; and 22 MPa in Pit 2 due to soil shrinkage.

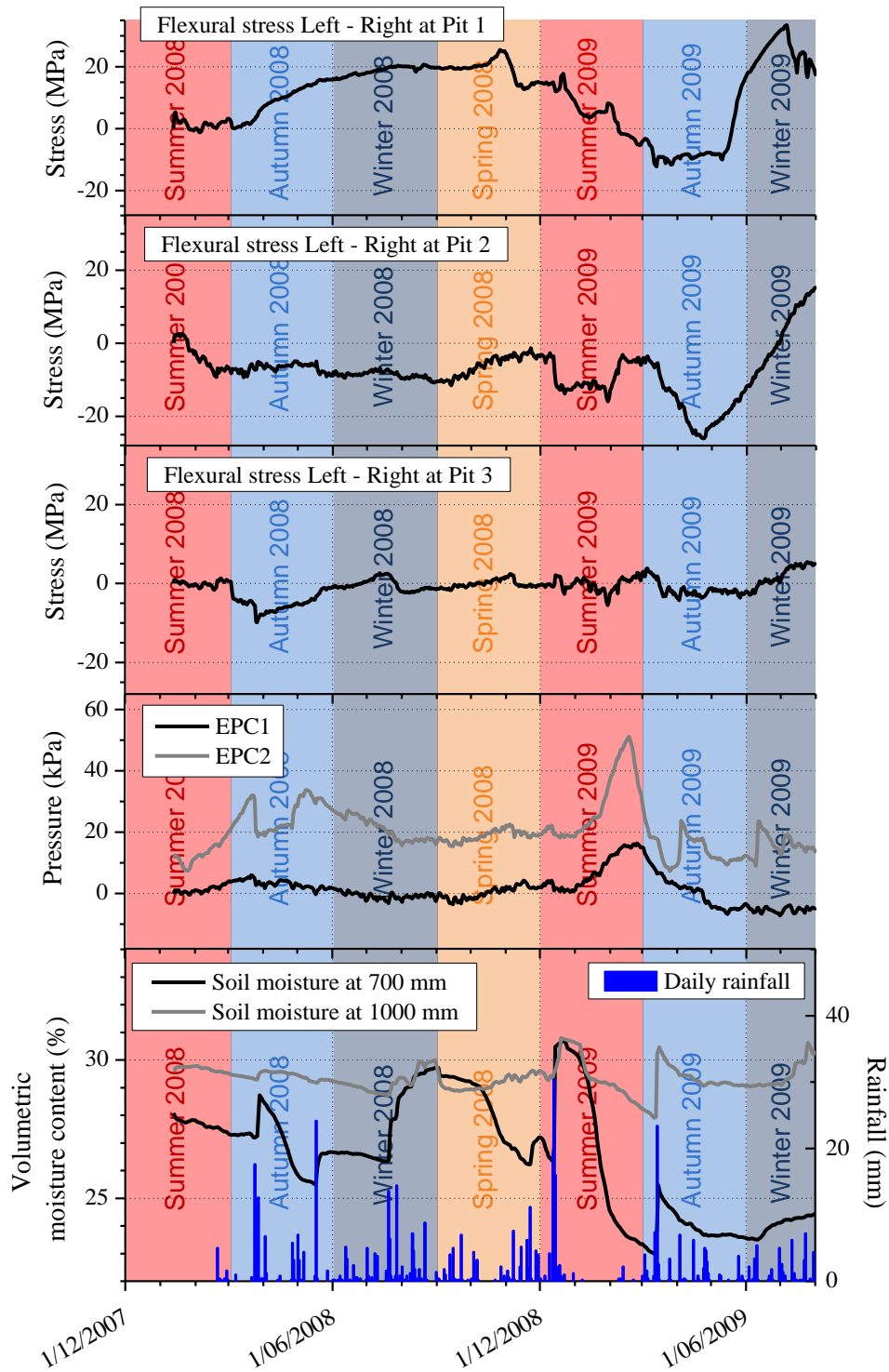


Figure 4-32 Flexural stress in horizontal direction in Altona North

4.7.3.2 Fawkner results

As noted previously two strain gauges on the springline of the gas pipe (Strain 2L and 10L) failed to function properly, and the flexural stress in the horizontal direction in Pits 1 and 3 could not be calculated. Therefore, flexural stress analysis was only performed in the vertical direction. Figure 4-33 shows the flexural stress in the vertical direction at each pit in Fawkner with soil pressure measured by EPC 1 and 5 at Pits 2 and 3, respectively. Soil moisture content measured at 500 and 700 mm, and rainfall are also included.

A general trend of decrease in pipe flexural stress was observed in all pits after the field instrumentation, indicating that the pipe was gradually bending upward throughout the monitoring period. Seasonal variations of soil moisture content were recorded throughout the monitoring period, where positive flexural stress (in tension) corresponded to a decrease in soil moisture content (i.e., summer to autumn of 2009 and 2010) and negative flexural stress (in compression) corresponds to increase in soil moisture content (i.e., winter to spring of 2009 and 2010). Similar to the understanding of pipe bending behaviour in Altona North, the gas pipe in Fawkner experienced minor downward bending in summer but significant upward bending at all other times. This behaviour was due to an increase of rainfall during 2009 to 2011 leading to swelling of soils, especially in late 2010 when a series of intense rainfall events occurred. Continuous decrease of flexural stress suggested that the pipe was subjected to upward bending due to soil swelling. Therefore, downward pipe bending did not occur in the wet summer in 2011. The maximum flexural stress measured on the gas pipe due to soil swelling was 58 MPa in Pit 3.

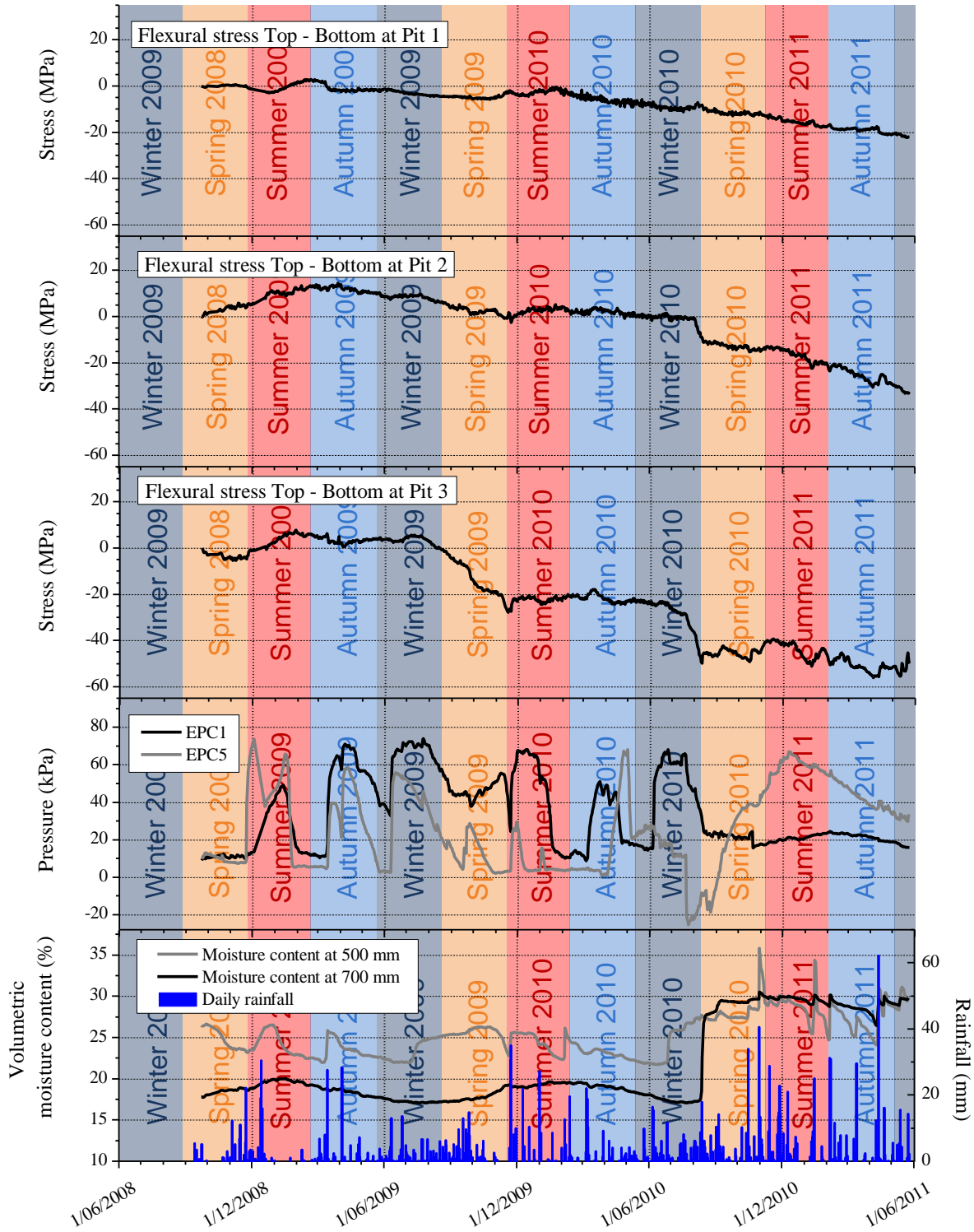


Figure 4-33 Flexural stress in vertical direction in Fawkner

4.7.3.3 Summary

The analysis of flexural stress from both of the instrumentation sites showed that in the vertical direction, a decrease of soil moisture content led to soil shrinkage and downward bending of the pipe, and an increase in soil moisture content led to swelling of soils and upward bending of the pipe. In the horizontal direction, based on the analysis of the pipe stress measurements in Altona North, changes in soil moisture content resulted in flexural pipe bending. The water pipe was bending toward the footpath when soils shrunk and toward the road when soils swelled.

The magnitude of flexural stress and of deflection on the pipes is possibly affected by the different fixity conditions at the pipe joints. The joints between each pipe sections can also have different fixity conditions when the pipe is bending about different axes, and therefore different flexural stress will be experienced by the pipe due to soil shrinkage and swelling. The maximum flexural stress was 35 MPa in Altona North and 58 MPa in Fawkner. According to the mechanical tests on cast iron pipes described in Chapter 3, maximum tensile strength of corroded and new cast iron pipes ranged from 25 to 250 MPa. Therefore, flexural stress due to pipe bending can lead to failure of aged and corroded cast iron pipes.

4.7.4 Behaviour of buried in-service pipes

The behaviour of in-service pipes buried in a typical driveway condition corresponding to changes in soil moisture content is illustrated in Figure 4-34 and Figure 4-35 in the vertical and horizontal directions, respectively. Figure 4-34 shows that shrinkage of soils in dry periods led to downward bending of the pipe, and the pipe top experienced greater tensile flexural stress than the bottom. Swelling of soils in the wet period led to upward bending of the pipe, and the pipe top experienced greater compressive flexural stress than the pipe bottom. Figure 4-35 shows that in the dry periods, the pipe bent toward the footpath due to soil shrinkage and this flexural bending introduced compressive stress on the pipe springline close to the footpath. A reverse action occurred in the wet period, when the pipe bent away from the footpath due to soil swelling and tensile stress was introduced on the pipe springline close to the road.

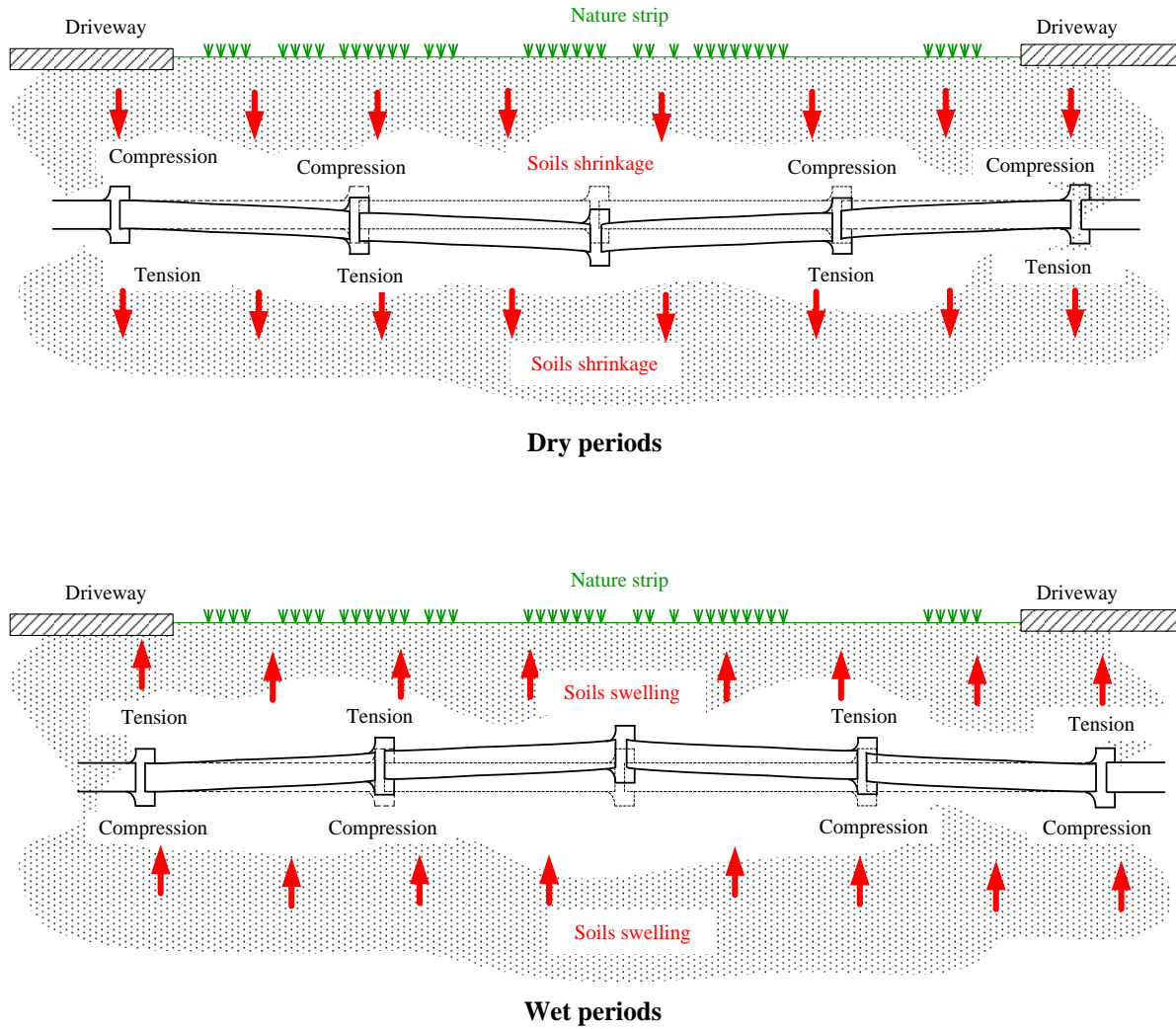


Figure 4-34 Behaviour of buried pipes in vertical direction due to changes in soil moisture content

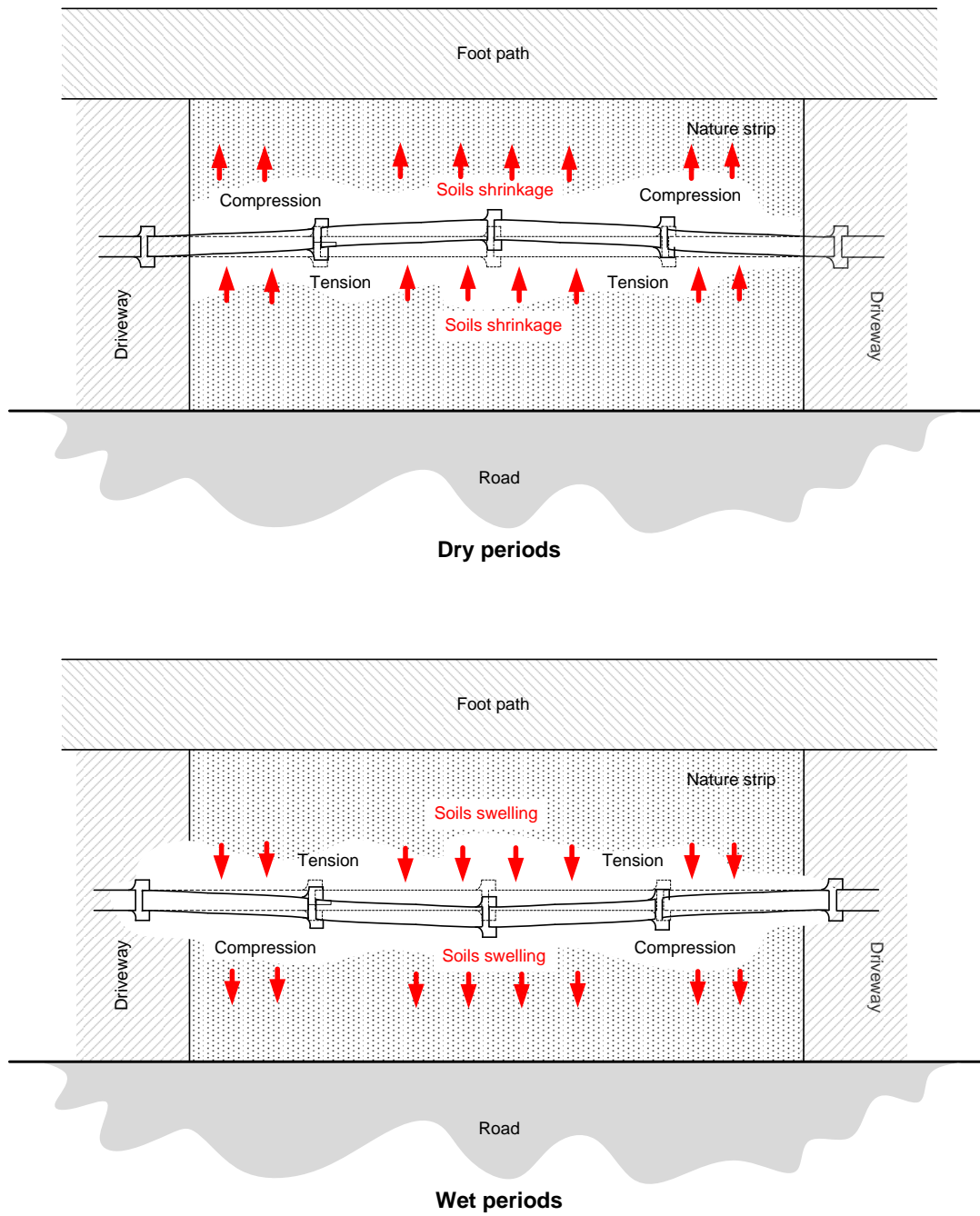


Figure 4-35 Behaviour of buried pipes in horizontal direction due to changes in soil moisture content

Previous studies of buried pipe failure in Victoria (Kassiff and Holland 1965; Ibrahimi 2005; Chan 2008; Gould and Kodikara 2008; Gould and Kodikara 2009) showed that higher failure rates were recorded in hot and dry summers when soil shrinkage occurred. In this study, it was found that upward and downward bending of pipes in the vertical direction occurred corresponding to increase and decrease of soil moisture content, respectively. Maximum flexural stress measured in both upward and downward bending suggested that failure of pipes could occur in both extreme conditions. Since pipe bending occurred due to both soils shrinkage and swelling, the reason of higher failure rates recorded in hot and dry summers might possibly be due to shrinkage of soils occurred more quickly than swelling of soils which occurred gradually as observed in Altona North. In addition, the cyclic upward and downward pipe bending due to wetting and drying of soils can also reduce the strength of the pipe and ultimately led to circumferential fractures.

4.8 Conclusions

The field data collected from both sites provides information on understanding of the effect of changes in soils and the prevailing climate on the behaviour of buried in-service pipes. Unfortunately, numerous sensors failed to work properly and could not provide data for analysis. It was shown that buried pipes were subjected to vertical and horizontal bending due to swelling and shrinkage of soils. The findings suggest that bending of the pipe is primarily due to seasonal variations of soil moisture content. The maximum flexural stress due to pipe bending can possibly lead to failure of aged and corroded cast iron pipes. Shrinkage of soils was found to occur more quickly than swelling, which is possibly related to higher pipe failure rates in hot and dry summers. Thus, the prevailing climate has a significant effect on the soil conditions which in turn lead to seasonal bending of the buried pipes.

CHAPTER 5

REGIONAL FIELD MEASUREMENT OF SOIL MOISTURE CONTENT

5.1 Introduction

The study on field behaviour of buried in-service pipes described in Chapter 4 identified that bending of pipes due to swelling and shrinking of soils could lead to failure of aged and corroded cast iron pipes. It follows then the knowledge of soil moisture variations close to the pipe is of substantial value in determining the possible pipe bending and failure prediction. In order to acquire a broader view of the variations of the soil moisture content, long-term monitoring program on regional Melbourne was implemented. The indirect neutron scattering method was used for the measurements of soil moisture content. This chapter presents the background theory of neutron scattering method, sensor calibration, field work, analysis of the measured soil moisture content, and

the variations of soil moisture content in sites with different soil types. Part of the information and data presented in this chapter were published in the research report, RR15 (Rajeev *et al.* 2010).

5.2 Overview of the Neutron Scattering Method

5.2.1 Principal of the neutron method

The neutron scattering method for measurement of soil moisture content is based on the principle of neutron thermalisation. Hydrogen nuclei within water molecules have a natural property of slowing down neutrons. When high energy neutrons emits from radioactive sources (e.g., americium-beryllium or radium-beryllium) the energy of the neutrons will be reduced to about the thermal energy of colliding atoms of a substance at room temperature, when collided with hydrogen nucleus. The choice of neutron for moisture measurement is based on consideration of both energy transfer and scattering cross-section, as it has a nucleus of about the same size and mass as hydrogen, which will produce a greater thermalising effect than any other elements. Thermalised neutron density can be easily measured with a detector, if the captured cross-section, except for that due to water, remains constant (i.e., chemical composition is constant), then the thermal neutron density may be calibrated against water concentration on a volume basis.

The neutron probe technology based on the neutron scattering method has been developed more than sixty years ago (Belcher *et al.* 1950). Soil moisture data collected using neutron probes can be used:

- to determine the soil moisture content at a given depth;
- to determine the total amount of soil moisture to a given depth, (e.g., 0.50 m); and
- to determine changes in soil moisture with time at a given depth.

Most commercially manufactured neutron probes are designed broadly to the same mechanical principles, although in detail they may differ considerably. It normally consists of a probe containing essentially a fast neutron source and a slow thermal neutron detector, a pulse counter, a cable connecting the two, and a transport shield. The 503DR hydroprobe manufactured by CPN International, Inc., which was used in this study, is shown in Figure 5-1.



Figure 5-1 503DR hydroprobe

The neutron source is a mixture of an alpha particle emitter (i.e., americium-241) and a fine powder of beryllium. When alpha particles bombarded the beryllium nuclei, the following reaction takes place ${}^9_4\text{Be} + {}^4_2\text{He} \rightarrow {}^1_0\text{n} + {}^{12}_6\text{C}$ so that fast neutrons diffuse in the soil medium and slowed down due to thermalisation. The strength of the source generally depends on the alpha particle emitter, measured in milliCuries (mCi) or in Becquerel (Bq). Most sources have an activity in the range of 5 to 50 mCi. Since most alpha emitters also emit some gamma radiation and most sources will emit alpha particles, gamma radiation and fast neutrons, radiation protection is an important issue. The container of the probe, which acts as a shield, has to be properly designed to protect the user from

exposure to radiation. The most widely used neutron source at present is $^{241}\text{Am-Be}$, as it produces a much lower level of gamma radiation than $^{226}\text{Ra-Be}$ source, hence lower level of shielding is required.

The thermal neutron detector and counter systems vary for different types of probe, but the basic design will include the amplifier, high-voltage source, timer, counter, rechargeable batteries, and microprocessor. The counting time is related to the statistical accuracy of estimating the soil moisture content, where the count is detected as the impulse originating from a slow neutron. The count data are then outputted in count per minute (cpm) or per second (cps) by the microprocessor.

5.2.2 Interaction of neutron and soils

During the measurement, high energy neutrons are emitted from the source, which interact with soil particles and soil water that surrounds the probe. Three processes occurred during the measurement of interaction; neutron absorption by nuclei, neutron scattering through collisions, and neutron disintegration.

Neutron absorption interaction occurs when a neutron enters a nucleus, and forming a new isotope in an excited state. It is usually rapidly relaxed by emitting gamma radiation. These reactions are strongly dependent on the neutron energy level. In ordinary soils, absorption of fast neutrons can usually be neglected as it is rapidly decreased for energies above the thermal range (IAEA 1970). In the reaction of neutron absorption, a nucleus, ^A_ZX will be transformed:



Neutron scattering interaction occurs when the kinetic energy of a neutron is partially or completely transferred to the impacted nuclei in successive collisions through elastic or inelastic scattering. Elastic scattering is the dominant mode of interaction for fast neutrons in soils. Fast and high energy neutrons ($> 2 \text{ MeV}$) will lose energy through collision with hydrogen atoms in water and become slow or thermal neutrons ($< 0.025 \text{ eV}$). A measurement of neutron count with higher thermal

neutrons represents higher soil moisture content, with the exception of soil organic matter, which may gradually fluctuate with time. Other soil materials containing constant amount of hydrogen are considered in the calibration equation.

Neutron disintegration interaction occurs under some circumstance when the new nucleus, ${}^{A+1}_{Z}X$ is unstable and disintegrates while emitting radiation. Nevertheless, this reaction will only occur with few nuclei presented in the soil, e.g., Ag, Au, IN, Fe, Al, and Mn, which in most cases, the concentrations are very low. Furthermore, the neutron flux emitted by the probe source has very low intensity, so that the chance of neutron absorption is extremely low (IAEA 1970). In some cases that a stable, radioactive nucleus is formed (e.g., ${}^{12}_{6}C + {}^1_0n \rightarrow {}^{13}_{6}C$, ${}^{14}_{7}N + {}^1_0n \rightarrow {}^{15}_{7}N$), it normally have a very short half-life and will not affect the measurement results.

5.2.3 Measurement procedure

A measurement of soil moisture content using the neutron probe can be done by fitting the transport shield to the top of the access tube made of aluminium or steel, which is transparent to thermal neutrons. The probe is lowered into the access tube to the required depth by the cable, which has a clamping depth indicator that can be mounted on the transport shield in order to maintain the depth of the probe. During the measurement, a spherical cloud of slow neutrons with diameters of approximately 300 mm is quickly develops in the soil around the source. The diameter of the cloud varies depending on the soil moisture content, where dry soils will have a relatively larger cloud than wet soils. The number of slow neutrons will be constant throughout the volume of the cloud and proportional to the soil moisture content. Therefore, the measurement of neutron count rate by the detector is proportional to the soil moisture content of the same volume. For a given counting rate, the counting time interval determines the precision of the measurement. A longer counting time provides more accurate data but then lesser measurements can be made in a day. In general, a count time of 16 seconds will provide sufficient precision for scheduling type operation, e.g., monthly basis measurement (CPN-International 2000). This count time was adopted for the study.

5.2.4 Calibration of neutron probe

Although the neutron probe has proven to be a convenient and effective means for monitoring long-term *in-situ* soil moisture variations (Schmugge *et al.* 1980; Silvestri *et al.* 1991), the correlation of neutron probe data (e.g., neutron counts) to absolute values of moisture content is not straightforward. Neutron count in wet soils are influenced by the moisture content, soil elemental composition, soil density, and proximity of the probe to the water table and soil surface (Dickey 1990). Neutron counts are also influenced by the strength of the neutron source, the size and type of the neutron detector, the position of the detector relative to the source, and the size and type of access tube (Schmugge *et al.* 1980; Stone 1990). Calibration is therefore necessary for each soil type covering the likely field moisture range and each access tube material, since it has been shown that the direct use of factory calibrations can often produce inaccurate results (Bell and McCulloch 1969; Rawls and Asmussen 1973; Vachaud *et al.* 1977; Carneiro and De Jong 1985; Chanasyk and Naeth 1996).

In general, the calibration of neutron probe is done by establishing a relationship between the neutron count rate, N in counts per minute (cpm) and the volumetric soil moisture content, θ_w . Soil samples with different moisture content are used in the calibration by measuring the neutron count rate with the probe then related to the soil moisture content measured by the traditional methods (e.g., oven drying). It is a simple procedure in theory but can be difficult and tedious to perform depending on the properties of the soil profile and the selected calibration method. One of the major problems in calibration is sampling. Theoretically, moisture content should be measured from the same sample which the neutron count rate was measured from, however the volume of sample measured by the neutron probe is not clearly defined. The sphere of influence has a diameter of approximately 300 mm but the samples used in the traditional method of soil moisture measurement are a lot smaller. This difference can be minimised by using several samples around the access tube for determination of traditional soil moisture content. Nevertheless, in most cases it is unable to guarantee that same volume of soils is used in both methods. This problem is worsening in soil profile with heterogeneous, layered or stony soils. Another practical problem is to obtain a wide range of moisture content for the same soil profile. Even though it can be achieved by wetting

and drying the soil artificially, it is a time consuming process as long periods of time is required for the infiltration of moisture into the soil. Since the soil do not wet or dry uniformly throughout the soil profile, the moisture content measured by the neutron probe are a spatial average over a volume of soils and the position and volume of soil to be considered in sampling is uncertain.

The calibration process can be undertaken in the laboratory or in the field. The laboratory calibration, also known as the drum calibration, is performed by packing a drum, having the diameter larger than the radius of influence of the neutron probe, with soils of know moisture and compact to the same density as in the field. The access tube is installed at the centre of the drum and neutron probe measurement is preceded. The drawback of laboratory calibration is usually the difficulty to reproduce soil fabric found *in-situ* in a drum (IAEA 1970). The process of field calibration is similar to the laboratory, where the access tube is installed in the field and neutron count rate measured along the soil profile is correlated with the estimated volumetric soil moisture content. Volumetric moisture content of the field soils are usually estimated from gravimetric soil moisture content and soil density (Li *et al.* 2003).

After the best set of data was achieved, the relationship between neutron count rate and volumetric soil moisture content can be obtained. According to Greacen and Schrale (1976) the neutron count rate obtained from the soil should not be used directly for calibration as these data may be affected by electronic drifts, temperature and other effects on the electronics of the neutron probe. It is advised that the neutron count ratio, n_{CR} defined by Equation 5-2 should be used,

$$n_{CR} = \frac{\text{count rate in soil}}{\text{count rate in standard}} = \frac{N}{N_s} = \frac{C \cdot T^{-1}}{C_s \cdot T^{-1}} \quad \text{Equation 5-2}$$

where C is number of counts measured in the soil during a period of time T in minutes; C_s is number of counts measured in a standard material during a period of time T_s ; N is the neutron count rate in the soil; and N_s is the neutron count rate in a standard material.

The bulk density correction of neutron count rate, n_c and moisture content, θ_c can be done by Equations 5-3 and 5-4 (Greacen and Schrale 1976),

$$n_c = n_{cR} \sqrt{\frac{\rho_{b,i}}{\rho_b}} \quad \text{Equation 5-3}$$

$$\theta_c = \theta_w \cdot \frac{\rho_{b,i}}{\rho_b} \quad \text{Equation 5-4}$$

where θ_w is the volumetric soil moisture content; $\rho_{b,i}$ is the bulk density of soil at a given depth; and ρ_b is the average bulk density of the soil profile. The volumetric soil moisture content, θ_w is calculated by:

$$\theta_w = \frac{\rho_b}{(1+\omega)\rho_w} \cdot a \quad \text{Equation 5-5}$$

where ω is the gravimetric soil moisture content and ρ_w is the density of water.

A least square linear regression of θ_c on n_c is also developed from the corrected data as Equation 5-6,

$$\theta_c = a + b \cdot n_c \quad \text{Equation 5-6}$$

where a is the y intercept and b is the slope of the calibration curve. The y intercept, a is depends on the soil and the type of probe, which does not necessary pass through the origin, as it is an extrapolated value out of the calibration range. Although there is no strong theoretical meaning given to the y intercept, it is nevertheless related to the residual moisture content of the soil. The slope, b is also depends on the soil and probe types. It is the derivative of the calibration curve and represents the sensitivity of the probe. The slope is generally the change of soil moisture content in per unit change of count ratio. The smaller the value, the greater the sensitivity of the probe, where a

small change in soil moisture content will result in a significant change in neutron count ratio. Since the calibration curve can be affected by the processes of neutron interaction in the soil, the geometry of the probe, the neutron detector types, the electronics of the probes, as well as the soil characteristics including, chemical composition, bulk density, a soil specific calibration curve may be required.

5.3 Field Measurement of Soil Moisture Content

5.3.1 Site selection criteria

The monitoring sites are selected by considering several criteria in order to be effective, safe, convenient, and least complicated for tube installations and field measurements. The site selection criteria were as follows:

- The site is clear of other utilities, e.g., service pipes, power cables, telecommunication cables, storm water pipes, and sewer pipes;
- A nature strip wide enough to allow for installation of the aluminium tube;
- No trees or other large vegetations located close to the aluminium tube; and
- A relatively quiet area with low traffic flow.

The geological maps of Melbourne (Rixon 1973; Greacen and Schrale 1976) and Victoria (Douglas and Spencer-Jones 1993) were used as a guide for selection of monitoring sites located in different geological formations. Large numbers of potential sites were selected using the drive-by and walking surveys according to the above criteria. A total of 50 sites were selected in the initial surveys. After contacting the corresponding authorities and local councils, and performing preliminary investigations, 23 sites were selected for the long term soil moisture content monitoring.

According to the Australian Standard of residential slab and footing design (Standards Australia 2011), the change of suction depth in Melbourne area ranged from 1.5 to 2.3 m, while the field

measurements presented in Chapter 4 showed that soil moisture content was relatively constant at the depths of 1.5 to 2.0 m. Therefore, aluminium tubes of 1.5 m long were installed at the 23 monitoring sites which allow for measurement of soil moisture content up to that depth. Shallow bed rocks were found at certain sites and the measurements were restricted to 1.0 to 1.2 m. Figure 5-2 shows the locations of all 23 monitored sites on a section of the Geological map of Victoria.

5.3.2 Site classification

5.3.2.1 Soil samples collection

In order to classify the soil properties of the selected sites disturbed soil samples were collected from the sites for laboratory soil testings. The soil samples were transported to the laboratory in sealed plastic bags and stored in a room with constant temperature prior to testing. The soil tests were performed in accordance with the relevant Australian Standards. The preliminary preparation of the soil samples was performed in accordance with the requirements of Australian Standard (Standards Australia 2001).

5.3.2.2 Soil particle size distribution

The Australian Standard sieving analysis and hydrometer analysis testing method (Standards Australia 2003) were used to analyse the particle size of the site soil samples. The procedure of the test was presented in Section 3.4.1 and will not be repeated here. The distribution curves of soil particles of Altona North and Fawkner were shown in Figure 3-6 in Chapter 3. The distribution curves for rest of the sites are presented in Appendix D. The results showed different grading of the soil samples depended on the location of the sites. Generally, Northern and Western regions of Melbourne have higher percentage of silts and clays, while sandy soils were found in the Southern region.

5.3.2.3 Atterberg limits

The Atterberg limit tests were conducted in accordance with the Australian Standard (Standards Australia, 2008; 2009a; 2009b). Details of these tests were presented in Section 3.4.2 and will not be repeated. The results of the monitoring sites, except Site 3 and 4 which contained coarse grained soils, are plotted in the plasticity chart (Standards Australia 1993) in Figure 5-3. All of the points in the plot are above the A-line within the regions of inorganic clays of low to high plasticity. According to the studies of soil reactivity based on plasticity index as discussed in Section 2.4.3, reactivity of soils is proportional to wPI. The wPI of the site soils were calculated using the clay content obtained from particle size distribution and presented in Table 5-1.

5.3.2.4 Geological profiles

The geological formation for each of the monitoring site was classified using the geological map and soil characterisation data. Three major categories according to the Australian Standard for residual slab and footing construction (Standards Australia 2011) were used; basaltic clay, non-basaltic clay, and Quaternary alluvials and Tertiary sediments. Basaltic clay is referred to residual and alluvial clay derived from basaltic and similar volcanic rocks, particularly the New Volcanins, which are highly to extremely reactive and corresponding to ground displacement with moisture change. Non-basaltic clay is residual clay derived from sedimentary, metamorphic and granitic rocks, which are moderately to highly reactive. Quaternary alluvials and tertiary sediments are deposits from delta, dune, lake, stream, colluvial and wind-laid, these soils are slightly to moderately reactive to changes in soil moisture content.

5.3.2.5 Summary of site classification

Table 5-1 shows the summary of tests results and site classification. Variations of soil moisture content primarily depended on the seasonal climate effect, e.g., rainfall, evaporation, and the hydraulic conductivity of soils. These factors will affect the time required for moisture to infiltrate the soil after rainfall and the evaporation of moisture from soil surface. It is expected that sites located in the western and northern regions will have smaller variations in moisture content at

greater depths (e.g., over 1000 mm) due to higher content of silts and clays, while greater variations in soil moisture content would likely to be observed in the sandy soils in the southern region. In terms of reactivity, monitoring sites in western and northern regions would be more sensitive to change in moisture content and would exhibit greater soil displacement than those in the southern region.

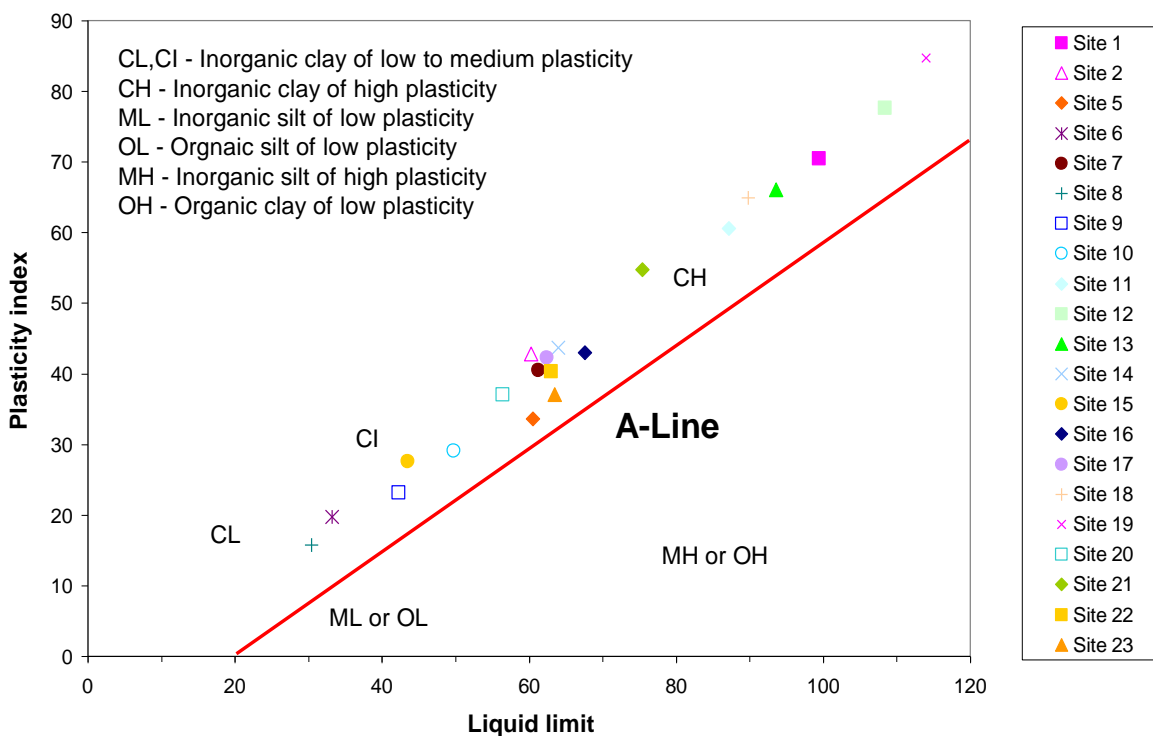


Figure 5-3 Plasticity chart for classification of fine grained soils

Table 5-1 Summary of soil properties of the monitoring sites

Site 1 Altona North		Site 2 Fawkner		Site 3 Carrum	
Plastic limit	28.9	Plastic limit	17.5	Plastic limit	-
Liquid limit	99.4	Liquid limit	60.3	Liquid limit	-
Plasticity index	70.5	Plasticity index	42.8	Plasticity index	-
Linear shrinkage	21.2%	Linear shrinkage	18.1%	Linear shrinkage	-
Soil group	CH	Soil group	CH	Soil group	SM
Geological profile	Basaltic clay	Geological profile	Basaltic clay	Geological profile	Quaternary alluvials
wPI	67.9	wPI	39.1	wPI	-
Reactivity	High	Reactivity	High	Reactivity	Low
Site 4 Oakleigh South		Site 5 Doveton		Site 6 Kew	
Plastic limit	-	Plastic limit	26.9	Plastic limit	13.5
Liquid limit	-	Liquid limit	60.5	Liquid limit	33.2
Plasticity index	-	Plasticity index	33.6	Plasticity index	19.7
Linear shrinkage	-	Linear shrinkage	11.4%	Linear shrinkage	11.8%
Soil group	SM	Soil group	CH	Soil group	SC
Geological profile	Quaternary alluvials	Geological profile	Quaternary alluvials	Geological profile	Non-basaltic clay
wPI	-	wPI	21.4	wPI	7.9
Reactivity	Low	Reactivity	Moderate	Reactivity	Medium
Site 7 Heidelberg West		Site 8 Mount Eliza		Site 9 Forest Hill	
Plastic limit	20.8	Plastic limit	14.7	Plastic limit	19.1
Liquid limit	61.3	Liquid limit	30.4	Liquid limit	42.3
Plasticity index	40.5	Plasticity index	15.7	Plasticity index	23.2
Linear shrinkage	16.2%	Linear shrinkage	7.5%	Linear shrinkage	8.3%
Soil group	CH	Soil group	SC	Soil group	CI
Geological profile	Non-basaltic clay	Geological profile	Quaternary alluvials	Geological profile	Non-basaltic clay
wPI	37.3	wPI	6.3	wPI	17.1
Reactivity	High	Reactivity	Medium	Reactivity	Moderate
Site 10 Bulleen		Site 11 Avondale Heights		Site 12 Deer Park	
Plastic limit	20.7	Plastic limit	26.4	Plastic limit	30.8
Liquid limit	49.8	Liquid limit	87.2	Liquid limit	108.4
Plasticity index	29.1	Plasticity index	60.6	Plasticity index	77.6
Linear shrinkage	14.2%	Linear shrinkage	22.8%	Linear shrinkage	25.6%
Soil group	CI	Soil group	CH	Soil group	CH
Geological profile	Non-basaltic clay	Geological profile	Basaltic clay	Geological profile	Basaltic clay
wPI	25.8	wPI	57.9	wPI	75.2
Reactivity	Moderate	Reactivity	High	Reactivity	High

Site 13 St Albans		Site 14 Coburg		Site 15 Keysborough	
Plastic limit	27.6	Plastic limit	20.3	Plastic limit	15.9
Liquid limit	93.6	Liquid limit	64	Liquid limit	43.5
Plasticity index	66	Plasticity index	43.7	Plasticity index	27.6
Linear shrinkage	20.4%	Linear shrinkage	18.1%	Linear shrinkage	13.4%
Soil group	CH	Soil group	CH	Soil group	SC
Geological profile	Basaltic clay	Geological profile	Basaltic clay	Geological profile	Quaternary alluvials
wPI	57.0	wPI	35.2	wPI	8.4
Reactivity	High	Reactivity	Moderate	Reactivity	Medium
Site 16 Fairfield		Site 17 Kingsbury		Site 18 Epping	
Plastic limit	24.6	Plastic limit	20.1	Plastic limit	24.9
Liquid limit	67.6	Liquid limit	62.4	Liquid limit	89.8
Plasticity index	43	Plasticity index	42.3	Plasticity index	64.9
Linear shrinkage	17.3%	Linear shrinkage	12.6%	Linear shrinkage	17.3%
Soil group	CH	Soil group	CH	Soil group	CH
Geological profile	Non-basaltic clay	Geological profile	Basaltic clay	Geological profile	Basaltic clay
wPI	38.9	wPI	39.0	wPI	46.9
Reactivity	High	Reactivity	High	Reactivity	High
Site 19 Maidstone		Site 20 Sunshine		Site 21 Gladstone Park	
Plastic limit	29.3	Plastic limit	19.4	Plastic limit	20.7
Liquid limit	114	Liquid limit	56.4	Liquid limit	75.4
Plasticity index	84.7	Plasticity index	37	Plasticity index	54.7
Linear shrinkage	30.4%	Linear shrinkage	15.4%	Linear shrinkage	19.3%
Soil group	CH	Soil group	CI	Soil group	CH
Geological profile	Basaltic clay	Geological profile	Basaltic clay	Geological profile	Basaltic clay
wPI	78.3	wPI	27.8	wPI	37.9
Reactivity	High	Reactivity	Moderate	Reactivity	High
Site 22 Lalor		Site 23 Laverton			
Plastic limit	22.7	Plastic limit	26.5		
Liquid limit	63	Liquid limit	63.5		
Plasticity index	40.3	Plasticity index	37		
Linear shrinkage	13.4%	Linear shrinkage	37.0%		
Soil group	CH	Soil group	CH		
Geological profile	Basaltic clay	Geological profile	Basaltic clay		
wPI	39.5	wPI	36.1		
Reactivity	High	Reactivity	High		

5.3.3 Field instrumentations

5.3.3.1 Requirements of access tube

An access tube is required at each monitoring site for measurements of soil moisture content along the soil profile. The main purpose of the tubes is to provide a constant access in the ground for measurement. Installation of the access tube needs to be undertaken properly in order to obtain accurate results.

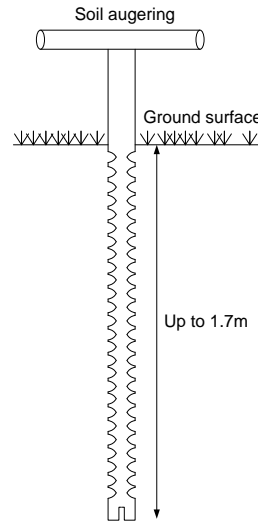
Different problems arose on each site during tube installation. The most common problem was the encountering of shallow rock layers which was solved by reducing the length of the access tubes. Aluminium, aluminium alloy, brass, stainless steel and plastic tubes are all being used as access tubes. The major considerations in the choice of materials were susceptibility to corrosion, mechanical strength, cost, intended depth of installation, and reaction to neutrons. Aluminium is the most transparent material to thermal neutrons; brass reduces the count rate slightly and may corrode in an alkaline soil; stainless steel is the most durable material but the large neutron absorption gives a considerably reduced count rate, the advantage is, it is strong enough to be flush-coupled, making it possible to reach greater depths. In this study, aluminium tubes were used as being cost-effective, allowing measurements up to moderate depth (i.e., 1 to 1.5 m), and being transparent to thermal neutrons. The selected access tubes have an outer diameter of 41.25 mm and wall thickness of 1.6 mm with the bottom closed by a tapered plug of the same material which may be either turned or casted.

5.3.3.2 Tube installation procedure

Tube installation on site was started by preparing a hole for the access tube using a hand auger or a motorised auger (Figure 5-4(a)). The depth of the hole was driven to approximately 200 mm longer than the length of the access tube, as shown in Figure 5-4(b). Small amount of water was added into the hole while drilling to soften the soil and allow the drilling work to progress easier.



(a)



(b)

Figure 5-4 Preparation of the access hole: (a) preparing an access hole with hand auger; (b) cross-section of soil augering

A hole prepared by augering may be unsatisfactory in some cases. The presence of stones can deflect the auger bit and when the stone is forced aside a cavity may be made in the side of the hole. Furthermore, the repeated vertical movement of the auger in the hole during drilling tended to enlarge the top of the hole, which created cavity for water to flow down along the outside boundary of the access tube. These problems can be overcome to some extent by backfilling from the ground surface and performing the installation carefully.

After the hole was prepared, it is important to ensure the access tube was tightly fitted to the tube by pushing the tube into the hole by hand as far as it could go (Figure 5-5(a)), then reverted to use a hammer to gently drove the tube the rest of the way (Figure 5-5(b)). An area of approximately 100 by 100 mm around the tube was excavated to a depth of 100 mm below the ground surface to allow for installation of a steel protection box. The access tube was then pushed further into the hole so that approximately 50 mm of the access tube was protruded above the soil surface after installation. A rubber bung was used as a stopper to seal off the top of the access tube in order to avoid water

and surface soil entering the tube, thus affecting the accuracy of soil moisture content measurements. The steel protection box (Figure 5-6(a)) was installed above the pipe to provide access during measurements, as well as protecting the tube against progressive damage and curiosity of animals and the public. The top of the steel box was flushed with the existing ground surface level to allow for mowing and minimised a tripping hazard (Figure 5-6(b)). Under favourable conditions, three to four tubes could be installed in a day. The tube installation work was carried out between February to May 2009 and moisture monitoring of the selected sites were started immediately after the tubes were installed.



(a)



(b)

Figure 5-5 Installation of the access tube: (a) push the tube by hand; (b) drove the tube with a hammer

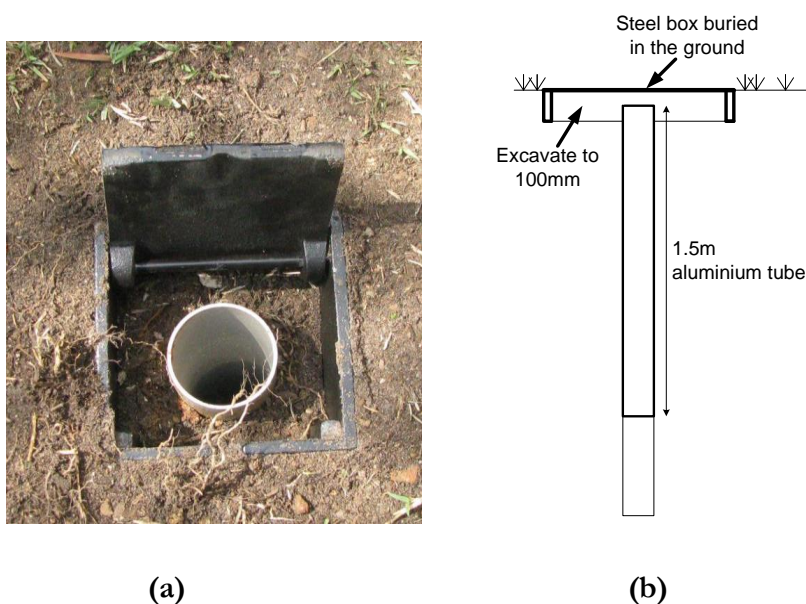


Figure 5-6 Installation of the protection box: (a) protection box installed above the tube; (b) cross-section of the tube and box after installation

5.3.4 Field calibrations

As noted previously in Section 5.2.4, the calibration of neutron probe is done by establishing the relationship between neutron count ratio and soil moisture content. It was decided that the field calibration method to be performed in this study, since it would be easier to undertake field measurement and collect soil samples at the sites than preparing calibration samples in the laboratory similar to the field conditions.

The field calibrations were performed on May 2009, after aluminium tubes were installed at all 23 monitoring sites. Seven different sites were selected so that the calibration could be finished within a day as well as covering a great variety of soil characteristic as the selected sites have contained basaltic clay, non-basaltic clay, and alluvial soils. The selected sites were Site 4 Oakleigh South, Site 5 Doveton, Site 7 Heidelberg West, Site 9 Forest Hill, Site 10 Bulleen, Site 11 Avondale Heights, and Site 12 Deer Park. The soil moisture content at each site was measured by the neutron probe

through the access tubes and push tube core soil samples were collected immediately at the same depths close to the access tube. Figure 5-7(a) shows the measurement of soil moisture content on site with the neutron probe. Chadwick Geotechnics, a company specialised in geotechnical investigation was employed to conduct the core soil sampling on site. Figure 5-7(b) shows the soil sampling in progress using the Terrier tracked dynamic sampling rig. The sampling was conducted by stepping down a sample barrel, which contained PVC lining of 100 mm diameter. Soil samples were collected in the PVC lining of 1 m length, the end of the lining were sealed with plastic bags and duct tape before transported to the laboratory for density and moisture content measurement. The core samples were collected at locations close to the access tube in each site to the same depth as the measuring depth of the access tube which was 1.5 m in most cases. A total of 62 core samples were collected from the seven sites.

The gravimetric soil moisture content, ω was determined by oven drying method and the bulk density, ρ_b at various depths were determined from volume and weight of the samples. Table 5-2 shows the bulk density measured at various depths of the selected calibration sites and the corresponding gravimetric moisture content data. The volumetric soil moisture content, θ_w was calculated by Equation 5-4. The corrected neutron count ratio, n_c and the corresponding volumetric soil moisture content, θ_c of the calibration sites were calculated using Equations 5-2 and 5-3. Figure 5-8 illustrates the plot of θ_c against n_c of all calibration sites with a least-squares linear regression line. A summary of the least-squares regression equation lines including the y-intercept, a , the slope, b and the coefficient of determination, R^2 of each plot is shown in Table 5-3.

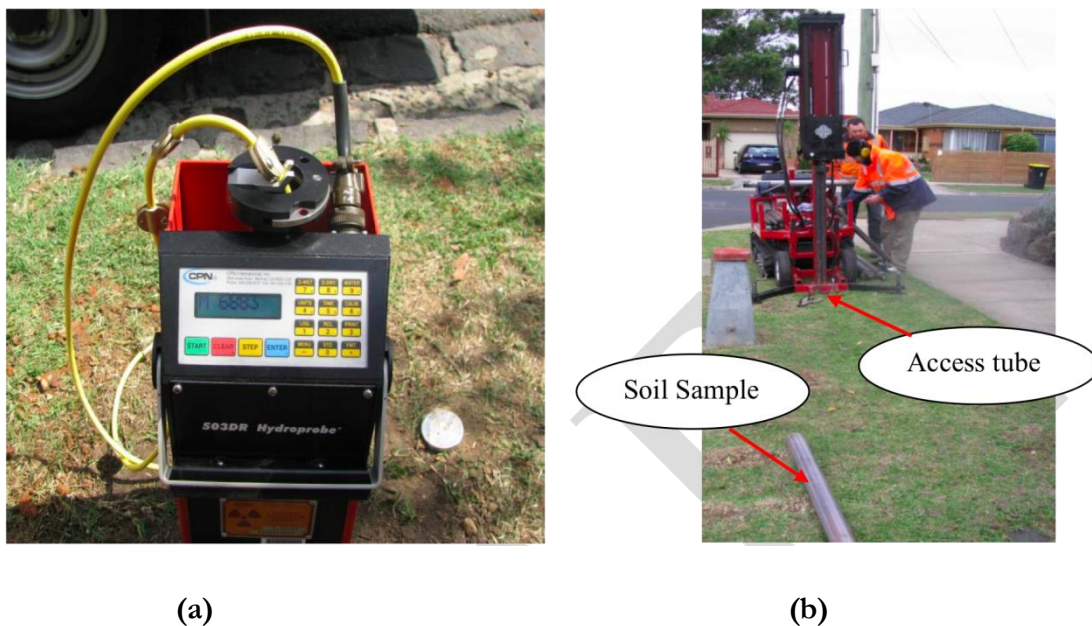
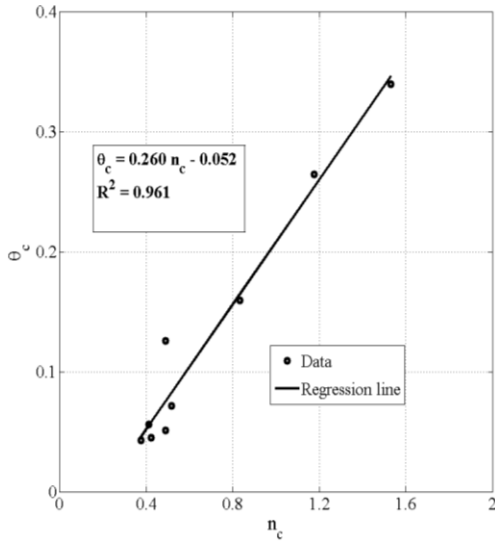


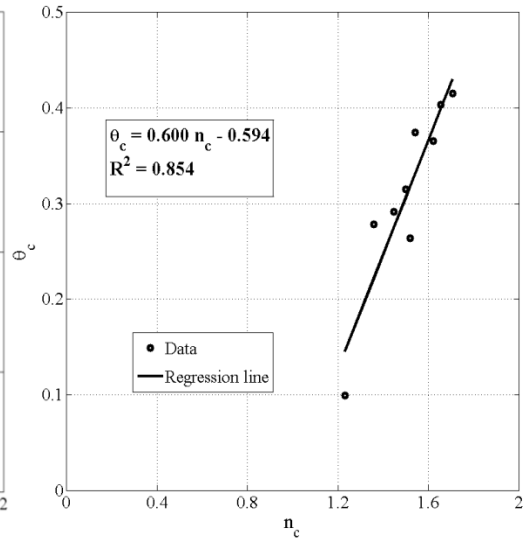
Figure 5-7 Field calibration of neutron probe: (a) moisture measurement with neutron probe; (b) core samples collected on site

Table 5-2 Soil bulk density of the calibration sites

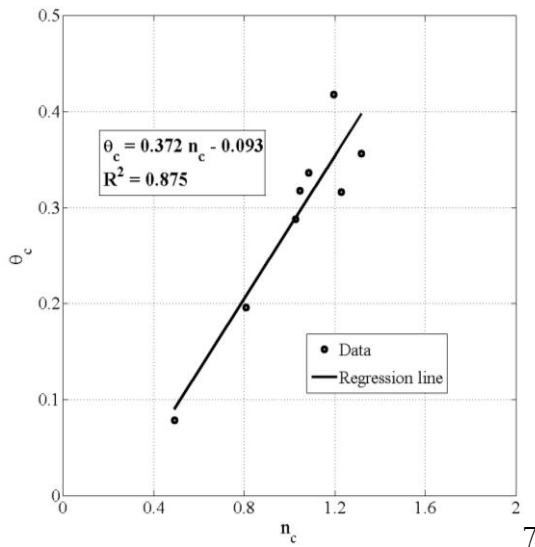
Depth (mm)	Site 4		Site 5		Site 7		Site 9		Site 10		Site 11		Site 12	
	Bulk Density (kg/m ³)	θ_c (%)	Bulk Density (kg/m ³)	θ_c (%)	Bulk Density (kg/m ³)	θ_c (%)	Bulk Density (kg/m ³)	θ_c (%)	Bulk Density (kg/m ³)	θ_c (%)	Bulk Density (kg/m ³)	θ_c (%)	Bulk Density (kg/m ³)	θ_c (%)
150	1560	5.4	1560	8.3	870	11.6	1950	25.1	1940	8.0	1960	13.9	1740	25.7
250	1450	3.9	1450	27.8	1530	14.1	2000	25.3	1940	7.7	2050	18.4	1560	28.9
350	1450	3.7	1930	25.9	2180	14.3	1920	20.0	1940	7.4	2040	26.3	1820	32.2
450	1590	4.0	2120	21.4	2000	15.6	2130	32.9	1940	25.0	2020	27.3	1760	32.5
550	1710	8.4	1980	21.5	2100	16.6	1970	23.3	1940	26.6	1810	26.4	1690	34.6
800	1480	4.3	2010	21.3	2090	21.8	1980	23.8	2010	18.6	2200	23.3	1760	35.6
1000	1620	3.6	1970	12.8	2070	15.9	1880	17.9	2010	18.2	1950	21.0	1770	33.7
1200	2050	13.7	2070	14.9	2110	17.6	2060	24.7	2120	13.1	1940	20.6	1750	31.3
1400	2180	16.3	2010	15.0	-	-	2110	23.3	2100	17.4	2200	19.5	1590	41.2
Ave	1677	7.0	1900	18.8	1869	15.9	2000	24.0	1993	15.8	2019	21.8	1716	32.9



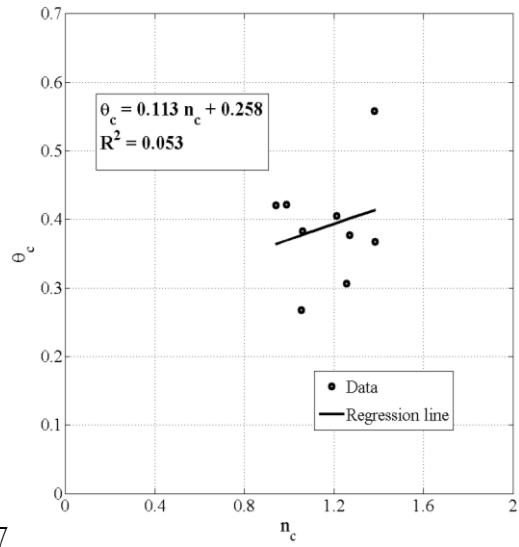
(a) Site 4 Oakleigh South



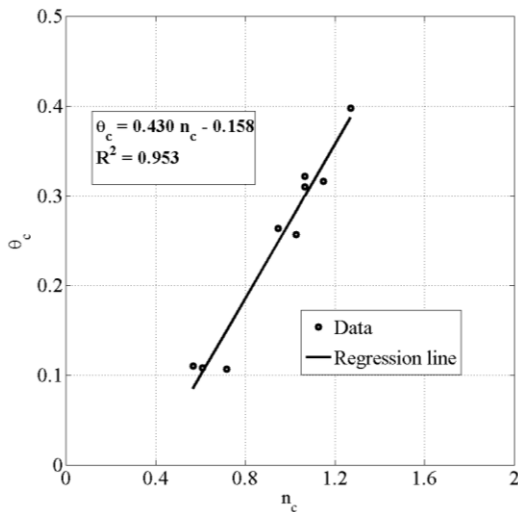
(b) Site 5 Doveton



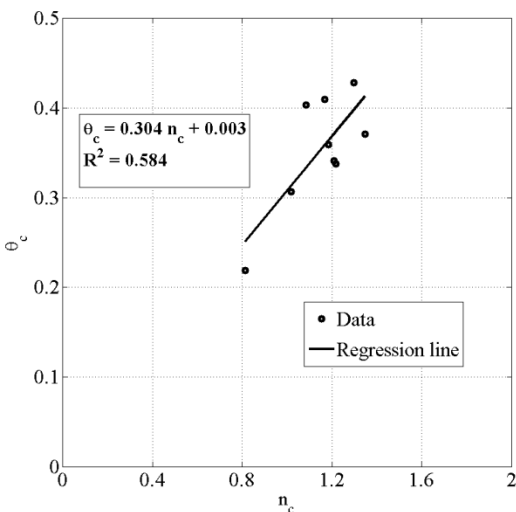
(c) Site 7 Heidelberg West



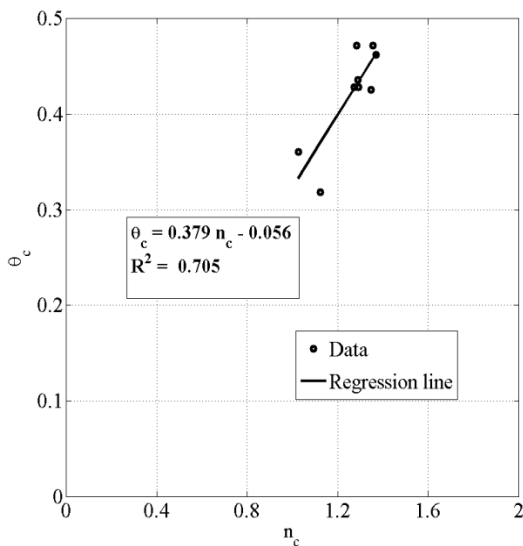
(d) Site 9 Forest Hill



(e) Site 10 Bulleen



(f) Site 11 Avondale Heights



(g) Site 12 Deer Park

Figure 5-8 Corrected volumetric soil moisture content against neutron count ratio of the calibration sites: (a) Site 4 Oakleigh South; (b) Site 5 Doveton; (c) Site 7 Heidelberg West; (d) Site 9 Forest Hill; (e) Site 10 Bulleen; (f) Site 11 Avondale Heights; (g) Site 12 Deer Park

Table 5-3 Summary of the least-squares linear regression equations of the calibration sites

Site No.	4	5	7	9	10	11	12
Number of data points	9	9	8	9	9	9	9
R^2	0.961	0.853	0.875	0.053	0.953	0.584	0.705
a	-0.052	-0.594	-0.093	0.258	-0.158	0.003	-0.056
b	0.26	0.6	0.372	0.113	0.43	0.304	0.379

The regression result of Site 9 Forest Hill showed a poor linear correlation, with R^2 of 0.053. It was suspected that uncertain sampling protocol and the highly stratified soil profile resulted in poor correlation on this occasion. To develop a general calibration equation for all 23 sites, the data collected from the six sites (except Site 9) were then combined for the regression analysis. The total number of data points used for the analysis was 53. Figure 5-9 shows the volumetric soil moisture content against corrected neutron count ratio together with the corresponding regression line for the combined data set with the $\pm \sigma$ and $\pm 2 \sigma$ lines from the mean.

The residuals (i.e., the difference between the measured values of soil moisture content and the corresponding values from the regression equation) were plotted as a function of the corrected count ratio to determine whether the data were homoscedastic such that the linear regression could be applied; and were such that residuals did not have outliers greater than two standard deviations away from zero. On the basis of this analysis, two more data points, which yielded the residuals greater than two standard deviations away from zero, were removed. Finally, after adjusting the data sets as described, a final least-square regression was performed and the residuals were checked for homoscedasticity compliance again. Altogether 37 data points out of 51 points lie between \pm one standard deviation from the regression line (i.e., more than 68% of the data lie within \pm one standard deviation). So the data were approximately normally distributed about the regression line.

Figure 5-10 shows the processed data and the corresponding regression line (total of 51 data points). This regression line was considered as the overall calibration equation for volumetric water content with corrected neutron count ratio and given as:

$$\theta_c = -0.050 + 0.318 \cdot n_c \quad \text{Equation 5-7}$$

This equation was used to determine the volumetric water content variation in 23 sites using the periodic neutron probe measurements, as described in the following section.

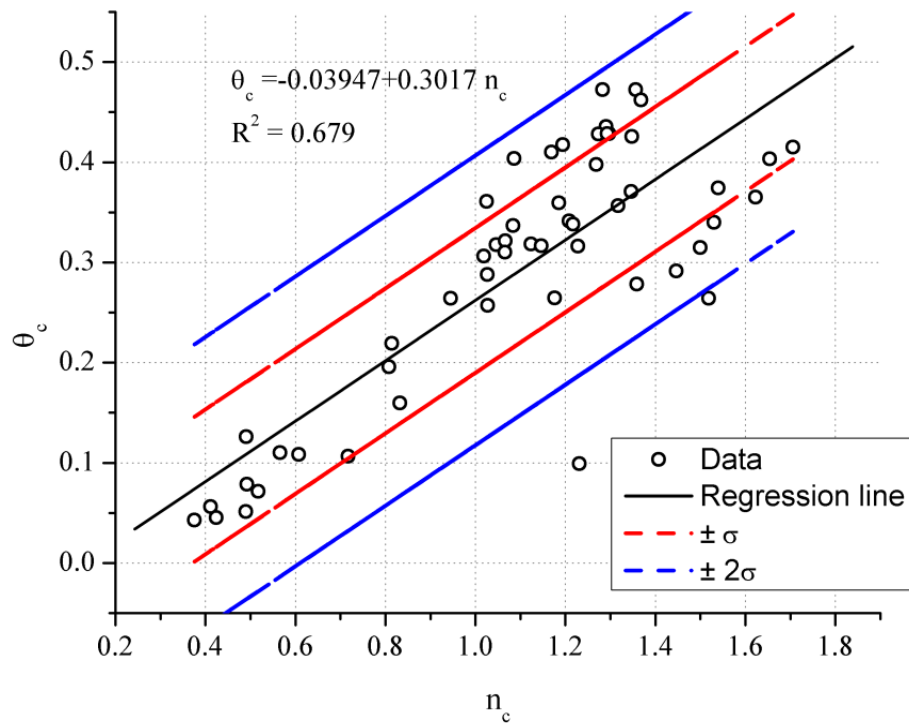


Figure 5-9 Combined data with linear regression line

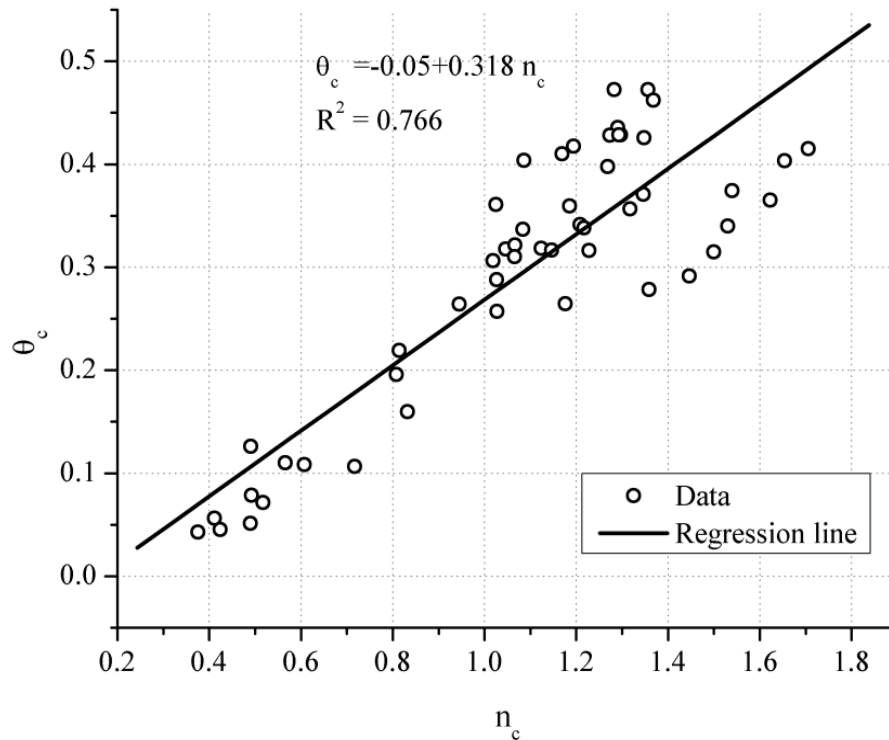


Figure 5-10 Cleaned data with linear regression line

5.4 Seasonal Variations of Soil Moisture Content

Monthly soil moisture content measurements were performed since the aluminium tubes were installed on February 2009. Moisture data measured up to October 2010 were used in the analysis. The measured changes in soil moisture content were similar for sites with same geological profiles and soil types, therefore only the measurements of nine selected sites are presented in this section. The measurements of the rest of the sites are presented in Appendix E.

Soil moisture content variations with time are given in Figure 5-11 to Figure 5-19 with rainfall for the nine selected sites. For each site, the corresponding rainfall data were obtained from the nearest monitoring station of the Department of Meteorology, Victoria. Each figure was divided into two plots; one from 150 to 550 mm as soil moisture content were highly sensitive to rainfall in these

depths, and the other one from 550 mm to the bottom of the aluminium tubes (i.e., 1000 to 1500 mm) using a larger scale for the soil moisture content, so that smaller changes could be observed.

In general, significant variations of soil moisture content due to rainfall could be observed at the soil depths down to 550 and 800 mm, while seasonal effects were more pronounced beyond a depth of 800 mm with the cyclic variations in soil moisture content recorded in some sites. These findings were same as the results obtained from the two field instrumentation sites in Altona North and Fawkner as described in Section 4.4. The geological profiles and soil types on site have significant effects on the magnitude of soil moisture content variations, especially at soil depths beyond 800 mm, since infiltration of moisture was faster in sandy than clayey soils.

Figure 5-11 to Figure 5-13 show the moisture variations of three selected sites contained basaltic clays, located in Western and North Western regions of Melbourne. The general geological profile of these sites was weathered Olivine basaltic clays with alkaline derivatives. Significant changes in soil moisture content could be observed in soil depths above 550 mm, and small variations of ± 2 to 3 % were recorded at soil depths of 1000 to 1400 mm. The time lapse in response to rainfall could be observed along the soil profile, as delays of two to three weeks occurred above the depths of 550 mm and delays of few weeks occurred below the depths of 550 mm. This behaviour was due to low hydraulic conductivity of basaltic clay soils on sites, where longer time was required for infiltrations of moisture into greater depths.

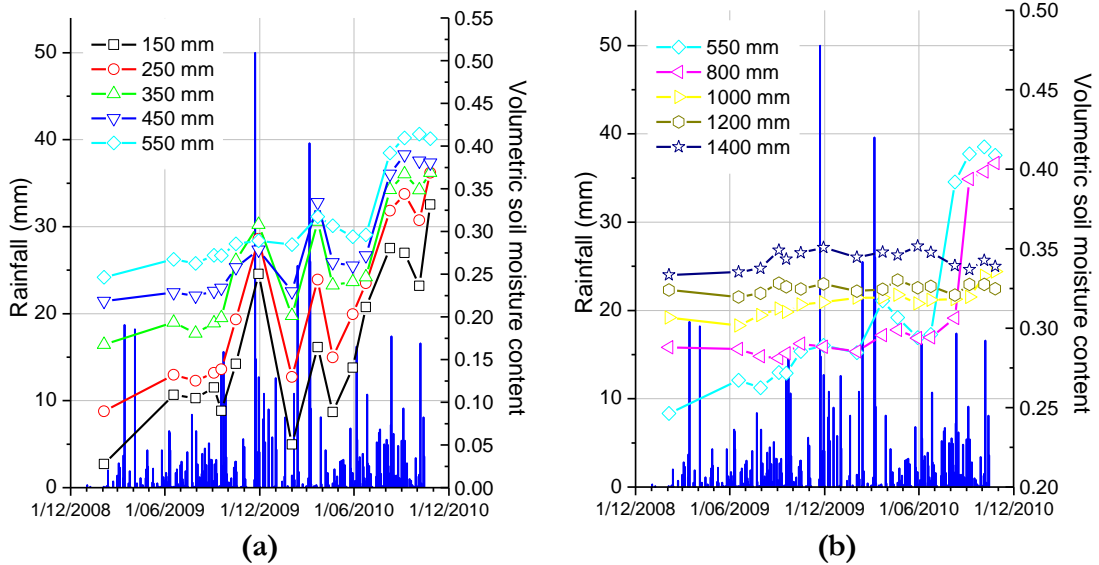


Figure 5-11 Volumetric soil moisture content in Site 1 Altona North: (a) 150 to 550 mm; (b) 550 to 1400 mm

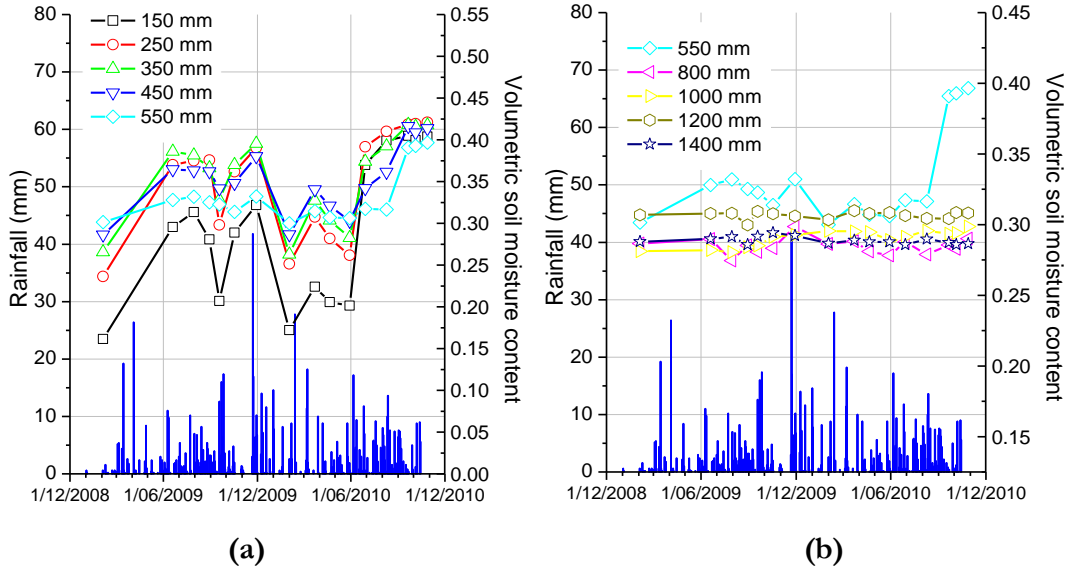


Figure 5-12 Volumetric soil moisture content in Site 2 Fawkner: (a) 150 to 550 mm; (b) 550 to 1400 mm

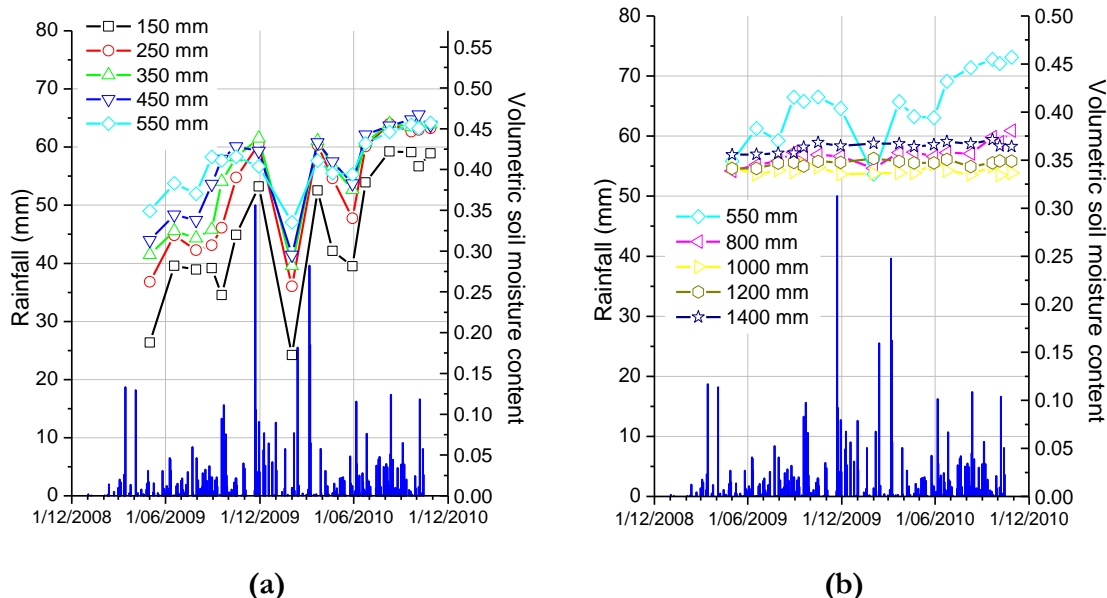
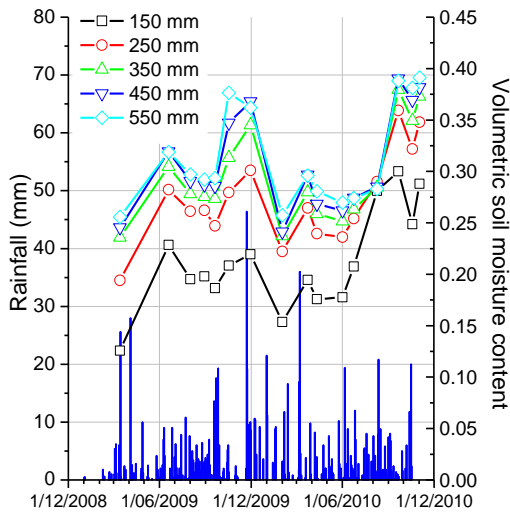
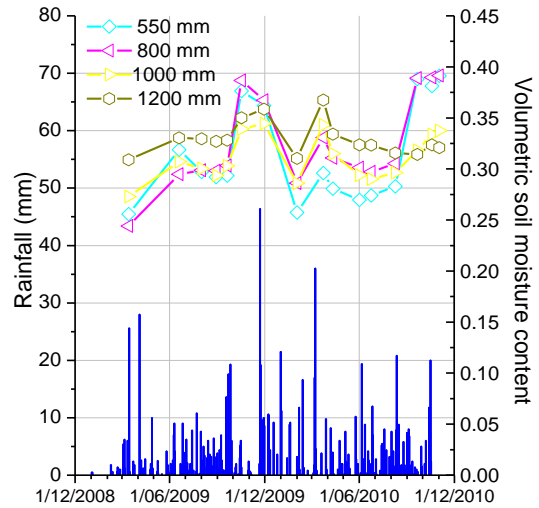


Figure 5-13 Volumetric soil moisture content in Site 11 Avondale Heights: (a) 150 to 550 mm; (b) 550 to 1400 mm

Figure 5-14 to Figure 5-16 show the soil moisture content variations of three sites contained non-basaltic clays, which located in the East and North Eastern regions of Melbourne. The geological profile of these sites was mixture of sandy clays and silts with laminated sandstone and interbedded mudstone and shale. Significant variations in soil moisture content of over $\pm 10\%$ could be observed at shallow depths, and approximately ± 5 to 10% variations occurred in greater depths (i.e., over 1000 mm) in these sites. The series of intense rainfall events at the end of 2010 increased the soil moisture content at all soil depths down to 1400 mm. This behaviour was due to the higher hydraulic conductivity of sandy clays at these sites than in the basaltic clay sites, which allowed faster infiltration of moisture into greater depths. The plots of soil particle size distribution in Appendix D show that the proportion of sand is 10 %, 30 % and 12 % in Site 7 Heidelberg West, Site 9 Forest Hill and Site 10 Bulleen, respectively, compares to approximately 5 % in average for the basaltic clay sites.

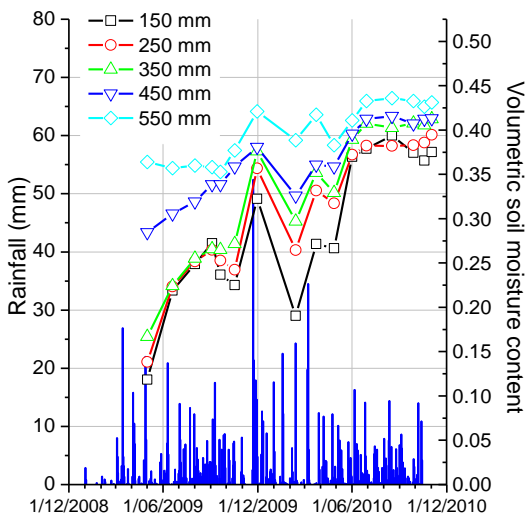


(a)

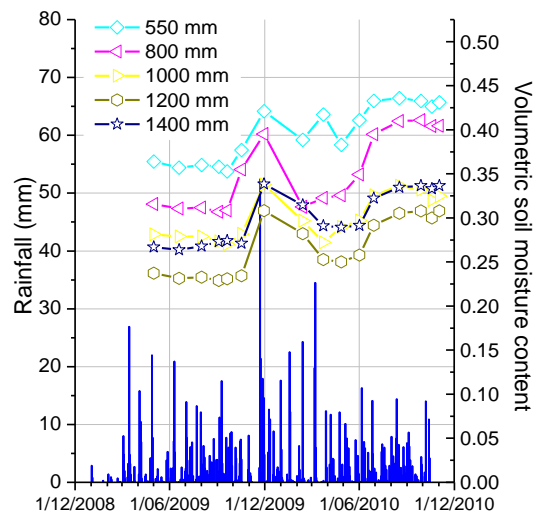


(b)

Figure 5-14 Volumetric soil moisture content in Site 7 Heidelberg West: (a) 150 to 550 mm; (b) 550 to 1200 mm



(a)



(b)

Figure 5-15 Volumetric soil moisture content in Site 9 Forest Hill: (a) 150 to 550 mm; (b) 550 to 1400 mm

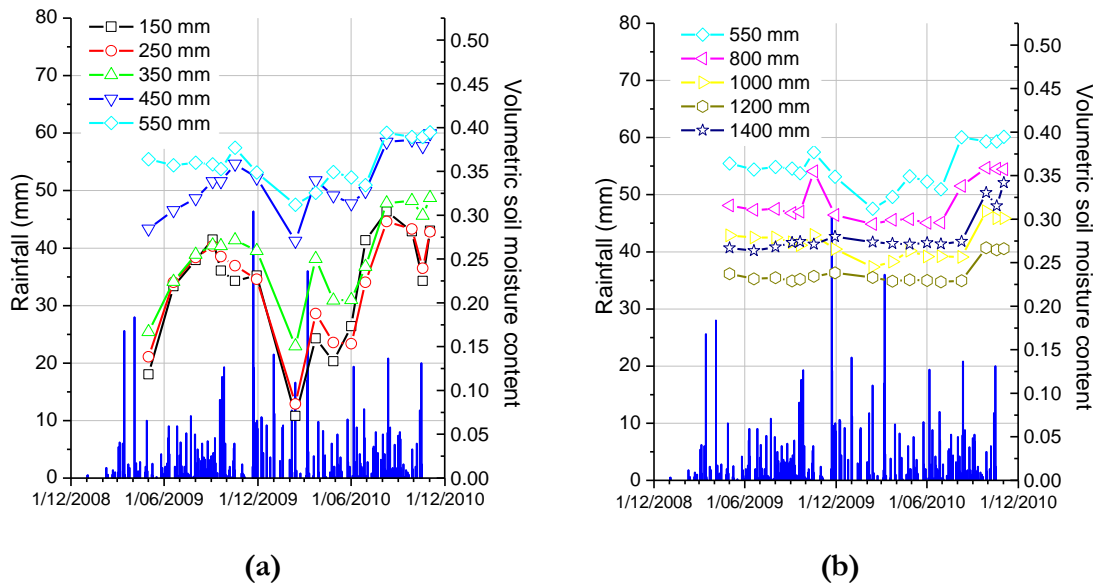
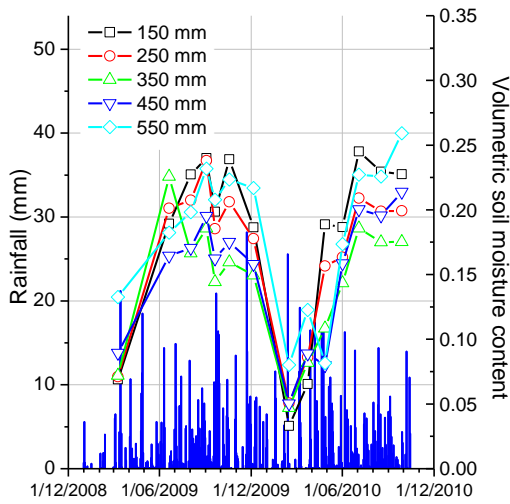
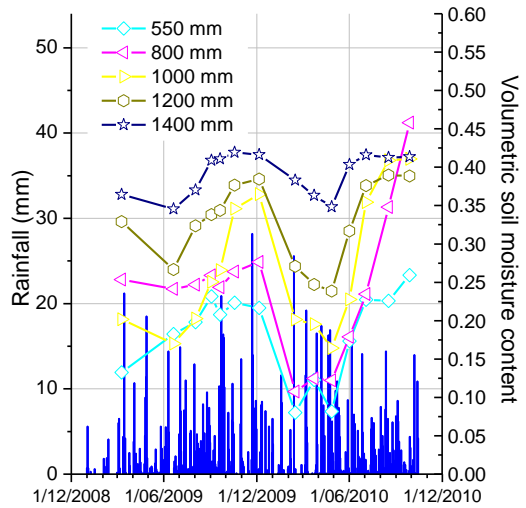


Figure 5-16 Volumetric soil moisture content in Site 10 Bulleen: (a) 150 to 550 mm; (b) 550 to 1400 mm

Figure 5-17 to Figure 5-19 show the moisture variations of the three selected sites contained Quaternary alluvial and tertiary sediments, situated in the South and South Eastern regions of Melbourne. The geological profile of these sites was alluvium and swamp deposits of gravel, sand, silt, clay, and black mud. The comparatively larger soil particles allowed faster infiltrations of moisture into the ground. Significant variations in soil moisture content could be observed over the full depths of the soil (i.e. 1400 mm). The changes in soil moisture content at these sites were closely related to the prevailing climate, immediate response to rainfall and drying events could be seen. The variations in soil moisture at shallow depths (i.e., 100 to 800 mm) were over $\pm 20\%$. At greater depths variations of $\pm 8\%$ were recorded at the depth of 1400 mm, which was very significant when compared with the changes of ± 2 to 3% measured at the depths of 1000 to 1400 mm in the basaltic clay sites.

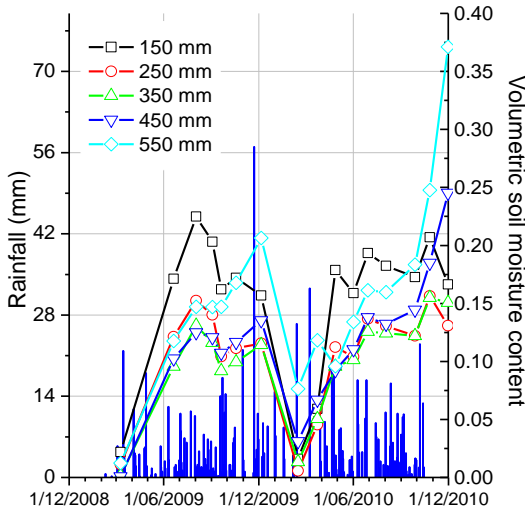


(a)

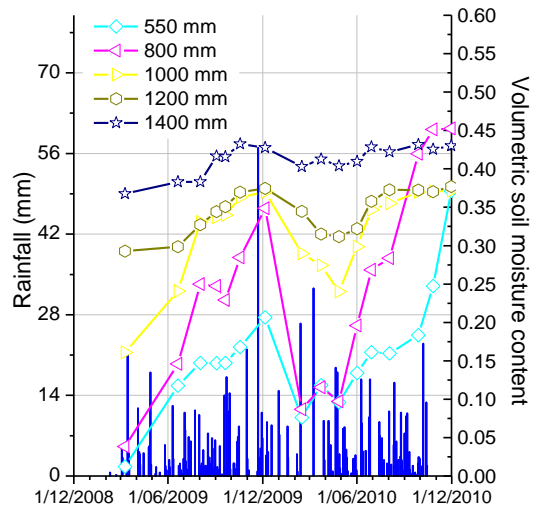


(b)

Figure 5-17 Volumetric soil moisture content in Site 3 Carrum: (a) 150 to 550 mm; (b) 550 to 1400 mm



(a)



(b)

Figure 5-18 Volumetric soil moisture content in Site 4 Oakleigh south: (a) 150 to 550 mm; (b) 550 to 1400 mm

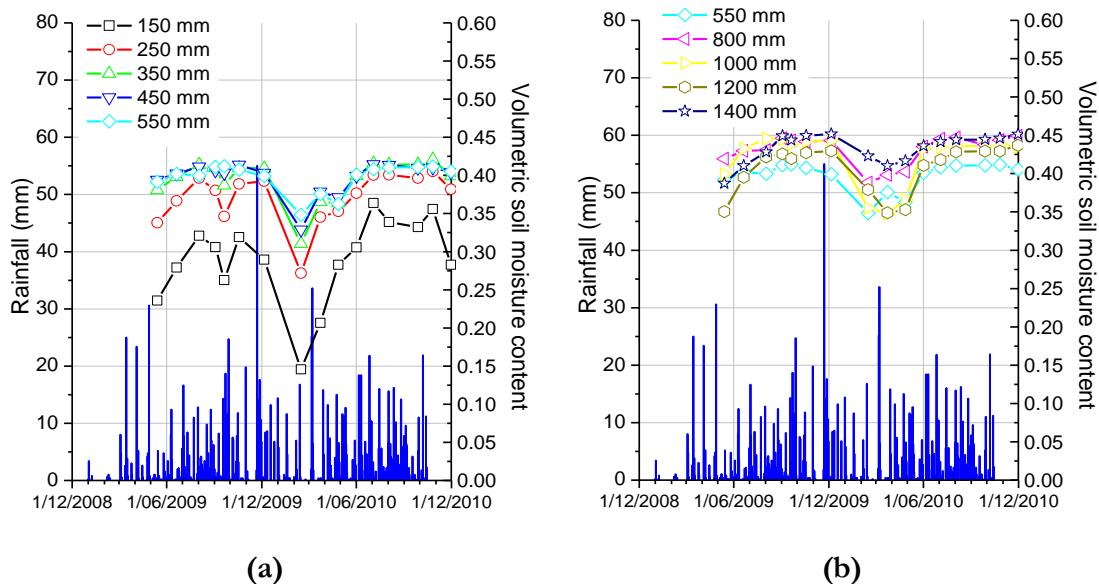


Figure 5-19 Volumetric soil moisture content in Site 15 Keysborough: (a) 150 to 550 mm; (b) 550 to 1400 mm

On the basis of the measured data and the magnitude of the moisture variations, analysis was undertaken by dividing the soil profile of each site into layers (e.g., above 800 mm, below 800 mm). Most of the sites were divided into two layers, except for sites that showed significant patterns of variations in soil moisture at various depths possibly due to a more complex soil profile, which were divided into three or more layers.

Table 5-4 shows the summary of soil moisture content variations analysis of the nine selected sites with site information. Summary for the rest of the sites is presented in Appendix F. The moisture changes were calculated on the basis of the difference between soil moisture content measured at the nominated depths, between the starting month and the ending month of a particular monitoring period. For example, 150-550 mm/ Jun 09–Nov 09/ increased: max 15%, min 2%; means that between the depths of 150 to 550 mm, the soil moisture content increased by a maximum of 15 % and a minimum of 2 % from the measurements on June 2009 to the measurements on November 2009.

Table 5-4 Analysis of seasonal soil moisture content variations

Site no.	Suburb	Soil symbol	Soil type	Geological formation	Seasonal soil moisture change		
					Depth (mm)	Months	
1	Altona North	CH	Inorganic clays of high plasticity	Basaltic clay	150-450	Jun 09-Nov 09	Increased: max 15%, min 2%
						Nov 09- Feb 10	Reduced: max 20%, min 1%
						Feb 10-Mar 10	Increased: max 11%, min 4%
						Mar 10-Jun 10	Reduced: max 3%, min 2%
					Jun 10-Oct 10	Increased: max 13%, min 11%	
					Jun 09-Nov 09	Increased: max 2%, min 1%	
					Nov 09-Feb 10	Reduced: less than 1%	
					Feb 10-Oct 10	Increased: max 24%, min 20%	
					Jun 09-Nov 09	Increased: max 2%, min 1%	
					Nov 09- Feb 10	Reduced: less than 1%	
Feb 10-Jun 10	Increased: less than 1%						
Jun 10-Oct 10	Reduced: less than 2%						
2	Fawkner	CH	Inorganic clays of high plasticity	Basaltic clay	150-550	Jun 09-Sep 09	Reduced: max 9%, min 2%
						Sep 09-Nov 09	Increased: max 11%, min 4%
						Nov 09-Jan 10	Reduced: max 15%, min 9%
						Jan 10-Mar 10	Increased: max 7%, min 5%
					Mar 10-Jun 10	Reduced: max 5%, min 2%	
					Jun 10-Oct 10	Increased: max 21%, min 9%	
					Jun 09-Oct 09	Increased: less than 1%	
					Oct 09-Jan 10	Reduced: less than 1%	
					Jan 10-Oct 10	Increased: less than 1%	
					Jun 09-Aug 09	Increased: max 5%, min 1%	
Aug 09-Sep 09	Reduced: max 5%, min 2%						
Sep 09 -Oct 09	Increased: max 4%, min 2%						
Oct 09-Feb 10	Reduced: max 21%, min 14%						
Feb 10-Oct 10	Increased: max 29%, min 10%						
Jun 09-Nov 09	Increased: max 19%, min 7%						
Nov 09-May 10	Reduced: max 10%, min 7%						
May 10-Oct 10	Increased: max 32%, min 11%						
3	Carrum	SM	Silty sands	Quaternary alluvial and tertiary sediments	150-800	Jun 09-Aug 09	Increased: max 5%, min 1%
						Aug 09-Sep 09	Reduced: max 5%, min 2%
						Sep 09 -Oct 09	Increased: max 4%, min 2%
						Oct 09-Feb 10	Reduced: max 21%, min 14%
					Feb 10-Oct 10	Increased: max 29%, min 10%	
					Jun 09-Nov 09	Increased: max 19%, min 7%	
					Nov 09-May 10	Reduced: max 10%, min 7%	
					May 10-Oct 10	Increased: max 32%, min 11%	
					800-1400	Jun 09-Oct 09	Increased: less than 1%
						Oct 09-Jan 10	Reduced: less than 1%
Jan 10-Oct 10	Increased: less than 1%						
Jun 09-Aug 09	Increased: max 5%, min 1%						
Aug 09-Sep 09	Reduced: max 5%, min 2%						
Sep 09 -Oct 09	Increased: max 4%, min 2%						
Oct 09-Feb 10	Reduced: max 21%, min 14%						
Feb 10-Oct 10	Increased: max 29%, min 10%						
Jun 09-Nov 09	Increased: max 19%, min 7%						
Nov 09-May 10	Reduced: max 10%, min 7%						
May 10-Oct 10	Increased: max 32%, min 11%						

Site no.	Suburb	Soil symbol	Soil type	Geological formation	Seasonal soil moisture change		
					Depth (mm)	Months	Mositure change (%)
4	Oakleigh South	SM	Silty sands	Quaternary alluvial and tertiary sediments, gravel, clay	150-800	Jun 09-Jul 09	Increased: max 10%, min 2%
						Jul 09-Sep 09	Reduced: max 6%, min 1%
						Sep 09-Dec 09	Increased: max 12%, min 1%
						Dec 09-Feb 10	Reduced: max 26%, min 10%
					1000-1400	Feb 10-Oct 10	Increased: max 21%, min 7%
						Jun 09-Dec 09	Increased: max 13%, min 5%
						Dec 09-Apr 10	Reduced: max 13%, min 3%
						Apr 10-Oct 10	Increased: max 29%, min 4%
7	Heidelberg West	CH	Inorganic clays of high plasticity	Non-basaltic clay	150-800	Jun 09-Sep 09	Reduced: max 3%, min 1%
						Sep 09-Nov 09	Increased: max 9%, min 3%
						Nov 09-Jan 10	Reduced: max 12%, min 8%
						Jan 10-Mar 10	Increased: max 4%, min 3%
						Mar 10-Jun 10	Reduced: max 3%, min 1%
						Jun 10-Oct 10	Increased: max 15%, min 10%
						Jun 09-Sep 09	Reduced: max 2%, min 1%
						Sep 09-Nov 09	Increased: max 5%, min 3%
						Nov 09-Jan 10	Reduced: max 5%, min 4%
						Jan 10-Mar 10	Increased: max 6%, min 5%
					1000-1200	Mar 10-Jun 10	Reduced: max 5%, min 4%
						Jun 10-Oct 10	Increased: max 12%, min 2%
						Jun 09-Sep 09	Increased: max 5%, min 4%
						Sep 09-Oct 09	Reduced: max 4%, min 3%
						Oct 09-Nov 09	Increased: max 12%, min 9%
						Nov 09-Feb 10	Reduced: max 13%, min 10%
						Feb 10-Mar 10	Increased: max 8%, min 7%
						Mar 10-Apr 10	Reduced: max 2%, min 1%
						Apr 10-Oct 10	Increased: max 10%, min 5%
						Jun 09-Nov 09	Increased: max 9%, min 6%
9	Forrest Hill	CL	Inorganic clays of low to medium plasticity	Non-basaltic clay	150-550	Nov 09-Mar 10	Reduced: max 8%, min 7%
						Mar 10-Apr 10	Reduced: max 2%, min 1%
						Apr 10-Oct 10	Increased: max 10%, min 5%
					800-1400	Jun 09-Nov 09	Increased: max 9%, min 6%
						Nov 09-Mar 10	Reduced: max 8%, min 5%
						Mar 10-Oct 10	Increased: max 9%, min 4%

Site no.	Suburb	Soil symbol	Soil type	Geological formation	Seasonal soil moisture change		
					Depth (mm)	Months	Mositure change (%)
10	Bulleen	CL	Inorganic clays of low to medium plasticity	Non-basaltic clay	150-350	Jun 09-Sep 09	Increased: max 5%, min 4%
						Sep 09-Feb 10	Reduced: max 20%, min 19%
						Feb 10-Mar 10	Increased: max 11%, min 9%
						Mar 10-Apr 10	Reduced: max 4%, min 3%
						Apr 10-Aug 10	Increased: max 4%, min 1%
						Aug 10-Oct 10	Reduced: max 6%, min 2%
						Jun 09-Oct 09	Increased: max 5%, min 1%
						Oct 09-Feb 10	Reduced: max 12%, min 4%
11	Avondale Heights	CH	Inorganic clays of high plasticity	Basaltic clay	450-800	Feb 10-Mar 10	Increased: max 10%, min 1%
						Mar 10-Jun 10	Reduced: max 5%, min 1%
						Jun 10-Oct 10	Increased: max 7%, min %
						Jun 09-Nov 09	Increased: max 2%, min 1%
						Nov 09-Jun 10	Reduced: less than 1 %
						Jun 10- Oct 10	Increased: les than 1%
						Jun 09-Nov 09	Increased: max 10%, min 1%
						Nov 09-Jan 10	Reduced: max 21%, min 2%
15	Keysborough	SC	Clayey sands	Quaternary alluvial and tertiary sediments, gravel, clay	150-800	Jan 10-Oct 10	Increased: max 21%, min 11%
						Jun 09-Nov 09	Increased: max 5%, min 1%
						Nov 09-Mar 10	Reduced: max 9%, min 4%
						Mar 10-Oct 10	Increased: max 7%, min 3%
						Jun 09-Oct 09	Increased: max 2%, min 1%
						Oct 09-Nov 09	Reduced: less than 1%
						Nov 09-Oct 10	Increased: less than 1%
						Jun 09-Oct 09	Increased: max 4%, min1%
Oct 09-Jan 10	Reduced: max 17%, min 6%						
15	Keysborough	SC	Clayey sands	Quaternary alluvial and tertiary sediments, gravel, clay	1000-1400	Jan 10-Oct 10	Increased: max 21%, min 11%
						Jun 09-Nov 09	Increased: max 5%, min 1%
						Nov 09-Mar 10	Reduced: max 9%, min 4%
						Mar 10-Oct 10	Increased: max 7%, min 3%
						Jun 09-Oct 09	Increased: max 2%, min 1%
						Oct 09-Nov 09	Reduced: less than 1%
						Nov 09-Oct 10	Increased: less than 1%
						Jun 09-Oct 09	Increased: max 4%, min1%
Oct 09-Jan 10	Reduced: max 17%, min 6%						

The variations of soil moisture content for the three categories of geological formations were summarised in Figure 5-20 to Figure 5-22 with respect to the soil moisture content measured to October 2010. The soil moisture content change was calculated with respect to the initial measured soil moisture content, as the starting date of measurement was different at each site the data collected on June 2009 were considered to be the initial values when monitoring for all sites was already started. The data labels in the figures showed that the increase or decrease in moisture content changes with respect to the previous value. Maximum moisture changes were used to plot the line while minimum moisture changes were shown in brackets.

Figure 5-20 shows the change in soil moisture content of the basaltic clay sites. The soil profiles were divided into three layers due to difference in moisture variations patterns. It was clear that the soil depths between 150 to 450 mm were highly sensitive to the rainfall as evident from the high moisture variations shown at lower depths of 550 to 800 mm and below 800 mm. Moisture variations were relatively low at these depths with wetting peak around March 2010, and driest period occurred around June 2010. The series of heavy rainfall events at the end of 2010 have caused significant increase in soil moisture up to the depths of 800 mm, maximum increase of over 20 % occurred in these depths. The soil moisture content below 1000 mm were still unaffected and showed similar variations to the previous year, possibly due to low hydraulic conductivity of the clay soils.

Figure 5-21 shows the change in soil moisture content of the non-basaltic clay sites. The soil profiles of these sites were simpler than that for the basaltic clay sites, and only two soil layers were used to represent the soil profiles. It was apparent that a significant peak and a relatively small peak of moisture content changes occurred within the first year for the depths between 150 to 800 mm. For the depths between 1000 to 1400 mm, the peak of soil moisture content changes only occurred in November 2009, arguably as a result of the smoothing effect of moisture content in deeper soils.

Figure 5-22 shows the change in soil moisture content of the Quaternary alluvials and Tertiary sediments sites. Since these formations were predominantly coarse grained soils, they were more sensitive to rainfall as moisture can seep relatively easily to deeper depths. It was apparent that soil

moisture content changes between the depths of 150 to 800 mm was similar to the other two categories of sites, but the changes between the depths of 1000 to 1400 mm were greater than in other two categories of sites. However, the changes of soil volume (i.e., shrinking and swelling) due to moisture are expected to be smaller in these less reactive sediments.

The variation of soil moisture measured by the neutron probe is a spot monthly measurement, which is unable to capture the frequent variations of soil moisture content compared to continuous measurement of moisture content with field instrumentations. However, the moisture data collected from the neutron probe can be used for calculation of possible change of soil volume due to moisture variations. The magnitudes of volume change are depended on the reactivity of the soil; hence change in volume of the soil at the Quaternary sites will be lower than the clay sites due to lower content of reactive soil particles and higher hydraulic conductivity.

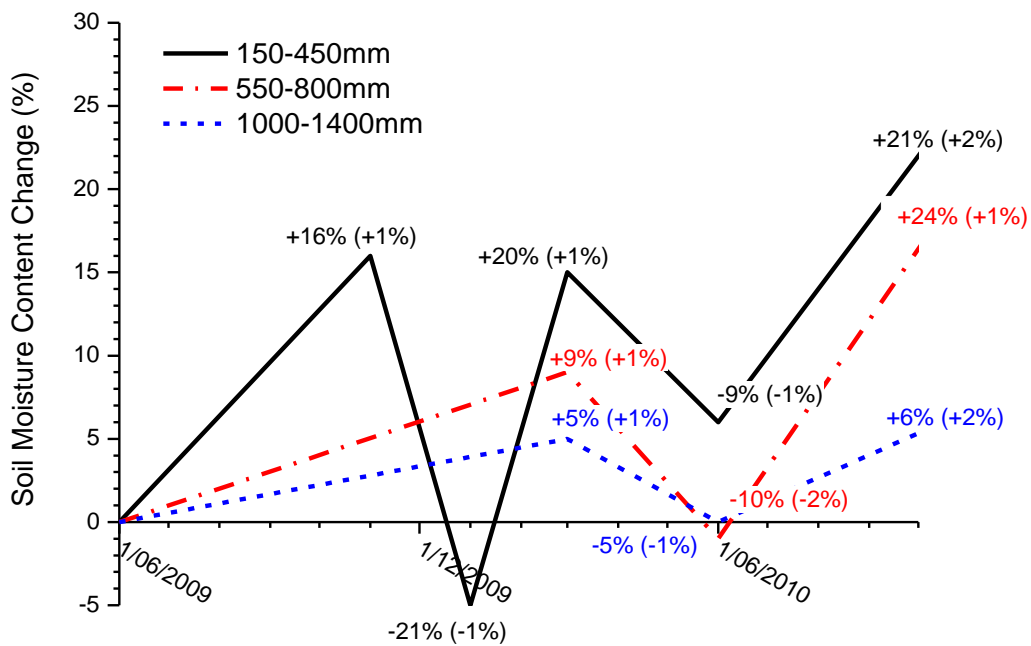


Figure 5-20 Soil moisture variations of basaltic clay sites

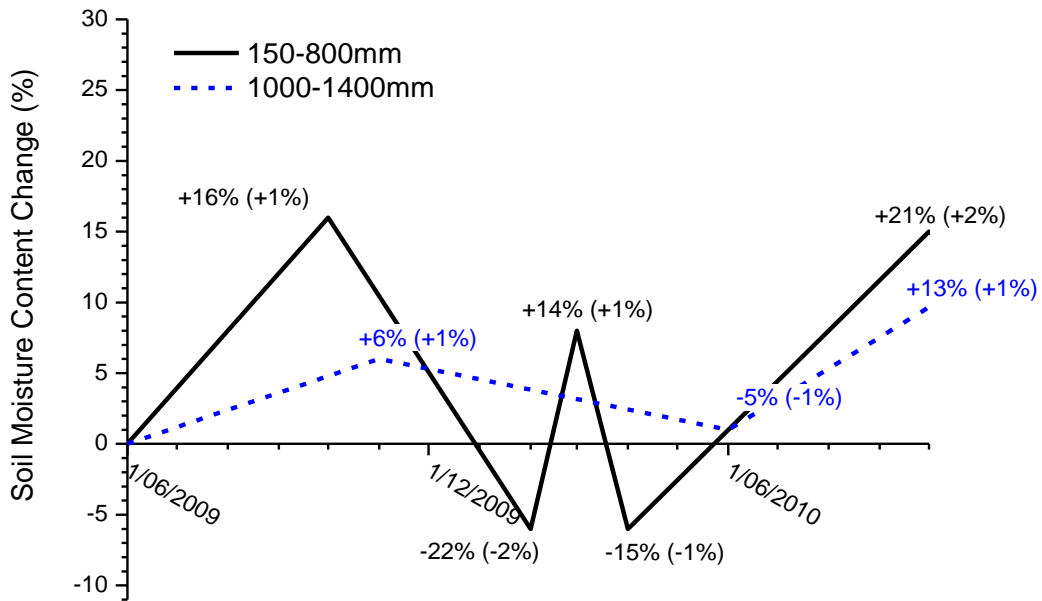


Figure 5-21 Soil moisture variations of non-basaltic clay sites

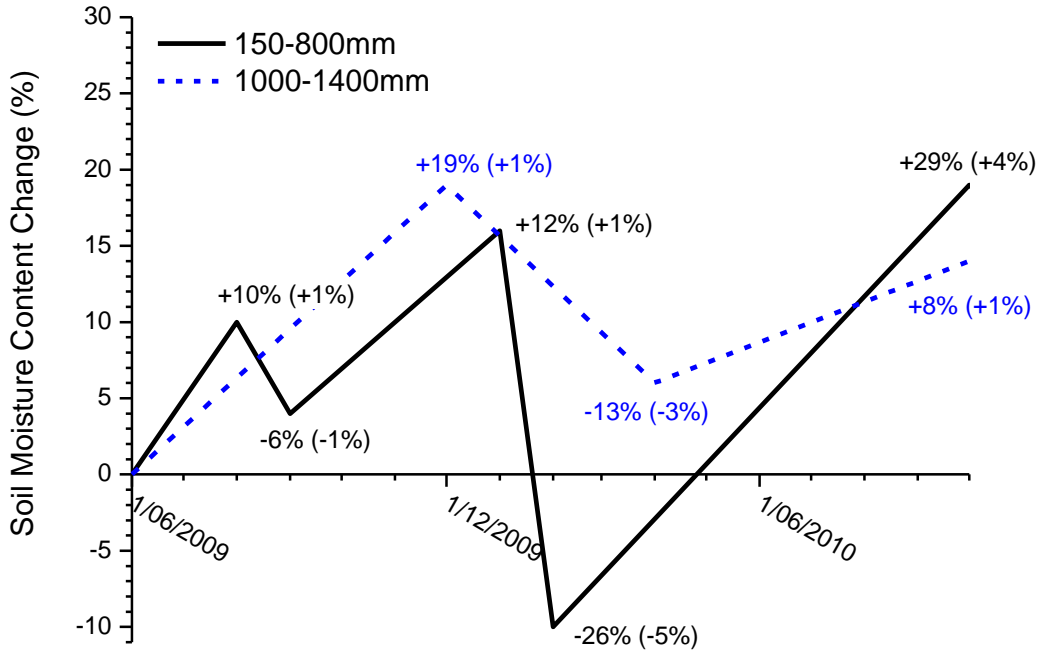


Figure 5-22 Soil moisture variations of Quaternary alluvials and Tertiary sediments sites

5.5 Conclusions

The work undertaken to study the soil moisture variation at different depths along the soil profiles of 23 sites around Melbourne region was described in this chapter. The neutron scattering method was used to monitor the soil moisture variation on monthly basis. Field calibrations of the neutron probe were performed and a single calibration equation was obtained for converting volumetric water content from the collected neutron counts.

The measured moisture data showed that variations of soil moisture content at a particular site depended on the soil type and the local climate variations. The soil moisture variations within shallower soil depths (i.e. up to 550 mm) closely followed the local events. If the soil is predominantly sandy, the water can infiltrate easily and the influence of local climate was felt to deeper soils (i.e., up to 1000 mm depth). In contrast, the infiltration of water was substantially slow in clayey soils (especially in basaltic clays), and therefore, the moisture variation within deeper soils depended also on the evaporation rate at the ground surface. Consequently, the moisture content changes within deeper soils could have a time lag of few weeks or more in comparison to shallower soils. The data also indicated that the soil moisture changes in deeper soils were cyclic in nature.

CHAPTER 6

GROUND-ATMOSPHERE INTERACTION MODELLING FOR PREDICTION OF SOIL MOISTURE CONTENT AND TEMPERATURE

6.1 Introduction

The behaviour of soils related to seasonal variations of soil moisture content within the soil profile is described in Chapters 5. Considering the time, cost and resources required for field moisture measurements, accurate and long term prediction of soil moisture content and temperature is very important for understanding the behaviour of buried pipes. In this study, the soil moisture content and temperature are predicted by ground-atmosphere interaction model using the Vadose/W software for the two instrumented sites, Altona North and Fawkner. This chapter presents the development of the one-dimensional model and describes the required soil properties and initial

conditions for each site. The soil moisture content and temperature computed by the model were compared with the field measurements in order to validate the reliability of the model capabilities.

6.2 Ground-atmosphere Modelling of Soil Column in Vadose/W

6.2.1 Governing equations

In this study the Vadose/W software developed by GEO-SLOPE International Ltd. was used for the ground-atmosphere modelling of one-dimensional soil column. Vadose/W is a two-dimensional software capable of mathematically simulating the real physical process of ground water flow in the vadose zone based on the physical process of seepage. In the software, the soil moisture content and temperature of a soil column are predicted by analysing the physical processes based on first principles of physics and balancing the ground-atmosphere condition. In the numerical model, the one-dimensional coupled processes of moisture and heat flow in porous soil are governed by Equations 6-1 and 6-2, respectively:

$$\frac{1}{\rho} \frac{\partial}{\partial z} \left(D_v \frac{\partial P_v}{\partial z} \right) + \frac{\partial}{\partial z} \left(k_z \frac{\partial \left(\frac{P}{\rho g} + z \right)}{\partial z} \right) + Q = \lambda \frac{\partial P}{\partial t} \quad \text{Equation 6-1}$$

$$L_v \frac{\partial}{\partial z} \left(D_v \frac{\partial P_v}{\partial z} \right) + \frac{\partial}{\partial z} \left(k_{tz} \frac{\partial T}{\partial z} \right) + Q_t + \rho c V_z \frac{\partial T}{\partial z} = \lambda_t \frac{\partial T}{\partial t} \quad \text{Equation 6-2}$$

where ρ is the water density; z is the elevation head; D_v is the vapour diffusivity coefficient; P_v is the vapour pressure of soil moisture; k_z is the hydraulic conductivity in z (vertical) direction (as a function of soil suction); P is the water pressure; g is the acceleration due to gravity; Q is the

applied boundary flux; λ is the slope of the volumetric water content function; t is time; L_v is the latent heat of vaporization; k_{tz} is the thermal conductivity in z-direction; T is the soil temperature; Q_t is the applied thermal boundary flux; ρc is the volumetric specific heat value; V_z is the Darcy's water velocity in vertical direction; and λ_t is the volumetric specific heat value.

The two equations are subjected to the ground-atmosphere flux at the ground surface. Equation 6-1 governs the moisture and vapour flow and conservation of these components, and Equation 6-2 governs the heat flow and conservation of heat energy between soil, water and water vapour. The coupling between the two equations arises from vapour diffusion and latent heat transfer during soil water evaporation within pores, both of which are dependent on the vapour pressure. The atmospheric coupling between the two equations can be achieved by calculating the soil evaporative flux based on the Penman-Wilson formulation (Wilson 1990; Wilson *et al.* 1994) as follows:

$$E = PE \left(\frac{h_r - \frac{V_{p.s \text{ air}}}{V_{p.s \text{ soil}}} h_A}{1 - \frac{V_{p.s \text{ air}}}{V_{p.s \text{ soil}}} h_A} \right) \quad \text{Equation 6-3}$$

where E is the evaporative flux; PE is the potential evaporation; h_r is relative humidity at the soil surface; $V_{p.s \text{ air}}$ is the saturated vapour pressure of air; $V_{p.s \text{ soil}}$ is the saturated vapour pressure at the soil surface; and h_A is the relative humidity of air above the soil surface. The relative humidity at the soil surface and the water vapour pressure at the soil surface are calculated using the relative humidity equation proposed by Edlefsen and Anderson (1943) on the basis of thermodynamic relationships. The saturated vapour pressure at the soil surface is a function of soil surface temperature and is calculated using the approach as explained by Lowe (1977).

The surface temperature may be estimated for no snow pack condition with the following relationship (Wilson 1990):

$$T_s = T_a + \frac{1}{\nu f(u)} (Q - E) \quad \text{Equation 6-4}$$

where T_s is the temperature at the soil surface; T_a is the temperature of the air above the soil surface; ν is a Psychrometric constant; $f(u)$ is a function dependent on wind speed, surface roughness and eddy diffusion ($f(u) = 0.35(1 + 0.15U_a)$); U_a is wind speed; Q is the net radiant available at the surface; and E is the evaporative flux.

In the Vadose/W software, the predications are done by solving Equations 6-1 and 6-2 using the Galerkin finite element method. Key input data required for numerical models includes the soil–water characteristic curve (SWCC), the hydraulic conductivity–suction function, thermal properties (i.e., soil thermal conductivity function and volumetric heat capacity function), and climate data (i.e. vegetation functions, air temperature, wind speed, solar radiation, rainfall, and relative humidity). The field and laboratory tests undertaken to obtain these input data and applied initial and boundary conditions to the model are described in the following section.

6.2.2 Soil water characteristic curves (SWCCs)

Most of the applications in practice normally employ drying SWCC and ignore hysteresis due to the difficulty in determining wetting SWCC for fine-textured soils (Adu-Wusu *et al.* 2007; Bohnhoff *et al.* 2009). Furthermore, the hydraulic hysteresis in SWWC will come to a minimum level for soils that have undergone large number of wet and dry cycles, which is called environmentally stabilised soil (Gould *et al.* 2011). Therefore, the drying SWCCs were measured using core samples collected from the field instrumentation sites at Altona North and Fawkner in accordance with the ASTM D5298-03 filter paper method (ASTM International 2003).

In general, three layers of soil can be found on the sites, the soil above the depth of 300 mm are the top soils which contains fill materials, organic soil, small proportion of sands and grass roots; the middle layer of soils at the depths of 500 to 800 mm are inorganic clays of high plasticity and in some occasion small rocks are embedded; the bottom layer of soils at the depth below 1000 mm are

usually a consistent layer of inorganic stiff clays down to the basaltic rock at approximately 2000 mm. Hence, according to the soil profiles; in Altona North, core samples from four different depths of 200 to 250 mm, 350 to 500 mm, 850 to 1000 mm, and 1400 to 1600 mm were used; in Fawkner, core samples from three different depths of 200 to 250 mm, 450 to 550 mm, and 800 to 1600 mm were used.

The core samples from the sites were cut into small specimens using steel rings with diameter of 45 mm and height of 12 mm. Initial moisture content of the specimens were determined in accordance with the oven drying method (Standards Australia 2005). Whatman No. 42 filter paper with 55 mm diameter was used for the test, which was prepared by drying overnight in an oven then stored in a sealed container over desiccant to keep the papers dry before testing. Physical contact between the soil and filter papers allowed fluid transfer including transfer of salts that may be dissolved in the pore water so that matric suction of the specimen can be measured (ASTM International 2003). Hence, measurement was carried out by placing three stacked filter papers directly under the soil specimens in the specimen container as shown in Figure 6-1(a). The centre filter paper was cut to a smaller diameter of 45 mm so that the two outer filter papers could prevent it from contamination due to contact with soils. The top of the specimen container was sealed with a layer of plastic wrap before the air tight lid was placed as shown in Figure 6-1(b). The sealed container was placed in an insulated chest in a temperature controlled room. The suction of the filter paper and the specimen was allowed to come to equilibrium for a minimum of seven days (ASTM International 2003). At the end of the equilibrium period the centre filter paper of the three-layer stack was transferred into a metal container and the moisture content was determined. Matric suction of the test specimens was determined from the equations which give the best fit to calibration data for Whatman No. 42 filter paper when measuring matric suction (Leong *et al.* 2002):

$$\log \psi_m = 4.945 - 0.0673w_f \quad w_r < 4.7 \quad \text{Equation 6-5}$$

$$\log \psi_m = 2.909 - 0.0229w_f \quad w_r \geq 4.7 \quad \text{Equation 6-6}$$

where $\log_{10} s$ is the logarithm of suction in base 10 and w_f is the moisture content of the filter paper in percentage.



(a)

(b)

Figure 6-1 SWCC test using filter papers: (a) soil specimen placed in the container with filter papers; (b) specimen container sealed with plastic wrap and lid

Two to four specimens were used in the test for at each layer of soils, and the same specimens were used repeatedly by drying to develop the entire curve. Drying of the specimens was performed by air-drying in a temperature controlled room of 20 ± 3 °C to the required moisture content (according to change in weight). The moisture content of the specimens at each stage was determined from the change in weight at the current stage and the weight at the initial moisture content. The soil moisture content of the specimens were measured by oven drying method when SWCC tests were completed

in order to cross check the results by back calculation of moisture content from the final stage to each of the previous stage.

Figure 6-2 and Figure 6-3 show the experimental data points and curves fitted using the Fredlund and Xing (1994) equation for SWCC at various depths of both sites together with the fitting parameters. The Fredlund and Xing (1994) equation was developed based on the pore size distribution of soil with a governing equation as follows:

$$\theta = C_{\psi} \frac{\theta_s}{\left\{ 1 + \left[e + \left(\frac{\psi}{a} \right)^n \right]^m \right\}} \quad \text{Equation 6-7}$$

where θ is the volumetric soil moisture content; C_{ψ} is a correction function; θ_s is the saturated soil moisture content; e is the natural number (2.71828); a is the inflection point with a unit of kPa; n is the slope control parameter; and m is the residual moisture content control parameter. The correction function, C_{ψ} is defined as:

$$C_{\psi} = \frac{-\ln\left(1 + \frac{\psi}{h}\right)}{\ln\left[1 + \left(\frac{1 \sigma}{h}\right)\right]} + 1 \quad \text{Equation 6-8}$$

where ψ is the soil suction and h is the suction corresponding to the residual moisture content. The SWCCs were determined using a fitting algorithm and applied to the experimental data points. These fitting curves were used as input material properties in the soil column models.

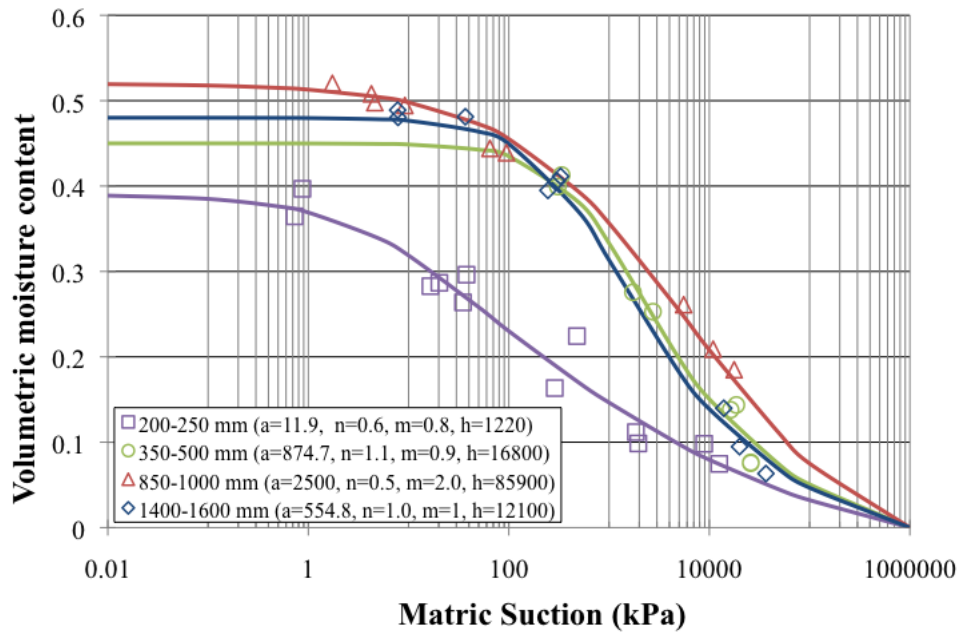


Figure 6-2 SWCCs of Altona North

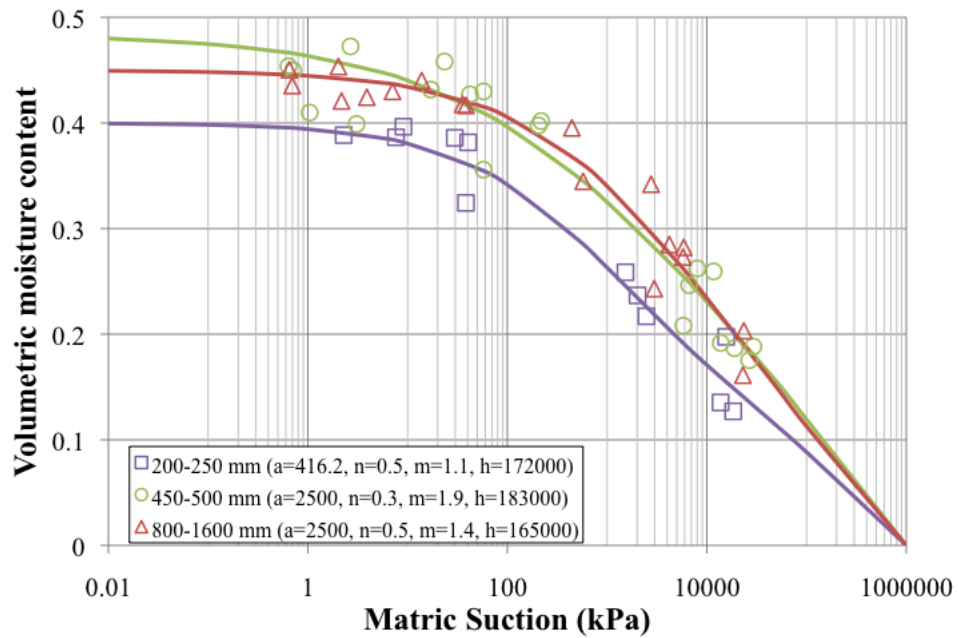


Figure 6-3 SWCCs of Fawkner

6.2.3 Hydraulic conductivity-suction functions

In general, water cannot flow through unsaturated soils with the same ease as through saturated soils because the unsaturated hydraulic conductivity is lower than that of a saturated soil. In saturated soils, once the air entry value is exceeded, air can enter some of the soil pores and increase the tortuosity of the flow paths. Therefore, hydraulic conductivity of soils decreases with increase of suction, as it is harder for water to flow through the soil when more pores become air-filled. It is then clear that the hydraulic conductivity of unsaturated soil depends on the moisture content, which is related to suction by the SWCC. Unsaturated hydraulic conductivity of soils is especially difficult to obtain, partly because of the extensive variability in the field, and partly because of measurement of this parameter is time consuming and expensive (van Genuchten 1980). This task is often overcome by predicting the hydraulic conductivity of unsaturated soil from particle size distribution or SWCC and saturated hydraulic conductivity. In this study, hydraulic conductivity-suction functions is predicted by the SWCCs obtained as described in the previous section and the saturated soil hydraulic conductivity.

The saturated soil hydraulic conductivity, k_{sat} of the two instrumentation sites was obtained by field and laboratory tests. Since the top layer of soils in the field (i.e., 0 to 300 mm) is generally loamy soils containing vegetations and their root systems, it is very difficult to obtain standard core samples for laboratory determination of k_{sat} . Therefore, the *in-situ* field test known as the air entry permeameter (AEP) method developed by Bouwer (1966) was performed. Figure 6-4 shows the AEP, which consists of a single ring infiltrometer and a vacuum gauge. The single ring infiltrometer essentially consists of a stainless steel ring, a top plate and a burette extending from the top plate. During the test, the ring is embedded in the test area from the ground surface if k_{sat} value of the top soil is to be determined. However, for measurement of k_{sat} at greater depths, pits or trenches must be prepared and relatively dry soil is required for easier detection of the wet front.

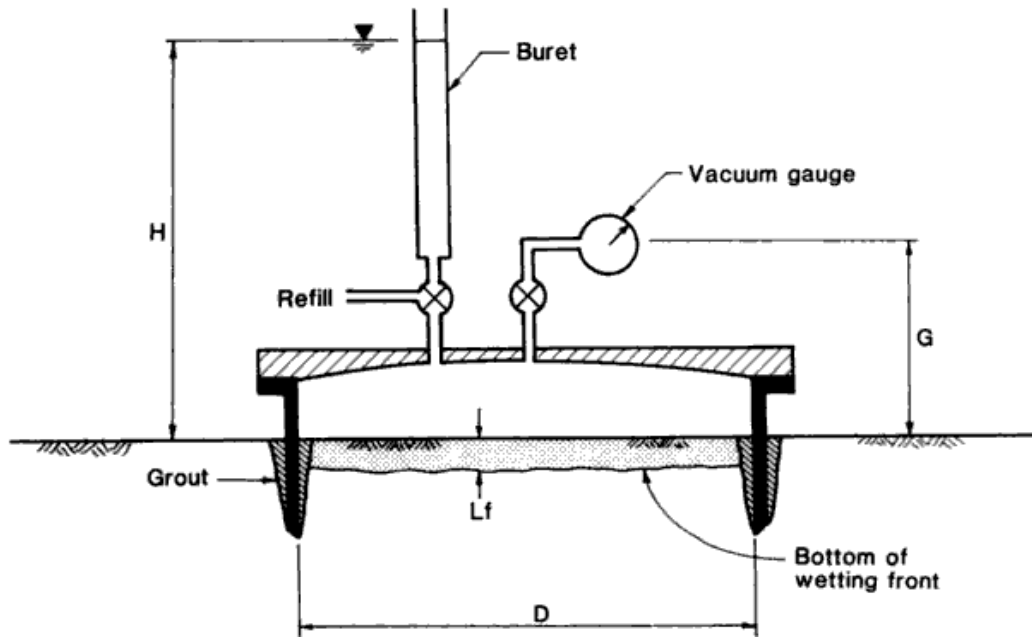


Figure 6-4 Schematic diagram of AEP (Daniel 1989)

During the test, the ring was hammered in the soil to the depth of approximately 100 mm as shown in Figure 6-5(a). Soils along the inner perimeter of the ring were then packed down using a hammer against the ring wall to ensure a good bond between the ring and the soil. The top plate was placed on the ring assembly to seal the ring (Figure 6-5(b)) before water was supplied from the plastic reservoir through the refill valve into the ring (Figure 6-5(c)). Water flow was maintained until the ring was full and all the air was driven out. Supply of water was then switched to the plastic cylinder as shown in Figure 6-5(d) so that the fall of water level could be observed. Water flow in the test area was in one-dimension as long as the depth to the bottom of the wetting front, L_f was less than the embedment depth. The one-dimensional flow rate was measured by noting the fall of water level in the cylinder with time until the wetting front reached the bottom of the ring, so that the water flow became three-dimensional (Trautwein and Boutwell 1994). The refill valve was then closed so that suction built up inside the permeameter, and the gauge valve was opened for measurement of suction with the manometer. Suction would continue to increase until the air entry value, AEV was

reached at which point air bubbles were driven out of the soil. The maximum suction, P_{\max} measured by the manometer was recorded, then the test setup was dismantled and the actual L_f was measured by pushing a metal ruler into the soil and observed the depth where the penetration resistance increased, indicating that the ruler has reached the dry soils zone.

The hydraulic conductivity, k of the test area is determined as follows:

$$k = \frac{I}{i} \quad \text{Equation 6-9}$$

where I is the infiltration of soils when the flow is still in one-dimension and i is the hydraulic gradient. The infiltration, I is determined as:

$$I = \frac{Q}{A \cdot t} \quad \text{Equation 6-10}$$

where Q is the volume of one-dimensional water flow (i.e., fall of water level in the cylinder); A is the area of flow (i.e., cross sectional area of the cylinder); and t is time interval in which Q is determined. The hydraulic gradient, i is determined as (Trautwein and Boutwell 1994):

$$i = \frac{H + L_f + \frac{AEV}{2}}{L_f} \quad \text{Equation 6-11}$$

where H is the height of the water level in cylinder above ground level; L_f is the depth to the bottom of the wetting front; and AEV is the air entry value of the wetted zone, which is assumed to be P_{\max} corrected with the elevation of the wet front (Bouwer 1966), therefore:

$$AEV_m = P_{\max} - G + L_f \quad \text{Equation 6-12}$$

where G is the height of the manometer above ground level (Figure 6-4).



(a)

(b)



(c)



(d)

Figure 6-5 Field hydraulic conductivity test using AEP: (a) the stainless steel ring embedded in soil; (b) the ring sealed with top plate; (c) filling of permeameter; (d) measurement of hydraulic conductivity with a plastic cylinder

The field test results of both sites are shown in Table 6- 6-1. The k_{sat} at the soil depths of 0 to 50 mm in Altona North and Fawkner are 2.24×10^{-5} m/s and 2.52×10^{-5} m/s, respectively. Typical saturated hydraulic conductivity ranged from 10^{-4} to 10^{-5} m/s and 10^{-5} to 10^{-7} m/s for fine sands and silty clays, respectively (Das 1998). The results suggested that the saturated soil hydraulic conductivity measurements of top soils on sites are similar to fine sands.

Table 6- 6-1 AEP test results

	Altona North	Fawkner
Test depth (mm)	50	50
P_{max} (PSI)	0.3	0.3
L_f (mm)	100	50
Rate of water fall (m/s)	0.0033	0.0028
k_{sat} (m/s)	2.24×10^{-5}	2.52×10^{-5}

The k_{sat} values of soils at greater depths of 350 to 450 mm and 750 to 850 mm were determined in the laboratory using core samples obtained from the sites. The tests were performed in a flexible wall apparatus using constant head method applied through flow pumps (Kodikara and Rahman 2002). Core samples with diameter of 100 mm were trimmed to specimens with height of 100 mm to maintain a 1:1 height to width ratio. The test specimen was assembled in the flexible permeameter with porous stones and filter papers positioned on top and bottom of the specimen. The specimen was then sealed to the top and bottom caps with silicon vacuum grease and o-rings, similar to a triaxial test set up, as shown in Figure 6-6. Saturation of the specimen was begun by applying a moderate cell pressure of 50 kPa, and top and bottom pressures of 30 kPa. The drainage port at the bottom of the cell was opened to bleed air from the supplying tube until air bubbles were virtually disappeared. A cell pressure of 130 kPa was applied to commence the saturation procedure with both top and bottom pressure raised to 100 kPa. The top and bottom pressures were increased by

increments of 100 kPa within time intervals of one hour, and the cell pressure was also increased at least 20 kPa greater than the top and bottom pressures. The Skempton's B test was conducted at various time intervals, and the saturation process was considered complete when a B value of 0.95 or higher was achieved. The hydraulic conductivity test was then began by maintaining a hydraulic gradient, i ranged from 3 to 10 in the specimen until a constant value of hydraulic conductivity was obtained; or when the inflow volume and outflow volume of the specimen became equal.

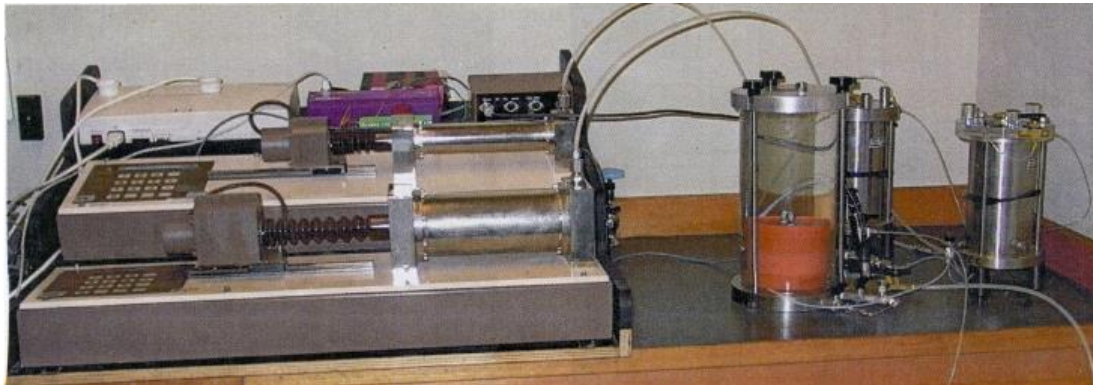


Figure 6-6 Constant head method with flow pumps (Lee 2004)

A study of hydraulic conductivity of compacted clay in Melbourne (Kodikara and Rahman 2002) indicated that k values does not have significant variation with i values up to 300. Therefore, the effect of consolidation on the specimen due to the i value employed in this study can be considered as negligible. The k values of the tests were determined using the Darcy's law as follows:

$$k = \frac{Q \cdot L \cdot \gamma_w}{P_u \cdot A}$$

Equation 6-13

where Q is the average flow rate (m^3/s) of inflow or outflow at steady state; L is the length of the specimen, γ_w is the unit weight of water; P_u is the pressure difference; and A is the cross section area of the specimen.

The test results of both sites are summarised in Table 6-2 and the plots are shown in Figure 6-7 and Figure 6-8. It can be observed that the k values were generally decreased with time and became stabilised in three to four days after the specimens were saturated. The measurements in Fawkner at soil depth of 350 to 450 mm showed a high variation in k during the first three days of the test. It is possibly due to fine particles clogged up the flow paths within the specimen, subsequently, however the steady state conditions were achieved in the fourth day. The k of the both sites at 350 mm and deeper ranged from 2.21×10^{-9} to 2.73×10^{-10} m/s, which are comparable to the typical k_{sat} value of clay soils as less than 10^{-8} m/s (Das 1998). Table 6-3 summaries the k_{sat} at various soil depths obtained from both field and laboratory tests in m/day.

Table 6-2 Laboratory hydraulic conductivity test results

Specimen	Altona North		Fawkner	
	350-450 mm	750-850 mm	350-450 mm	750-850 mm
Depth	350-450 mm	750-850 mm	350-450 mm	750-850 mm
Skempton's B value	0.97	0.95	0.96	0.96
P_u (kPa)	8	8	3	8
i	8.16	8.15	3.07	8.15
k_{sat} (m/s)	2.21×10^{-9}	1.28×10^{-9}	1.93×10^{-9}	2.73×10^{-10}

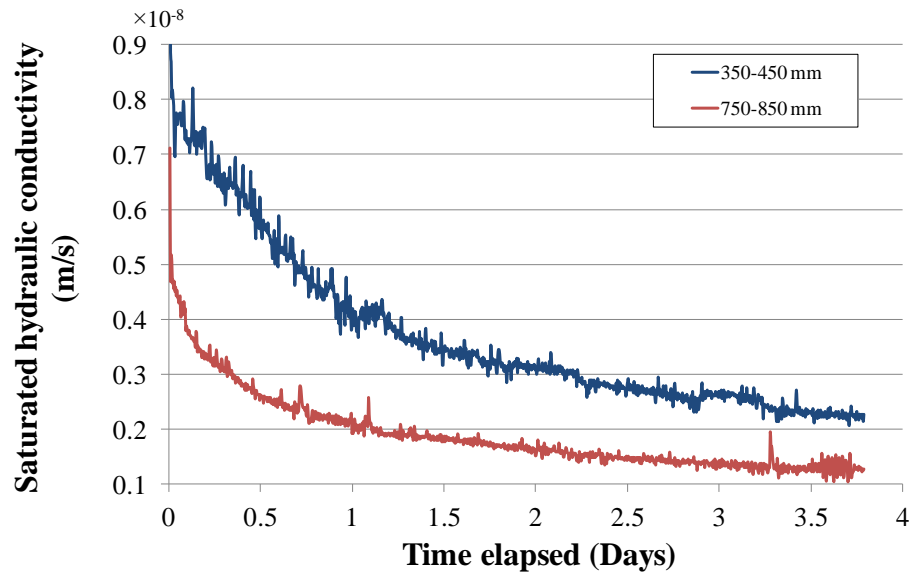


Figure 6-7 Saturated hydraulic conductivity plot of Altona North

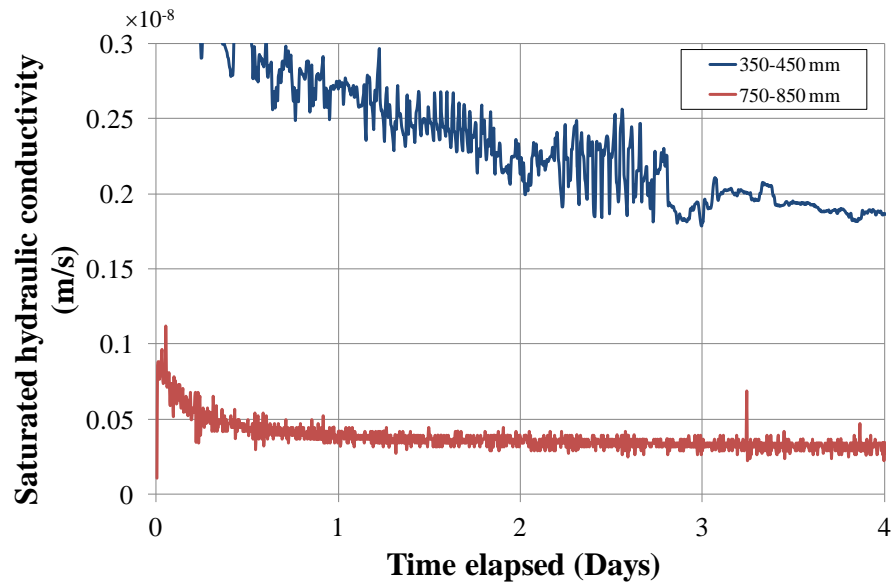


Figure 6-8 Saturated hydraulic conductivity plot of Fawkner

Table 6-3 Summary of hydraulic conductivity of the field instrumentation sites

Specimen depth (mm)	k_{sat} (m/day)	
	Altona North	Fawkner
0 - 50	1.935	2.177
350 - 450	0.00019	0.00017
750 - 850	0.00011	0.00002

In this study, the hydraulic conductivity-suction functions of the field soils at various depths were estimated according to the methods by van Genuchten (1980) and Fredlund et al. (1994) based on the k_{sat} and the SWCCs obtained. The prediction of the hydraulic conductivity-suction functions for clayey soils is generally less accurate than that for sandy soils for both methods. A comparison of predicted and experimental data of Yolo light clay by Fredlund et al. (1994) methods showed a close prediction only when the soil suction is less than 4 kPa. The predictions obtained for Beit Netofa clay by van Genuchten (1980) were found to be less accurate at low suction, where the conductivity values are seriously under predicted. Therefore the average of the functions estimated from both methods was used as the soil column models input. The hydraulic conductivity-suction functions corresponding to various depths at both sites are shown in Figure 6-9 and Figure 6-10. Hydraulic conductivity at greater depths is found to be lower due to the increase of clay content and visibly more homogenous and intact composition.

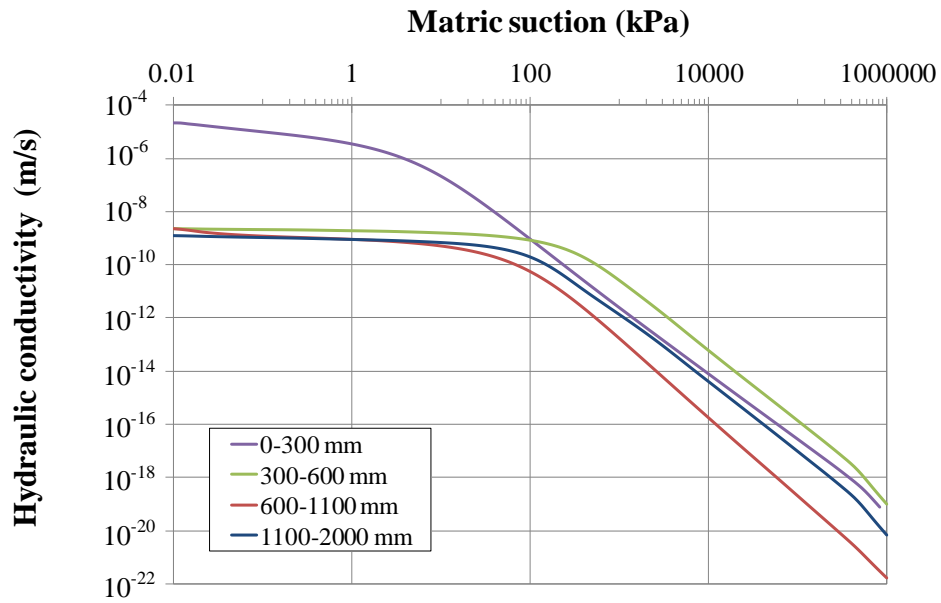


Figure 6-9 Hydraulic conductivity-suction functions of Altona North

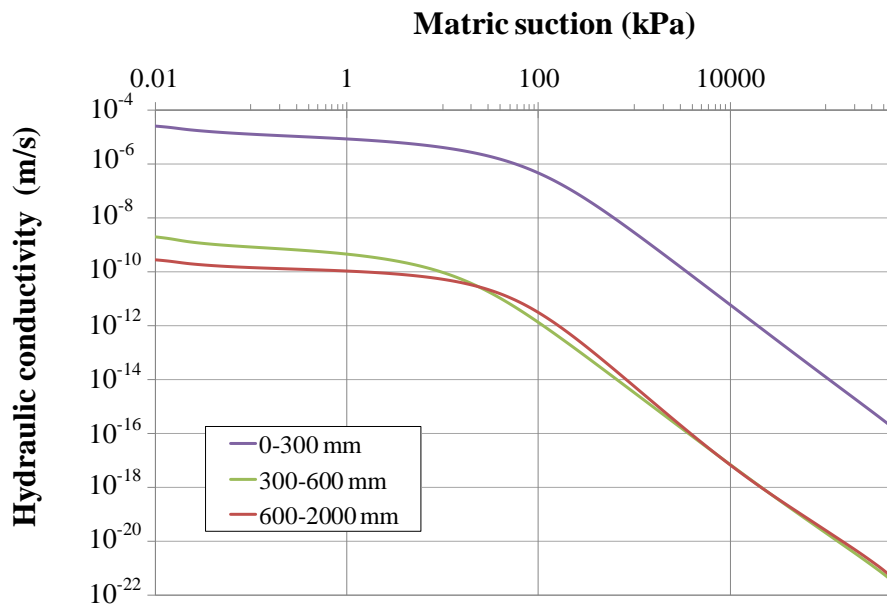


Figure 6-10 Hydraulic conductivity-suction functions of Fawkner

6.2.4 Soil thermal conductivities and volumetric heat capacities

The thermal properties of the soil were measured in the laboratory using the KD2 Pro thermal properties analyser manufactured by Decagon Devices, Inc. (Figure 6-11). The principle of the thermal measurement is based on the change of temperature of a heated sensor over a set heating time. The dual-needle of the device is capable of analysing the temperature against time relationship for the separate needle and yield information on diffusivity, heat capacity, and thermal conductivity. The measurement range of the device is 0.02 to 2.0 W/(m.K) for thermal conductivity and 0.5 to 4.0 mJ/(m³.K) for volumetric heat capacity. During measurement, data were collected at one second interval in the heating time of 30 seconds and cooling time of 30 seconds with a resolution of 0.001 °C. The short heating time minimised errors due to thermally induced water movement and temperature drift of the sample (Decagon Device Inc. 2009).

Soil specimens used for the SWCC tests were used for measurement of thermal properties. The measurement was done by inserting the dual-needle sensor into the soil specimens and selected the type of measurement to be performed. It is important to maintain good contact between the soil and the needles as well as keeping the needles parallel to each other. Figure 6-12 and Figure 6-13 show the measured thermal conductivity, and Figure 6-14 and Figure 6-15 show the volumetric heat capacity. The figures are plotted as a function of volumetric moisture content with respect to soil depths in each site. Barry-Macaulay et al. (2011) reported the thermal conductivity and volumetric heat capacity for basaltic clays at different dry densities as 17.3 to 121 kJ/day.m.°C and 1300 to 3600 kJ/m³/°C, respectively, which is similar to the findings in this study. The measured thermal properties were inputted in the soil column models as fitted curves.



Figure 6-11 KD2 Pro thermal properties analyser

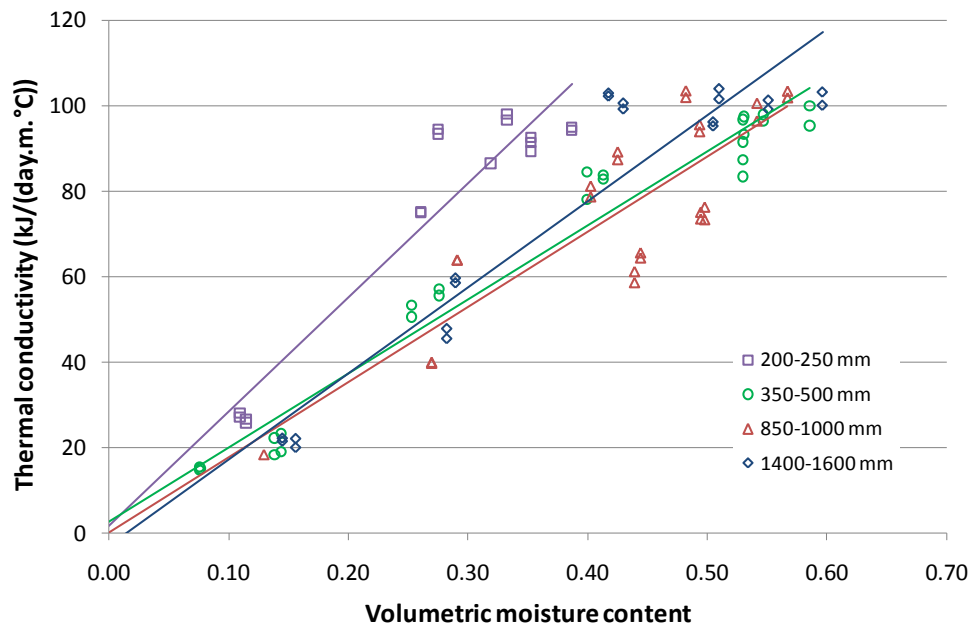


Figure 6-12 Thermal conductivity functions of Altona North

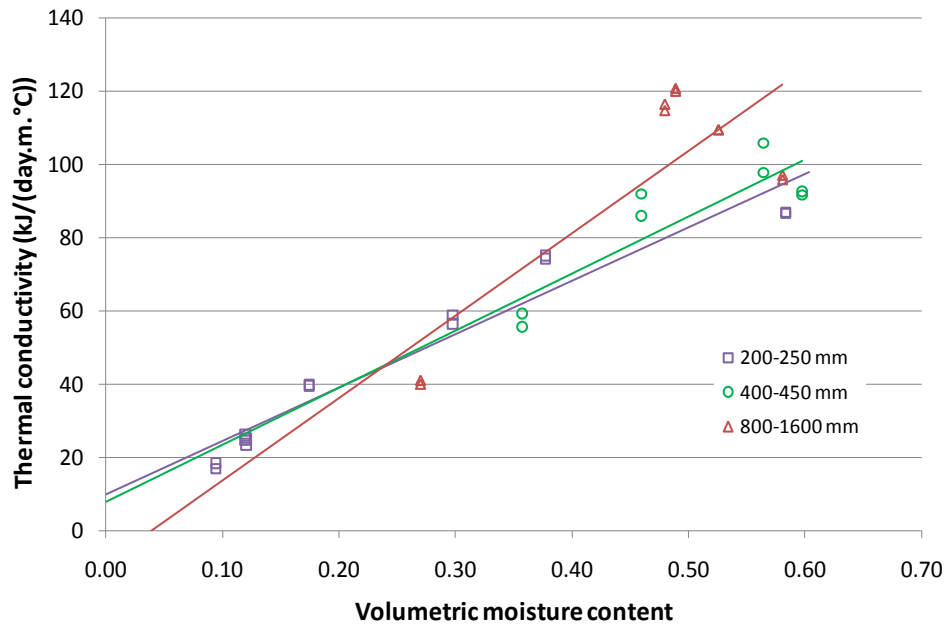


Figure 6-13 Thermal conductivity functions of Fawkner

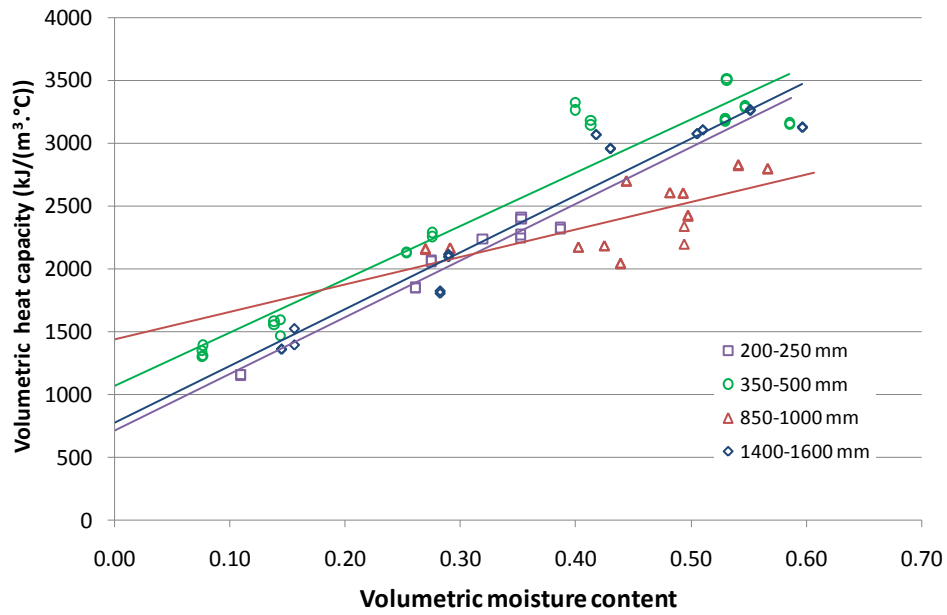


Figure 6-14 Volumetric heat capacity functions of Altona North

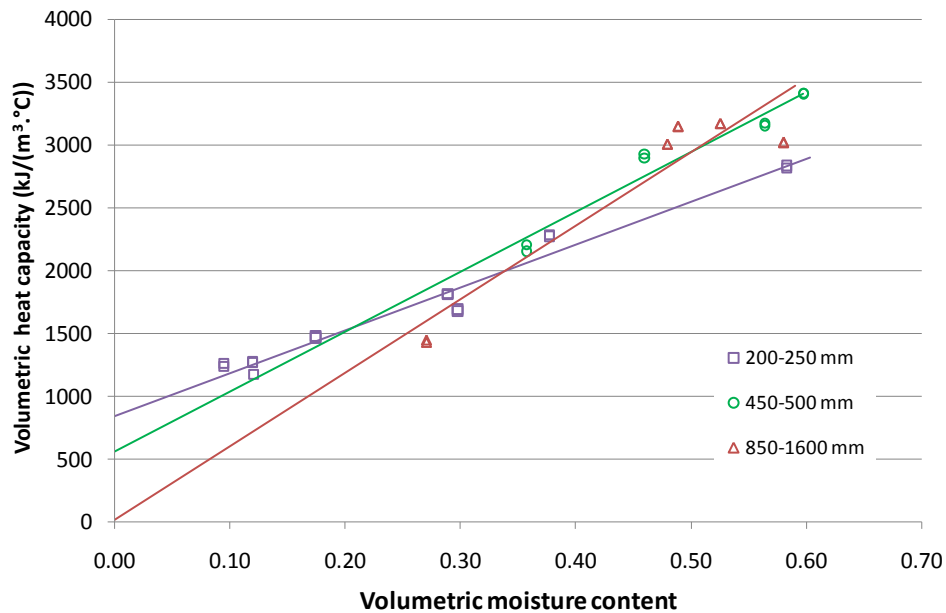


Figure 6-15 Volumetric heat capacity functions of Fawkner

6.2.5 Vegetation functions

It is necessary to input data related to the vegetation at the sites, which were predominantly grass. The evapotranspiration from the grass was inputted as a combination of functions of leaf area index (LAI), root depth (RD) and plant moisture limits (PML) in the soil column models. The evapotranspiration process of the grass was incorporated by the nodal vegetation uptake combined with the ground surface energy in the model. The amount of nodal uptake was depended on RD and suction. The percentage of the vegetation ability to draw water due to change in soil suction was determined by PML. While LAI governed the amount of energy intercepting the soil surface, which in turn affect the computed actual evaporation (GEO-SLOPE International 2010).

The dimensionless LAI function describes the ratio of the leaf area that is actively transpiring vegetation to the nominal surface area of the ground on which vegetation is growing. In general, minimum LAI occurred in bare ground as zero and the value increases from 1.0 to 3.0 for the

presence of poor grass to good stand of grass, respectively. This function was estimated on the basis of the start and end day of the growing season and the quality of grass using the Vadose/W built-in function. The start of the growing season is based on the mean daily temperature and plant species. According to a study of vegetation growth pattern in North east Victoria (Clifton et al. 2000) the growth season in Victoria starts on March and ends on December. The LAI functions for both sites were then input as started on the 60th days of the year (March) and ended on the 365th days of the year (December). The quality of the grass was based on the observation at the site, where moderate grass (LAI = 2.0) and poor grass (LAI = 1.0) were selected for Altona North and Fawkner, respectively. The LAI functions for both sites are shown in Figure 6-16.

The RD function is defined as the relationship between simulation day and maximum root depth from the surface. In general, plants with deeper root systems will have access to more soil water and able to sustain greater rates of evaporation during the drier months of the year (Clifton *et al.* 2000). The root depth of the grass on the field sites were generally range from 0.1 to 0.4 m below the ground surface as observed during filed instrumentations. The duration of growing season was considered as the same as LAI and a maximum root depth of 0.4 m was specified. Figure 6-17 shows the estimated RD function featured growing season starting in March and ending in December. The shape of the roots can be selected in Vadose/W to be applied over the depth. A triangular shape of roots will potentially draw more water out of the roots toward the surface, while a rectangular shape will potentially draw the same amount of water over the full root depth. The rate of root uptake is a function of the potential rates multiplied by PML value that corresponding to the actual negative water pressure in ground. Therefore, the plant will not be able to transpire any water if the negative pressure is too high (GEO-SLOPE International 2010). The shape of root depth distribution was selected to be rectangular in the soil column models, as observed on sites that the grass root system was distributed across the nature strip at approximately the same depth.

PML is known as the relationship between negative pressure and plant moisture limiting factor. It shows the percentage of the plant ability to draw water from the ground with suction. In the field, all vegetations growing on the ground is drying the soil by applying tension to the pore water through evapotranspiration. Initially, drying of ground soils is in a constant rate governed by evaporative

conditions. A gradient is developed in the soil profile that water is moving upward to the soil surface to be evaporated or transpired off. When drying of soils continues, the soil moisture content is in equilibrium with the atmosphere. At this stage the drying rate begins to decrease. Therefore, for any vegetation to draw water from the soil, suction higher than the soil suction must be applied. Most plants can apply suction up to 1 to 2 MPa before reaching the wilting point (Taylor and Ashcroft 1972). When the suction of the soil exceeds the wilting point of the plant the transpiration rate is reduced and growth of the plant is virtually ceased. The PML functions of the grass on the sites are not available, hence a typical function from the Vadose/W database for various types of vegetation was chosen and shown in Figure 6-18. The typical function has a suction of 100 kPa, where the plants will start to reach the uptake limit; and by the wilting point of 1500 kPa the plants will not be able to transpire any water from the ground.

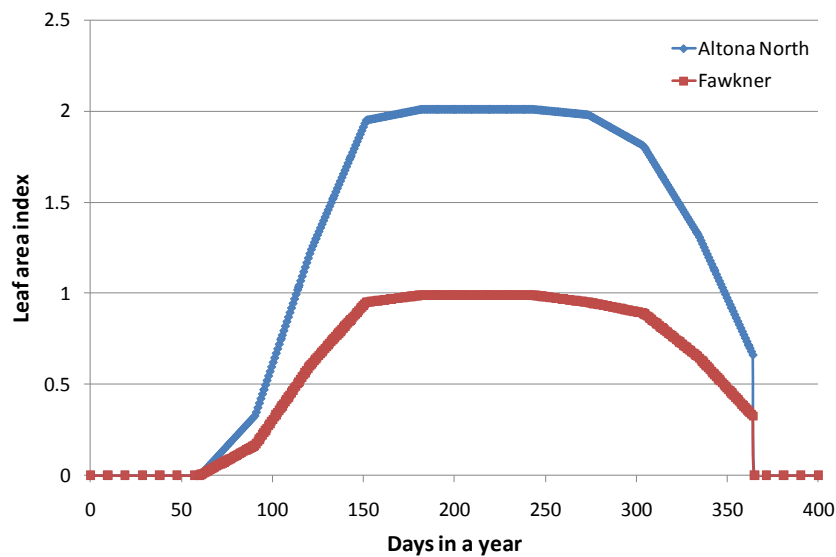


Figure 6-16 Estimated LAI function for both sites

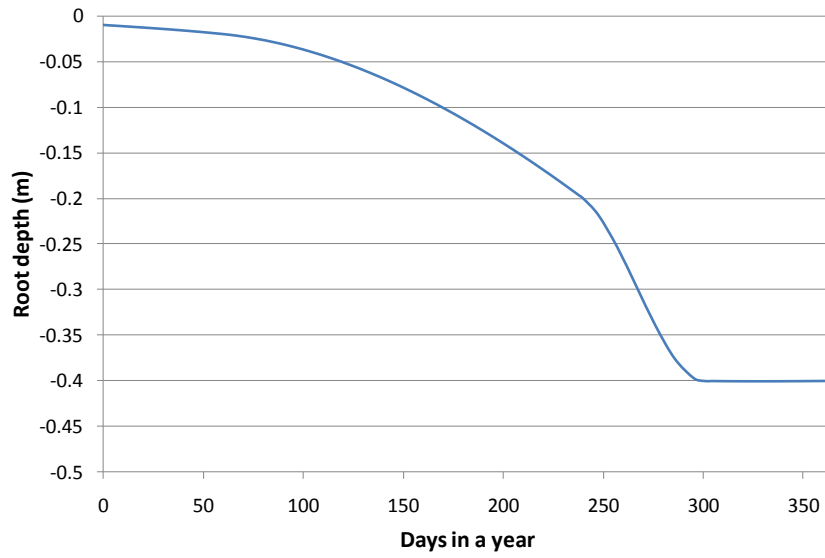


Figure 6-17 Estimated root depth function

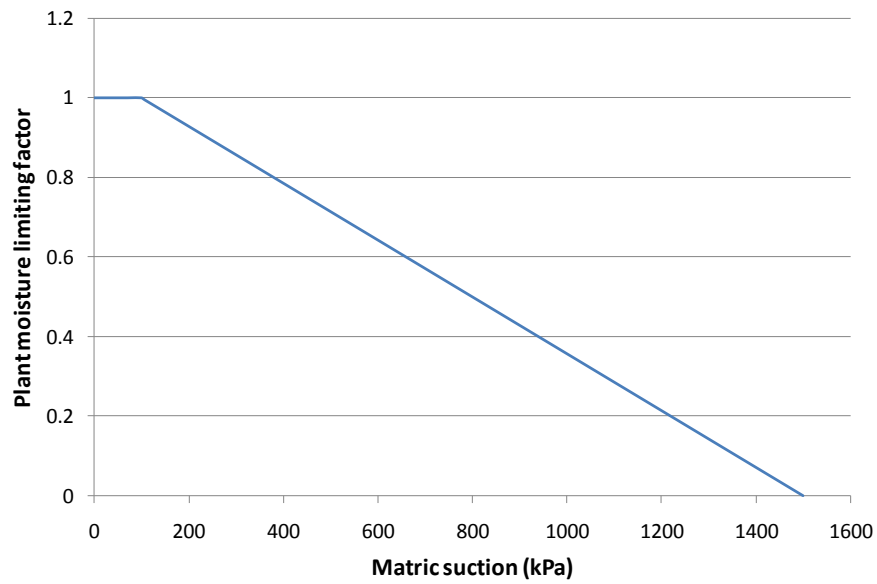


Figure 6-18 Typical PML function for most types of vegetation

The soil evaporative flux at the surface of the model as shown in Equation 6-3 is modified by the grass transpiration functions with Equation 6-14, so that a portion of the available energy is to be partitioned to the plants based on the leaf area function:

$$E = E_s \left[1 - (-0.21 + 0.7 \cdot \sqrt{LAI}) \right] \quad \text{Equation 6-14}$$

The potential transpiration (PT) which represents the energy available to the vegetation is then determined as:

$$PT = PE \cdot (-0.21 + 0.7 \cdot \sqrt{LAI}) \quad \text{Equation 6-15}$$

Full amount of the potential transpiration energy will be applied to the plant roots according to the RD function for saturated soils. The transpiration energy will be further reduced for vegetation in unsaturated soils, which is according to the PML function as follows:

$$T = PRU \cdot PM \quad \text{Equation 6-16}$$

where T is nodal transpiration, and

$$PRU = \frac{2PT}{R_T} \left(1 - \frac{R_n}{R_T} \right) A_n \quad \text{Equation 6-17}$$

where R_T is the total thickness of root zone; R_n is the depth to the node in question; and A_n is the nodal contributing area of the node in question.

The nodal vegetation uptake in the model is recorded as transpiration at the surface, and on the basis of the criterion of conservation of energy, the sum of evaporation and transpiration can never be greater than the potential evapotranspiration at the surface node.

6.2.6 Initial and boundary conditions

Ground-atmosphere simulation of the soil column requires the initial conditions, i.e., suction and temperature profiles) and the boundary conditions, i.e., climate, heat sink, and no-flow boundaries, to be setup in the model.

The initial suction profile used in each model were established from the SWCCs using the soil moisture content measured with the neutron probe in the field as described in Chapter 5, at the start date of the analysis (i.e., June 2009). Figure 6-19 shows the initial moisture and suction profiles used in the models for each site. In order to provide more accurate modelling which took into account the varying suction along the soil profiles, each of the soil column model was divided into 11 thin layers where the activation suction value for each layer was interpolated from Figure 6-19.

The initial temperature profiles were taken as the average soil temperature measured at each depth on both sites on the start date of the analysis. The initial temperature profiles are shown in Figure 6-20 and the activation temperature for each of the 11 layers was interpolated from this figure. Since soil temperature was only measured at four depths, the temperature between each depth was assumed to be linear.

The climate boundary condition applied at the ground-atmosphere interface of the soil column model requires measurements of air temperature, relative humidity, precipitation, wind speed and solar radiation. These data were obtained from the weather stations installed at the instrumentation sites measured between the periods of January 2009 to October 2010. This weather data are presented in Appendix G.

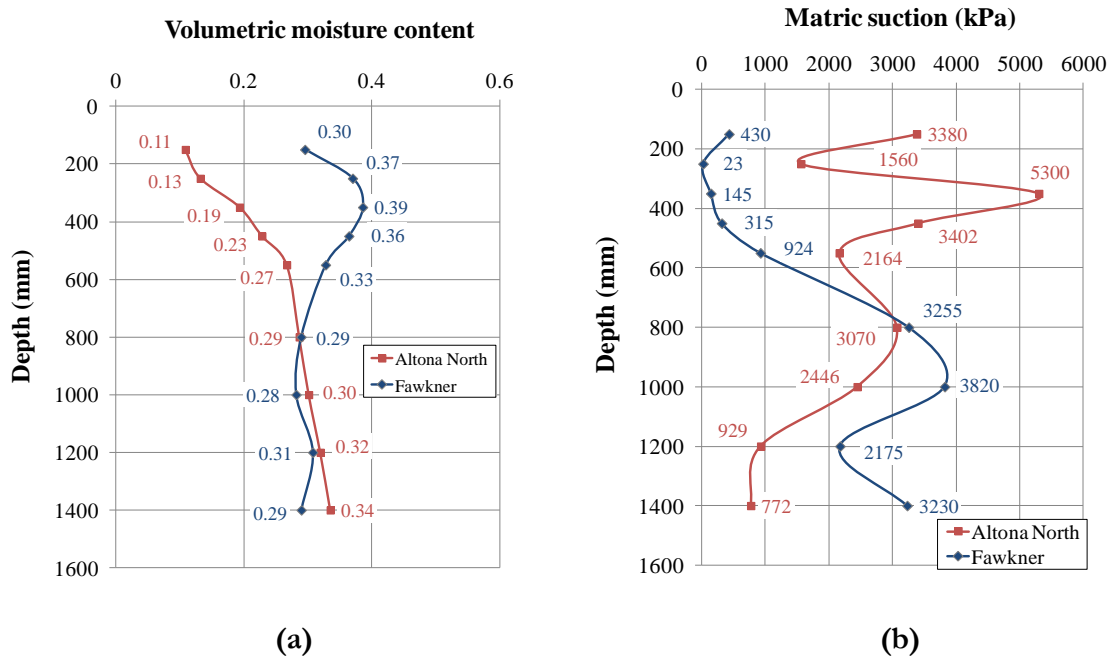


Figure 6-19 Initial soil profiles : (a) moisture content; (b) suction

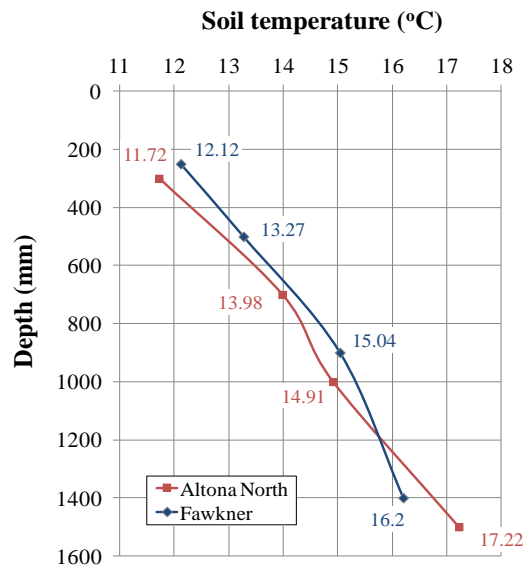


Figure 6-20 Initial soil temperature profiles

The heat sink boundary in the form of heat unit flux was applied at the bottom of the models to remove excess heat energy as the heat energy within the in one-dimensional soil column model can only be dissipated in the vertical direction. Preliminary analyses undertaken indicated that the without the heat sink boundary, the model prediction of soil temperature were very high due to excess heat energy stored in the model. The values of heat unit flux applied on each model were obtained from parametric study of the effect of heat sink on the predicted soil temperature. Multiple model runs by trial and error were performed to estimate the bottom unit flux of heat loss. These values were obtained as $-465 \text{ kJ}/(\text{day}\cdot\text{m})$ and $-930 \text{ kJ}/(\text{day}\cdot\text{m})$ for the Altona North and Fawkner models, respectively.

A no flow boundary was applied at the bottom of the soil column at each site to imitate the layer of basalt found at the depth of 2000 mm at the sites (as described in Chapter 3). The basalt rock was considered to be slightly weathered with small cracks on the first meter and then became tight with no crack at greater depths. Hence, the no flow boundary was applied at one meter below the basalt layer (i.e. 3000 mm from ground surface) in the soil column to prevent infiltration of moisture below this depth.

6.2.7 Summary of the Vadose/W models

The soil properties and boundary conditions assigned for the models were:

- Hydraulic properties:
 - SWCCs;
 - Hydraulic conductivity-suction functions ;
 - Initial soil suction.
- Thermal properties:
 - Thermal conductivity functions;
 - Volumetric heat capacities;

- Initial soil temperature.
- Boundary conditions:
 - Vegetation functions;
 - Climate boundary;
 - Heat sink boundary;
 - No flow boundary.

The numerical models of the soil column of both sites are shown in Figure 6-21 and Figure 6-22. Both models were constructed as a soil column with 12 sub-layers consists of three meshes. The surface mesh was sub-layers 1 to 9, the middle mesh was sub-layers 10 and 11, and the bottom mesh was sub-layer 12 representing the basalt. A fine discretisation was performed by dividing the surface mesh four times finer than the other meshes as greater variations in soil moisture content and temperature were experienced by the soil at this layer due to the prevailing climate conditions.

6.2.8 Numerical analysis of soil column

The soil columns were analysed using the full thermal conditions with adaptive time stepping (with initial time step as one day) that is required for solving climate boundary conditions where the daily climate data are used (GEO-SLOPE International 2010). The analysis time in a desktop computer (i.e., Intel Pentium 4 CPU, 3 GHz, 1 GB RAM) was approximately 1 hour for 1 to 2 years.

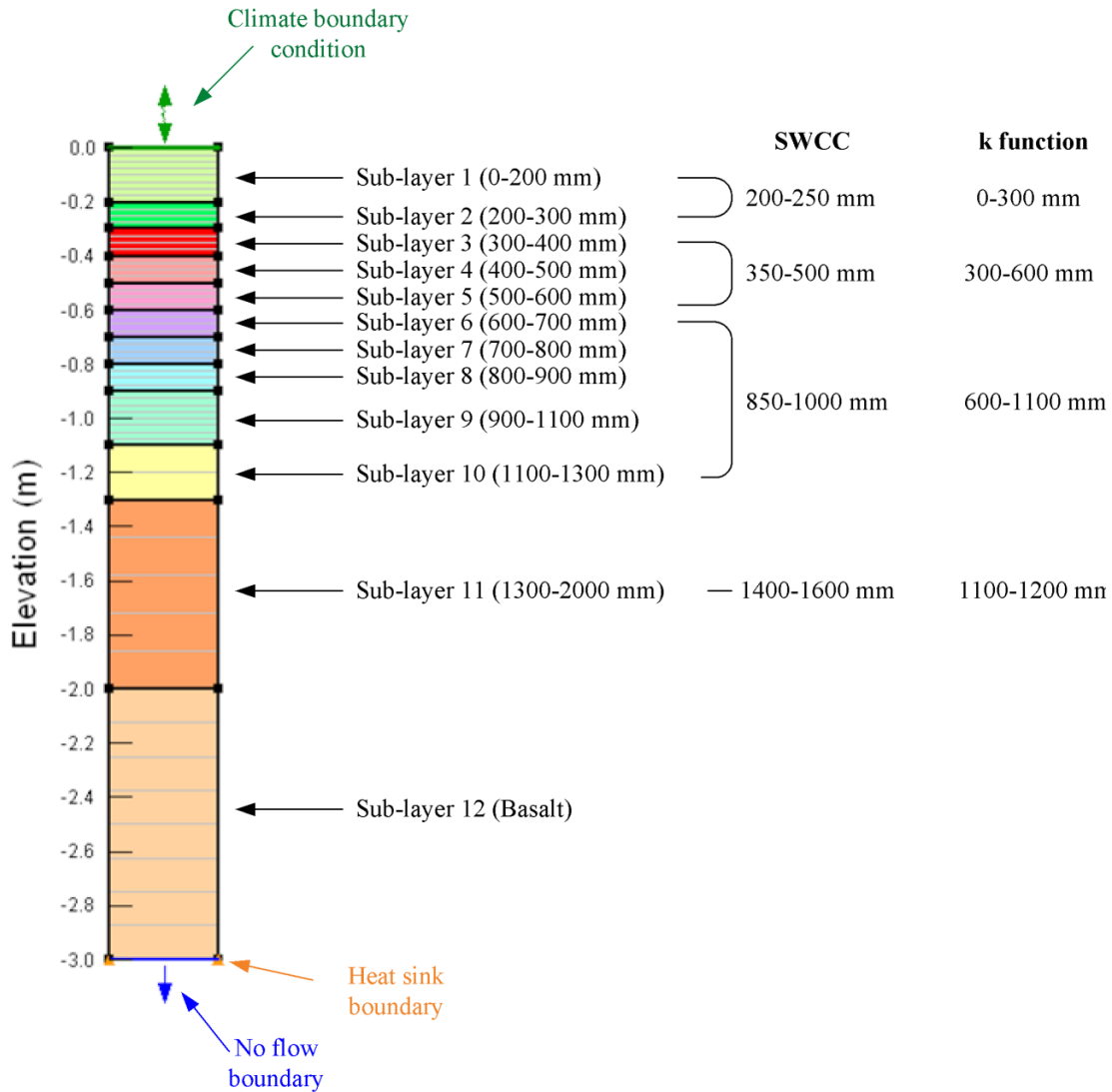


Figure 6-21 Summary of the Vadose/W model of Altona North (SWCC in Figure 6-2 and *k* function in Figure 6-9)

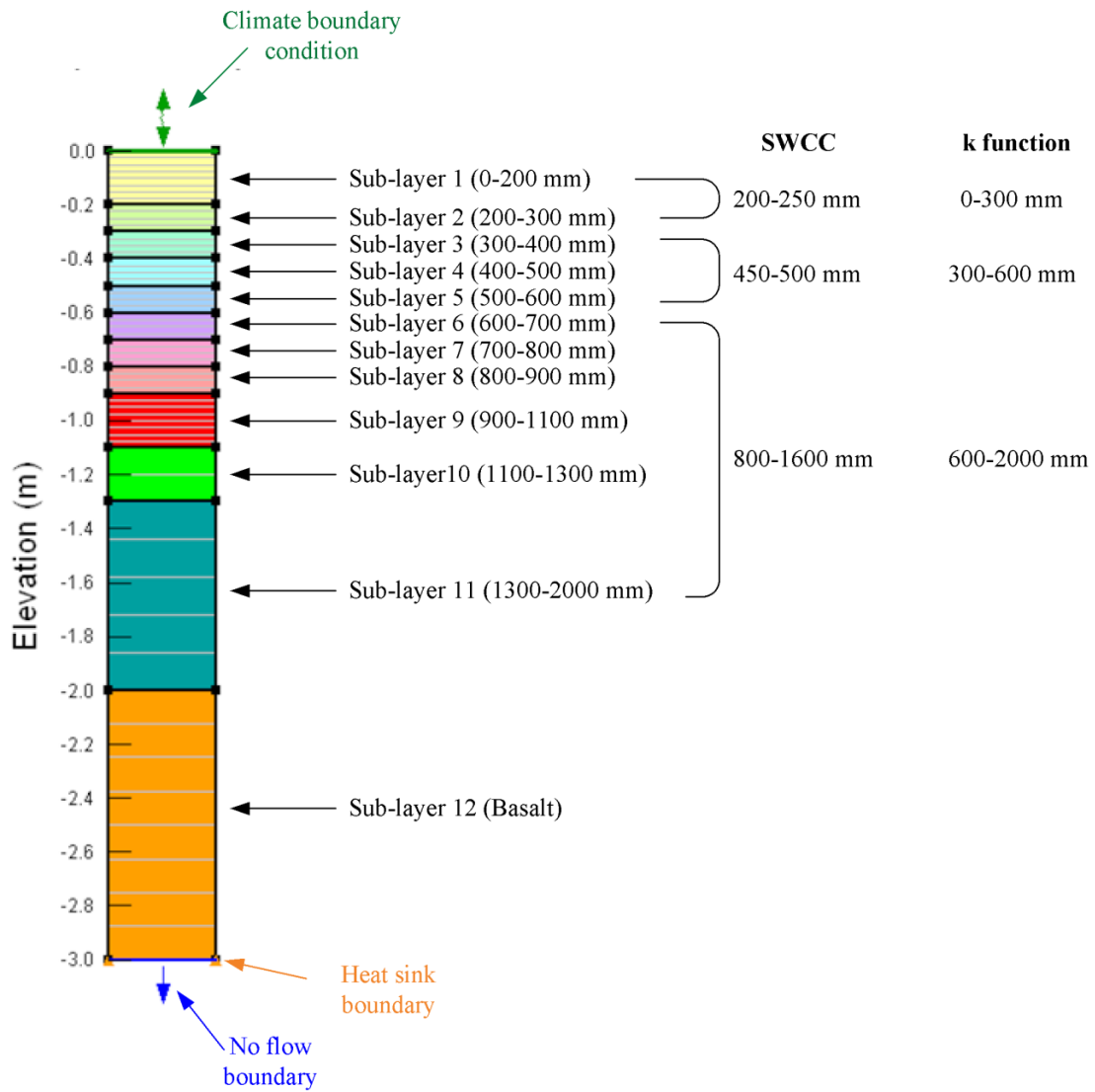


Figure 6-22 Summary of the Vadose/W model of Fawkner North (SWCC in Figure 6-3 and *k* function in Figure 6-10)

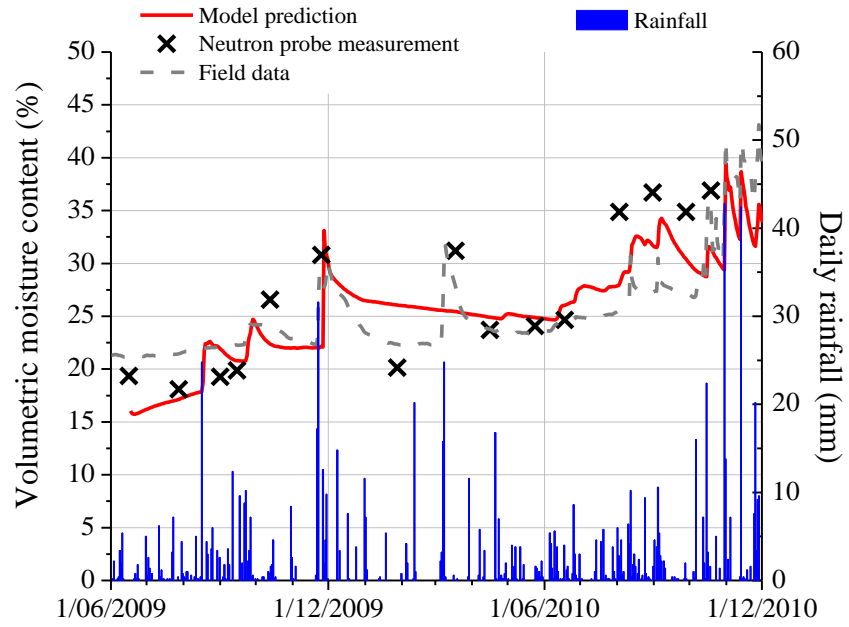
6.3 Ground-atmosphere Model Prediction

The ground-atmosphere models are developed to be used as a base condition for long term predictions (i.e., 20 years) of soil moisture content variations in the field sites, which will be described in the next chapter. Model predictions for the base condition made for the duration of the neutron probe measurement period of June 2009 to December 2010 are verified in this section by comparing with the field measured data.

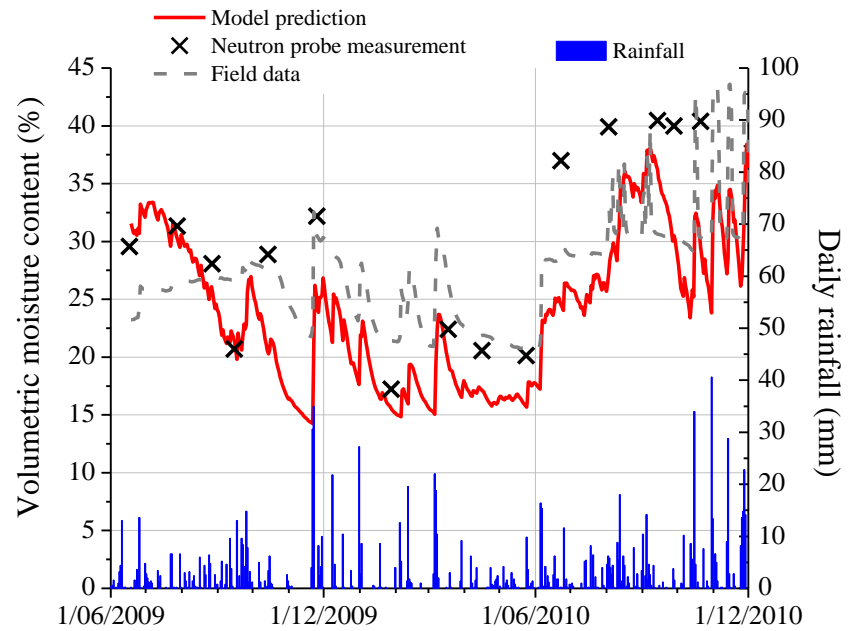
6.3.1 Prediction of soil moisture content

The model predicted volumetric soil moisture content values are plotted with the neutron probe measurements, field measurements from Theta probes at some specific depths and the daily rainfall measured at the site. The predicted moisture content is given in Figure 6-23 to Figure 6-25 for depths of 300, 800 and 1000 mm for Altona North, and 250, 500 and 1000 mm for Fawkner.

According to the field measurements shown in Chapter 4, the influence of atmospheric forcing is generally decreases with depth, and this trend is captured by the model. At soil depths close to the ground surface (Figure 6-23), the soil moisture content is directly affected by rainfall and evaporation events, as the fluctuations of soil moisture content correlates well with daily rainfall. As expected, the soil moisture content predicted by the models increases corresponding to high rainfall events and decreases in low rainfall or dry periods. The model predictions match reasonably well with both neutron probe and Theta probe measurements. At depths of 500 and 800 mm at both sites (Figure 6-24), the field measurements indicate that the predicted moisture content were close to field measurements. At greater depths over 1000 mm (Figure 6-25), again the predicted values matched well with the field measurements.

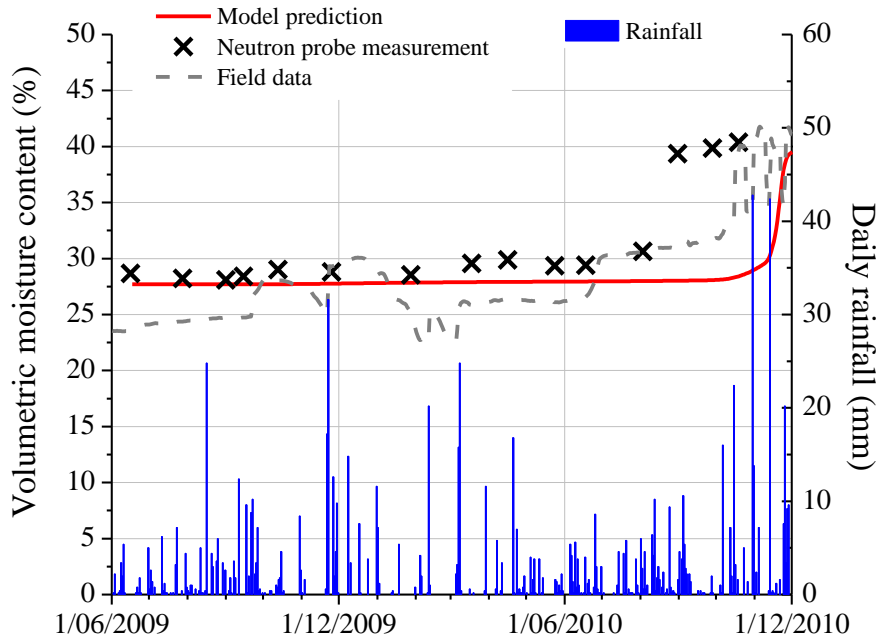


(a)

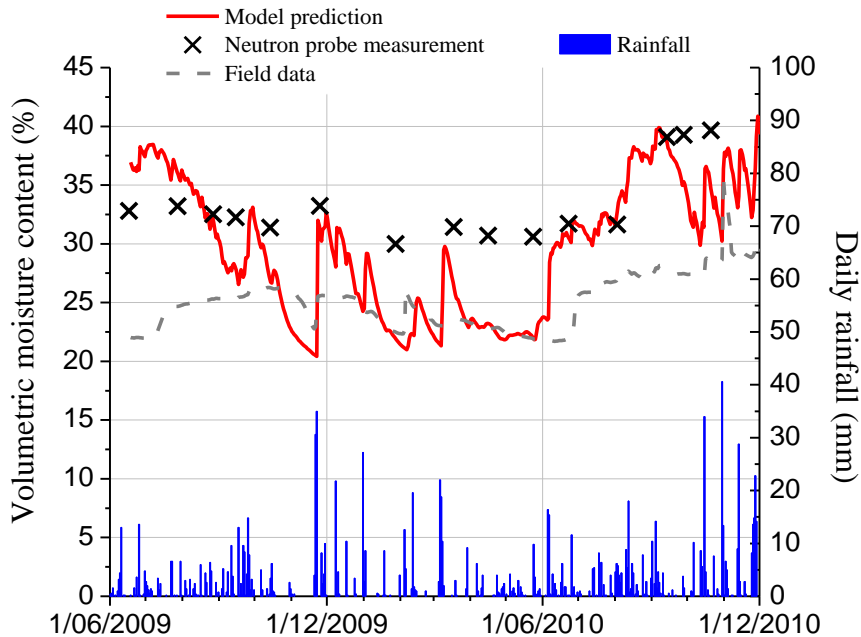


(b)

Figure 6-23 Volumetric moisture content output: (a) Altona North at 300 mm; (b) Fawkner at 250 mm

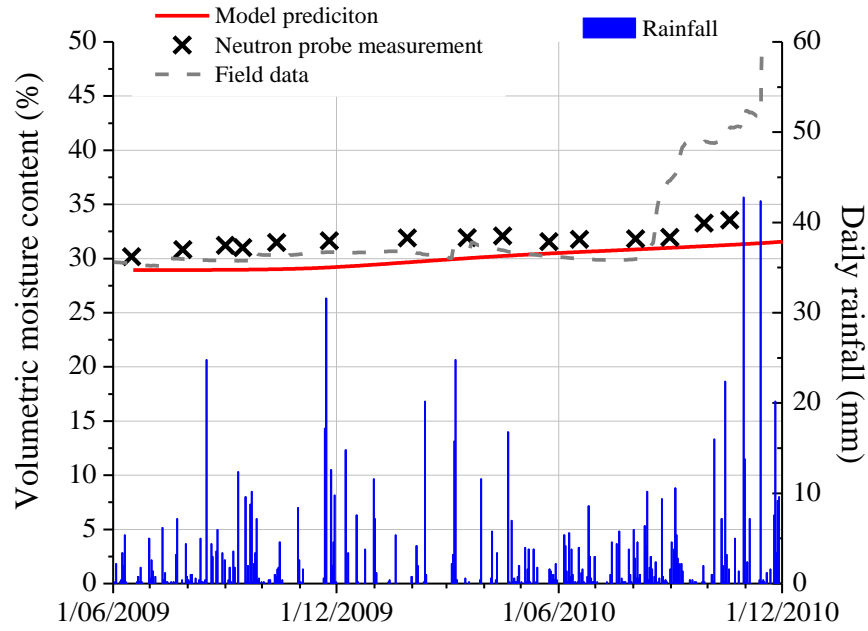


(a)

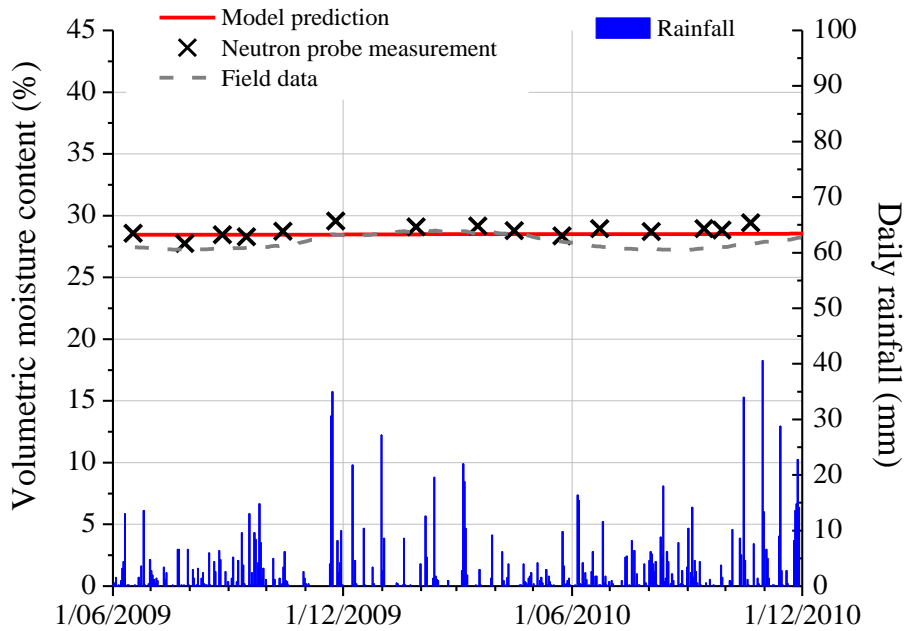


(b)

Figure 6-24 Volumetric moisture content output: (a) Altona North at 800 mm; (b) Fawkner at 500 mm



(a)



(b)

Figure 6-25 Volumetric moisture content output: (a) Altona North at 1000 mm; (b) Fawkner at 1000 mm

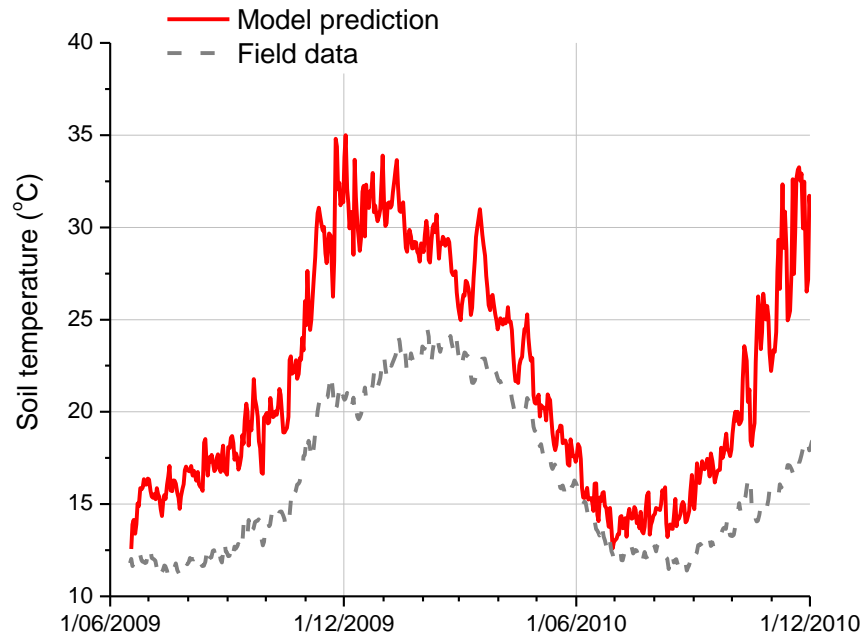
In Altona North, an overall increment in soil moisture content was observed towards the end of the 2010. This increase in moisture content was captured by the model at soil depths of 300 and 800 mm. At the depth of 1000 mm, the model prediction matched the neutron probe and Theta probe measurements. At the end of 2010 when the Theta probe showed a significant increase in soil moisture content due to series intense rainfall events, however such increase were not recorded by neutron probe and the model prediction was still matched well with the neutron probe measurements.

In Fawkner, the model predictions generally capture the soil moisture content variations, although at certain periods it underestimated the moisture variation at a depth of 250 mm. In particular, the model predictions were more accurate at greater soil depths (i.e., greater than 800 mm), possibly due to the lesser variations by the prevailing climate and more consistent soil profiles (i.e. same layer of clay soils).

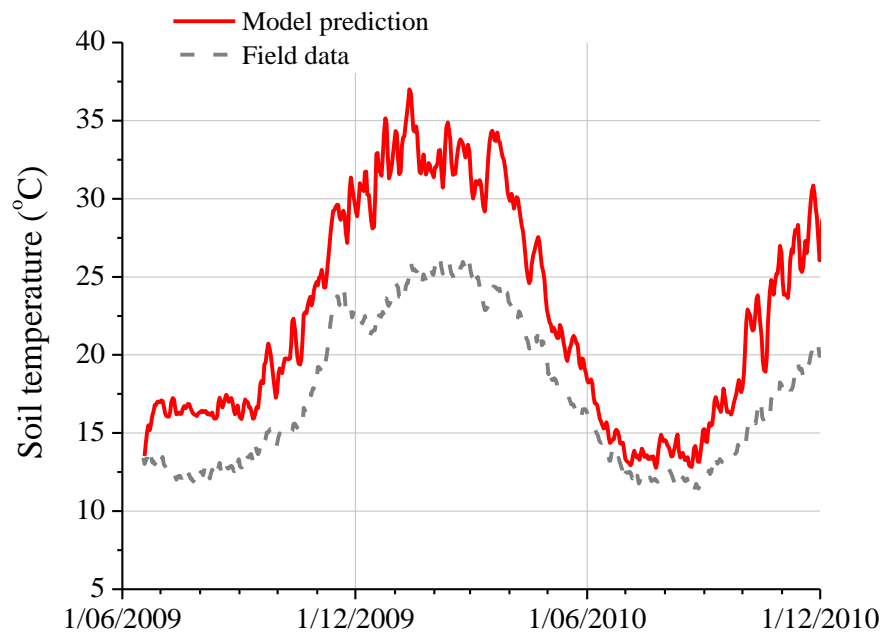
6.3.2 Prediction of soil temperature

As reported in Chapter 4, soil temperature was measured by thermocouples at various depths at the field sites. The comparison of field data and model predictions of soil temperature are shown in Figure 6-26 to Figure 6-28. In general, the models predicted temperatures higher than the measured field soil temperature at shallow depths (i.e., above 800 mm) and provide better predictions at greater depths.

At the shallow depths of 250 and 300 mm (Figure 6-26), the discrepancy between model predictions and field data are basically due to the limitations of the one-dimensional models. As the heat sink boundary was applied at the bottom of the soil column, it had greater effect on the elements close to the bottom, and thus better predictions were made by the model at greater depths (i.e., 700 and 1000 mm) as shown in Figure 6-27 and Figure 6-28. Overall, the models are able to capture the temperature variation at these depths with reasonably good accuracy with a discrepancy of approximately ± 8 °C.

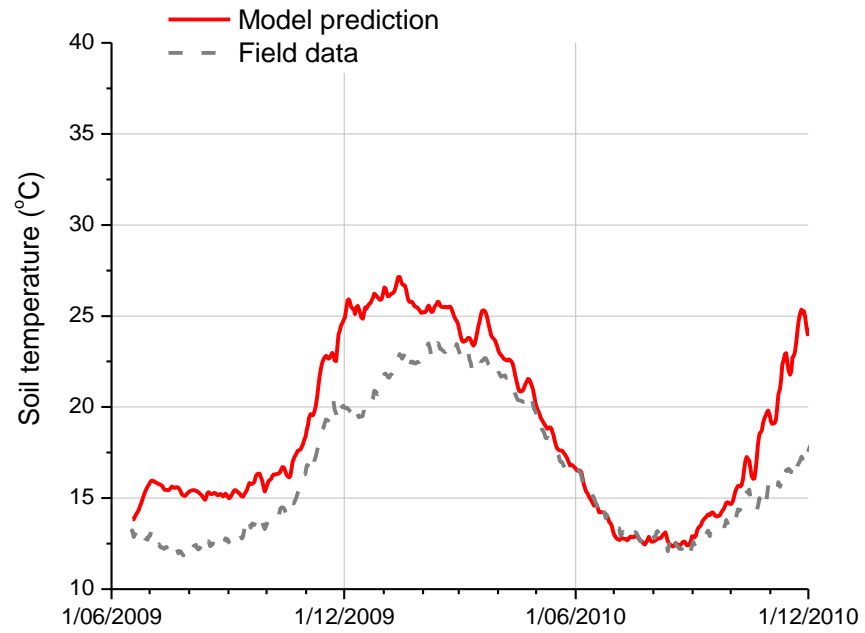


(a)

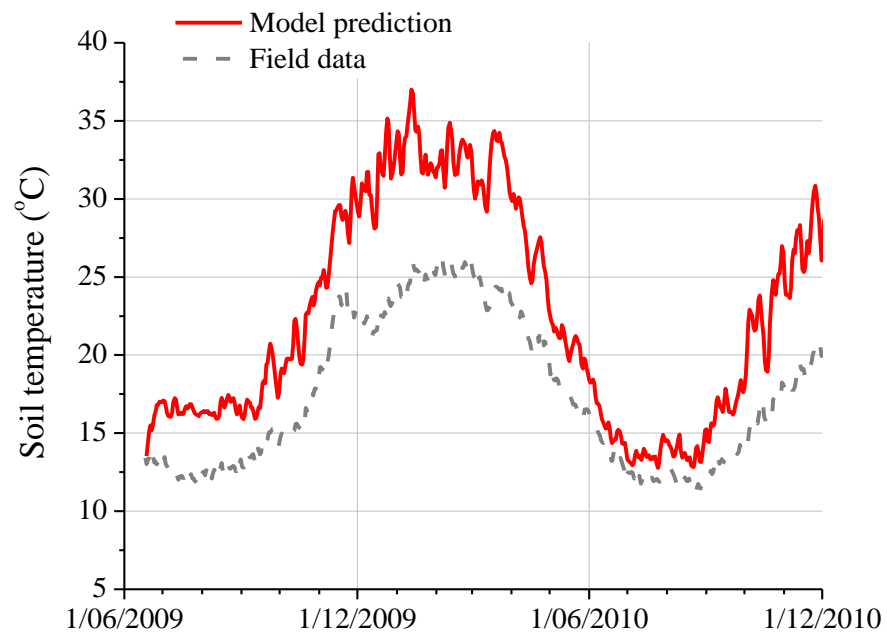


(b)

Figure 6-26 Temperature output: (a) Altona North at 300 mm; (b) Fawkner at 250 mm

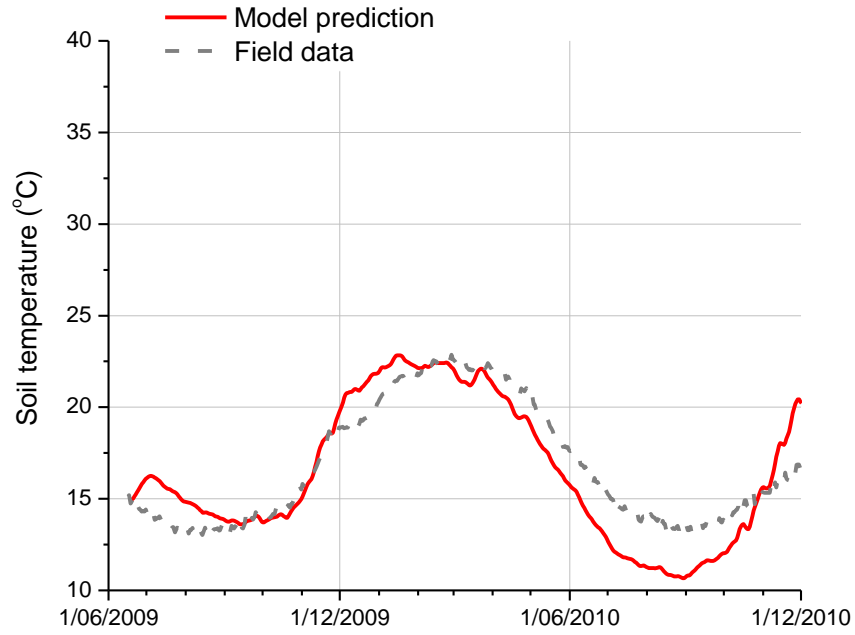


(a)

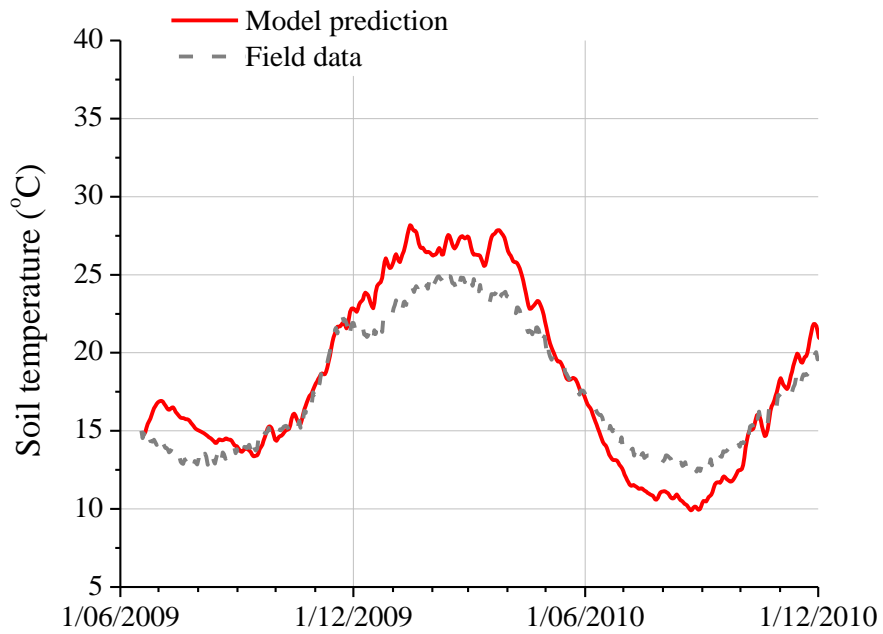


(b)

Figure 6-27 Temperature output: (a) Altona North at 800 mm; (b) Fawkner at 500 mm



(a)



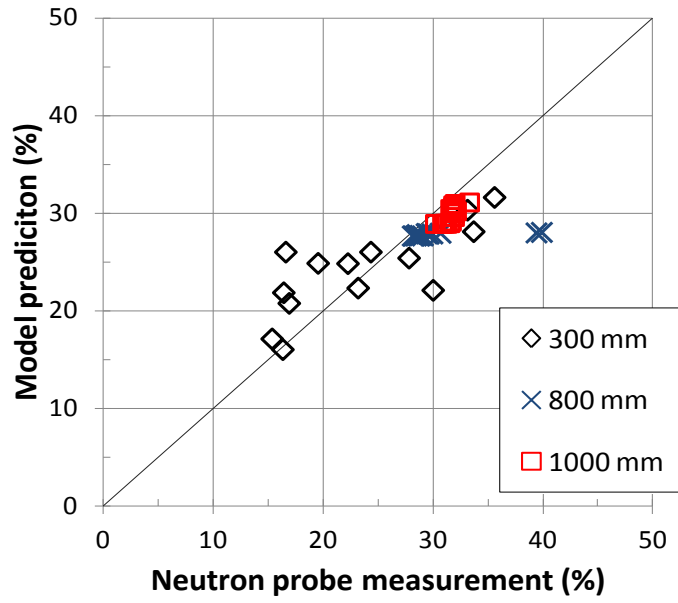
(b)

Figure 6-28 Temperature output: (a) Altona North at 1000 mm; (b) Fawkner at 900 mm

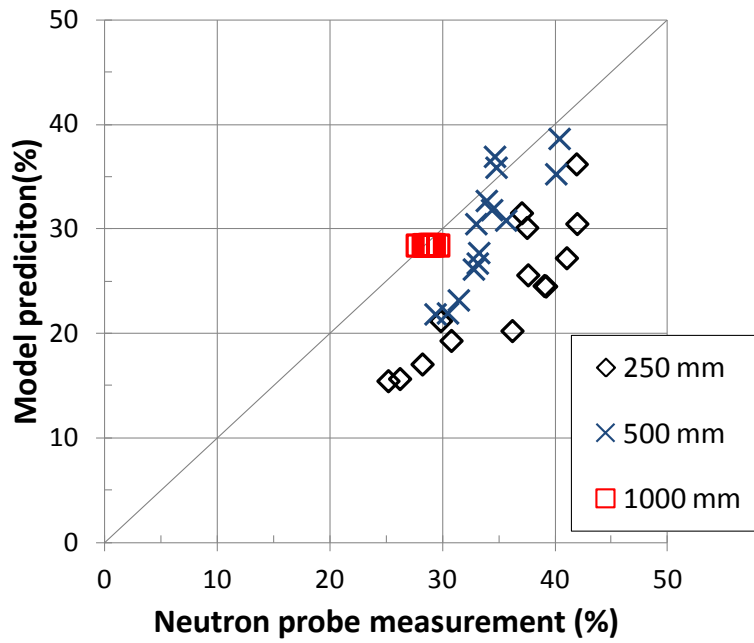
6.3.3 Comparison of field measurements and model predictions

A comparison of the field measured neutron probe and thermocouple data and the model predictions for both sites is shown graphically in Figure 6-29 for soil moisture content, and Figure 6-30 for soil temperature.

As noted previously, the model predictions for both sites were more accurate at greater depths. As shown in the comparison plots of soil moisture content (Figure 6-29), the data points at 1000 mm are generally located closer to the 1:1 line than the data points at depths of 150 to 800 mm. Similarly, the data points of soil temperature (Figure 6-30) at depths of 900 and 1000 mm are closer to the 1:1 line than the data points corresponding to shallower depths. The Fawkner site has some variability compared to Altona North, where the soil moisture content is underestimated. A possible explanation to this is the localise flow characteristic (e.g. macropores) around the neutron probe measurement location.

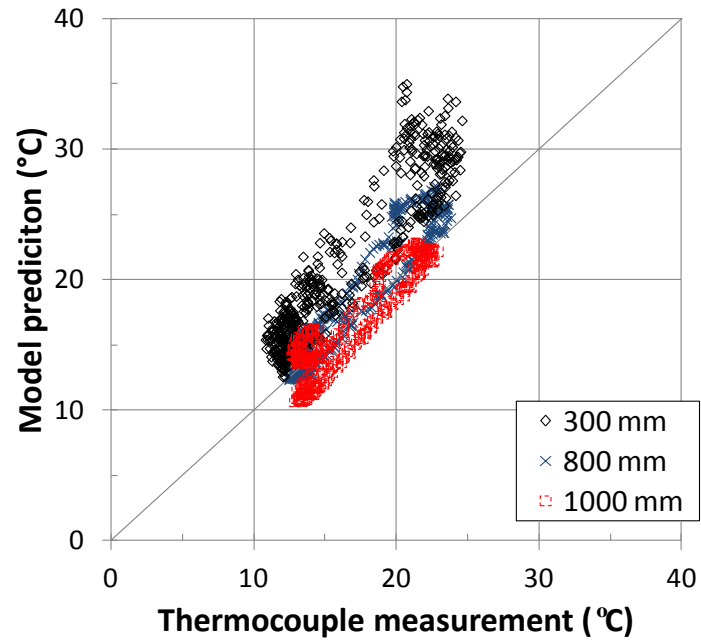


(a)

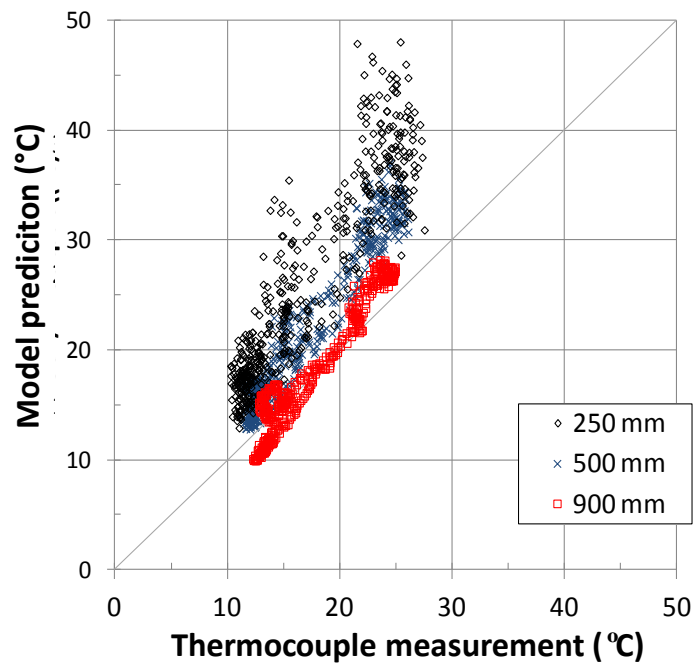


(b)

Figure 6-29 Model prediction against neutron probe measurement: (a) Altona North; (b) Fawkner



(a)



(b)

Figure 6-30 Model prediction against thermocouple measurement: (a) Altona North; (b) Fawkner

6.4 Conclusions

Modelling of the ground-atmosphere interaction of the two instrumented field sites is presented in this chapter. One-dimensional soil column of each site was modelled in Vadose/W using soil thermal and hydraulic properties determined from field and laboratory tests. The developed numerical models were validated against the field measurements. The models predictions were generally in good agreement with the field measurements and provided better predictions at greater soil depths than at shallow depths. The developed soil column of both sites will be used for long term predictions of soil moisture content with randomised climate events, and report of this work is presented in the next chapter.

CHAPTER 7

PROBABILITY OF PIPE FAILURES DUE TO CHANGES OF SOIL MOISTURE CONTENT OVER TIME

7.1 Introduction

The one-dimensional ground-atmosphere interaction models described in the previous chapter are capable of predicting soil moisture content and temperature of the field sites reasonably well in the monitoring period. Long term modelling can also be undertaken using climate data for longer period (e.g., ten years or longer) to predict variations of soil moisture content that can impact adversely on buried pipes. The first part of this chapter presents the long term prediction of soil moisture content for Altona North. The Winkler models are then used to simulate the pipe-soil interaction and calculate the pipe flexural stresses associated with change in soil moisture content. Finally, pipe failure probability is estimated from pipe flexural stresses and deterioration of the pipe material, therefore the relationship between pipe failure and pipe age can be obtained.

7.2 Long Term Ground-atmosphere Model

7.2.1 Overview of long term ground-atmosphere model

In order to calculate the soil displacement and pipe stress that could be experienced by the pipe buried on site, a long term ground-atmosphere model was set up to predict the soil moisture variations due to possible extreme climate events. The soil column models described in Chapter 6 capable of predicting soil moisture content of the field sites for the monitoring period were used for long term prediction of soil moisture content.

In general, both the soil column models for Altona North and Fawkner could be used for the long term prediction. However considering the time required for model analysis, only one site was used. In this instance, the Altona North model was used for long term prediction with the same hydraulic properties, thermal properties, initial conditions, and boundary conditions, but with extended climate data. Historical climate data obtained from the Australian Bureau of Meteorology, corresponding to a weather station located approximately 10.3 km from the Altona North site was used. Since only data of 10 year period (1997 to 2006) was available, a 20 years dataset was created by using the same data twice.

The long term simulation began at the same date as the previous simulation (i.e., June 2009) and continued for a total period of 20 years until December 2029. A simulation period of 20 years was chosen on the basis of the findings that extreme weather conditions (i.e., extremely hot and dry seasons) which believed to lead to pipe failures occurred in three to four years intervals (Ibrahimi 2005; Chan 2008). The long term model was analysed using the same desktop computer as described in Chapter 6. The analysis time for a 20 years model was approximately a day.

7.2.2 Prediction of soil moisture content

Prediction on soil moisture content from the long term model at different depths is shown in Figure 7-1. Similar to previous model predictions and the field measurements, higher variations

occurred close to the ground surface and these variations diminished with depth. For example, at depths of 150 mm, soil moisture content variation of $\pm 26\%$ was recorded; soil moisture content variation of $\pm 15\%$ was recorded. At greater depths of 800 mm and below, relatively low soil moisture content variation of $\pm 9\%$ was recorded. Furthermore, the variation of soil moisture content at greater depths showed a cyclic peaking behaviour. These peaking occurred at significantly wet period after a long relatively dry period at an interval of four to five years. After a significant wet period, the soil moisture content depleted continuously for four to five years until another significant wet period began. This pattern of soil moisture content variation may explain why soil shrinkage is the predominant ground movement that is considered to be responsible for pipe failures in Victoria, since soils were experiencing continuous drying through a period of four to five years.

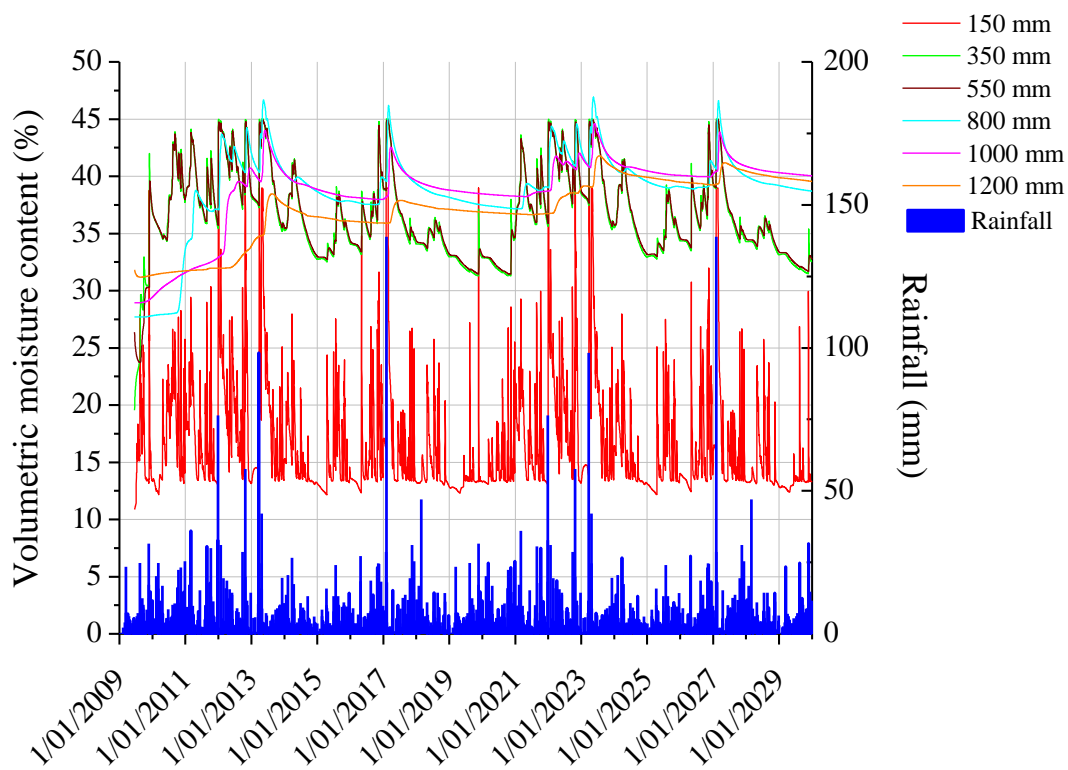


Figure 7-1 Long term prediction of soil moisture content in Altona North

7.3 Probability of Soil Moisture Content Variations

In order to provide better prediction of soil moisture content variations, a study of the original 10 years climate data from the Australian Bureau of Meteorology was carried out. It was found that the rainfall and relative humidity of the Altona North area decreased by a maximum of 50 % and increased by a maximum 80 % (from the original value) in the years of extremely dry and wet climate. Therefore, to simulate the possible extreme climate events the random climate datasets was created by applying a randomly generated ratio range from 0.5 (decrease by 50 %) to 1.8 (increase by 80 %) to the rainfall and relative humidity in each year of the 20 years climate data described in the previous section. Five random climate datasets of 20 years were created following this approach, where the rainfall and relative humidity in each year was multiplied by a random ratio. These datasets were inputted into the long term Altona North model for prediction of soil moisture content taken into account the extreme climate conditions.

Figure 7-2 shows the soil moisture content at soil depth of 800 mm predicted by the original climate data and the random climate datasets. Variation of soil moisture content was approximately 37 % to 50 % at this depth for each datasets, and different cyclic variations could be identified. A maximum and a minimum soil moisture content can occur in the same period for different datasets, suggesting that the randomised climate events had significant effect on the soil moisture content. Using these model outputs the change in soil moisture content can be calculated as the differences between the soil moisture content at each time step (i.e., one day) and the average soil moisture content (e.g., average soil moisture content of the corresponding soil depth) of all datasets outputs. The change in soil moisture content could practically be calculated at any depth along the soil column, but since the pipe stress corresponding to variations in soil moisture content were the interest of this study, the change in soil moisture content close to nominal pipe depth at 800 mm was used.

Figure 7-3 shows the histogram developed from the change in soil moisture content at soil depth of 800 mm. A negative change in moisture content represents a decrease from the average value (i.e., 43 % at soil depth of 800 mm) and a positive change in moisture content represents an increase

from the average value. It was found that soil moisture can decrease by a maximum of 8 % and increase by a maximum of 6 %, respectively.

The change in soil moisture content was used for analysis of pipe-soil interaction, where pipe flexural stress corresponding to a particular increase or decrease in soil moisture content was calculated. Hence, the probability of change in moisture content could be converted to the probability of flexural stress experienced by the pipe buried on site. The numerical modelling of pipe-soil interaction is described in the following sections.

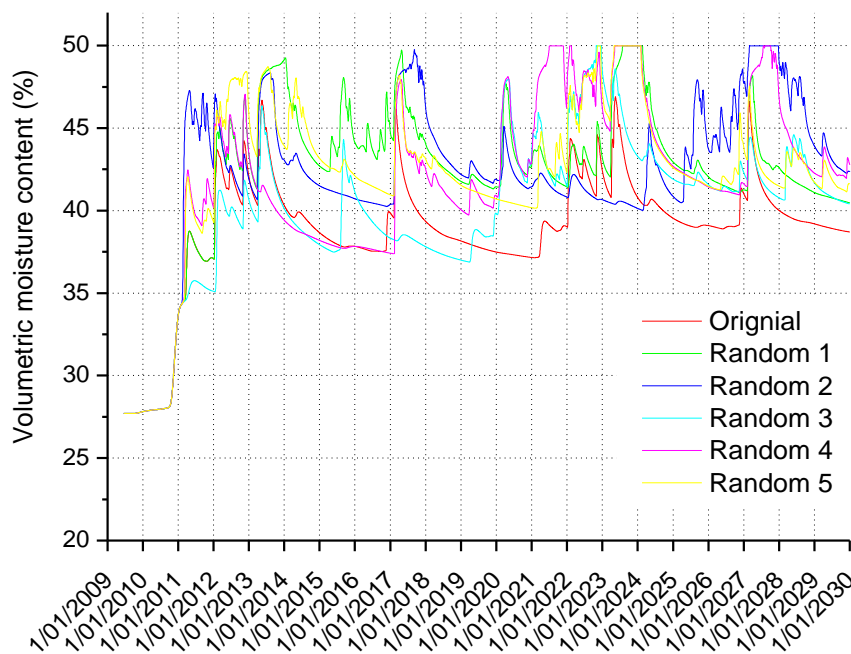


Figure 7-2 Long term prediction of soil moisture content in Altona North with random climate at 800 mm

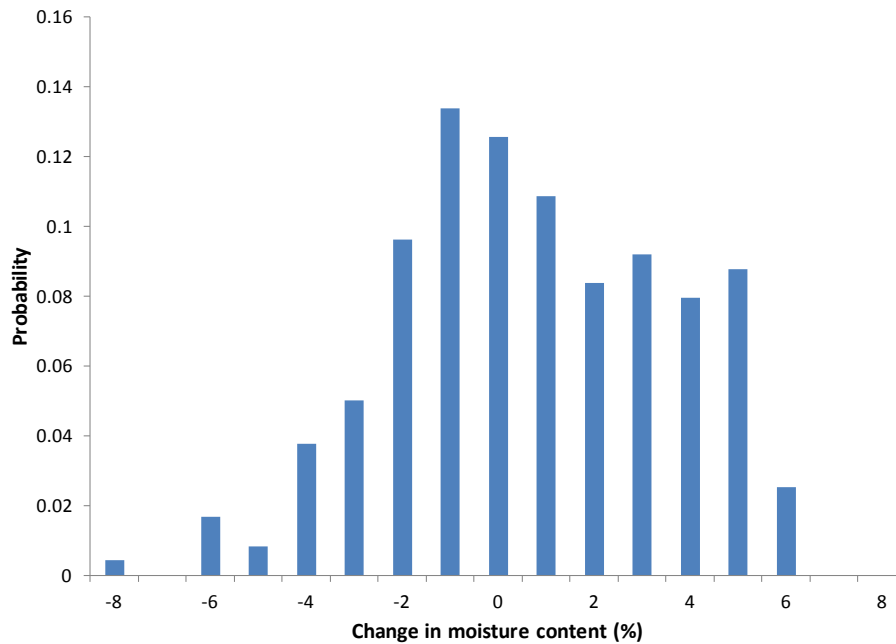


Figure 7-3 Change in soil moisture content at soil depth of 800 mm

7.4 Numerical Modelling of Pipe-Soil Interaction

7.4.1 Overview of numerical pipe-soil models

There are two commonly used techniques for numerical modelling of pipes buried in unsaturated soil; the Winkler spring models and the three-dimensional continuum models. The Winkler models represent the situation in two-dimensions with special beam type elements to represent the pipe and series of separate spring of known stiffness to represent the soil (Rajani *et al.* 1996; Rajani and Tesfamariam 2004). The three-dimensional continuum models use continuous finite element or finite difference or boundary elements methods to represent both the soil and pipe.

In general, the Winkler models are commonly used in practice due to its simplicity and lesser computational time (Gould 2011). However, assuming the soil by springs with no direct interaction

in-between may be an approximate approach, especially in the case of reactive soils where the swelling and shrinkage behaviour can be non-linear (Rajeev and Kodikara 2011). Conversely, the three-dimensional continuum models provide a better representation of unsaturated soil by direct interaction of the soil particles with interconnected elements. However, the disadvantage of such models is the requirement of additional parameters to describe the soil properties which can be difficult to obtain as well as substantially increasing the complexity of the model.

The Winkler spring models described by Gould (2011) are used in this study due to its simplicity and good agreement with the field measured data. A simplified application of these models using the change in soil moisture content presented in Figure 7-3 as input is demonstrated in the following sections.

7.4.2 Theoretical framework of pipe-soil interaction

Swelling and shrinking of soils are primary due to change in moisture content. Change of soil volume in the form of void ratio are commonly related to soil suction as it is considered to be a stress state variable in controlling mechanical properties of partially saturated soils (Fredlund and Morgenstern 1977). However accurate measurement of soil suction is difficult, while hydraulic hysteresis is presented between wetting and drying cycles of soils (Chu and Mou 1973). The use of soil moisture content related to void ratio is advocated as a practical way to overcome this problem (Fityus 1999; Briaud *et al.* 2003; Rajeev and Kodikara 2011; Kodikara 2012). The relationship between soil moisture content and void ratio does not exhibit significant hysteresis, especially for soil that have experienced multiple wetting and drying cycles (Fleureau *et al.* 2002; Tripathy *et al.* 2002; Gould *et al.* 2011), therefore it is used in this study to model the swelling and shrinking behaviour of soils. This approach provides a more straightforward analysis of the problem avoiding the difficulty in measurement of soil suction and hydraulic hysteresis in wetting and drying of soils.

The theoretical framework for determination of deformation in a pipe-soil system due to change in soil moisture content was described in detail by Gould (2011) and will only be briefly repeated in here. Gould (2011) developed Equation 7 – 1 known as the void ratio – water content – net stress (

) surface applicable to environmentally stabilised soils, such as the reactive clays in Altona North and Fawkner. The equation relates the response of soils to change in gravimetric moisture content and stress as follows:

$$e(\omega) = f(\omega, a) - f(\omega, b) - f(0, a) + f(0, b) + e_r \quad \text{Equation 7 - 1}$$

where

$$f(x, y) = -\frac{m}{\phi \cdot \pi} \left[\phi(x-y) \cdot \tan^{-1}(\phi(x-y)) - \frac{1}{2} \ln(1 + (\phi(x-y))^2) \right] \quad \text{Equation 7 - 2}$$

$$e_r = \alpha_{er} \ln \left(1 + \frac{\sigma}{\sigma_0} \right) + e_{r0} \quad \text{Equation 7 - 3}$$

$$a = \alpha_a \ln \left(1 + \frac{\sigma}{\sigma_0} \right) + a_0 \quad \text{Equation 7 - 4}$$

e is the soil void ratio, ω is the soil moisture content, σ is the soil net stress, σ_0 is the nominal net stress, b , α_{er} , e_{r0} , α_a , a_0 and m are the fitting parameters. Figure 7-4 shows an idealised surface relationship between e , ω , and σ . It is important to note that this surface is relevant only for soils that have experienced multiple wetting and drying cycles, where the behaviour of the soil is stabilised.

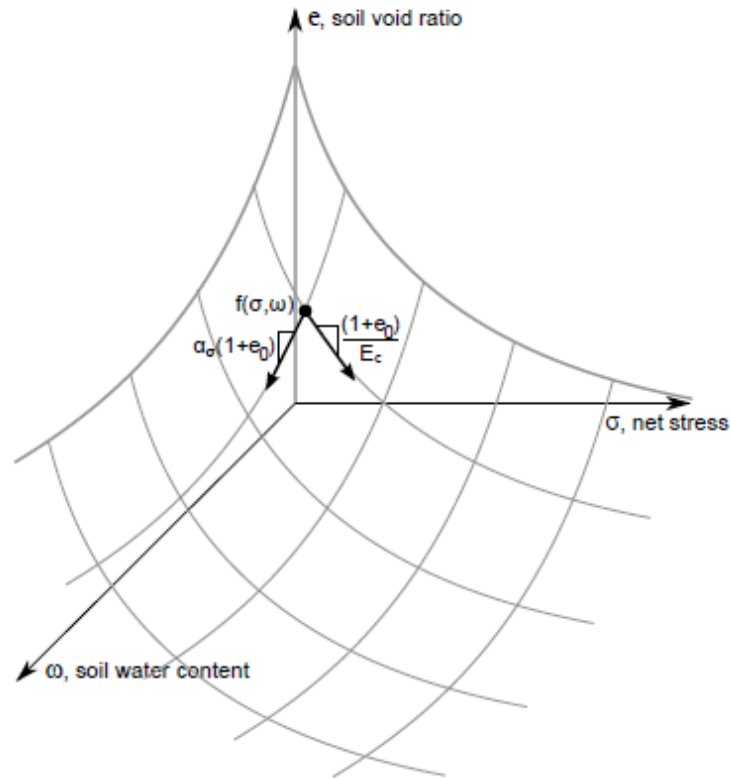


Figure 7-4 Idealised surface between void ratio, moisture content, and net stress (Gould 2011)

In the assumption of one-dimensional soil volume change, the change in soil volume can be considered as the change in soil height. The relationship of change in soil void ratio, e to soil moisture content, w , and net stress, σ can be represented by the following equation:

$$de = \left(\frac{\partial e}{\partial \sigma} \right)_w \cdot d\sigma + \left(\frac{\partial e}{\partial w} \right)_\sigma \cdot dw \quad \text{Equation 7 - 5}$$

Equation 7 – 5 can be rewritten in terms of soil strain, ε as Equation 7 – 6 by dividing $1 + e_0$,

$$d\varepsilon = \frac{1}{E_c} \cdot d\sigma - \alpha_\sigma \cdot dw \quad \text{Equation 7 - 6}$$

where

$$d\varepsilon = \frac{de}{1 + e_0} \quad \text{Equation 7 - 7}$$

$$\frac{1}{E_c} = - \frac{\left(\frac{\partial e}{\partial \sigma} \right)_\omega}{1 + e_0} \quad \text{Equation 7 - 8}$$

$$\alpha_\sigma = - \frac{\left(\frac{\partial e}{\partial \omega} \right)_\sigma}{1 + e_0} \quad \text{Equation 7 - 9}$$

e_0 is the initial void ratio, $d\varepsilon$ is the change in soil strain, $\frac{1}{E_c}$ is the one-dimensional soil constrained modulus at the state (σ, ω) and α_σ is the one-dimensional soil expansion coefficient at the state (σ, ω) .

Equation 7 - 6 can then be rewritten to Equation 7 - 2, so that the relationship of change in ω and/or σ to change in soil height in one-dimension can be obtained:

$$d\varepsilon = - \frac{dh}{dz} = \frac{1}{E_c} \cdot d\sigma - \alpha_\sigma \cdot d\omega \quad \text{Equation 7 - 10}$$

where dh is the change in height of a soil element and dz is the height of a soil element.

The change in soil height of the soil layer, Δh can be calculated as the integration over the total layer height of the soil. And by separating the terms of ω and σ resulting in:

$$\Delta h = - \int_0^H \frac{1}{E_c} \cdot d\sigma \cdot dz + \int_0^H \alpha_\sigma \cdot d\omega \cdot dz \quad \text{Equation 7 - 11}$$

$$\int_0^H \frac{1}{E_C} \cdot d\sigma \cdot dz = \underbrace{\int_0^H \alpha_\sigma \cdot d\omega \cdot dz}_{\Delta h_\omega} - \Delta h \quad \text{Equation 7 - 12}$$

In a simplified approximation, the change in soil height due to average change in soil moisture content, $\Delta\omega$ can be written as:

$$\text{Equation 7 - 13}$$

where α_σ is considered to be the average one-dimensional soil expansion coefficient over the layer.

According to Equation 7 – 12, the change in σ can be calculated when both Δh and Δh_ω is known. Therefore Equation 7 – 12 can be rewritten as:

$$\int_0^H \frac{1}{E_C} \cdot \Delta\sigma \cdot dz = \Delta h_\omega - \Delta h \quad \text{Equation 7 - 14}$$

Elastic soil foundation theory was used to account for the attenuation of stress imparted to the soil directly beneath the pipe as depth increases (Das 2007). Figure 7-5 shows a schematic diagram representing the attenuation of soil stress due to a point load beneath the pipe as depth increases. The solution of Equation 7 – 14 is obtained using the Steinbrenner (1934) solution for stress induced in an infinite layer due to a footing of known length and width:

$$\begin{aligned} \Delta h_\omega - \Delta h &= \Delta\sigma_p \left[4 \cdot \frac{D(1-\nu)}{2 E_C} \cdot I_S \cdot I_f \right] \\ &= \Delta\sigma_p \cdot \frac{1}{k_S} \end{aligned} \quad \text{Equation 7 - 15}$$

where Δh_ω is the free expansion of the pipe, Δh is the actual vertical pipe displacement, $\Delta\sigma_p$ is change in stress at pipe level, D is the pipe diameter, ν is the Poisson's ratio of soil (assumed to be 0.4), I_S is the shape factor (Steinbrenner 1934), I_f is the depth factor (Fox 1948) which accounts

for the attenuation of net stress beneath the pipe as depth increase, and k_s is the soil spring modulus.

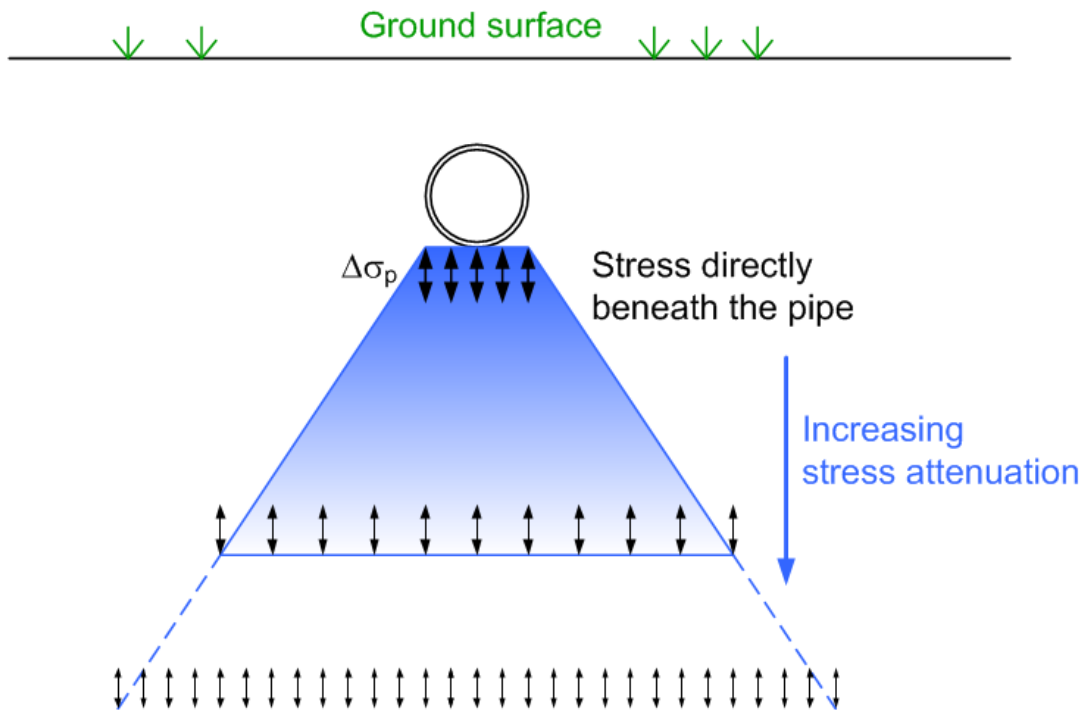


Figure 7-5 Schematic diagram of attenuation of stress with depth (after Gould 2011)

As shown in Equation 7 – 15, k_s can be calculated as:

$$k_s = \frac{E_c}{2.1 \cdot I_s} \tag{Equation 7 - 16}$$

where

$$I_s = F_1 + \frac{1 - 2\nu}{1 + \nu} \cdot E_c \tag{Equation 7 - 17}$$

$$F_1 = \frac{1}{\pi} (A_0 + A_1) \quad \text{Equation 7 - 18}$$

$$F_2 = \frac{n'}{2} t \quad \text{Equation 7 - 19}$$

$$A_0 = m' \cdot 1 \frac{(1 + \sqrt{m'^2 + 1}) \sqrt{m'^2 + n'^2}}{m' (1 + \sqrt{m'^2 + n'^2 + 1})} \quad \text{Equation 7 - 20}$$

$$A_1 = 1 \frac{(m' + \sqrt{m'^2 + 1}) \sqrt{1 + n'}}{m' + \sqrt{m'^2 + n'^2 + 1}} \quad \text{Equation 7 - 21}$$

$$A_2 = \frac{m'}{n' (\sqrt{m'^2 + n'^2 + 1})} \quad \text{Equation 7 - 22}$$

$$m' = \frac{L}{D} \quad \text{Equation 7 - 23}$$

$$n' = \frac{H}{\left(\frac{D}{2}\right)} \quad \text{Equation 7 - 24}$$

H is the total height of soil beneath the pipe and L is the distance between soil springs (i.e., length of the modelled pipe section).

The theoretical framework can be used to determine the deformation at the pipe level due to change in soil moisture content. Flexural stresses experienced by the pipe can be then be calculated on the basis of the pipe-soil interaction. Application of this framework for pipe stresses calculation is described in the following section.

7.4.3 Setup of pipe-soil interaction model

7.4.3.1 Description of model

The pipe-soil interaction model adopted for the calculation of flexural pipe stress from change in moisture content is based on the Winkler models. The modelling procedure is illustrated by the flowchart in Figure 7-6. Different magnitude of change in soil moisture content as obtained from the long term model prediction shown in Figure 7-3 was imposed in the model at each time step. Based on the theoretical framework described in the previous section, the change in soil height due to change in moisture content, Δh_w (soil shrink or swell) at each time step was determined and applied to the model incrementally. The change in soil stress corresponding to Δh_w is then determined.

Figure 7-7 illustrates the schematic diagram of the model. The buried pipe was modelled as a linear elastic beam with either fixed or pinned end supports at the interface of soils beneath nature strip and driveway in order to simulate the “driveway effect” described in Chapter 3. The use of two end support conditions was based on the studies of Chan (2008) and Gould (2011) that the end condition of buried pipes is in-between fixed and pinned end. Overburden soil load acting on the pipe was modelled as a uniformly distributed dead load. The soil springs were spread at a distance of 2 % of the total pipe length along the modelled pipe. Complete contact was assumed between the soil and pipe. The numerical model is intended only to predict the flexural stress developed in the pipe, while axial stress is assumed to remain constant due to change in soil volume.

The Winkler models were simulated using a finite element software package, OpenSEES developed by UC Regents. A Newton line search algorithm object was constructed in OpenSEES where a limiting ratio was specified to be check at each incremental update. The Newton-Raphson method with line search was used to advance to the next time step in the iterative solution until system equilibrium was reached. A fibre section with linear elastic material properties was used to represent the pipe in OpenSEES, and equilibrium was determined by input of α_σ , k_s , and h_w to the model. Determinations of these values are described in the following sections.

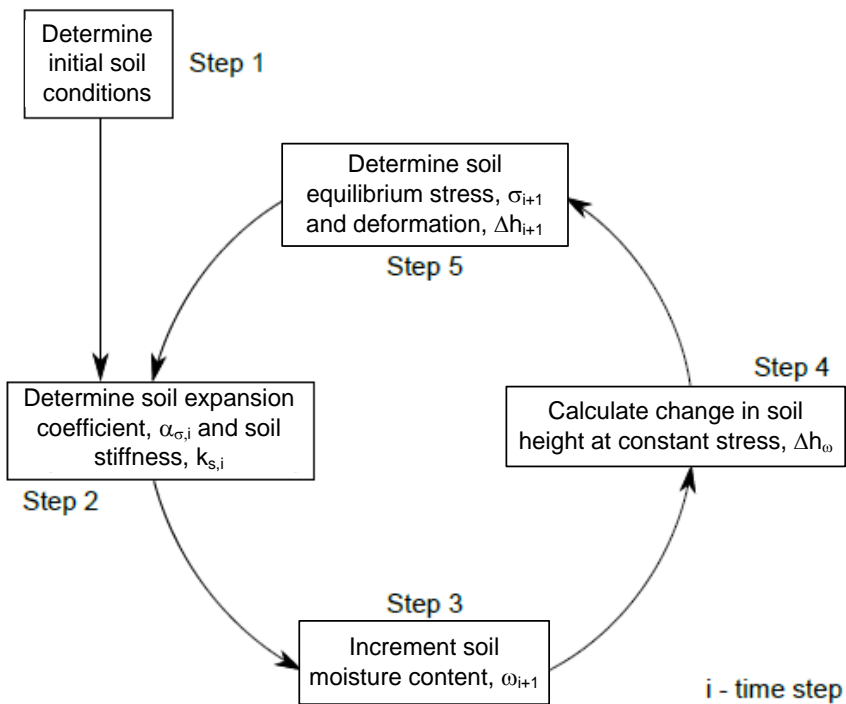


Figure 7-6 Flowchart of pipe-soil interaction modelling procedure (after Gould 2011)

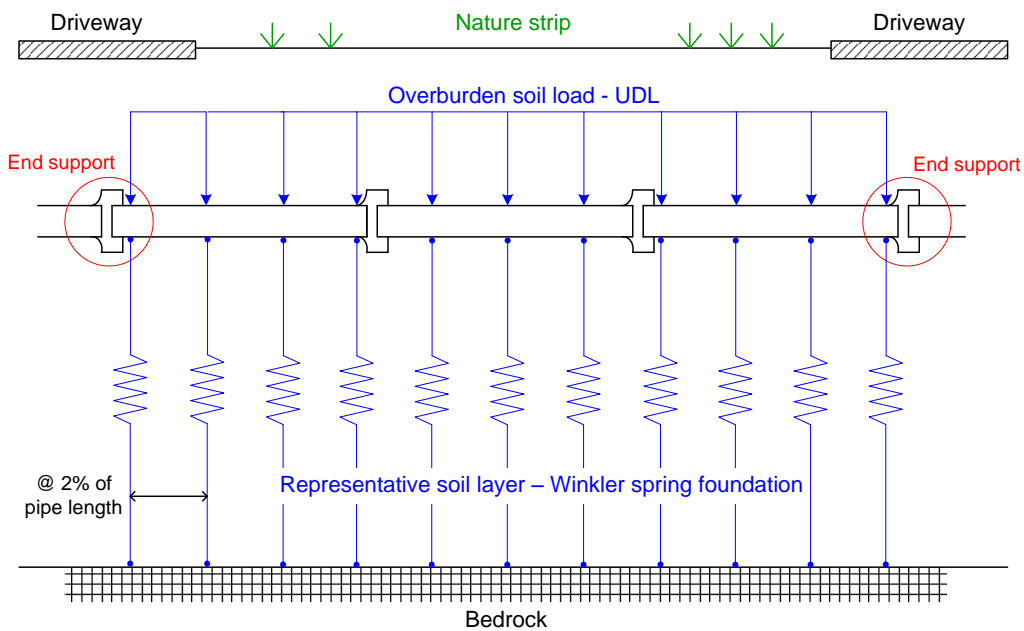


Figure 7-7 Schematic diagram of Winkler spring model

7.4.3.2 Determination of linear soil expansion coefficient, α_e

In an isotropic condition volume change of soil is assumed to be linearly relating to the change in soil moisture content to certain extent. The shrinkage of soil can then be represented by the shrinkage curve in a plot of void ratio versus moisture content. An ideal shrinkage curve is shown in Figure 7-8. For environmentally stabilised soils, the $e - \omega$ relationship does not display significant hysteresis; hence the relationship presented by the shrinkage curve is valid for both wetting and drying (swelling and shrinkage) conditions. The swelling and shrinkage of soil can be modelled as linearly proportional to the change in moisture content.

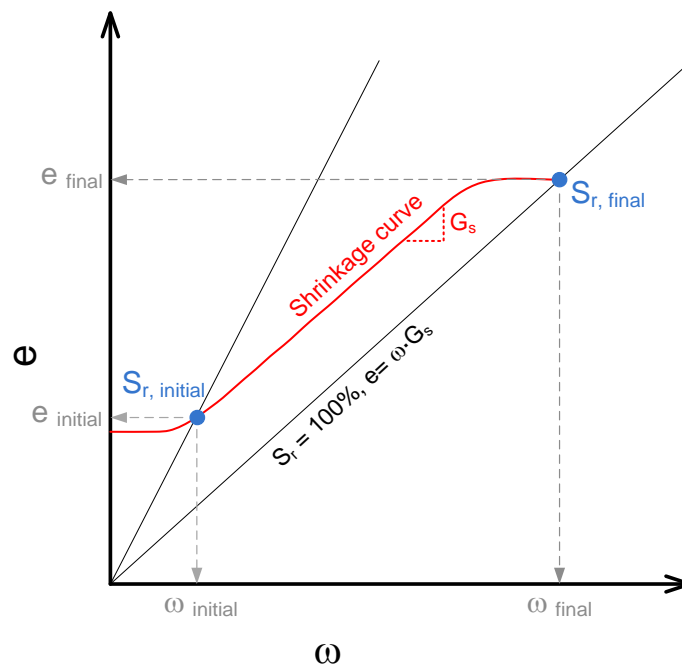


Figure 7-8 Plot of void ratio against moisture content

When soil is swelling, void ratio will increase from the initial state when degree of saturation is smaller than 1 ($S_r < 1$) to the final state ($S_r \approx 1$) as shown in Figure 7-8 by the two blue dots. The increase of volumetric soil strain, $\Delta \varepsilon_v$ can be calculated as following:

$$\Delta \varepsilon_v = \frac{\Delta e}{1 + e_0} = 3 \alpha \cdot \Delta a \quad \text{Equation 7 - 25}$$

where Δe is the change in void ratio, e_0 is the initial void ratio, α is the soil expansion coefficient and $\Delta \omega$ is the change in gravimetric moisture content.

Equation 7 – 25 can be rewritten in terms of Δe and $\Delta \omega$:

$$\frac{\Delta e}{\Delta \omega} = 3 \alpha \cdot (1 + e_0) \quad \text{Equation 7 - 26}$$

In this condition linear swelling of soil is assumed to be following the shrinkage curve, where at certain limit increase in moisture content will not have significant change in the void ratio. The gradient of the linear proportion of the shrinkage curve is represented by the gradient as:

$$\frac{\Delta e}{\Delta \omega} = G_s \quad \text{Equation 7 - 27}$$

where G_s is the specific gravity of soil.

The soil expansion coefficient, α is obtained by combining Equation 7 – 26 and 7 – 27:

$$\alpha = \frac{G_s}{3(1+e_0)} \quad \text{Equation 7 - 28}$$

α is considered as $\alpha_{\sigma,i}$ in the initial conditions of the numerical model. Under general condition, α_{σ} at other time steps is calculated by the following equation:

$$\alpha_{\sigma} = \frac{\left(\frac{\partial e}{\partial \omega}\right)_{\sigma}}{1 + e_0} \quad \text{Equation 7 - 29}$$

where $\left(\frac{\partial e}{\partial \omega}\right)_{\sigma}$ is obtained from the partial derivative of Equation 7 – 1 with respect to ω at each time step:

$$\left(\frac{\partial e}{\partial \omega}\right)_{\sigma} = -\frac{m}{\pi} \cdot \tan^{-1} \left(\phi \left(\omega - \left(\alpha_a \cdot \ln \left(1 + \frac{\sigma}{\sigma_0} \right) + a_0 \right) \right) \right) + \frac{m}{\pi} \cdot \tan^{-1} (\phi(\omega - b)) \quad \text{Equation 7 - 30}$$

However, unless the soil gets very wet or dry, α_{σ} will remain close to that given in Equation 7-28.

7.4.3.3 Determination of soil spring modulus, k_s

In the initial conditions, k_s is calculated by Equation 7 – 16. The one-dimensional soil constrained modulus, E_c is similar to elastic modulus of soil, E_s with the restriction that the soil does not deform perpendicular to the applied load. It can be calculated by the following equation:

$$E_c = \frac{E_s(1-\nu)}{(1+\nu)(1-2\nu)} \quad \text{Equation 7 - 31}$$

where ν is the Poisson's ratio of soils (assumed to be 0.4).

E_s is determined based on the correlation between soil's elastic modulus and moisture content in Altona North. This relationship was obtained from the oedometer test results presented in Chapter 4. The stress-strain relationship of the soil samples were used to determine the elastic modulus for the soil moisture contents close to the range observed from the long term moisture content prediction as described in Section 7.3 (i.e., $36 \% \leq \omega \leq 50 \%$).

In general, k_s in the Winkler models is divided into several layers with different moisture content and stress condition according to the soil profile on site. Each soil layer is represented by an

individual spring with the soil spring modulus, k_s , and a series of springs are combined to represent the soil at full depth. However, investigation on the change in k_s over the range of soil moisture content and net stresses found little change in k_s (Gould 2011). Therefore, the numerical model is simplified by calculating k_s at the initial conditions and then kept constant to represent the soil layer beneath the pipe at all time steps (Figure 7-9). The representative spring modulus, $k_{s,rep}$ is calculated by the following equation:

$$\frac{1}{k_{s,rep}} = \sum_{j=1}^n \frac{1}{k_{s,j}} \quad \text{Equation 7 - 32}$$

where n is the number of soil layers beneath the pipe and $k_{s,j}$ is the k_s at layer j .

7.4.3.4 Soil and pipe properties

The soil and pipe properties of Altona North site were inputted to the pipe-soil interaction model for calculation of pipe stresses. Table 7-1 shows the soil and pipe properties used in the model. α_σ and k_s were determined as described in the previous sections, and the pipe properties were obtained from the cast iron water pipe buried in Altona North.

The model analysis was preceded with the assumption that the soil in Altona North was environmentally stabilised since the ground had experienced many cycles of shrinkage and swelling. Furthermore, the analysis consider only the displacement of the soil due to moisture change with the assumption that shrinkage of soils would not cause downward dragging of the pipe. The creeping behaviour of soils was not considered.

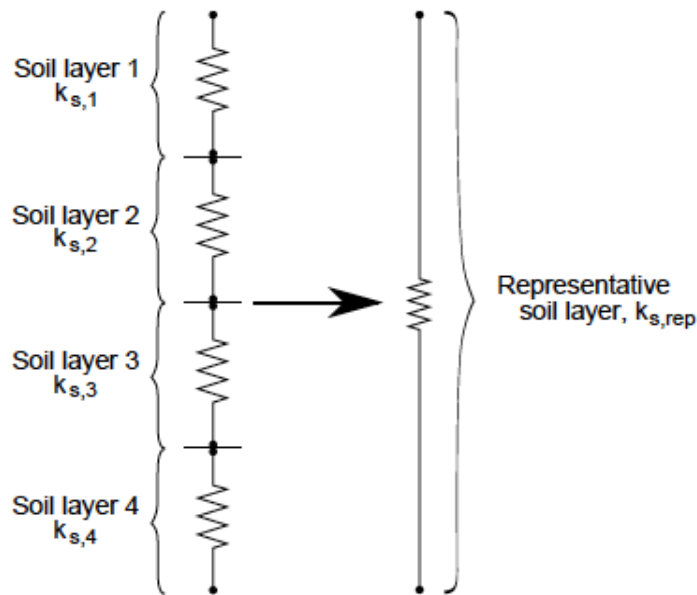


Figure 7-9 Simplified springs at all soil layers to the representative layer

Table 7-1 Soil and pipe properties used in the pipe-soil interaction model

α_σ	0.4 – 0.6
k_s	0.11 – 0.20
Cast iron pipe elastic modulus	150 GPa
Outer diameter	126 mm
Inner diameter	110 mm
Pipe length	20 m

7.4.4 Pipe-soil interaction modelling results

This section presents the results from the pipe-soil interaction models with change in soil moisture content from Figure 7-3 and different end support conditions. The changes in soil moisture content used in the model were increment and decrement of 0.5 %, 1 %, 5 %, and 10 % (i.e., cover the range of +6 % to -8 %). Figure 7-10 and Figure 7-11 shows the bending moment predicted by the model

for pinned end support and fixed end support conditions, respectively. For pinned end condition, maximum bending moment occurred at approximately one-third of the pipe length from the support when the soil shrunk, and approximately 6 % of the pipe length from the support when soil swelled. For fixed end condition, maximum bending moment always occurred at the end supports.

The maximum flexural pipe stresses resulted from the model due to change in soil moisture content are shown in Table 7-2. The average stresses of both end support conditions were also calculated as previously stated that buried pipe support condition in field was found to be in-between the two conditions. The average flexural stresses associated with different magnitude of change in soil moisture content is used for estimation of the pipe life described in next section.

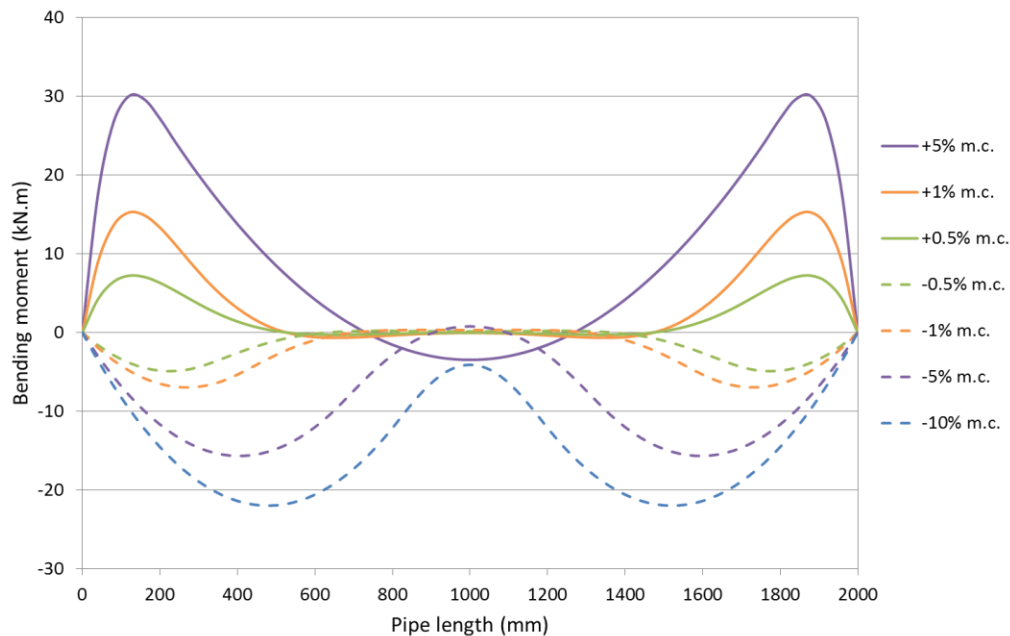


Figure 7-10 Model prediction for pinned end support conditions

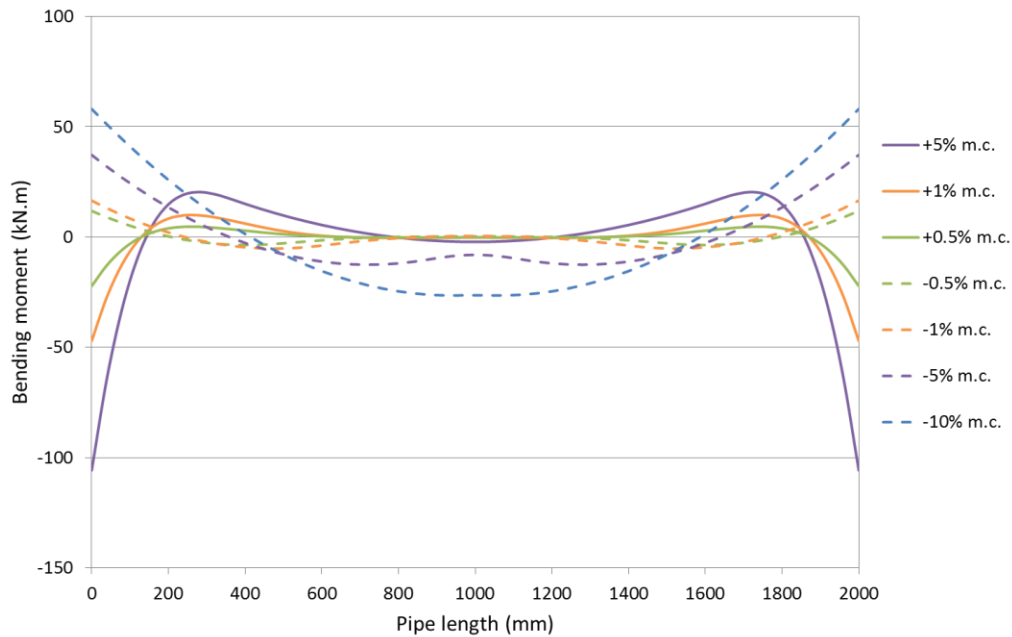


Figure 7-11 Model outputs of bending moment for fixed end support conditions

Table 7-2 Model outputs of maximum flexural stress

Change in moisture content (%)	Maximum flexural stress (MPa)		
	Pinned end	Fixed end	Average
+5	25.6	68.6	47.1
+1	11.6	35.7	23.7
+0.5	5.5	16.9	11.2
-0.5	3.7	9.0	6.4
-1	5.3	12.6	8.9
-5	11.9	28.3	20.1
-10	16.7	44.1	30.4

7.5 Estimation of Buried Pipe Life

7.5.1 Change in pipe stresses

The pipe-soil interaction model predicts the flexural pipe stress due to change in soil moisture content. The histogram of change in soil moisture content as shown in Figure 7-3 can then be converted to a histogram of flexural pipe stress by inputting the soil moisture content into the pipe-soil model. The pipe flexural stress predicted by the model corresponding to the change in soil moisture content in Figure 7-3 is plotted in the histogram as shown in Figure 7-12 from the average end support conditions. The frequency generally decreases with increases of pipe stress, which can be represented by a log-normal distribution curve. It is important to note that the flexural stresses resulted from soil shrinkage and swelling were grouped into the same bin in the histogram regardless of the direction of the stress (i.e., tension and compression) since pipe failure is considered as the applied stress exceeds the material strength of the pipe in the analysis, which can be caused by both tensile and compressive stresses.

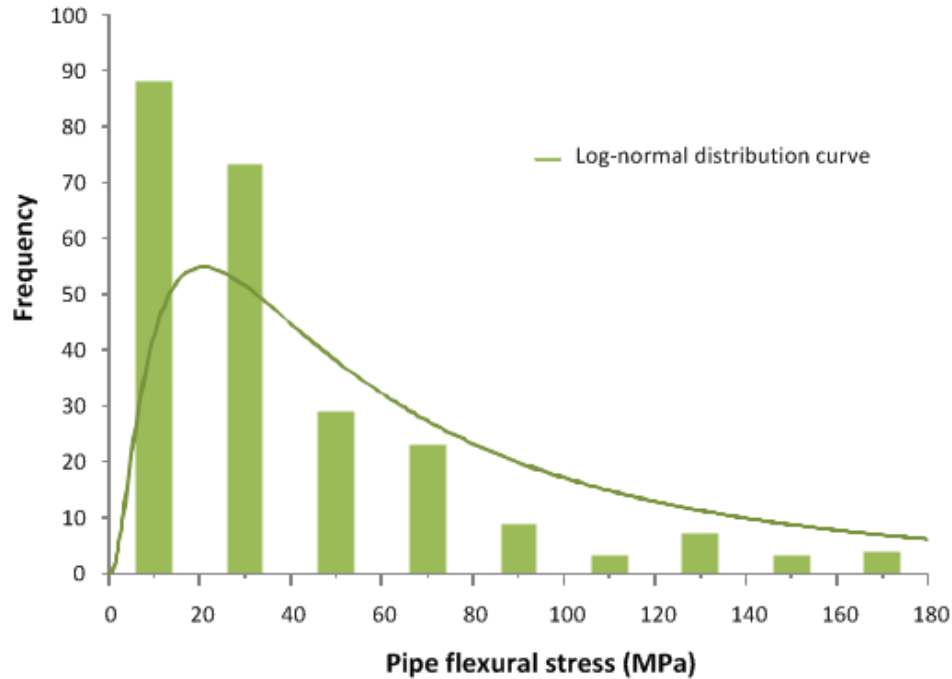


Figure 7-12 Pipe flexural stress with average support condition

7.5.2 Relationship between pipe strength and pipe failure

Pipe failure probability due to flexural stress can be obtained from the stress probability plot in Figure 7-12. For example, a cast iron pipe with tensile strength of 150 MPa will fail when the flexural stress exceeds this amount, so that the failure probability of the pipe can be calculated from the area under the log-normal curve in Figure 7-12 for pipe stress ≥ 150 MPa (i.e., integral of the log-normal curve). Figure 7-13 shows the relationship between failure probability of pipe under the average support condition and pipe strength. The pipe failure probability was presented to the maximum of 1, which means 100 % failure, when pipe strength becomes 0 MPa. Maximum pipe strength was considered to be 250 MPa, based on the maximum tensile strength of cast iron pipe from mechanical test results as described in Chapter 3. It is clear that probability of failure increases when strength of the pipe decreases.

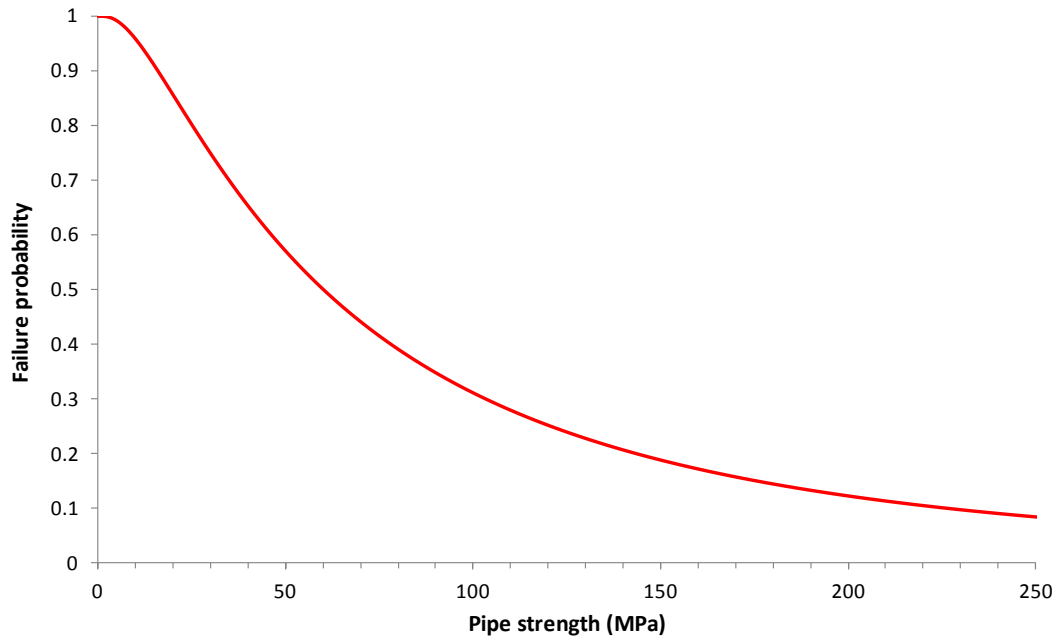


Figure 7-13 Correlation between pipe strength and pipe failure probability

7.5.3 Relationship between pipe strength and pipe age

Failures of buried pipes due to ageing are attributed to the deterioration of pipe structural capacity and increase of applied load. The deterioration of cast iron and other metallic pipes is predominantly as a result of electro-chemical corrosion (Makar 1999; Rajani and Kleiner 2001). In this study, the reduction of pipe strength is modelled on the basis of the growth of the graphitisation depth on the pipe wall. Rajani et al. (2000) proposed an exponential equation for nonlinear corrosion growth rate

P_{cr} :

$$P_{cr} = a + b \cdot c \cdot e^{-ct} \quad \text{Equation 7 - 33}$$

where t is the exposure time in year, constant a is corresponding to the minimum corrosion rate and $a + b \cdot c$ represents the maximum corrosion rate. Typical values of the constant, a , b and c

are shown in Table 7-3. Gould (2011) performed tensile testing with a total of 50 specimens machined from 12 cast iron pipe samples with age ranging from 34 to 123 years. The effect of graphitisation on tensile strength of pipe was showed in Figure 7-14, where the maximum graphitisation depth was measured on the fractured pipe surface. The correlation of tensile strength can be represented by the two equations in Figure 7-14 for spun cast and pit cast iron pipes.

In this study, the capacity of the modelled pipe was reduced with the corrosion growth rate calculated by Equation 7 – 28, where the graphitisation depth increase per year was substituted into the two equations in Figure 7-14. Reduction in tensile strength of the modelled pipe was then calculated according to the increase of pipe age. The pipe strength and age for both spun cast and pit cast iron pipes subjected to average and maximum corrosion rates are plotted in Figure 7-15. It is observed that under average corrosion rate, the strength of both types of pipe reduced to approximately 150 MPa in 300 years, while under maximum corrosion rate the strength of spun cast iron pipe reduced to 0 MPa in 150 years, and the strength of pit cast iron pipe reduced to 0 MPa in 250 years. The correlation between pipe strength and pipe age is used to obtain the relationship between pipe failure and pipe age as described in the following section.

Table 7-3 Typical constants for exponential corrosion equation (Rajani *et al.* 2000)

Corrosion rate (mm/year)	a (mm/year)	b (mm)	c (/year)
Average	0.0042	1.95	0.058
Maximum	0.0125	5.85	0.058

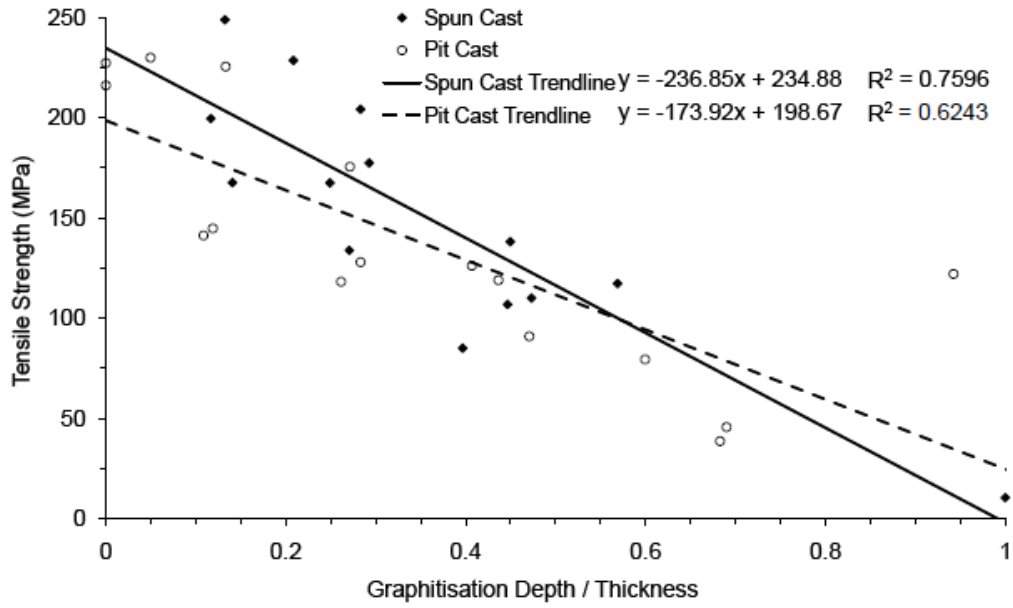


Figure 7-14 Correlation between graphitization depth to specimen thickness ratio and tensile strength (Gould *et al.* 2009)

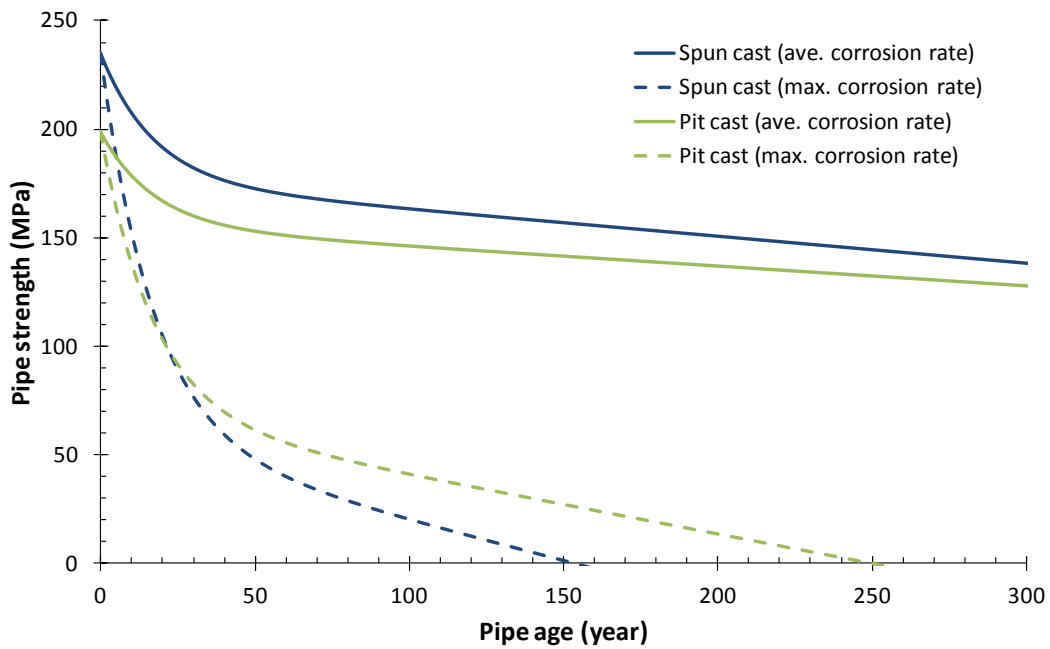


Figure 7-15 Correlation between pipe strength and pipe age

7.5.4 Relationship between pipe failure and pipe age

As noted previously, pipe failure occurs when the applied stress exceeds the pipe strength. Therefore when the relationship between pipe strength and pipe age, and the relationship between failure probability and pipe strength are known, the relationship between failure probability and pipe age can be obtained. Figure 7-16 shows the failure probability of both spun cast and pit cast iron pipes with age.

As expected the pipe failure probability was relatively low under average corrosion rate for both spun and pit cast iron pipes, as the failure probability is approximately 0.2 at the pipe age of 200 years. In the case of maximum corrosion rate the failure probability increase rapidly with pipe age in the first 50 years then became more gradual. The failure probability of spun cast iron pipes is 0.6 at the age of 50 years, and increase to 1 at the age of 140 years. The failure probability of pit cast iron pipes is 0.5 at the age of 50 years, and increase to 0.9 at the age of 200 years. These results can be used as a guide for estimation of the life of pipes buried in the Altona North area. This same approach can also be undertaken for pipes at other locations where the soil properties and climate data are available.

It is important to note that the estimated failure probability assumes the pipe is subjected to the soil movement due to variation in soil moisture content only. Since the pipe strength was continuously deteriorating when the pipe age increased, pipe failure could occurred earlier if the pipe subjected to extra loading (i.e., pressure transient, traffic loading, additional loading on ground surface etc.).

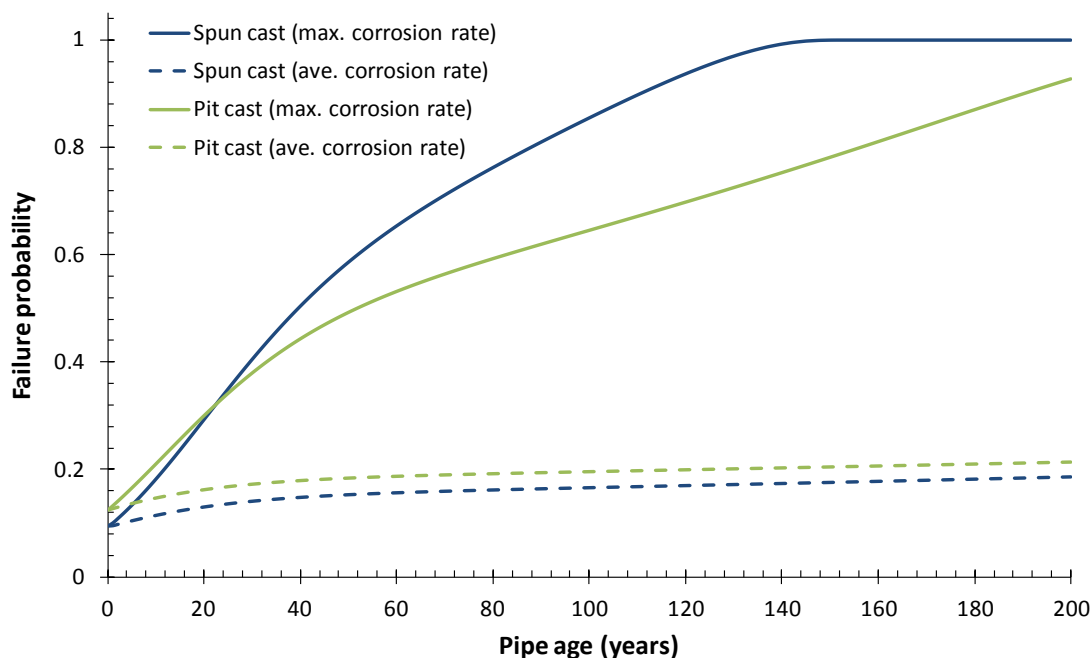


Figure 7-16 Correlation between pipe age and failure probability

7.6 Conclusions

The long term prediction of soil moisture content variation was presented in this chapter. The long term prediction model for the Altona North site was used for prediction of soil moisture variation corresponding to the extremely wet and dry climate events using random climate datasets. It was found that soil moisture could decrease by a maximum of 8 % and increase by a maximum of 6 % from the average value of 43 % at soil depth of 800 mm under extreme climate conditions.

The theoretical framework of numerically modelling of pipe-soil interaction was presented. A 2D Winkler models on the basis of the theoretical framework was used for simulation of the flexural pipe stress due to soil displacement as a result of change in soil moisture content. The model outputs were used to develop the stress probability and pipe failure probability curves. The relationship between pipe age and failure probability was obtained for spun cast and pit cast iron

pipes under average and maximum corrosion rates. This study provides a greater understanding of the behaviour of buried cast iron pipes due to variation of soil moisture content. The relationship between pipe age and failure probability can be obtained for other locations following the procedures described in this chapter.

CHAPTER 8

CONCLUSIONS AND RECOMMENDATIONS

8.1 Conclusions

The major aim of this research project was to extend current knowledge the interaction between pipes, soils and climate. The primary study area of the project was Melbourne, Australia where field instrumentations of in-service buried pipes were undertaken in the Western and North Western Melbourne. Long term monitoring of soil moisture content was also undertaken for 23 sites across the regional Melbourne. The collected field data were analysed for understanding of pipe-soil behaviour due to seasonal climate changes.

One-dimensional ground-atmosphere modelling was carried out on the basis of field data and site properties. Long term prediction of soil moisture content was undertaken using random climate data and the probability of change in soil moisture content was obtained. Deformation of buried pipes due to variation of soil moisture content was simulated using the Winkler spring models.

Relationship between pipe flexural stress, pipe strength and failure probability was developed, where pipe failure probability could be estimated by deterioration of pipe strength due to ageing. A summary of the conclusions drawn is presented as follows:

1. Analysis of the field data showed that changes in soil moisture content, suction and temperature were closely related to the seasonal climate variations and the depth of soils. At soil depth above 500 mm, immediate response to rainfall and temperature could be observed, and undergoes multiple wetting and drying cycles. At soil depth below 500 mm, response to the prevailing climate was slower with delays in temperature change and seasonal cyclic fluctuation of soil moisture content. The difference in soil temperature in summer and winter were approximately +2.5 to +3 °C per meter depth and -2.5 to -3 °C per meter depth. The responding time of soil moisture content to rainfall also increased with depth. In soils at depths of 800 mm and greater, the moisture content took two to three weeks to a month to respond to rainfall events.
2. Field measurement of soil moisture content and pipe stress analysis showed that swelling of soils due to increase of soil moisture content caused upward pipe bending, while shrinkage of soils due to decrease of soil moisture content caused downward pipe bending. In the horizontal direction, pipe bending was found to be toward the footpath when soils shrunk and toward the road when soils swelled. In general, pipe failure in Victoria, Australia was dominated by soil shrinkage where higher pipe failure rate was recorded in hot and dry summers. In this study, it was found that upward and downward bending of pipes in the vertical direction occurred corresponding to increase and decrease of soil moisture content, respectively. Maximum tensile and compressive flexural stresses measured during upward and downward bending of the pipe suggested that failure of pipes could occur in both extreme conditions. The reason of higher failure rates recorded in hot and dry summers might possibly due to shrinkage of soils occurred more quickly than swelling of soils which occurred gradually.

3. Monitoring of soil moisture content in regional Melbourne showed that variation of soil moisture content was primarily related to the geological formation of the site. The monitoring sites were divided into three categories of geological formations: basaltic clay, non-basaltic clay, and Quaternary alluvials and Tertiary sediments. While significant changes in soil moisture content were observed in the Quaternary sites due to larger particle size, the low reactive sandy soils would have small change in volume. By contrast, the basaltic and non-basaltic clay sites were more reactive and sensitive to moisture change. However due to relatively low hydraulic conductivity, the soil moisture content change at deeper depths could have a time lag of few weeks or more in comparison to shallower depths. Cyclic variations of soil moisture were also observed in deeper depths.
4. Based on the field climate data and soil properties, ground-atmosphere modelling of one-dimensional soil column of the field sites was performed using VADOSE/W. The models were validated against the field measurement and showed the capability of simulating the field soil conditions with reasonable accuracy. Long term prediction of soil moisture content was performed using 20 years climate data as input. Cyclic peaking of soil moisture content could be observed at 800 mm and deeper, where after the soil moisture content peaked at a significant wet period, then continuously depleted in the following years until the soil moisture content came to a minimum prior to another significant wetting period. This pattern of soil moisture content variation implied that the soils were drying most of the time and it might explain why soil shrinkage was the predominant ground movement considered to be responsible for pipe failures in Victoria.
5. Pipe-soil interaction was simulated by the Winkler spring models, and the maximum pipe flexural stresses as a result of change in soil volume due to change in soil moisture content were calculated. Relationship between pipe flexural stress, pipe strength and failure probability was developed. According to deterioration of pipe strength with age, the relationship between pipe failure probability and pipe age was developed. This relationship could also be developed at other location following the same procedure.

The overall interaction between pipe, soil and climate was investigated and presented in this thesis. The behaviour of in-service pipes buried in soils and the pipe bending mechanism due to seasonal variations of soil moisture content were described. The field data was used to develop numerical models that can predict the failure probability of pipes in order to provide generalisable information for implications for pipe repairs, maintenance or replacement.

8.2 Recommendations for Future Research

This research project focused on the field investigation and studied the pipe-soil-climate interaction with the development of numerical models and pipe failure probability. However, further research can be performed to extend the research in the following areas:

1. The pipe behaviour in the field was measured over years of relatively high rainfalls. The monitoring period could be extended to monitor years with hot and dry seasons, which is more typical of the Victoria climate, to study the response of the pipe due to continuous drying of soils.
2. Field measurements of soil moisture content in the regional Melbourne area were undertaken from February 2009 to October 2010. The measurement could be continued for a longer period of two to three years in order to capture multiple cycles of soil moisture variation between wet and dry years. The number of monitoring sites within each region (i.e., suburbs) could be increased to provide more data for analysis and cross-check the measurements. In addition, field measurements could be performed at shorter interval (e.g., on a fortnightly basis) to improve the understanding of moisture content variations within shorter period of time.
3. The soil moisture content and temperature of the two instrumentation sites were predicted by ground-atmosphere interaction model, which contain reactive basaltic clays. Similar predictions could be performed for sites with different geological formations (i.e., non-basaltic clay and Quaternary alluvials and Tertiary sediments) to predict the behaviour of

soils in these formations. The model predictions could also be used to develop the failure probability of pipes buried in these formations.

4. The pipe-soil interaction was simulated using the 2D Winkler spring models where the beam element was used to represent the pipe and the series of springs was used to represent the soil. The modelling results could be improved by adopting 3D continuum models which use continuous finite element or finite difference or boundary elements to represent both the soils and pipe. The use of 3D models could provide better representation of unsaturated soils with direct interaction of the soil particles with interconnected elements. The creeping behaviour and possible downward dragging of pipe during soil shrinkage could also be considered in the 3D models. Behaviour of the buried pipe and the corresponding stresses could then be studied in detail.
5. The study of pipe flexural stresses from the field data and the pipe-soil interaction models have not considered rotation of the joints between the pipe sections. The joints of the buried pipes, depends on the joint types, could rotate to certain degree of angles and therefore the pipe could resist greater bending. Laboratory experiments could also be set up to study the degrees of rotation and the strength of the joint connection to study the behaviour of different types of pipe joints and the distribution of stresses along the pipe sections under bending. These findings could be used to improve the pipe elements in the pipe-soil interaction models, which were considered as continuous linear elastic beams in this study.

REFERENCES

Adu-Wusu, C., Yanful, E. K., Lanteigne, L. and O'Kane, M. (2007). "Prediction of the water balance of two soil cover systems." *Geotechnical and Geological Engineering*, 25(2): 215-237.

Ahamed, M. and Melchers, R. E. (1994). "Reliability of underground pipelines subject to corrosion." *ASCE Journal of Transportation Engineering*, 120: 989-1003.

Andreou, S. A., Marks, D. H. and Clark, R. M. (1987). "A new methodology for modelling break failure patterns in deteriorating water distribution systems: Theory." *Advance in Water Resources*, 10: 2-10.

APIA (2011a). APIA Fact sheet 3- 2011, The Australian Pipeline Industry Association Ltd.: p.9.

APIA (2011b). APIA Fact sheet 6- 2011, The Australian Pipeline Industry Association Ltd.: p.9.

Ascher, H. and Feingold, H. (1984). "Repairable systems: Modelling, inference, misconceptions and their causes.", Marcel Dekker, New York.

ASTM International (2003). ASTM D 5298 - 03: Standard test methods for measurement of soil potential (suction) using filter paper PA, US, American Society for Testing and Materials.

ASTM International (2008). ASTM D 4546 – 08: Standard test method for one-dimensional swell or settlement potential of cohesive soils, American Society for Testing and Materials.

ASTM International (2011). ASTM D4829: Standard test methods for expansion index of soils, American Society for Testing and Materials.

Bahmanyar, H. G. and Edil, T. B. (1983). Cold weather effects on underground pipeline failures. *ASCE Conference on Pipelines in Adverse Environments*. New York: 579-593.

Baracos, A., Hurst, W. D. and Legget, R. F. (1955). "Effects of physical environment on cast iron pipe." *Journal of American Water Works Association*, 42: 1195-1206.

Barry-Macaulay, D., Bouazza, A. and Singh, R. M. (2011). Study of thermal properties of a basaltic clay. *Geo-Frontiers 2011: Advances in Geotechnical Engineering Dallas, TX, United states*: 480-487.

Barshad, I. (1955). "Adsorptive and swelling properties of clay-water system", *Proceeding of 1st National Conference on Clays and Clay Technology Oct 1966, California Department of National Resources, Division of Mines*.

Belcher, D. J., Cuykendall, T. R. and Sack, H. S. (1950). The measurement of soil moisture and density by neutron and gamma-ray scattering, *Civil Aeronautics Administration Technical Development, Report no. 127*.

Bell, J. P. and McCulloch, J. S. P. (1969). "Soil moisture estimation by the neutron method in Britain." *Journal of Hydrology*, 7: 425-433.

Birch, W. (2003). "Geology of Victoria", *Geological Society of Australia, Victoria, Australia*.

Bohnhoff, G. L., Ogorzale, A. S., Benson, C. H., Shackelford, C. D. and Apiwantragoon, P. (2009). "Field data and water-balance predictions for a monolithic cover in a semiarid climate." *Geotechnical and Geoenvironmental Engineering*, 135(3): 333-348.

Bouwer, H. (1966). "Rapid field measurement of air entry value and hydraulic conductivity of soil as significant parameters in flow system analysis." *Water Resources Research*, 2(4): 729-738.

Briaud, J.-L., Zhang, X. and Moon, S. (2003). "Shrink test - water content method for shrink and swell predictions." *Journal of Geotechnical and Geoenvironmental Engineering*, 129(7): 590-600.

Cameron, D. A. (1989). Test for reactivity and prediction of ground movement. *Civil Engineering Transactions, Institution of Engineers, Australia*. CE31: 121-132.

Cameron, D. A. and Walsh, P. F. (1984). "Damage to buildings on clay soils", Australian Council of National Trusts, Melbourne, Australia.

Carneiro, C. and De Jong, E. (1985). "In situ determination of the slope of the calibration curve of a neutron probe using a volumetric technique." *Soil Science*, 139: 250-254.

Chan, D. (2008). Performance of water and gas pipes buried in reactive soil. Department of Civil Engineering. Melbourne, Australia, Monash University. MEngSc thesis.

Chan, D., Kodikara, J. K., Gould, S., Ranjith, P., Choi, X. and Davis, P. (2007). Data analysis and laboratory investigation of the behaviour of pipes buried in reactive clay. *Common Ground, Proceedings of the 10th ANZ Conference on Geomechanics*. Ameratunge, J. e. a. Queensland, Australia. 2: 206-211.

Chan, D., Rajeev, P. and Kodikara, J. (2010a). Field Measurement of the Behaviour of an In-Service Water Reticulation Pipe Buried in Reactive Soil (Altona North, Vic) – Part 2, Monash University, Research Report, RR16, December 2010.

Chan, D., Rajeev, P., Kodikara, J. K. and Gallage, C. (2010b). "Regional field measurement of soil moisture content with neutron probe", 17SEAGC, 10th -13th May, Taipei, Taiwan.

Chanasyk, D. S. and Naeth, M. A. (1996). "Field measurement of soil moisture using neutron probe." *Canadian Journal of Soil Science* 76: 317–323.

Chu, T. Y. and Mou, C. H. (1973). "Volume change characteristics of expansive soils determined by controlled suction test", *Proceedings of 3rd International Conference on Expansive Soils*, Haifa.

Clark, C. M. (1971). "Expansive-soil effect on buried pipe." *Journal of American water works association*, 63: 424-427.

Clark, R. M., Stafford, C. L. and Goodrich, J. A. (1982). "Water distribution systems: A spatial and cost evaluation." *ASCE Journal of Water Resources Planning and Management Division*, 108(3): 243-256.

Clayton, C. R. I., Xu, M., Whiter, J. T., Ham, A. and Rust, M. (2010). "Stresses in cast-iron pipes due to seasonal shrink-swell of clay soils." *of the Institution of Civil Engineers: Water Management*, 163: 157-162.

Clifton, C., Reid, M. and Ockenden, P. (2000). "Managing dryland salinity with vegetation in North East Victoria - North east salinity strategy July 2000", Department of Natural Resources and Environment.

Constantine, A. G. and Darroch, J. (1993). *Stochastic Models in Engineering Technology and Management*, Australia-Japan Workshop on Stochastic Models in Engineering, Technology and Management, Osaki, S. and Murthy, D. N. P., Singapore: World Scientific: 86-95, 14-16 July.

Constantine, A. G., Darroch, J. and Miller, R. (1996). "Predicting underground pipe failure", Australian Water Works Association.

CPN-International (2000). "503DR Hydroprobe Moisture Gauge Operating Manual", CA, United States.

CSIRO (2010). Sustainable asset management fact sheet: Urban water research theme - Water for a healthy country flagship, CSIRO, National Research Flagships.

Daniel, D. E. (1989). "In situ hydraulic conductivity tests for compacted clay." *Journal of Geotechnical Engineering*, 115(9): 1205-1226.

Das, B. M. (1998). "Principles of Geotechnical Engineering", PWS Publishing Company, Boston, MA.

Das, B. M. (2007). "Principles of Foundation Engineering", Thomson, 6th Edition.

Davis, P., Burn, S., Moglia, M. and Gould, S. (2007). "A physical probabilistic model to predict failure rates in buried PVC pipelines." *Reliability Engineering & System Safety*, 92(9): 1258-1266.

Davis, P. and Burn, L. S. (2002). *Physical failure models for buried pipelines*, Highett, Australia, CSIRO Building Construction and Engineering.

Decagon Device Inc. (2009). "KD2 Pro compliance to ASTM and IEEE Standards - Application note", Pullman, WA, USA.

Delta-T (1999). "ThetaProbe soil moisture sensor user manual", Ltd., D.-T. D. (Ed.), Cambridge, England.

Dickey, G. L. (1990). Factors affecting neutron gauge calibration. In S.R. Harris (ed.) *Proceeding of National Conference of Irrigation and drainage*. Durango, CO, American Society of Civil Engineering, New York: 9–20.

Douglas, J. and Spencer-Jones, D. (1993). "Geological map of Victoria ", *Geology by Geological Survey of Victoria from 1 : 250 000 geological series*.

Dye, H. B. (2008). *Moisture movement through expansive soil and impact on performance of residential structures*. Arizona, USA, Arizona State University. PhD thesis.

Edlefsen, N. E. and Anderson, A. B. C. (1943). "Thermodynamics of soil moisture." *The Journal of Agricultural Science*, 15(2): 31-297.

Evet, S. R. and Steiner, J. L. (1995). "Precision of neutron scattering and capacitance type moisture gages based on field calibration." *Journal of Soil Science Society American*, 59: 961–968.

Fantozzi, M. (2000). "Acoustic Emission Technique the optimum solution for leakage detection and location on water pipelines", *15th World Conference on Nondestructive Testing*, 15th-21st October 2000, Roma, Italy.

Farouki, O. T. (1986). "Thermal properties of soils", Series on Rock and soil Mechanics Vol.11, Clausthal-Zellerfeld: Trans Tech Publications.

Fityus, S. G. (1999). "A soil moisture based method of estimating γ_s ." Australian Geomechanics, 34(3): 15-23.

Fleureau, J. M., Verbrugge, J. C., Huergo, P. J., Correia, A. G. and Kheirbek-Saoud, S. (2002). "Aspects of the behaviour of compacted clayey soils on drying and wetting paths." Canadian Geotechnical Journal, 39(6): 1341-1357.

Fox, E. N. (1948). The mean elastic settlement of a uniformly loaded area at a depth below the ground surface. 2nd International Conference on Soil Mechanics and Foundation Engineering. 1: 129-132.

Fredlund, D. G. (1996). "The emergence of unsaturated soil mechanics", A&M University Press, Texas, US.

Fredlund, D. G. and Morgenstern, N. R. (1977). "Stress state variables for unsaturated soils." ASCE Journal of Geotechnical Engineering, 103: 447-466.

Fredlund, D. G. and Rahardjo, H. (1993). "Soil mechanics for unsaturated soils", John Wiley & Sons, Inc., New York, USA.

Fredlund, D. G. and Xing, A. (1994). "Equations for the soil-water characteristic curve." Canadian Geotechnical Journal, 31: 521-532.

Fredlund, D. G., Xing, A. and Huang, S. (1994). "Predicting the permeability function for unsaturated soils using the soil-water characteristic curve." Canadian Geotechnical Journal, 31(3): 533-546.

Gallage, C., Gould, S., Chan, D. and Kodikara, J. (2008). Field measurement of the behaviour of an in-service water reticulation pipe buried in reactive soil (Altona North, VIC), Monash University, Research Report, RR10, October 2008.

Gallage, C., Gould, S., Chan, D. and Kodikara, J. (2009). Field measurement of the behaviour of an in-service gas reticulation pipe buried in reactive soil (Fawkner, VIC), Monash University, Research Report, RR13, February 2009.

GEO-SLOPE International (2010). "Vadose zone modeling with VADOSE/W 2007 - An Engineering Methodology Fourth Edition", GEO-SLOPE International Ltd, Alberta, Canada.

Geotechnical Systems Australia (2011). "Series 4000 - Displacement monitoring - Borehole." Retrieved 7th January, 2011, from <http://www.geotechsystems.com.au/products/4000bore.html#4000>.

Gould, S. (2011). A study of the failure of buried reticulation pipes in reactive soils. Civil Engineering. Melbourne, Monash University. PhD thesis.

Gould, S., Gallage, C., Chan, D. and Kodikara, J. K. (2009). Material Investigation of Failed Cast Iron Water Reticulation Main Pipe and Surrounding Soils (Melbourne, Australia), RR14.

Gould, S. and Kodikara, J. (2009). Exploratory Statistical Analysis of Gas Reticulation Main Failures (Melbourne, Australia), Monash University, Research Report, RR12, January 2009.

Gould, S. and Kodikara, J. K. (2008). Exploratory Statistical Analysis of Water Reticulation Main Failures, Technical report, Melbourne, Australia, Monash University, RR11, October 2008.

Gould, S., Kodikara, J. K., Rajeev, P., Zhao, X.-L. and Burn, S. (2011). "A void ratio – water content – net stress model for environmentally stabilized expansive soils." *Canadian Geotechnical Journal*, 48(6): 867-877.

Goulter, I. C., Davidson, L. and Jacobs, P. (1993). "Predicting watermain breakage rate." ASCE Journal of Water Resources Planning and Management Division, 119(4): 419-436.

Goulter, I. C. and Kazemi, A. (1988). "Spatial and temporal groupings of water main pipe breakage in Winnipeg." Canadian Journal of Civil Engineering, 15(1): 91-97.

Greacen, E. L. (1981). "Soil water assessment by the neutron method", East Melbourne, Victoria, Australia, CSIRO.

Greacen, E. L. and Schrale, G. (1976). "The effect of bulk density on neutron meter calibration." Australian Journal of Soil Research, 14: 159-169.

Grim, R. E. (1962). "Applied clay mineralogy", McGraw-Hill, New York, U.S.

Gustafson and Clancy (1999a). "Modelling the occurrence of breaks in cast iron water mains using methods of survival analysis", Proceedings of the AWWA Annual Conference, Chicago.

Gustafson and Clancy (1999b). "Using Monte-Carlo simulation to develop economic decision criteria for the replacement of cast iron water mains", Proceedings of the AWWA Annual Conference, Chicago.

Habibian, A. (1994). "Effects of temperature changes on water mainsbreaks." Journal of Transportation Engineering, ASCE, 120(2): 312-321.

Hertzler, P. C. and Davies, C. (1997). "The cost of infrastructure needs." Journal of American Water Works Association, 89: 55-61.

Herz, R. K. (1998). "Exploring rehabilitation needs and strategies for water distribution networks." Journal of Water SRT-Aqua, 47: 275-283.

Herz, R. K. (1996). "Ageing processes and rehabilitation needs of drinking water distribution networks." AQUA - Journal of Supply: Research and Technology, 45(5): 221-231.

Holtz, W. G. and Gibbs, H. J. (1956). "Engineering properties of expansive clays." *Transaction ASCE*, 121: p641-677.

Hu, Y. and Hubble, D. (2007). "Factors contributing to the failure of asbestos cement water mains." *Canadian Journal of Civil Engineering*, 34(5): 608-621.

Hu, Y., Rudaba, C. and Shahid, A. (2010). Behaviour of expansive soils at a water distribution pipe site. 63rd Canadian Geotechnical Conference & 1st Joint CGS/CNC-IPA Permafrost Specially Conference (GeoCalgary). Calgary, AB., Canada: 1426-1434.

Hu, Y. and Vu, H. Q. (2006). "Field performance of water mains buried in expansive soil", 1st International Structural Specialty Conference, May 23-26, Calgary, Alberta.

Hu, Y. and Vu, H. Q. (2011). "Analysis of soil conditions and pipe behaviour at a field site." *Canadian Geotechnical Journal*, 48(6): 847-866.

Hu, Y., Vu, H. Q. and Kaveh, L. (2008). "Instrumentation of a section of AC pipe in expansive soil", *ASCE International Pipelines Conference 2008*, 22-24 July, 2008, Atlanta, GA., US.

IAEA (1970). "Neutron Moisture Gauges", INTERNATIONAL ATOMIC ENERGY AGENCY (IAEA), Vienna.

Ibrahimi, F. (2005). Seasonal Variations in Water Main Breaks Due to Climate Variability and Ground movement. *Proceedings of the Australian Water (Ozwater) Conference*. Brisbane, Australia, Australian Water Association: 28-35.

ICT International (2007). "Soil Science Instrumentation", Australia.

Jarrett, R., Hussain, O., Veevers, A. and Van der Touw, J. (2001a). A review of asset management models available for water pipeline networks. *Proceedings of International Conference of Maintenance Societies (ICOMS)*. Melbourne, Australia: 49-57.

Jarrett, R., Hussain, O., Veevers, A. and Van der Touw, J. (2001b). "Predictive models for pipeline failures and identification of pipes for replacement", Pipeline Asset Planning & Operations Workshop, Melbourne, Australia.

Jeon, S. S., O'Rourke, T. D. and Neravali, A. N. (2004). "Repetitive loading effects on cast iron pipelines with cast-in-place pipe lining systems." *Journal of Transportation Engineering*, 130(6): 692-705.

Johansen, O. (1975). *Thermal conductivity of soils*, University of Trondheim, Norway. PhD thesis: 236.

Johnston, G. H., Ladanyi, B., Morgenstern, N. R. and Penner, E. (1981). "Engineering characteristics of frozen and thawing soils", In *Permafrost: Engineering design and construction*, G. H. Johnston (Ed.), Toronto : Wiley: 73–147.

Karaa, F. D. and Marks, D. H. (1990). "Performance of water distribution networks: Integrated approach." *Journal of performance of constructed facilities*, 4(1): 51-67.

Kassiff, G. and Holland, J. E. (1965). "The behaviour of pipes buried in expansive clays Part III: Field study of bedding of asbestos-cement pipes in Dooen clays", State Rivers and Water Supply Commission, Melbourne.

Kassiff, G. and Holland, J. E. (1966). "The expansive properties of dooen clays as applied to buried pipes." *Institution of Engineers, Australia -- Civil Engineering Transactions*, v CE 8(n 2): 133 - 142.

Kassiff, G. and Zeitlen, J. G. (1962). "Behaviour of pipes buried in expansive clays." *Journal of Soil Mechanics and Foundations division, Proceedings of the American Society of Civil Engineers*, 88(SM 2): 132-148.

Keen, B. A. and Raczkowski, H. J. (1921). "The relation between the clay content and certain physical properties of a soil." *The Journal of Agricultural Science*, 11: 441-449.

Kettler, A. J. and Goulter, I. C. (1985). "An analysis of pipe breakage in urban water distribution networks." *Canadian Journal of Civil Engineering*, 12: 286-293.

Kiefner, J. F. and Vieth, P. H. (1989). Project PR-3-805: A modified criterion for evaluating the remaining strength of corroded pipe, Pipeline Corrosion Supervisory Committee of the Pipeline Research Committee of the American Gas Association.

Kleiner, Y. and Rajani, B. (2001). "Comprehensive review of structural deterioration of water mains: statistical models." *Urban Water*, 3(3): 131-150.

Kleiner, Y. and Rajani, B. (2002). "Forecasting variations and trends in water-main breaks." *Journal of infrastructure systems*, December: p122-131.

Kodikara, J. (2012). "New framework for volumetric constitutive behaviour of compacted unsaturated soils." *Canadian Geotechnical Journal*, 49(11): 1227-1243.

Kodikara, J. K. and Rahman, F. (2002). "Effects of specimen consolidation on the laboratory hydraulic conductivity measurement." *Canadian Geotechnical Journal*, 39(4): 908-923.

Kuraoka, S., Rajani, B. and Zhan, C. (1996a). "Pip soil interaction analysis of field tests of buried PVC pipe." *Journal of infrastructure systems*, December: p162-170.

Kuraoka, S., Rajani, B. and Zhan, C. (1996b). "Pipe soil interaction analysis of field tests of buried PVC pipe." *Journal of infrastructure systems*, December: p162-170.

Ladd, C. C. (1960). "Mechanisms of swelling by compacted clays." *Highway Research Board Bulletin*, 245: p. 10-26.

Lee, K. Y. (2004). Cementitious stabilisation of scoria for pavement construction. Department of Civil Engineering. Melbourne, Monash University. MEngSc thesis: p179-185.

Leong, E. C., He, L. and Rahardjo, H. (2002). "Factors affecting the filter paper method for total and matric suction measurements." *Geotechnical testing journal*, 25(3): 322-333.

Li, J., Smith, D., Fityus, S. and Sheng, D. (2003). "Numerical Analysis of Neutron Moisture Probe Measurements." *International Journal of Geomechanics*, 3: 11-20.

Liu, S., Li, L., Cui, J. and Li, T. (2000). "Acoustic Emission Detection of Underground Pipeline Leakage", 15th World Conference on Nondestructive Testing, 15th-21st October 2000, Roma, Italy.

Lochbaum, B. S. (1993). "PSE&G develop models to predict main breaks." *Pipeline and gas journal*, 220: p.20-27.

Lowe, P. R. (1977). "An approximating polynomial for the computation of saturation vapour pressure." *Journal of Applied Meteorology*, 16(1): 100-103.

Makar, J. (1999). *Failure Analysis for Grey Cast Iron Water Pipes*. AWWA Distribution System Symposium. Reno, Nevada.

Marks, H. D., Andreou, S. A., Jeffrey, L. A., Park, C. and Zaslavski, A. (1987). *Statistical models for water main failures*, Boston, MA, US Environmental Protection Agency (Co-operative Agreement CR8 1 0558) M.I.T. Office of Sponsored Projects No. 94211.

Miller, R. B. (1993). "Personal communications", CSIRO Division of Mathematics and Statistics, Glen Osmond, Australia.

Mordak, J. and Wheeler, J. (1988). *Deterioration of asbestos cement water mains*. Final report to the Department of the Environment. Water research centre, Wiltshire, UK.

Morris, R. E. (1967). "Principal causes and remedies of water main breaks." *Journal of American water works association*, 54: 782-798.

Moser, A. P. (2001). "Buried pipe design", McGraw-Hill Companies Inc., Utah, USA.

Needham, D. and Howe, M. (1981). "Why gas main fail. Part 1." Pipe line industry, 55: p.47-50.

Nelson, J. D., Reichler, D. K. and Cumbers, J. M. (2006). "Parameters for heave prediction by oedometer tests", Proceedings of the 4th International Conference on Unsaturated Soils, Arizona.

Newport, R. (1981). "Factors influencing the occurrence of bursts in iron water mains." Water Supply and Management, 3: 274-278.

O'Day, K. D. (1982). "Organizing and analysing leak and break data for making main replacement decisions." Journal of American Water Work Association, 74(11): 589-594.

Pandey, M. D. (1998). "Probabilistic models for condition assessment of oil and gas pipeline." NDT & E International, 31(5): 349-358.

Puppala, A. J., Wejrungsikul, T., Puljan, V. and Manosuthikij, T. (2012). "Measurements of shrinkage induced pressure (SIP) in unsaturated expansive clays." Geotechnical Engineering Journal of the SEAGS & AGSSEA, 43(1): 40-47.

Rajani, B. and Kleiner, Y. (2001). "Comprehensive review of structural deterioration of water mains: physically based models." Urban Water, 3(3): 151-164.

Rajani, B., Makar, J., McDonald, S. E., Zhan, C., Kuraoka, S., Jen, C. and Viens, M. (2000). "Investigation of grey cast iron water mains to develop a methodology for estimating service life", AWWARF, Denver, CO.

Rajani, B. and Tesfamariam, S. (2004). "Uncoupled axial, flexural, and circumferential pipe-soil interaction analyses of partially supported jointed water mains." Canadian Geotechnical Journal, 41(6): pp. 997-1010.

Rajani, B. and Tesfamariam, S. (2007). "Estimating time to failure of cast-iron water mains." Proceedings of the Institution of Civil Engineers Water Management, 160(WM2): 83-88.

Rajani, B., Zhan, C. and Kuraoka, S. (1996). "Pipe-soil interaction analysis of jointed water mains." *Canadian Geotechnical Journal*, 33(3): p. 393-404.

Rajeev, P., Chan, D. and Kodikara, J. K. (2010). *Field Measurement of Soil Moisture Content with Neutron Moisture Probe*, Monash University, Research Report, RR15, December 2010.

Rajeev, P. and Kodikara, J. K. (2011). "Numerical analysis of an experimental pipe buried in swelling soil." *Computers and Geotechnics*, 38(7): 897-904.

Rao, S. M., Ed. (2006). "Identification and classification of expansive soils". *Expansive soils, Recent advances in characterization and treatment*. London, UK, Taylor & Francis Group.

Rawls, W. J. and Asmussen, L. E. (1973). "Neutron probe field calibration for soils in the Georgia coastal plain." *Soil Science*, 116: 262-265.

Ring, G. W. (1965). "Shrink-swell potential of soils", 44th Annual Meeting of the Highway Research Board, Jan 1965, Washington, D.C.

Rixon, C. H. (1973). *Geological Map of Victoria*, Geological Survey of Victoria.

Rossum, J. R. (1969). "Prediction of pitting rates in ferrous metals from soil parameters." *Journal AWWA*, 61(6): 305-310.

Rowe, R. (2001). "Geotechnical and geoenvironmental engineering handbook ", Kluwer Academic, Boston, US.

Sargand, S., Masada, T., Tarawneh, B. and Gruver, D. (2008). "Deeply buried thermoplastic pipe field performance over five years." *Journal of Geotechnical and Geoenvironmental Engineering*(August): 1181-1191.

Schmugge, T. J., Jackson, T. J. and McKim, H. L. (1980). "Survey of methods for soil moisture determination." *Water Resources Research*, 16(16): 961-979.

Seddon, K. D. (1992). Reactive soils. Engineering Geology of Melbourne. Peck, W. A., Neilson, J. L., Olds, R. J. and Seddon, K. D. Rotterdam, A. A. Balkema Publishers: 33-37.

Seed, H. B., Mitchell, J. K. and Chan, C. K. (1962a). "Studies of swell and swell pressure characteristics of compacted clays." Highway Research Board Bulletin, 313: p.12-39.

Seed, H. B., Woodard, R. J. and Lundgren, R. (1962b). "Prediction of swelling potential for compacted clays." Journal of soil mechanics and foundation division ASCE, 88: p.53-87.

Shamir, U. and Howard, C. D. D. (1979). "An analytical approach to scheduling pipe replacement." Journal AWWA, 71(5): 248-258.

Siemens AG (2011). "SITRANS P ZD Pressure transmitter." Retrieved 7th January, 2011, from <http://www.automation.siemens.com/w1/automation-technology-sitrans-p-zd-18608.htm>.

Silvestri, V., Sarkis, G., Bekkouche, N., Soulie, M. and Tabib, C. (1991). "Laboratory and field calibration of a neutron depth moisture gauge for use in high water content soils." Geotechnical Testing Journal 14(1): 64–70.

Standards Australia (1993). "AS1726 Geotechnical site investigations", Homebush, NSW, Australia.

Standards Australia (1996). "AS2870 Residential slabs and footings", Sydney, Australia.

Standards Australia (2001). "AS 1289.1.1 Preparation of disturbed soil samples for testing ", Sydney, Australia.

Standards Australia (2003). "AS1289.3.6.3 Determination of the particle size distribution of a soil - Standard method of fine analysis using a hydrometer", Sydney, Australia.

Standards Australia (2005). "AS1289.2.1.1 Determination of the moisture content of a soil – Oven drying method", Sydney, Australia.

Standards Australia (2008). "AS1289.3.4.1 Determination of linear shrinkage of a soil", Sydney, Australia.

Standards Australia (2009a). "AS1289.3.1.1 Determination of the liquid limit of a soil – Four point Casagrande method", Sydney, Australia.

Standards Australia (2009b). "AS1289.3.2.1 Determination of the plastic limit of a soil", Sydney, Australia.

Standards Australia (2011). "AS2870 Residential slabs and footings", Sydney, Australia.

Steinbrenner, W. (1934). "Tafeln zur setzungsberechnung." *Die Strasse*, 1: 121-124.

Stone, J. F. (1990). Neutron physics considerations in moisture probe design. *Proceeding National Conference ASCE Irrigation and Drainage Division ASCE*. New York: 1–8.

Taylor, S. and Ashcroft, G. (1972). "Physical edaphology", Freeman and Co., San Francisco, CA.

Terzaghi, K. (1931). "The influence of elasticity and permeability on swelling of two-phase systems." *Colloid Chemistry*, 3: p. 65-88.

Trautwein, S. J. and Boutwell, G. P. (1994). "In situ hydraulic conductivity tests for compacted soil liners and caps", *Hydraulic Conductivity and Waste Contaminant Transport in Soil*, ASTM STP 1142, Daniel, D. E. and Trautwein, S. J. (Ed.), Philadelphia, US, American Society for Testing and Materials.

Trewin, B. and Jones, D. (2004). "Notable Recent Rainfall Anomalies in Australia", 16th Australia New Zealand Climate Forum, 8-10 November, Lorne.

Tripathy, S., Rao, K. S. S. and Fredlund, D. G. (2002). "Water content-void ratio swell-shrink paths of compacted expansive soils." *Canadian Geotechnical Journal*, 39(4): 938-959.

Vachaud, G., Royer, J. M. and Cooper, J. D. (1977). "Comparison of methods of calibration of a neutron probe by gravimetry or neutroncapture model." *Journal of Hydrology* 34: 343–356.

van Genuchten, M. T. (1980). "A closed-form equation for predicting the hydraulic conductivity of unsaturated soils." *Soil Science Society of America Journal*, 44(5): 892-898.

Walski, T. M. and Pelliccia, A. (1982). "Economic analysis of water main breaks." *Journal AWWA*, 74(3): 140-147.

Watkins, R. K. and Spangler, M. G. (1958). "Some characteristics of the modulus of passive resistance of soil - a study similitude." *Highway Research Board Proceedings*, 37: 576-583.

Wilson, G. W. (1990). Soil evaporation fluxes for geotechnical engineering problems. University of Saskatchewan, Saskatchewan, Canada. PhD thesis.

Wilson, G. W., Fredlund, D. G. and Barbour, S. L. (1994). "Coupled soilatmosphere modelling for soil evaporation." *Canadian Geotechnical Journal*, 31(2): 151-161.

Winterkorn, H. and Bayer, L. D. (1934). "Sorption of liquids by soil colloids: I. Liquid intake and swelling by soil colloidal materials." *Soil Science*, 38: 291-298.

WSAA (2010a). Annual report 2009-2010, Water Services Association of Australia Ltd: p.9.

WSAA (2010b). WSAA Report Card 2009/10, Water Services Association of Australia Ltd: p.9.

Young, O. C. and Trott, J. J. (1997). "Buried rigid pipe", Elsevier Applied Science Publishers, London.

Zapata, C. E. (1999). Uncertainty in soil-water-characteristic curve and impacts on unsaturated shear strength predictions. Arizona, USA, Arizona State University. PhD thesis.

Zapata, C. E., Houston, S. L., Houston, W. N. and Dye, H. (2006). "Expansion index and its relationship with other index properties", The fourth international conference on unsaturated soils, Arizona.

Zhang, T. Q. and Shao, W. Y. (2000). "Numerical analysis of buried pipe characteristics." Journal of Zhejiang University, 1(2): 144-147.

APPENDIX A

PLOT OF SOIL PRESSURE

The plot of soil pressure and volumetric moisture content versus time in Pit 3 of Fawkner includes the erratic measurements recorded by EPC 6.

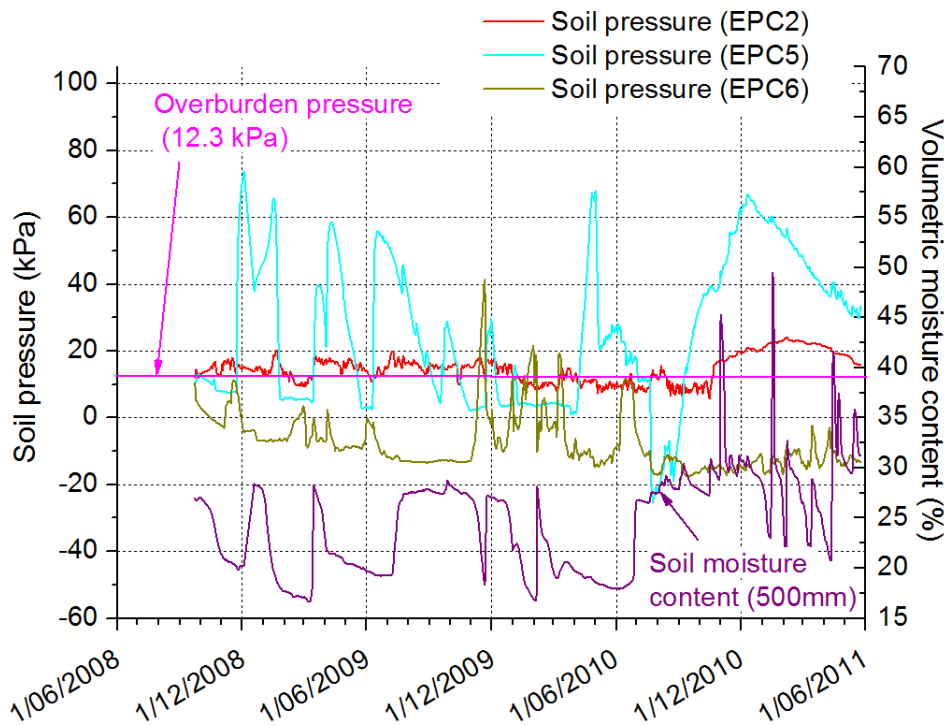


Figure A- 1 Soil pressure and volumetric moisture content versus time in Pit 2 of Fawkner

APPENDIX B

PLOTS OF PIPE STRAINS

The sign convention for the strain plots is positive for tension and negative for compression.

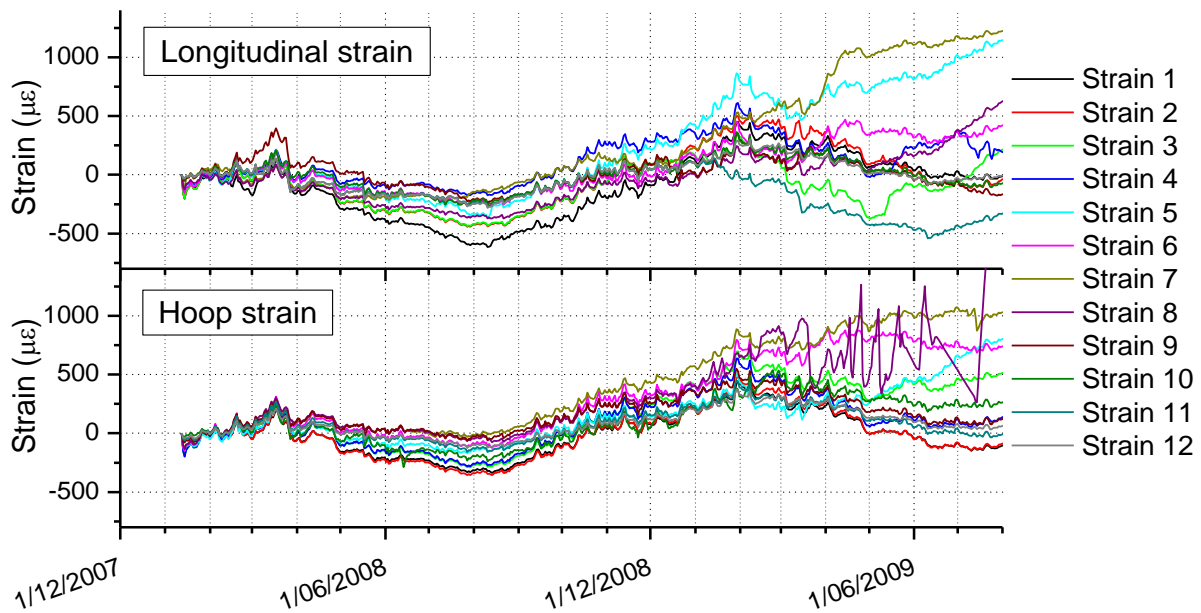


Figure B- 2 Longitudinal and hoop strains of water pipe

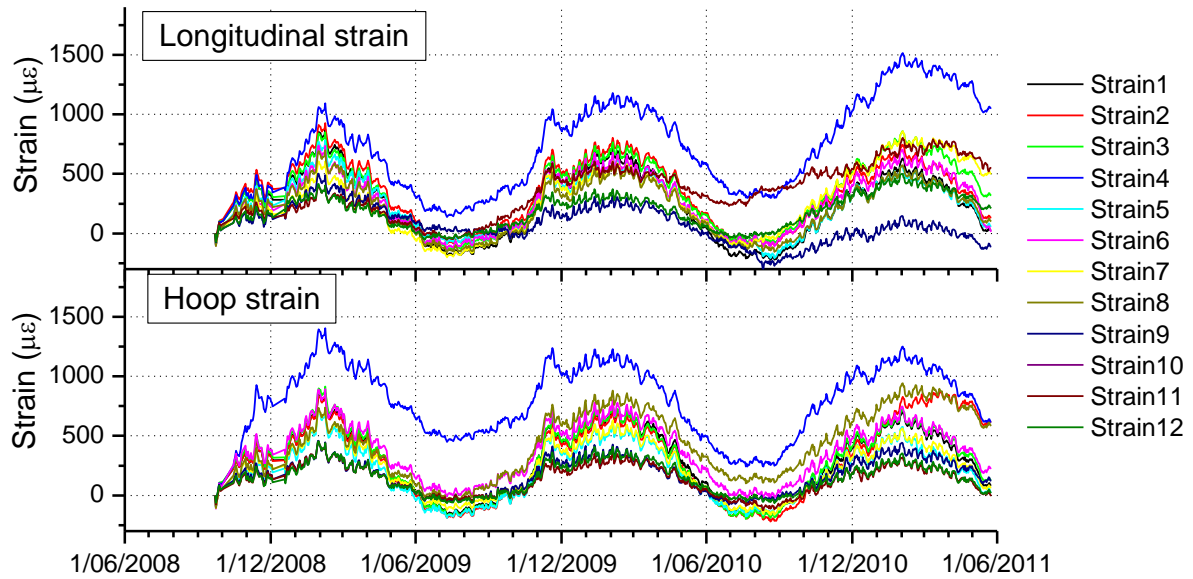


Figure B- 3 Longitudinal and hoop strains of gas pipe

APPENDIX C

LABORATORY STRAIN GAUGES TEST

The measured apparent thermal expansion coefficient, α' , used for pipe stress calculation is dependent on the type of the strain gauge. In order to obtain the apparent thermal expansion coefficient of the cast iron pipe a laboratory test was undertaken using the same type of biaxial strain gauge used in the Altona North instrumentation site. The strain gauges were attached to a cast iron water pipe section collected during the forensic investigations. The pipe section was then placed in an oven and subjected to temperature change. The measured apparent thermal expansion coefficient, α' , was calculated as the average of the gradients from the longitudinal strain against temperature and circumferential strain against temperature plots (Figure C- 1 and Figure C- 2). The average apparent thermal expansion coefficient was calculated as $40 \times 10^{-6}/^{\circ}\text{C}$.

The Poisson's ratio, ν , of the cast iron pipe was obtained from a pipe loading test. Biaxial strain gauges were installed in a two meter cast iron water pipe collected during the forensic investigations. The pipe was tested in a three points bending load test as shown in Figure C- 3. The Poisson's ratio was calculated from the longitudinal and hoop strains measured on the tension surface of the pipe. Figure C- 4 and Figure C- 5 show the plot of strains on two gauges. The average Poisson's ratio was found to be 0.21, which was similar to the nominal value of cast iron.

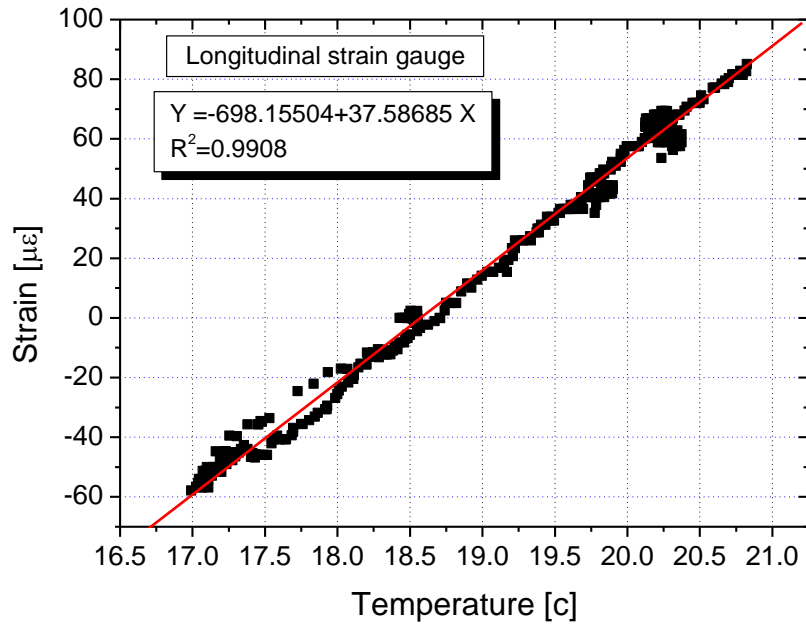


Figure C- 1 Longitudinal strain against temperature change

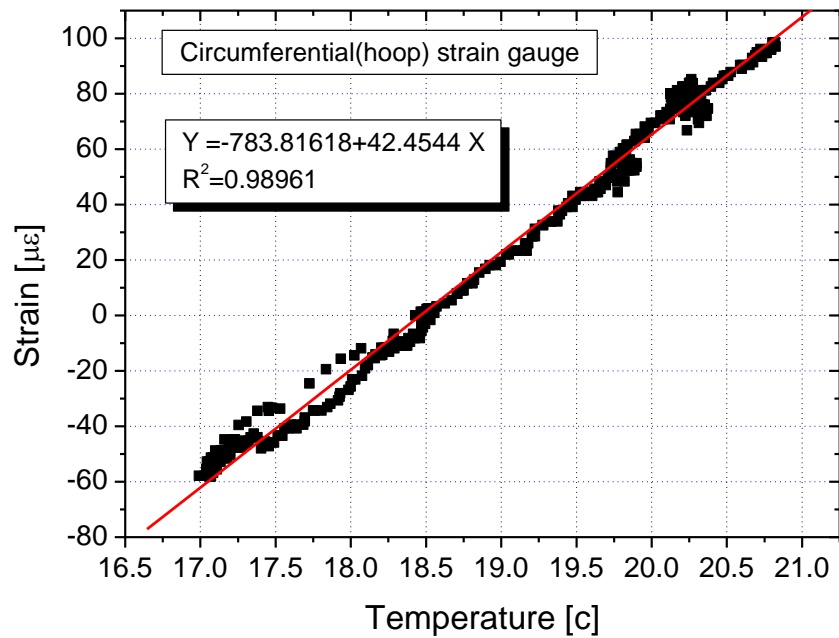


Figure C- 2 Hoop strain against temperature change



Figure C- 3 Three points bending test of the water pipe

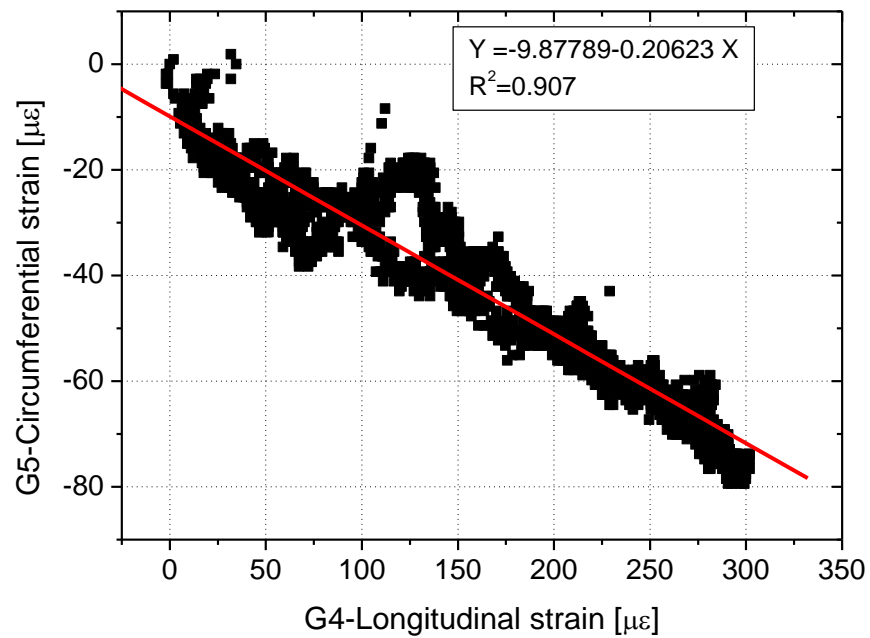


Figure C- 4 Hoop strain against longitudinal strain at Gauge 1

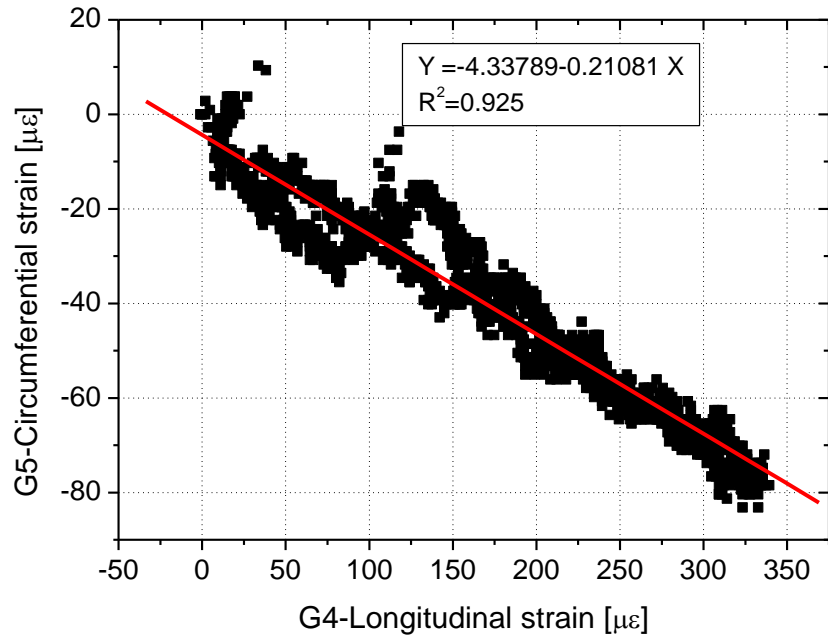


Figure C- 5 Hoop strain against longitudinal strain at Gauge 2

APPENDIX D

THERMAL EXPANSION OF THE DUMMY PIPE

The dummy pipe buried at the Fawkner instrumentation site was used to monitor the effects of temperature on strain measurements. Figure D- 1 shows the measured strain and temperature on the dummy pipe during the observation period of October 2008 to February 2009. The magnitude of longitudinal expansion of the dummy pipe was same as the circumferential expansion, and the pipe temperature was increased by approximately 11 °C. Figure D- 2 shows the plot of temperature change against measured change in longitudinal strain on the dummy pipe. The gradient of this plot is considered as the measured apparent thermal expansion coefficient, α' of the cast iron pipe. The data points are scattered and it is not possible to define a unique gradient. Therefore, it is evident that α' is not constant and varies with temperature.

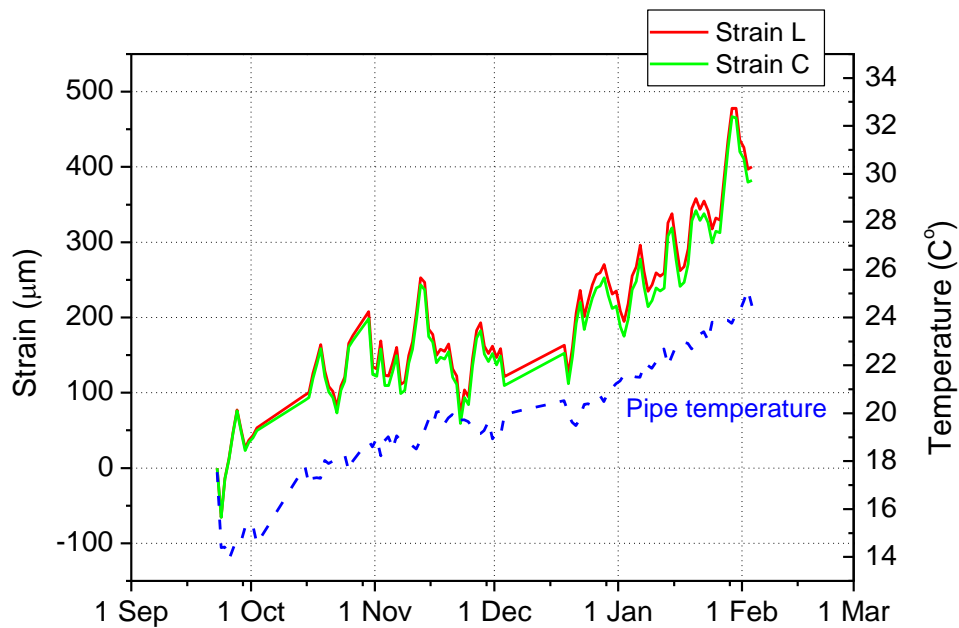


Figure D- 1 Average strain at dummy pipe from October 2008 to February 2009

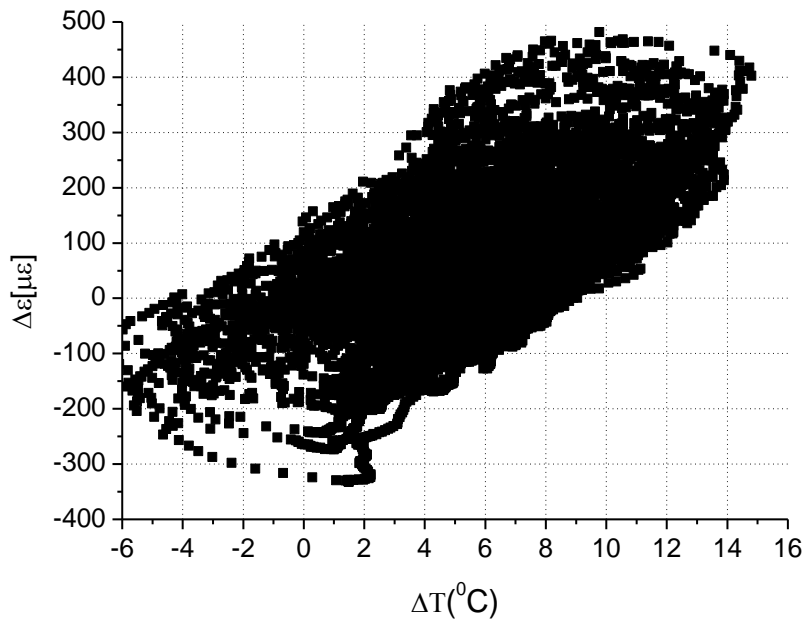


Figure D- 2 Dummy pipe strain against temperature change

APPENDIX E

SOIL PARTICLE SIZE DISTRIBUTION CURVES OF THE MOISTURE CONTENT MONITORING SITES 3 TO 23

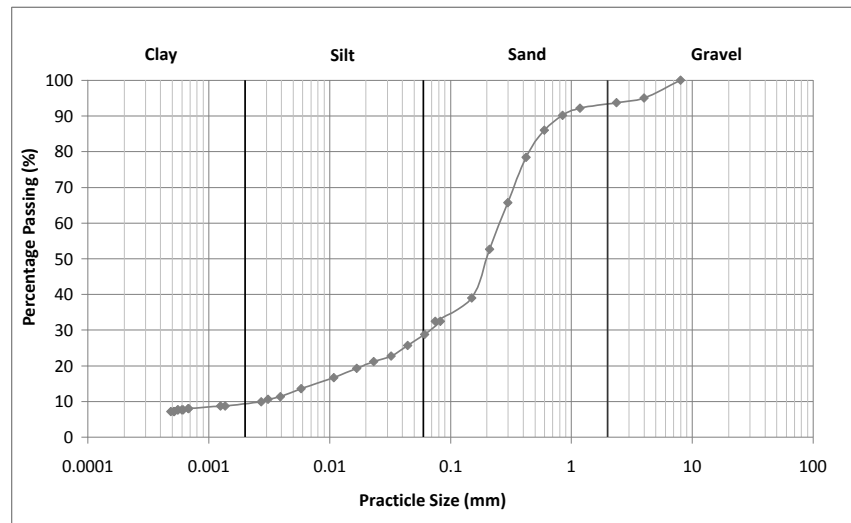


Figure E- 1 Particle size distribution of Site 3 Carrum

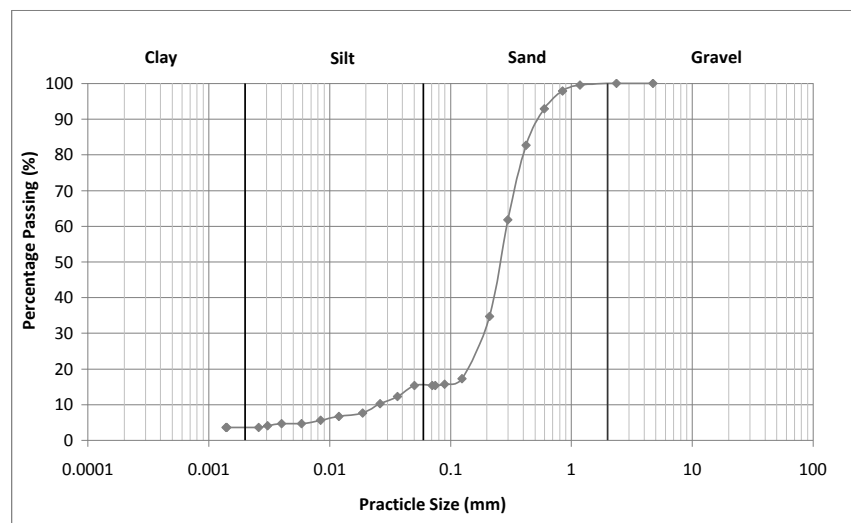


Figure E- 2 Particle size distribution of Site 4 Oakleigh South

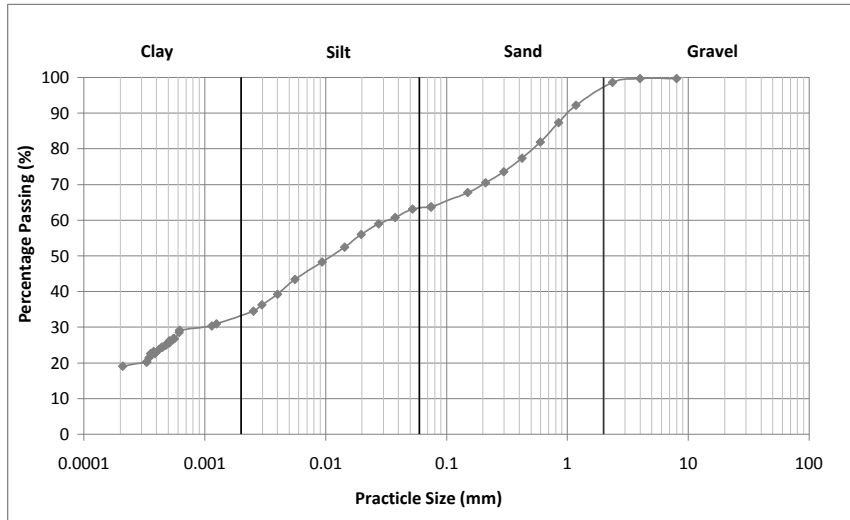


Figure E- 3 Particle size distribution of Site 5 Doveton

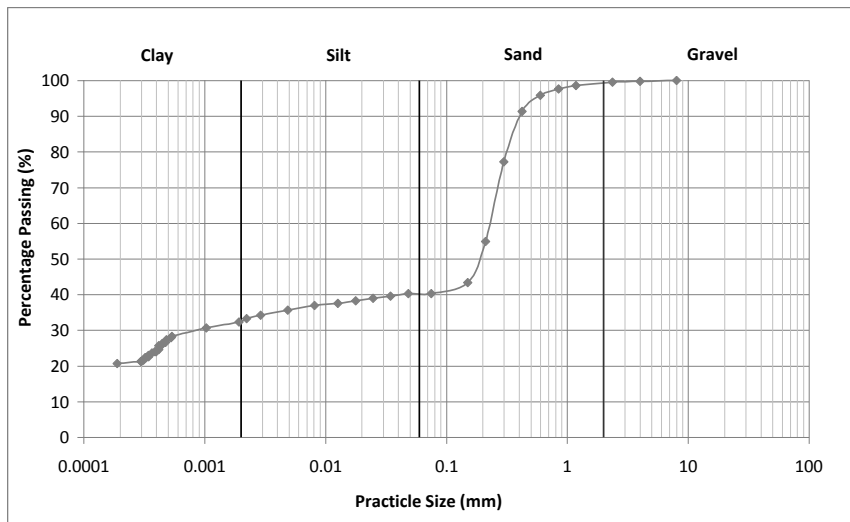


Figure E- 4 Particle size distribution of Site 6 Kew

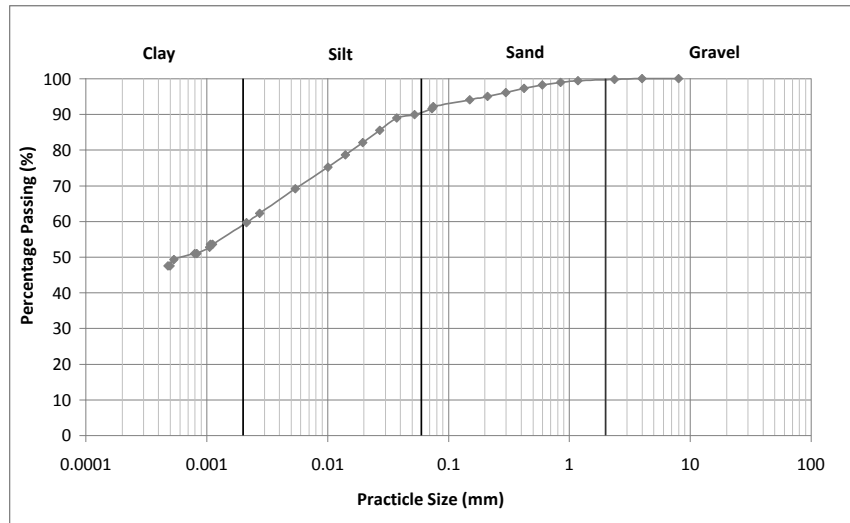


Figure E- 5 Particle size distribution of Site 7 Heidelberg West

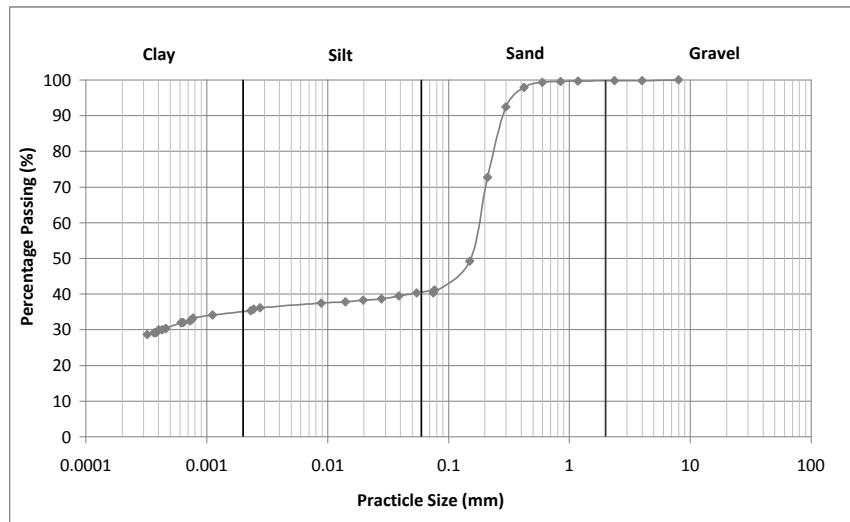


Figure E- 6 Particle size distribution of Site 8 Mt Eliza

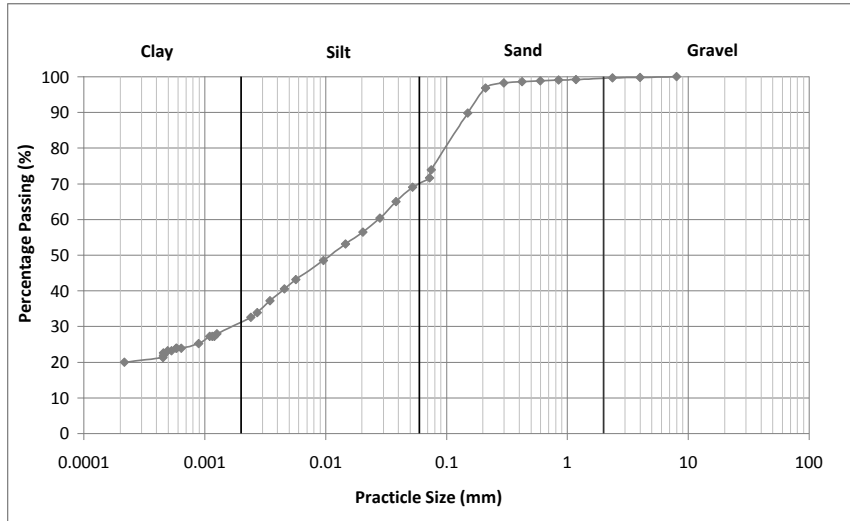


Figure E- 7 Particle size distribution of Site 9 Forest Hill

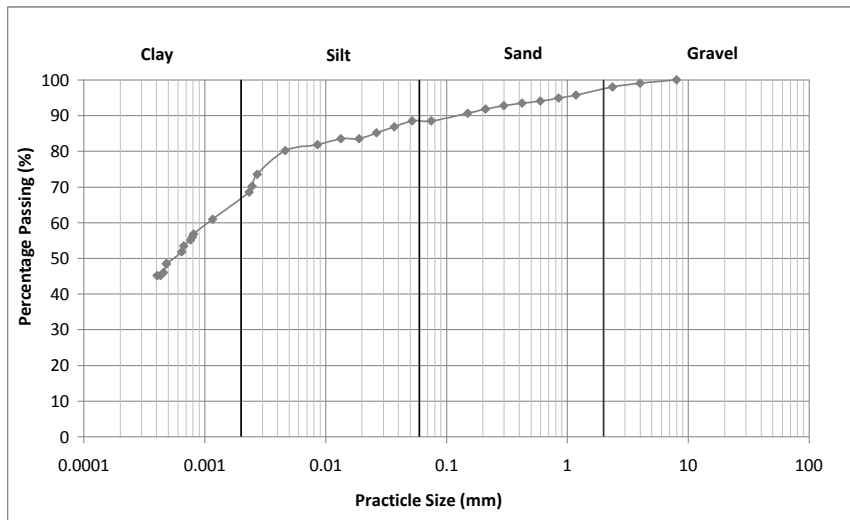


Figure E- 8 Particle size distribution of Site 10 Bulleen

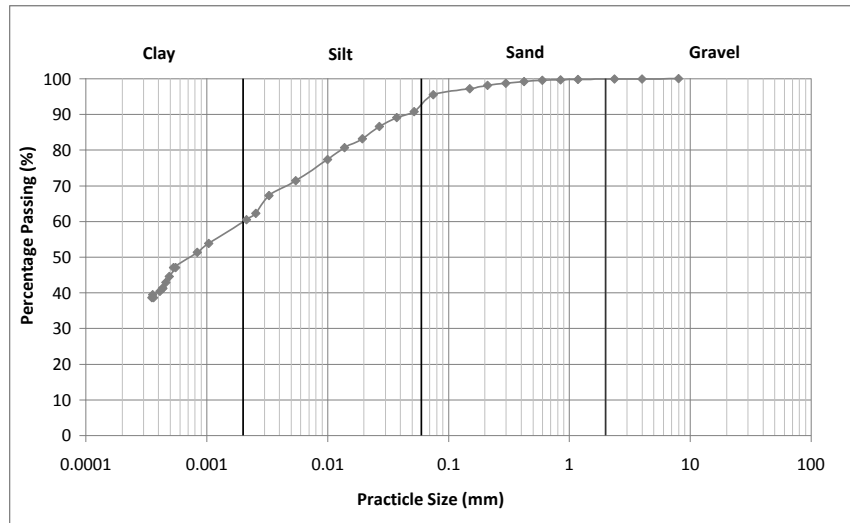


Figure E- 9 Particle size distribution of Site 11 Avondale Heights

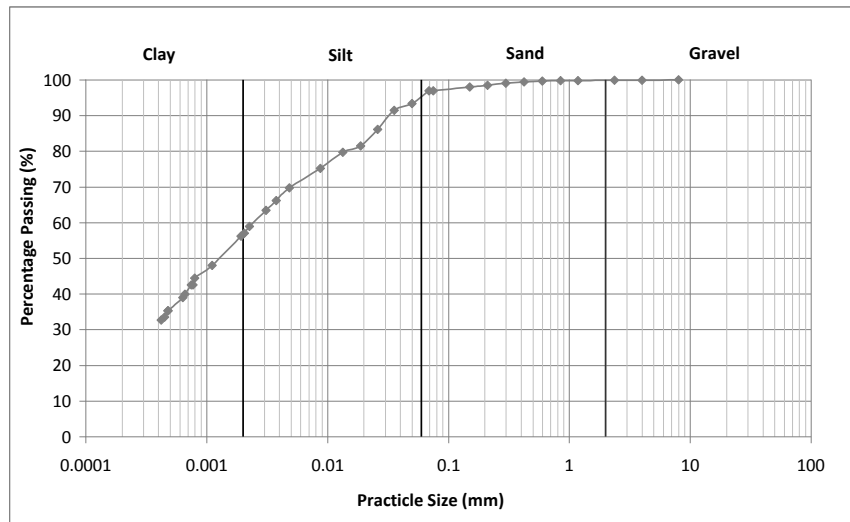


Figure E- 10 Particle size distribution of Site 12 Deer Park

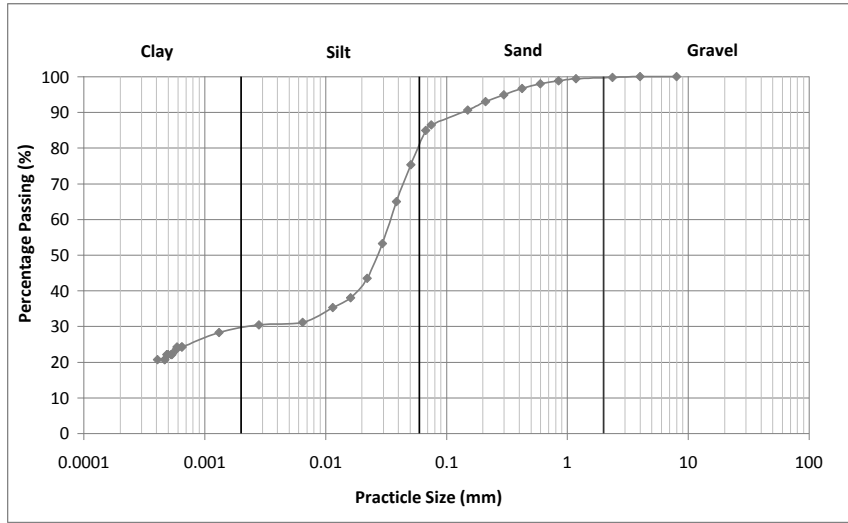


Figure E- 11 Particle size distribution of Site 13 St Albans

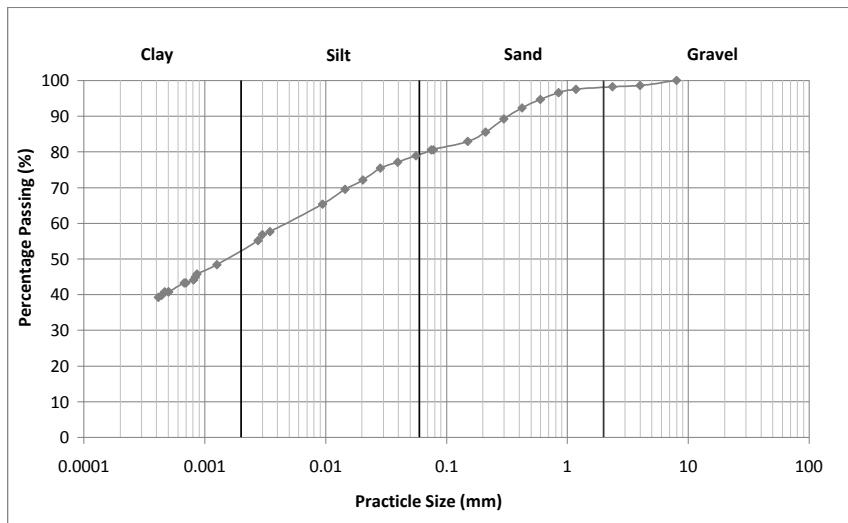


Figure E- 12 Particle size distribution of Site 14 Coburg

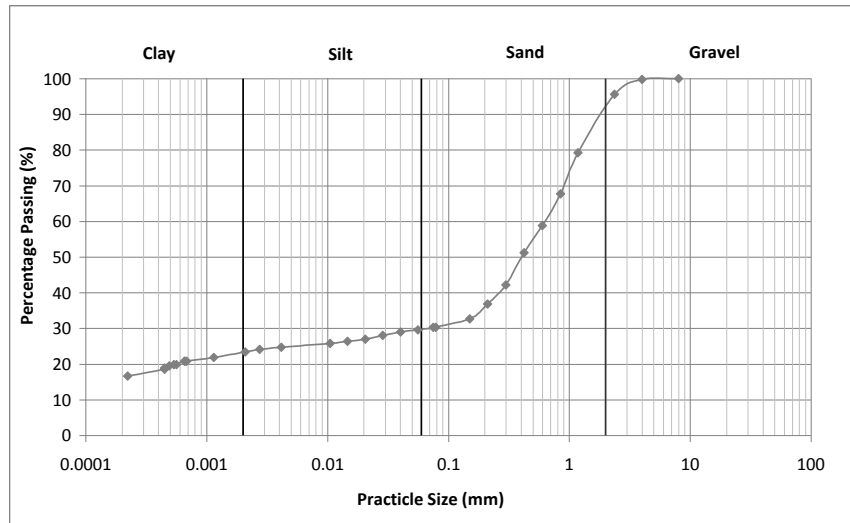


Figure E- 13 Particle size distribution of Site 15 Keysborough

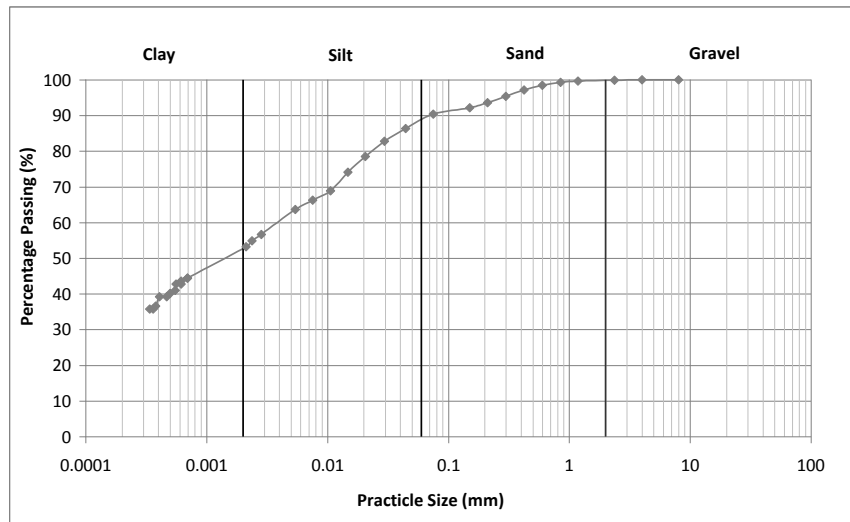


Figure E- 14 Particle size distribution of Site 16 Fairfield

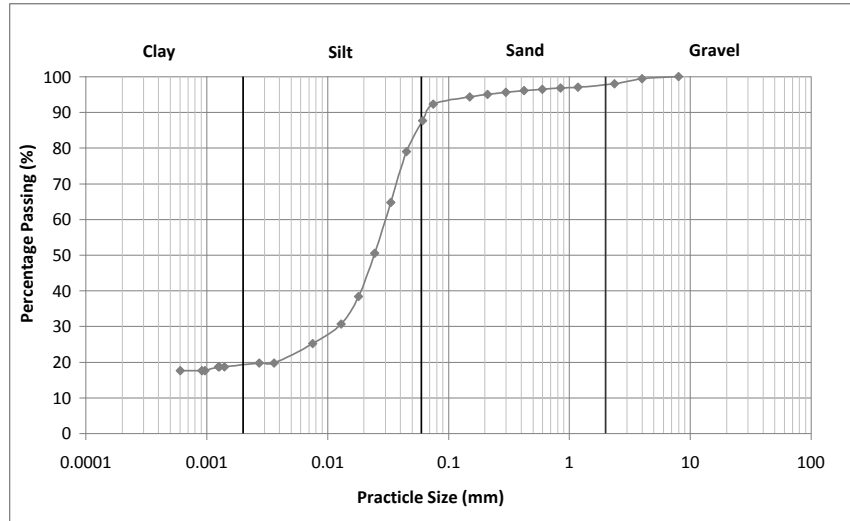


Figure E- 15 Particle size distribution of Site 17 Kingsbury

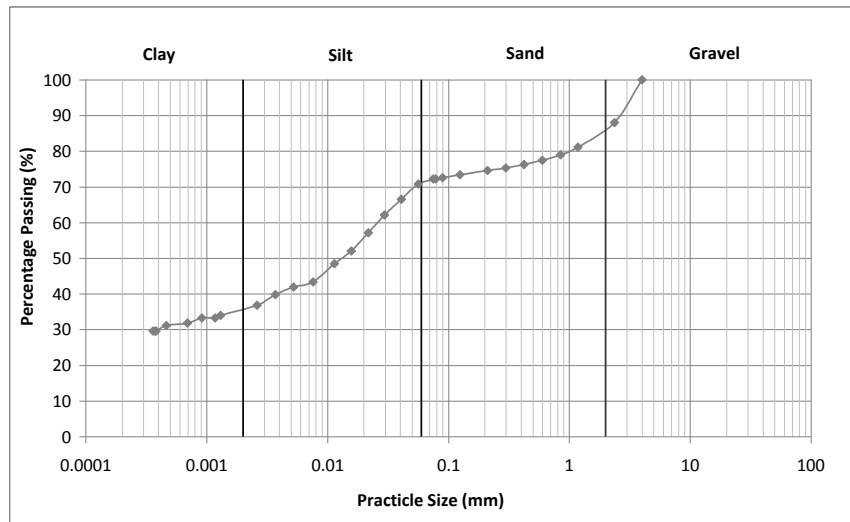


Figure E- 16 Particle size distribution of Site 18 Epping

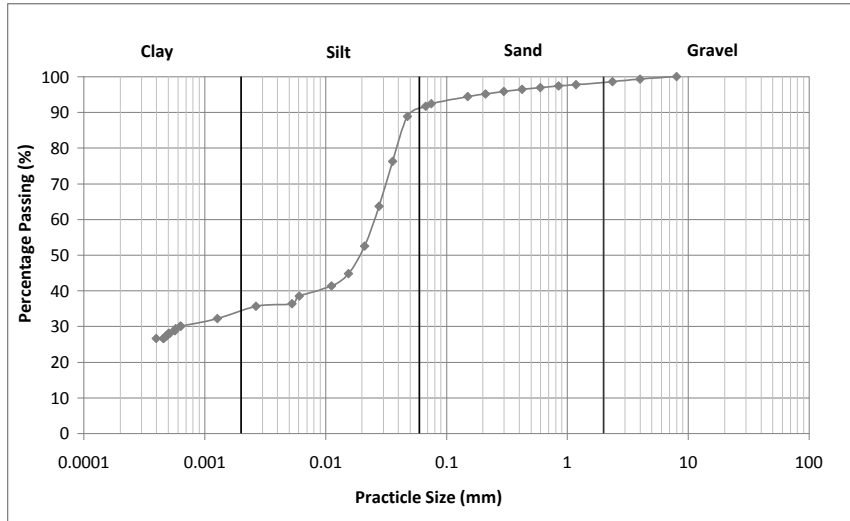


Figure E- 17 Particle size distribution of Site 19 Maidstone

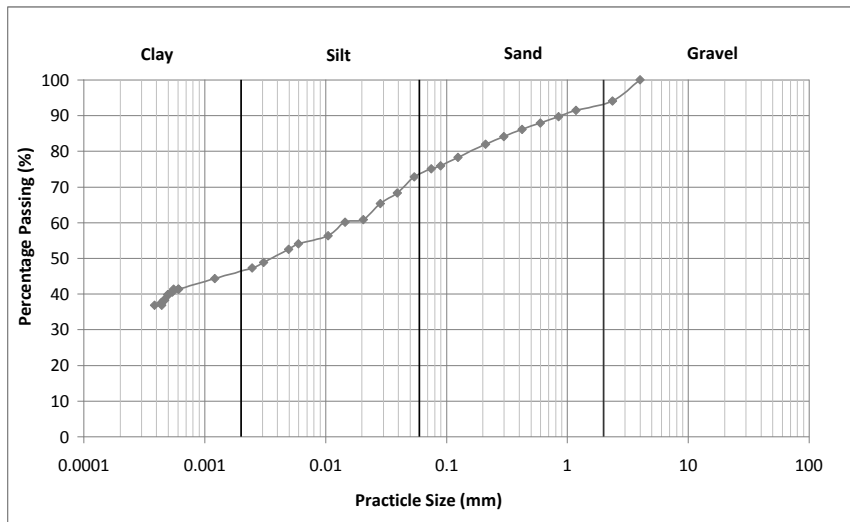


Figure E- 18 Particle size distribution of Site 20 Sunshine

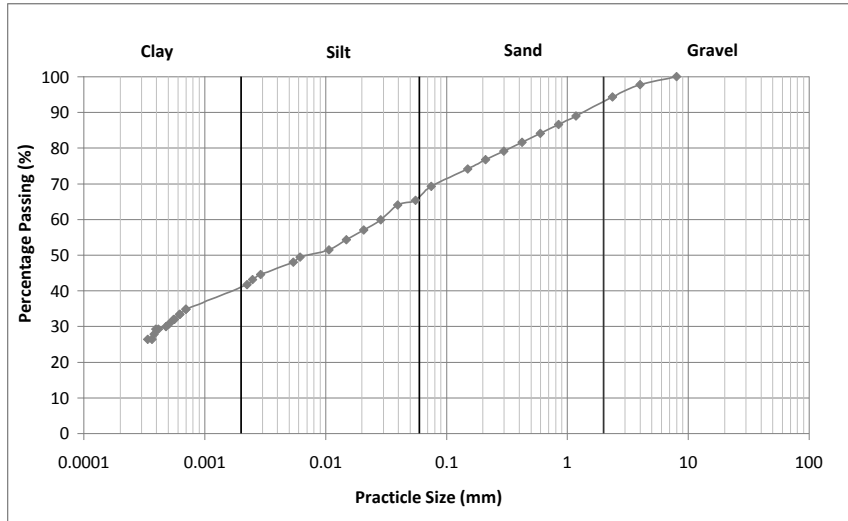


Figure E- 19 Particle size distribution of Site 21 Gladstone Park

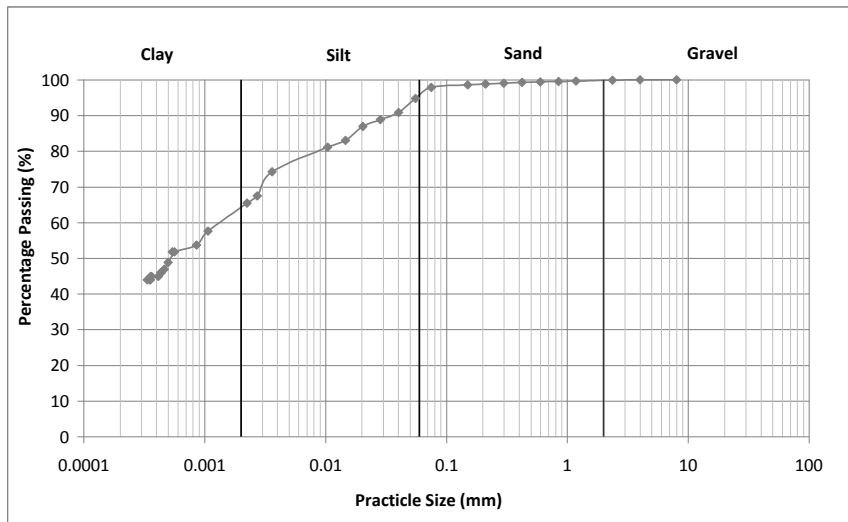


Figure E- 20 Particle size distribution of Site 22 Lalor

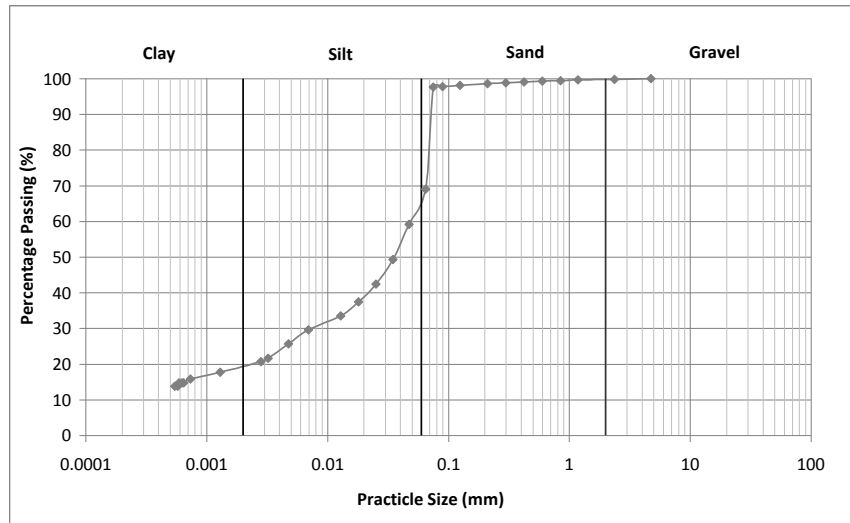


Figure E- 21 Particle size distribution of Site 23 Laverton

APPENDIX F

SOIL MOISTURE CONTENT PLOTS OF UNSELECTED SITES

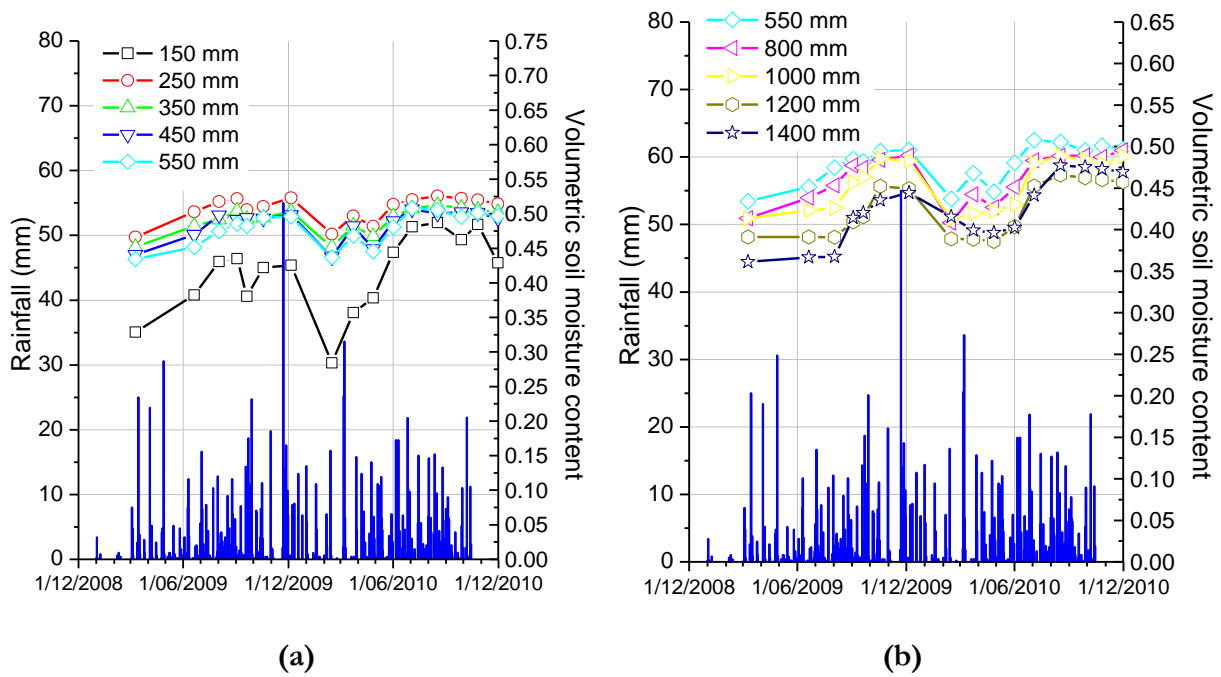


Figure F- 1 Volumetric soil moisture content in Site 5 Doveton: (a) 150 to 550 mm; (b) 550 to 1400 mm

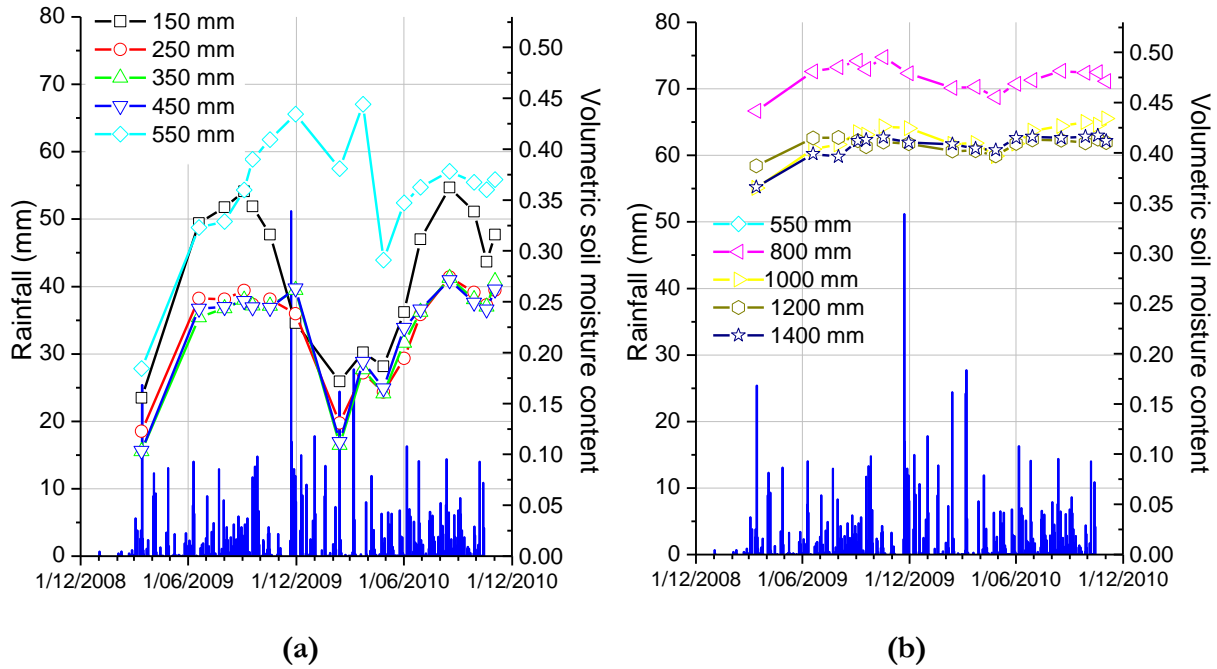


Figure F- 2 Volumetric soil moisture content in Site 6 Kew: (a) 150 to 550 mm; (b) 550 to 1400 mm

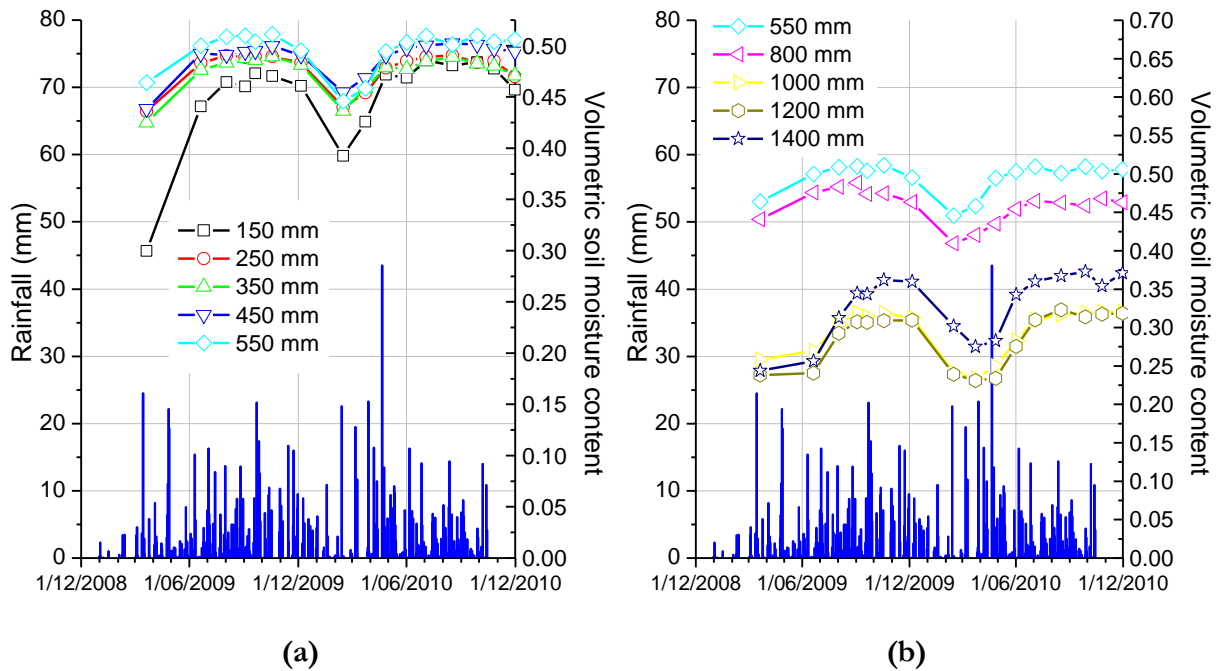
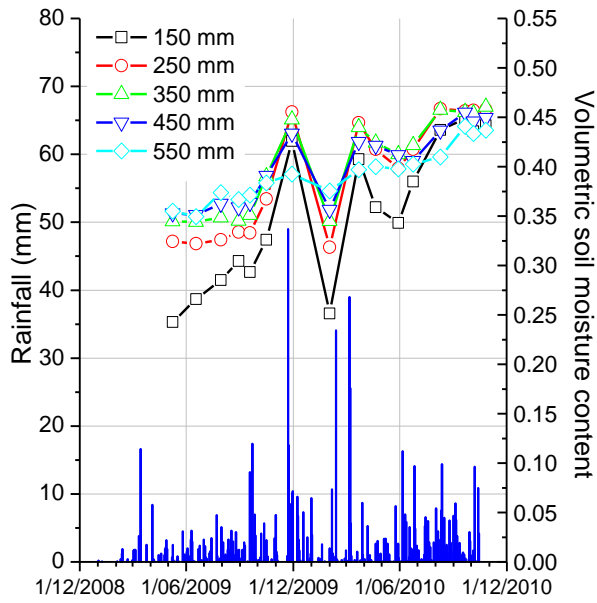
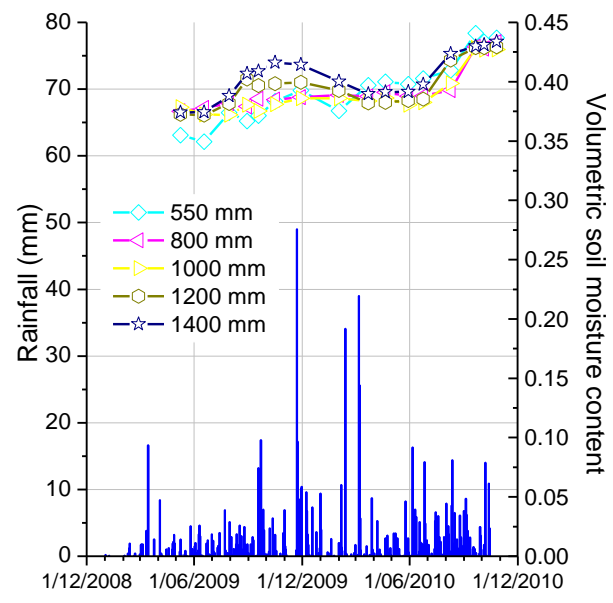


Figure F- 3 Volumetric soil moisture content in Site 8 Mount Eliza: (a) 150 to 550 mm; (b) 550 to 1400 mm

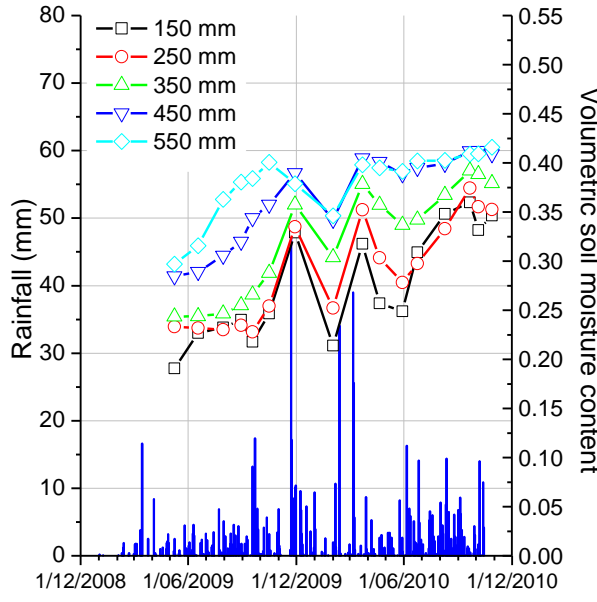


(a)

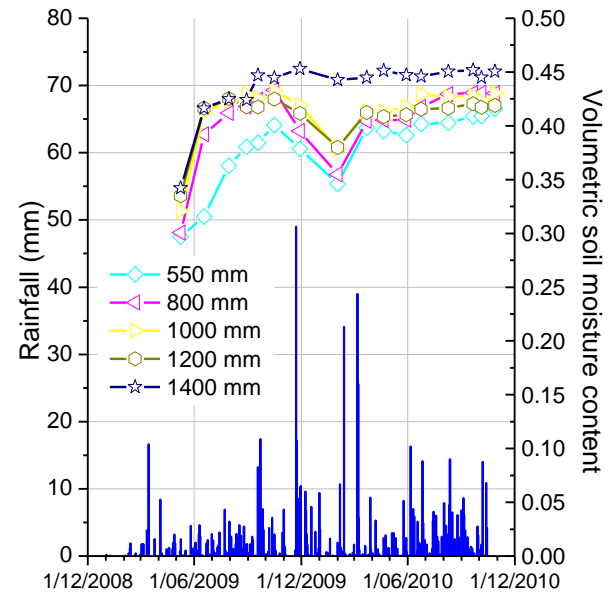


(b)

Figure F- 4 Volumetric soil moisture content in Site 12 Deer Park: (a) 150 to 550 mm; (b) 550 to 1400 mm



(a)



(b)

Figure F- 5 Volumetric soil moisture content in Site 13 St Albans: (a) 150 to 550 mm; (b) 550 to 1400 mm

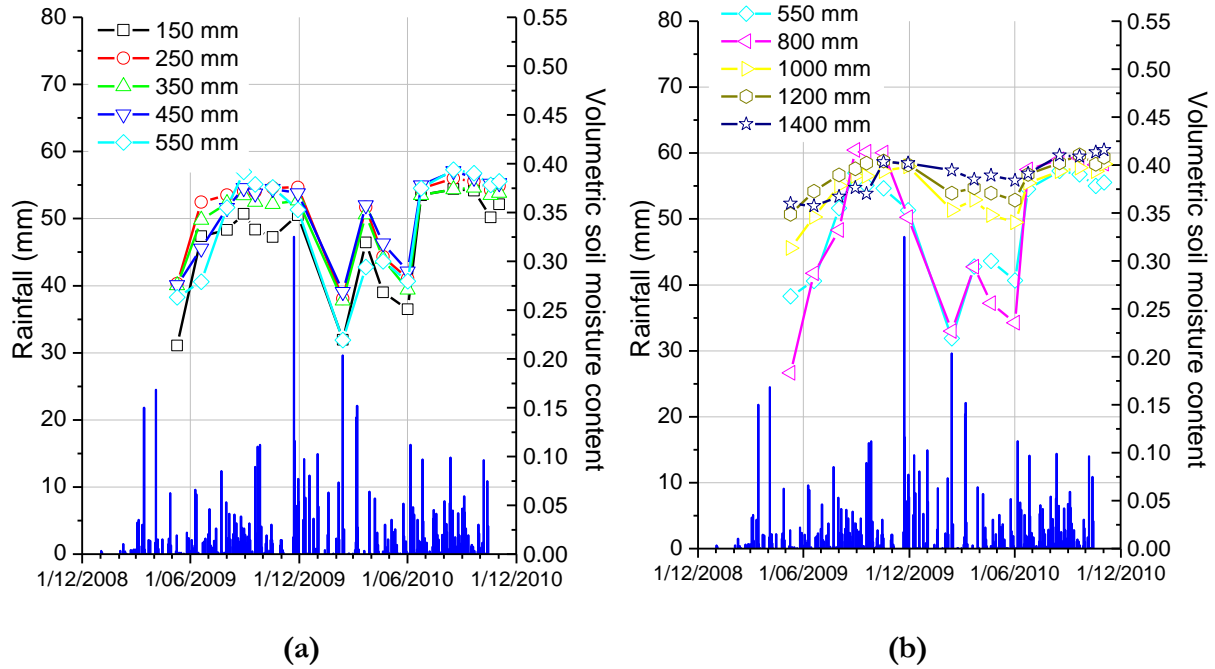


Figure F- 6 Volumetric soil moisture content in Site 14 Coburg: (a) 150 to 550 mm; (b) 550 to 1400 mm

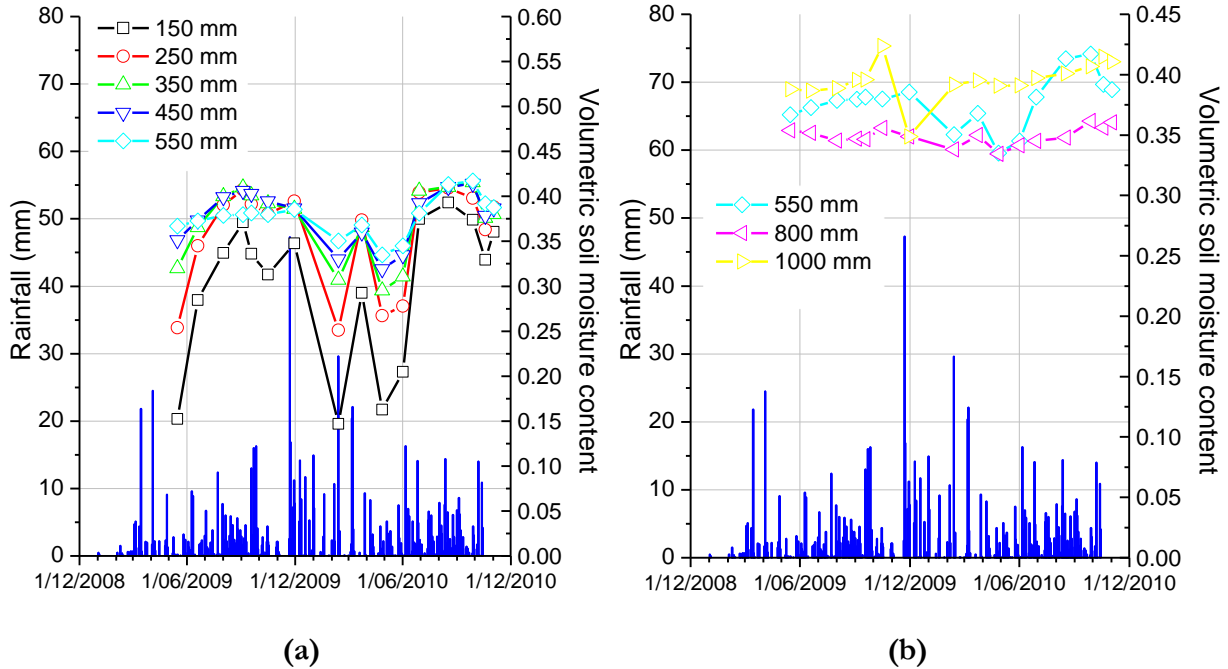
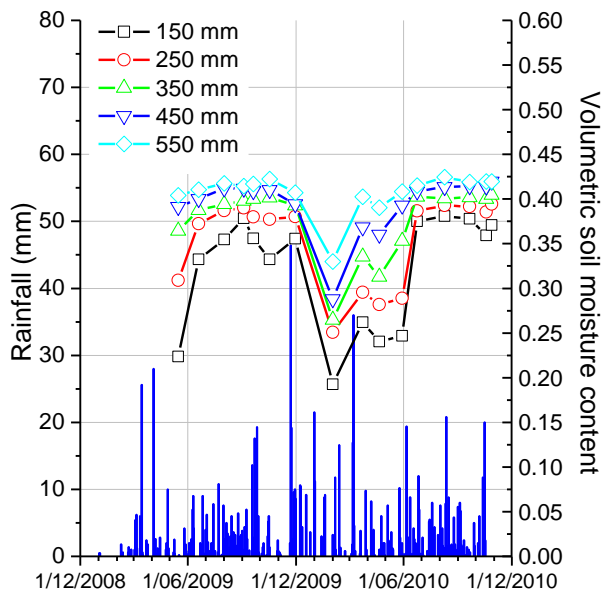
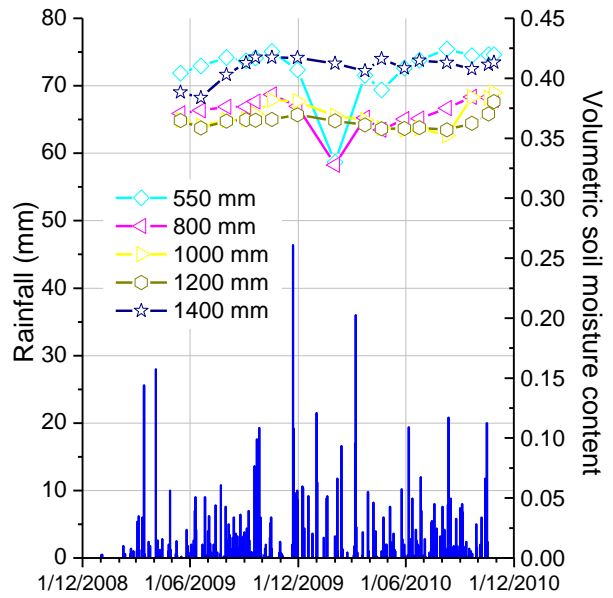


Figure F- 7 Volumetric soil moisture content in Site 16 Fairfield: (a) 150 to 550 mm; (b) 550 to 1000 mm

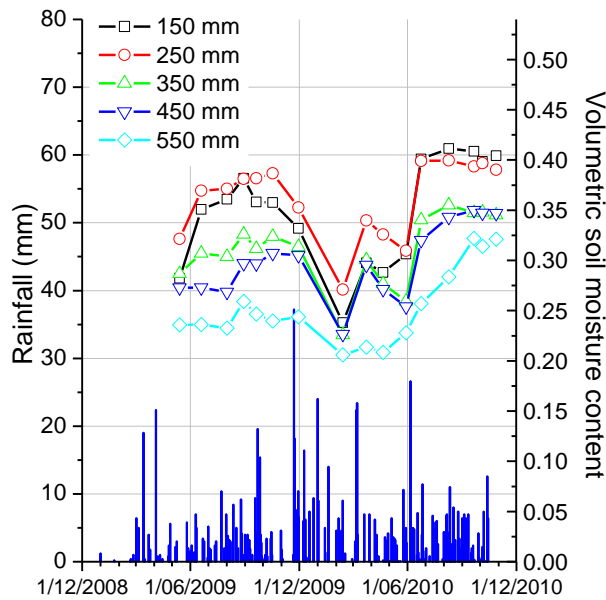


(a)

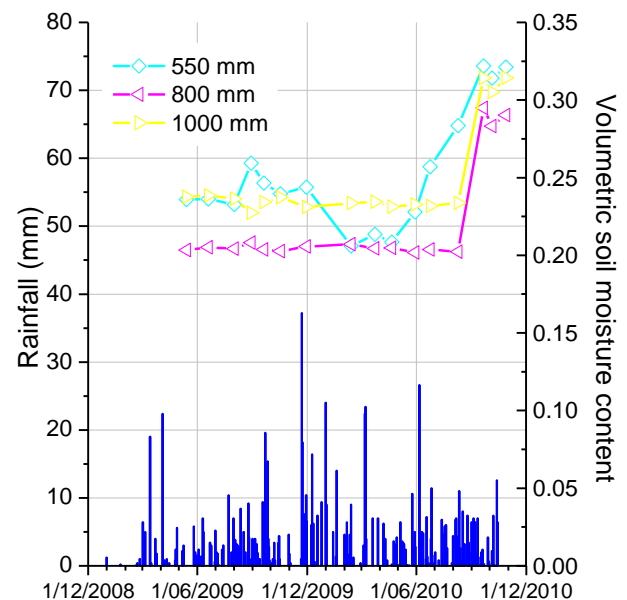


(b)

Figure F- 8 Volumetric soil moisture content in Site 17 Kingsbury: (a) 150 to 550 mm; (b) 550 to 1400 mm



(a)



(b)

Figure F- 9 Volumetric soil moisture content in Site 18 Epping: (a) 150 to 550 mm; (b) 550 to 1000 mm

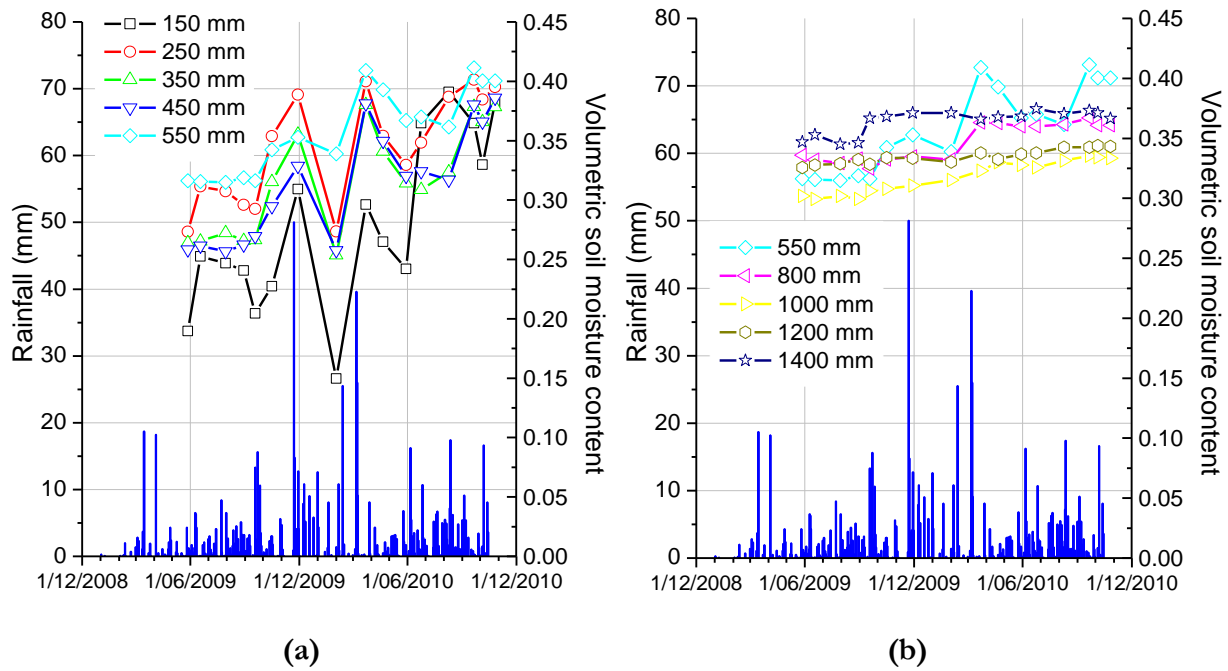


Figure F- 10 Volumetric soil moisture content in Site 19 Maidstone: (a) 150 to 550 mm; (b) 550 to 1400 mm

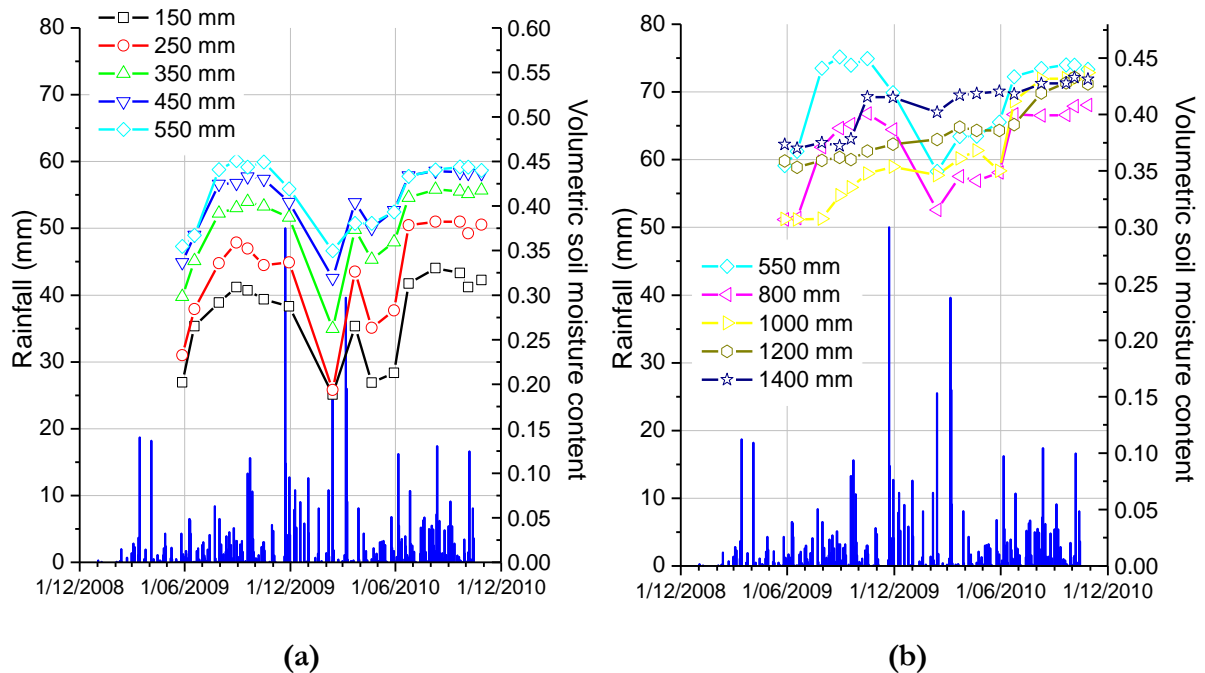


Figure F- 11 Volumetric soil moisture content in Site 20 Sunshine: (a) 150 to 550 mm; (b) 550 to 1400 mm

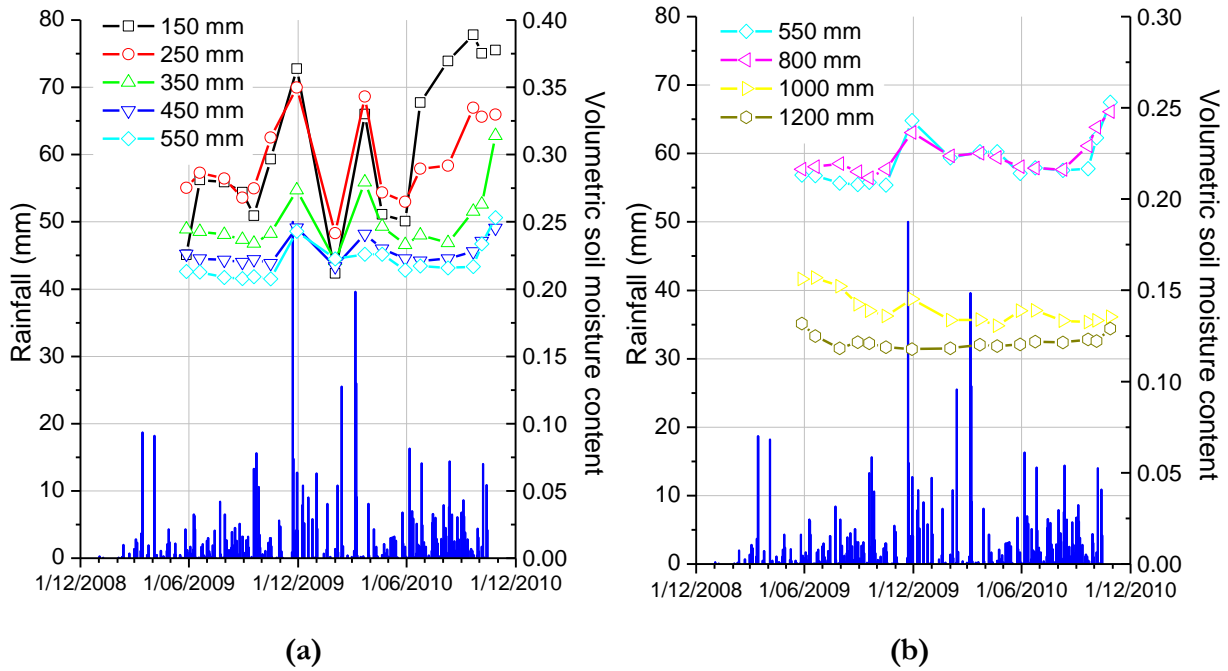


Figure F- 12 Volumetric soil moisture content in Site 21 Gladstone Park: (a) 150 to 550 mm; (b) 550 to 1200 mm

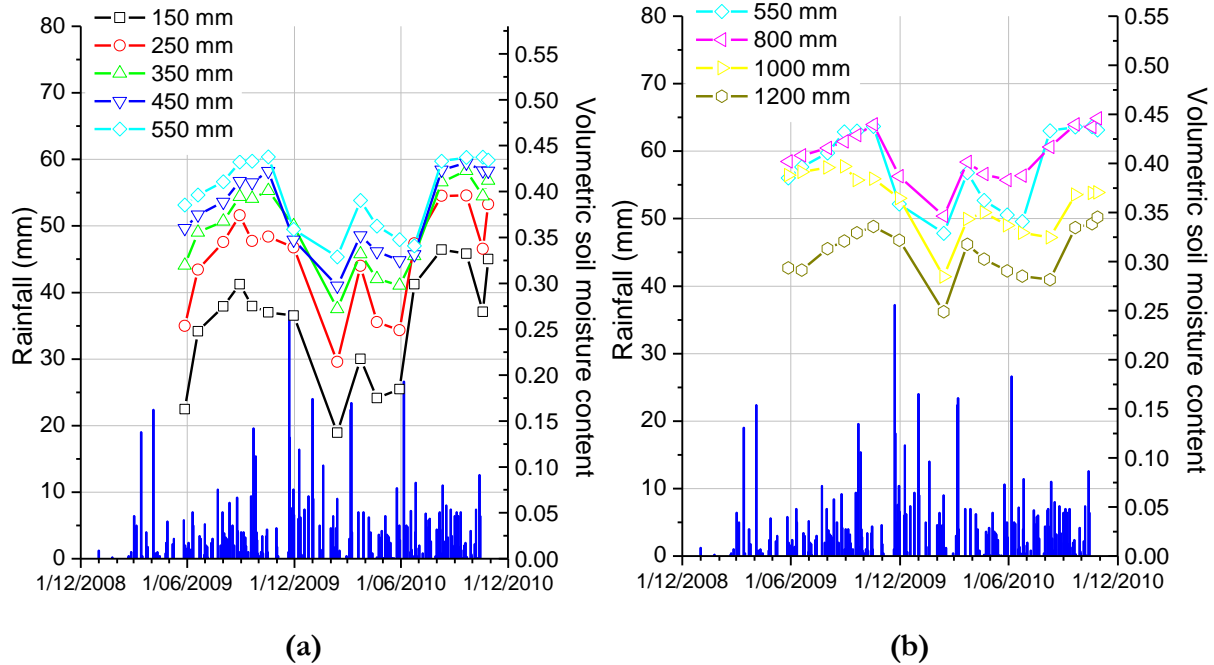


Figure F- 13 Volumetric soil moisture content in Site 22 Lalor: (a) 150 to 550 mm; (b) 550 to 1200 mm

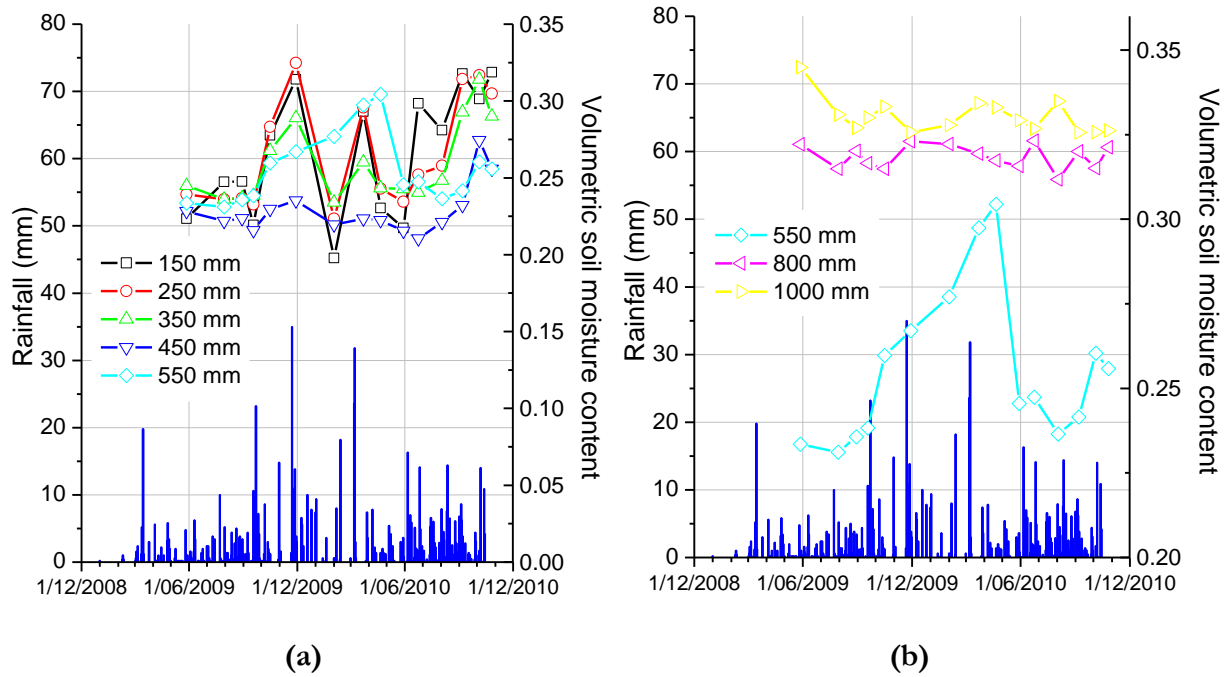


Figure F- 14 Volumetric soil moisture content in Site 23 Laverton: (a) 150 to 550 mm; (b) 550 to 1000 mm

APPENDIX G

ANALYSIS OF SEASONAL SOIL MOISTURE CONTENT VARIATIONS OF UNSELECTED SITES

Site no.	Suburb	Soil symbol	Soil type	Geological formation	Seasonal soil moisture change							
					Depth (mm)	Months	Moisture change (%)					
5	Doveton	CH	Inorganic clays of high plasticity	Quaternary alluvial and tertiary sediments, gravel, clay	150-800	Jun 09-Aug 09	Increased: max 5%, min 2%					
						Aug 09-Sep 09	Reduced: max 6%, min 1%					
						Sep 09-Dec 09	Increased: max 5%, min 2%					
						Dec 09-Feb 10	Reduced: max 15%, min 5%					
											Feb 10-Oct 10	Increased: max 22%, min 4%
					1000-1400	Jun 09-Dec 09	Increased: max 7%, min 6%					
						Dec 09-Apr 10	Reduced: max 6%, min 4%					
						Apr 10-Oct 10	Increased: max 20%, min 8%					
6	Kew	SC	Clayey sands	Non-basaltic clay	150-550	Jun 09-Sep 09	Increased: max 11%, min 1%					
						Sep 09-Feb 10	Reduced: max 19%, min 5%					
						Feb 10-Oct 10	Increased: max 25%, min 20%					
					800-1400	Jun 09 -Oct 09	Increased: max 3%, min 2%					
						Oct 09-Apr 10	Reduced: max 4%, min 1%					
						Apr 10-Oct 10	Increased: max 2%, min 1%					

Site no.	Suburb	Soil symbol	Soil type	Geological formation	Seasonal soil moisture change		
					Depth (mm)	Site no.	Suburb
8	Mount Eliza	SC	Clayey sands	Quaternary alluvial and tertiary sediments, gravel, clay	150-800	Jun 09-Oct 09	Increased: max 3%, min 1%
						Oct 09-Feb 10	Reduced: max 8%, min 5%
						Feb 10-Oct 10	Increased: max 9%, min 4%
					1000-1400	Jun 09-Oct 09	Increased: max 7%, min 5%
						Oct 09-Mar 10	Reduced: max 9%, min 8%
						Mar 10-Oct 10	Increased: max 9%, min 5%
12	Deer Park	CH	Inorganic clays of high plasticity	Basaltic clay	150-800	Jun 09-Nov 09	Increased: max 16%, min 8%
						Nov 09-Jan 10	Reduced: max 18%, min 7%
						Jan 10-Mar 10	Increased: max 16%, min 7%
						Mar 10-Jun 10	Reduced: max 7%, min 2%
						Jun 10-Oct 10	Increased: max 11%, min 4%
					1000-1400	Jun 09-Jan 10	Increased: max 2%, min 1%
						Jan 10-Mar 10	Reduced: less than 1%
						Mar 10-Apr 10	Increased: less than 1%
						Apr 10-Jun 10	Reduced: 1%
						Jun 10-Oct 10	Increased: max 2%, min 1%

Site no.	Suburb	Soil symbol	Soil type	Geological formation	Seasonal soil moisture change		
					Depth (mm)	Site no. Suburb	
13	St Albans	CH	Inorganic clays of high plasticity	Basaltic clay	150-450	Jun 09-Nov 09	Increased: max 12%, min 10%
						Nov 09-Jan 10	Reduced: max 12%, min 6%
						Jan 10-Mar 10	Increased: max 11%, min 6%
						Mar 10-Jun 10	Reduced: max 7%, min 1%
						Jun 10-Oct 10	Increased: max 11%, min 2%
					550-1400	Jun 09-Oct 09	Increased: max 8%, min 1%
						Oct 09-Jan 10	Reduced: max 5%, min 1%
						Jan 10-Mar 10	Increased: max 5%, min 1%
						Mar 10-Jun 10	Reduced: max 2%, min 1%
						Jun 10-Oct 10	Increased: max 3%, min 1%
14	Coburg	CH	Inorganic clays of high plasticity	Basaltic clay	150-800	Jun 09-Aug 09	Increased: max 13%, min 1%
						Aug 09-Feb 10	Reduced: max 18%, min 10%
						Feb 10-Mar 10	Increased: max 11%, min 10%
						Mar 10-Jun 10	Reduced: max 8%, min 7%
					1000-1400	Jun 10-Oct 10	Increased: max 12%, min 9%
						Jun 09-Nov 09	Increased: max 5%, min 3%
						Nov 09-Jun 10	Reduced: max 6%, min 2%
						Jun 10-Oct 10	Increased: max 17%, min 1%

Site no.	Suburb	Soil symbol	Soil type	Geological formation	Seasonal soil moisture change							
					Depth (mm)	Site no.	Suburb					
16	Fairfield	CH	Inorganic clays of high plasticity	Non-basaltic clay	150-800	Jun 09-Oct 09	Increased: max 7%, min 2%					
						Oct 09-Feb 10	Reduced: max 22%, min 2%					
						Feb 10-Mar 10	Increased: max 14%, min 1%					
						Mar 10-Apr 10	Reduced: max 13%, min 2%					
						Apr 10-Oct 10	Increased: max 23%, min 2%					
					1000-1400	Jun 09-Oct 09	Increased: 3%					
						Oct 09-Nov 09	Reduced: 7%					
						Nov 09-Oct 10	Increased: 2%					
					17	Kingsbury	CH	Inorganic clays of high plasticity	Basaltic clay	150-800	Jun 09-Oct 09	Increased: max 5%, min 1%
											Oct 09-Jan 10	Reduced: max 19%, min 6%
Jan 10-Oct 10	Increased: max 19%, min 5%											
1000-1400	Jun 09-Oct 09	Increased: max 4%, min 1%										
	Oct 09-Jun 10	Reduced: max 2%, min 1%										
	Jun 10-Oct 10	Increased: max 2%, min 1%										
18	Epping	CH	Inorganic clays of high plasticity	Basaltic clay	150-550	Jun 09-Oct 09	Increased: max 3%, min 1%					
						Oct 09-Feb 10	Reduced: max 14%, min 5%					
						Feb 10-Oct 10	Increased: max 17%, min 11%					
					800-1000	Jun 09-Oct 09	Increased: less than 1%					
						Oct 09-Jun 10	Reduced: less than 1%					
						Jun 10-Oct 10	Increased: max 9%, min 8%					

Site no.	Suburb	Soil symbol	Soil type	Geological formation	Seasonal soil moisture change		
					Depth (mm)	Site no.	Suburb
19	Maidstone	CH	Inorganic clays of high plasticity	Basaltic clay	150-450	Jun 09-Nov 09	Increased: max 6%, min 3%
						Nov 09-Jan 10	Reduced: max 16%, min 1%
						Jan 10-Mar 10	Increased: max 15%, min 7%
						Mar 10-Jun 10	Reduced: max 6%, min 1%
						Jun 10-Oct 10	Increased: max 16%, min 2%
					550-800	Jun 09-Mar 10	Increased: max 9%, min 3%
						Mar 10-Jun 10	Reduced: max 5%, min 1%
						Jun 10-Oct 10	Increased: max 4%, min 1%
						Jun 09-Nov 09	Increased: max 3%, min 1%
						Nov 09-Jun 10	Reduced: max 2%, min 1%
1000-1400	Jun 10-Oct 10	Increased: max 2%, min 1%					
	Jun 09-Oct 09	Increased: max 8%, min 4%					
20	Sunshine	CL	Inorganic clays of low to medium plasticity	Basaltic clay	150-450	Oct 09-Feb 10	Reduced: max 12%, min 10%
						Feb 10-Mar 10	Increased: max 14%, min 3%
						Mar 10-Jun 10	Reduced: max 6%, min 1%
						Jun 10-Oct 10	Increased: max 12%, min 6%
						Jun 09-Oct 09	Increased: max 9%, min 8%
					550-800	Oct 09-Feb 10	Reduced: max 10%, min 8%
						Feb 10-Oct 10	Increased: max 9%, min 8%
						Jun 09-Nov 09	Increased: max 5%, min 2%
						Nov 09-Feb 10	Reduced: max 2%, min 1%
						Feb 10-Oct 10	Increased: max 8%, min 1%
1000-1400	Jun 09-Nov 09	Increased: max 5%, min 2%					
	Nov 09-Feb 10	Reduced: max 2%, min 1%					
					Feb 10-Oct 10	Increased: max 8%, min 1%	

Site no.	Suburb	Soil symbol	Soil type	Geological formation	Seasonal soil moisture change		
					Depth (mm)	Site no.	Suburb
21	Gladstone Park	CH	Inorganic clays of high plasticity	Basaltic clay	150-550	Jun 09-Sep 09	Reduced: max 3%, min 1%
						Sep 09-Nov 09	Increased: max 11%, min 3%
						Nov 09-Jan 10	Reduced: max 15%, min 2%
						Jan 10-Mar 10	Increased: max 12%, min 1%
						Mar 10-Jun 10	Reduced: max 8%, min 2%
					Jun 10-Oct 10	Reduced: max 14%, min 2%	
					800-1100	Jun 09-Oct 09	Reduced: max 2%, min 1%
						Oct 09-Jun 10	Increased: less than 1%
						Jun 10-Oct 10	Reduced: less than 1%
					22	Lalor	CH
Aug 09-Feb 10	Reduced: max 21%, min 16%						
Feb 10-Mar 10	Increased: max 11%, min 8%						
Mar 10-Jun 10	Reduced: max 7%, min 4%						
Jun 10-Oct 10	Increased: max 16%, min 4%						
800-1200	Jun 09-Oct 09	Increased: max 5%, min 4%					
	Oct 09-Feb 10	Reduced: max 13%, min 11%					
	Feb 10-Mar 10	Increased: max 6%, min 5%					
	Mar 10-Aug 10	Reduced: max 4%, min 2%					
	Aug 10-Oct 10	Reduced: max 5%, min 4%					

Site no.	Suburb	Soil symbol	Soil type	Geological formation	Seasonal soil moisture change		
					Depth (mm)	Suburb	
23	Laverton	CH	Inorganic clays of high plasticity	Basaltic clay	150-450	Jun 09-Nov 10	Increased: max 8%, min 2%
						Nov 09-Jan 10	Reduced: max 11%, min 2%
						Jan 10-Mar 10	Increased: max 9%, min 1%
						Mar 10-Jun 10	Reduced: max 7%, min 1%
						Jun 10-Oct 10	Increased: max 10%, min 6%
					550	Jun 09-Apr 10	Increased: 7%
						Apr 09-Jul 10	Reduced: 5%
						Jul 10-Oct 10	Increased: 2%
					800-1000	Jun 09-Nov 10	Increased: less than 1%
						Nov 09-May 10	Reduced: less than 1%
May 10-Oct 10	Increased: less than 1%						

APPENDIX H

CLIMATE DATA USED AS INPUT FOR THE GROUND-ATMOSPHERE INTERACTION MODELLING

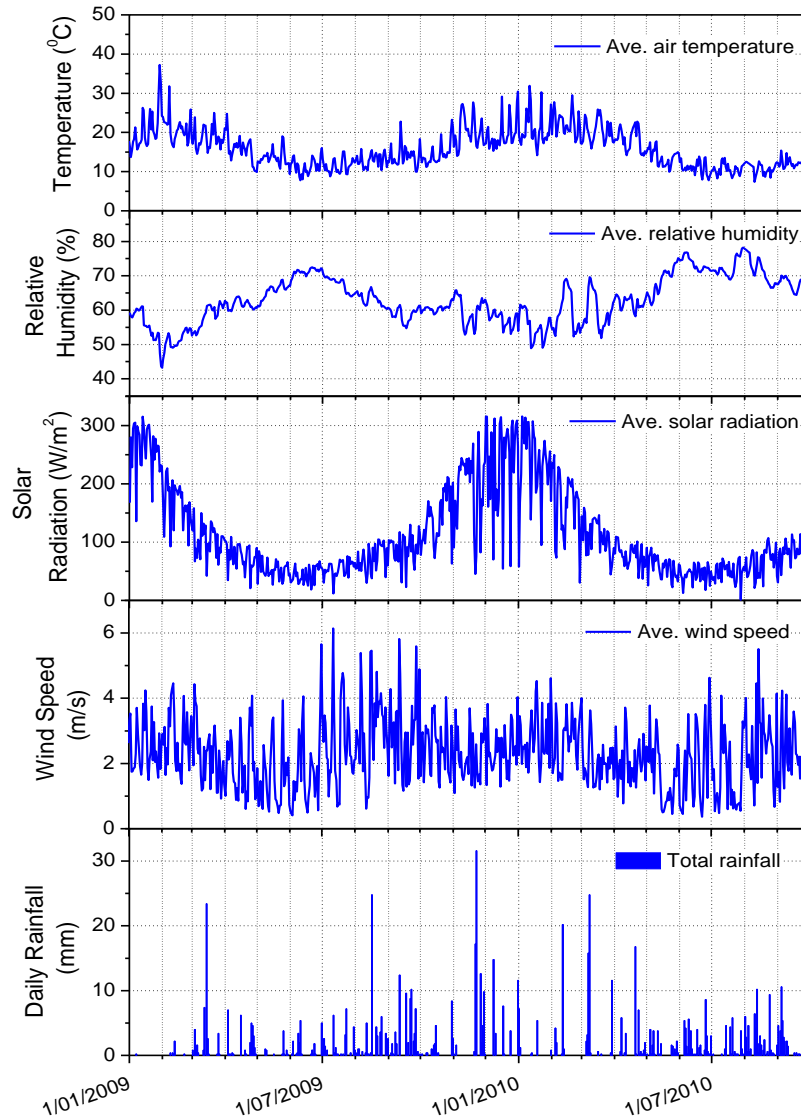


Figure H- 1 Average air temperature, relative humidity, solar radiation, wind speed and total daily rainfall in Altona North

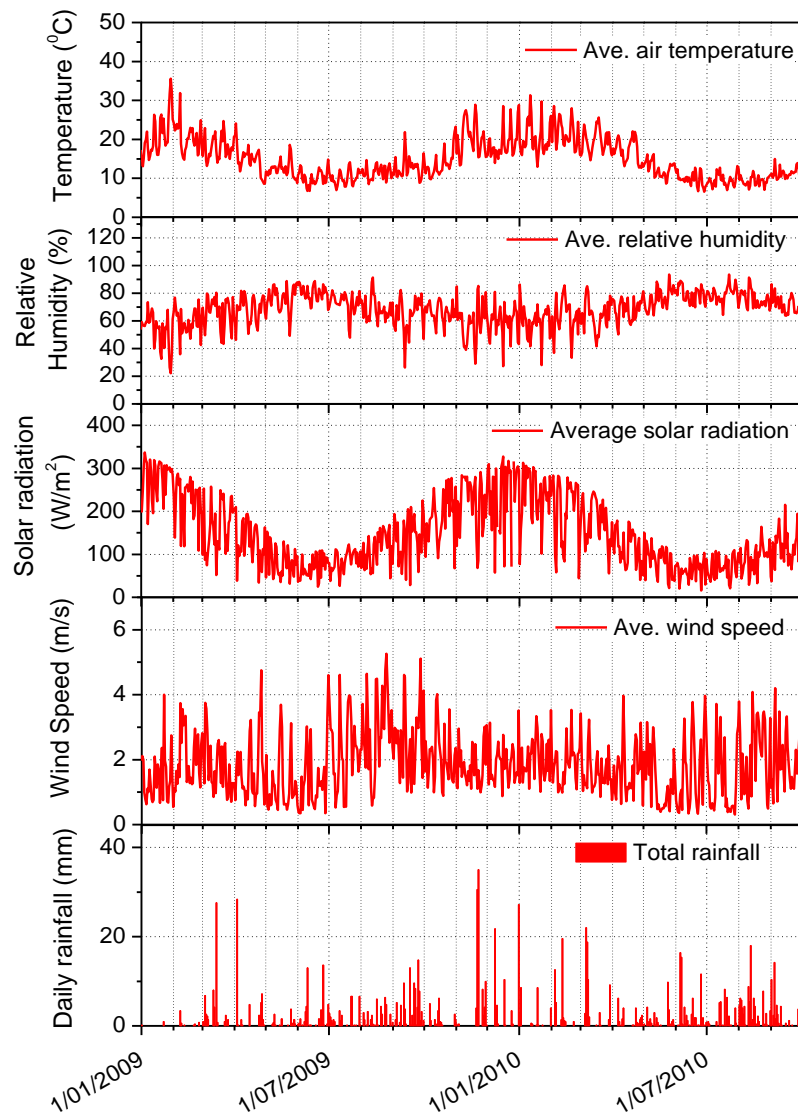


Figure H- 2 Average air temperature, relative humidity, solar radiation, wind speed and total daily rainfall in Fawkner